SÉBASTIEN MORIN

Motions, Order and Consistency
A Story Based on the Study of the Dynamics of the Class A β-Lactamase PSE-4 by NMR

Thèse présentée
à la Faculté des études supérieures de l'Université Laval
dans le cadre du programme de doctorat en Biochimie
pour l'obtention du grade de Philosophiæ Doctor (Ph. D.)

Département de biochimie et de microbiologie
Faculté des sciences et de génie
UNIVERSITÉ LAVAL
QUÉBEC

2010

À mes deux grands amours :
Alexia et Diana...

Somewhere, something incredible is
waiting to be known.
(Carl Sagan)

Remerciements

Je remercie d'abord tous ceux qui ont croisé ma route durant ces années d'études graduées. Je remercie les différents membres du laboratoire de Stéphane M. Gagné, présents et passés, particulièrement Jean-Baptiste, Olivier et Pierre-Yves. Merci les mecs !

Ensuite, je remercie les membres de mon comité aviseur, Michèle Auger et Roger C. Levesque, ainsi que Jacques Lapointe et Walter J. Chazin, tous deux membres de mon jury de thèse. Plusieurs personnes m'ont conseillé et/ou aidé au cours de mon doctorat (Pierre Audet, Edward J. d'Auvergne, Richard Daigle, Nicolas Doucet, Michel Guertin, Pierre Lavigne, Anthony Mittermaier, Joëlle N. Pelletier, Tara Sprules), je les remercie !

Je remercie aussi mon directeur Stéphane pour m'avoir motivé et poussé à me dépasser intellectuellement. Merci Stéphane ! Tu as été mon mentor pendant toutes ces années et je suis maintenant ce scientifique passionné en grande partie grâce à toi !

Évidemment, toutes ces années auraient été bien plus difficiles sans aide financière. Je remercie donc le CRSNG, le FRSQ, la Fondation J.-Arthur Vincent, PROTEO (anciennement le CREFSIP), la Faculté des sciences et de génie et le Département de biochimie et de microbiologie de l'Université Laval.

Finalement, je remercie mes proches pour m'avoir soutenu pendant toutes ces années !

Merci à maman, papa et Maryse pour m'avoir encouragé ! Un merci spécial à maman et papa pour m'avoir, dès mon très jeune âge, enseigné l'importance des études et m'avoir ainsi valorisé tout au long de mon cheminement ! Merci !

Merci Diana ! Depuis le début, tu m'as soutenu quand j'ai douté de moi ! Sans toi, je n'aurais jamais réussi ! Merci mon amour !

Merci finalement à Alexia pour m'avoir inspiré et donné le goût de me dépasser !

Résumé

Partie I L'analyse de données de relaxation des spins à l'aide de l'approche model-free est très répandue pour obtenir des informations sur la dynamique des protéines aux échelles de temps ps-ns et μs-ms. Afin d'extraire des informations de qualité, les données sont enregistrées à plusieurs champs magnétiques. Combiner de telles données est cependant sujet aux erreurs expérimentales. Ainsi, la consistence des données de relaxation à plusieurs champs doit être vérifiée. Malheureusement, cela s'effectue rarement, *i.e.* on assume simplement que les données sont correctes. Nous proposons donc une approche simple pour la vérification de la consistence de données de relaxation enregistrées à plusieurs champs. L'utilisation des test proposés améliore l'analyse et réduit la présence artéfactuelle d'échange conformationnel. Ainsi, comme les données d'échange conformationnel sont souvent discutées en terme de liaison de substrat ou de catalyse, s'assurer de leur validité améliore la compréhension biologique du système étudié.

Partie II Les β-lactamases de classe A sont impliquées dans la résistance aux antibiotiques. Elles y participent en hydrolysant les β-lactamines. Ces enzymes ont été étudiées par différentes approches : études mutationnelles, simulations de dynamique moléculaire, cristallographie des rayons X et RMN. L'enzyme modèle de cette classe, TEM-1, a précédemment été étudiée par RMN dans notre laboratoire. TEM-1 est très rigide sur l'échelle de temps des ps-ns, mais subit des mouvements lents μs-ms au niveau du site actif. Afin de mieux caractériser la dynamique des β-lactamases de classe A, l'homologue PSE-4 a aussi été étudié par RMN avec des données de relaxation des spins, de dispersion de relaxation par CPMG et d'échange d'amides. Les mêmes conclusions que pour TEM-1 ont été obtenues : rigidité générale élevée et présence de mouvements lents près du site actif. Ces mouvements pourraient être conservés chez les β-lactamases de classe A et ainsi avoir un lien avec la catalyse enzymatique. Cette hypothèse est renforcée par les données RMN pour cTEM-17m, une chimère TEM-1/PSE-4, pour laquelle plusieurs résonances près du site actif sont non observées dû à un élargissement causé par ces mouvements lents.

Summary

Part I The analysis of spin relaxation data using the model-free formalism is a widely used approach to get insights into protein dynamics on the ps-ns and μs-ms timescales. In order to extract high quality data, multiple magnetic field datasets are required. Combining datasets recorded using different NMR magnets is prone to experimental errors. Hence, the consistency of multiple field spin relaxation data must be carefully verified. Analysis of multiple field spin relaxation data generally proceeds without verification of consistency, *i.e.* with only the assumption that data is fine. We propose a simple approach to verify the consistency of multiple field relaxation data. Using the proposed tests improves the analytical approach by reducing the presence of artifactual conformational exchange terms. Since these terms are often rationalised in relation with ligand binding or catalysis, improving their confidence yields a better understanding in terms of biology.

Part II Class A β-lactamases are involved in antibiotics resistance. They do so by hydrolysing the β-lactam antibiotics. These enzymes have been widely studied by different approaches including mutational studies, MD simulations, X-ray crystallography and NMR. The model enzyme for this class of proteins, TEM-1, has previously been studied by NMR in the laboratory. It was observed that TEM-1 is a highly ordered protein on the ps-ns timescale, with slower μs-ms motions clustered around the active site. In order to characterize further the backbone dynamics of class A β-lactamases, the homologous enzyme PSE-4 was studied by NMR using different approaches such as spin relaxation, CPMG relaxation dispersion, and amide exchange experiments. The same conclusions as for TEM-1 were obtained with a high rigidity along the sequence balanced by slower motions in the vicinity of the active site. These motions might be conserved in class A β-lactamases and potentially be important for catalysis. This hypothesis is further enforced by the backbone resonance assignments for cTEM-17m, a TEM-1/PSE-4 chimera, where many resonances are unobservable around the active site, potentially suffering from line broadening caused by slow motions.

Foreword

This thesis is presented in two parts. Part I discusses improvements to the analysis of spin relaxation data. Part II discusses the dynamics of class A β-lactamases (mostly PSE-4).

Publications

Most of this thesis has been published. The references to the corresponding publications are:

- Sébastien MORIN, Roger C. LEVESQUE & Stéphane M. GAGNÉ (2006) ^{1}H, ^{13}C and ^{15}N backbone resonance assignments for PSE-4, a 29.5 kDa class A β-lactamase from *Pseudomonas aeruginosa*. *Journal of Biomolecular NMR*, **36 Suppl. 1:** 11.
  → See Chapter 5 and [196].

- Sébastien MORIN & Stéphane M. GAGNÉ (2009) NMR dynamics of PSE-4 β-lactamase: An interplay of ps-ns order and *μ*s-ms motions in the active site. *Biophysical Journal*, **96:** 4681–4691.
  → See Chapter 7 (except Section 7.3.4) and [194].

- Sébastien MORIN & Stéphane M. GAGNÉ (2009) Simple tests for the validation of multiple field spin relaxation data. *Journal of Biomolecular NMR*, **45:** 361–372.
  → See Chapter 2 and [195].

- Sébastien MORIN, Christopher M. CLOUTHIER, Sophie GOBEIL, Joëlle N. PELLETIER & Stéphane M. GAGNÉ (In press) Backbone resonance assignments of a TEM-1/PSE-4 class A β-lactamase chimera. *Biomolecular NMR Assignments*.
  → See Chapter 8 and [193].

Manuscript in preparation

One last part is currently in preparation and will not be included in this thesis:

- Christopher M. CLOUTHIER, Sébastien MORIN, Sophie GOBEIL, Joëlle N. PELLETIER & Stéphane M. GAGNÉ (In preparation) Dynamics and function of the β-lactamase chimera cTEM-17m.

Contributions

Data presented in this thesis has been collected and analysed by me, Sébastien Morin, under the supervision of Pr. Stéphane M. Gagné. Additionally, all text (including publications) has been prepared by myself under the guidance of Stéphane.

One exception concerns the backbone chemical shifts assignment of the TEM-1/PSE-4 chimera cTEM-17m (see Chapter 8) and [193]). Indeed, as the list of authors of the article shows, there were other participants in this work. Both Christopher M. Clouthier (Université de Montréal) and I were considered as first author in this manuscript. Christopher performed a considerable amount of assignment and all kinetics experiments (for which Sophie Gobeil – Université de Montréal – also participated). My participation in this work thus consisted in approximately half the assignment as well as NMR data collection. Moreover, I participated in the preparation of the manuscript in writing most of the document. Finally, this work was supervised both by Pr. Stéphane M. Gagné and Pr. Joëlle N. Pelletier (Université de Montréal).

Permissions and Rights

Table of Contents

List of Tables

List of Figures

Abbreviations

aa	Amino acid
Å	Ångström (0.1 nm)
A	Alanine *or* Amplitude *or* Ampere
A_{280nm}	Absorbance at a wavelength of 280 nm
AIC	Akaike's information criteria [3]
AICc	Small sample size corrected AIC [120]
Ala	Alanine
Arg	Arginine
ASA	Accessible surface area
Asn	Asparagine
Asp	Aspartic acid (or Aspartate)
B	Static magnetic field vector
B_0	Static magnetic field strength
BIC	Schwarz or bayesian information criteria [245]
BLIP	β-lactamase inhibitor protein
BLIP-I	β-lactamase inhibitor protein I
BLIP-II	β-lactamase inhibitor protein II
BMRB	Biological Magnetic Resonance Bank (also known as BioMagResBank) http://www.bmrb.wisc.edu/ [269]
C	Cysteine *or* Carbon
C(τ)	Correlation function
χ^2	Chi-squared function
cal	Calorie (equivalent to 4.1868 J)
CPMG	Carr–Purcell–Meiboom–Gill [30, 183]
CSA	Chemical shift anisotropy
CSI	Chemical shift index
Cys	Cysteine

D	Aspartic acid (or Aspartate) *or* Deuterium (^{2}H)
δ	Chemical shift
$\Delta\varepsilon$	Molar extinction coefficient
ΔG_{HX}	Apparent stabilisation free energy of the structure protecting the N-H group from exchange
$\Delta\omega$	Chemical shift difference between states *A* and *B*
$\Delta\sigma$	Chemical shift anisotropy
$\mathfrak{D}_{\parallel}$	Spheroid diffusion tensor component of the principal axis
$\mathfrak{D}_{\perp}$	Spheroid diffusion tensor component of the perpendicular axis
$\mathfrak{D}_a$	Anisotropic component of diffusion
$\mathfrak{D}_{iso}$	Isotropic component of diffusion
$\mathfrak{D}_r$	Rhombic component of diffusion
$\mathfrak{D}_{ratio}$	$\mathfrak{D}_{\parallel}/\mathfrak{D}_{\perp}$
$\mathfrak{D}_x$	Diffusion constant for the *x* axis of diffusion
$\mathfrak{D}_y$	Diffusion constant for the *y* axis of diffusion
$\mathfrak{D}_z$	Diffusion constant for the *z* axis of diffusion
Da	Dalton (1/12 the mass of a ^{12}C atom, *i.e.* the mass of a hydrogen atom)
DSS	Sodium 2,2-dimethyl-2-silapentane-5-sulfonate
E	Glutamic acid (or Glutamate)
ESBL	Extended-spectrum β-lactamase
F	Phenylalanine
f_r	Rotational frictional drag coefficient for a sphere of radius *R*
FID	Free induction decay (*i.e.* the NMR signal)
G	Glycine
γ	Gyromagnetic ratio
Gln	Glutamine
Glu	Glutamic acid (or Glutamate)
Gly	Glycine
h	Planck's constant
$\bar{h}$	Planck's constant divided by 2π
h	Hour
H	Histidine *or* Hydrogen

η	Cross-correlation rate between the ^{15}N *CSA* and the ^{15}N-^{1}H dipolar interaction
η_{visc}	Viscosity
His	Histidine
HSQC	Heteronuclear single-quantum coherence
Hz	Hertz
I	Isoleucine
I	Nuclear spin angular momentum quantum number
Ile	Isoleucine
Inhibitor 105	N-[5-methyl-3-O-tolyl-isoxazole-4-carboxylic acid amide] boronic acid
Inhibitor BJH	1(R)-1-acetamido-2-(3-carboxy-2-hydroxyphenyl)ethyl boronic acid
Inhibitor BJI	1(R)-1-acetamido-2-(3-carboxyphenyl)ethyl boronic acid
Inhibitor BJP	(1R)-2-phenylacetamido-2-(3-carboxyphenyl)ethyl boronic acid
Inhibitor CB4	Pinacol[[2-amino-α-(1-carboxy-1-methylethoxyimino)-4-thiazoleacetyl] amino]methaneboronate
Inhibitor CBT	N,N-bis(4-chlorobenzyl)-1H-1,2,3,4-tetraazol-5-amine
Inhibitor CXB	[(2-amino-α-methoxyimino-4-thiazolylacetyl)amino]methylboronic acid
Inhibitor EPE	4-(2-hydroxyethyl)-1-piperazine ethanesulfonic acid
Inhibitor FOS	[[N-(benzyloxycarbonyl)amino]methyl]phosphate
Inhibitor FTA	3-(4-phenylamino-phenylamino)-2-(1H-tetrazol-5-yl)-acrylonitrile
Inhibitor NBF	[(2-ethoxy-1-naphthoyl)amino]methylboronic acid
Inhibitor SM2	(1R)-1-(2-thienylacetylamino)-1-(3-carboxyphenyl)methylboronic acid
IPTG	Isopropyl β-D-thiogalactoside
$^{1}J_{NH}$	One bond ^{15}N-^{1}H scalar coupling (also known as J-coupling)
J	Joule (equivalent to 0.2388459 cal)
$J(\omega)$	Spectral density function
K	Lysine *or* Kelvin
k_A	Exchange rate from state *A* to state *B*
k_B	Boltzmann constant *or* Exchange rate from state *B* to state *A*
k_{cat}	Catalytic turnover constant
k_{cat}/k_{inact}	Partition ratio for turnover and inhibition
k_{cat}/K_M	Catalytic efficiency
k_{close}	Closing rate of the structure protecting the N-H group from exchange
k_{ex}	Apparent exchange rate between states *A* and *B*

k_{HX}	Amide exchange rate
K_i	Inhibitor constant
	(concentration of inhibitor needed for half maximum inhibition)
k_{inact}	Rate of enzyme inhibition
k_{int}	Intrinsic rate of amide exchange (unprotected exchange rate)
K_M	Michaelis constant
k_{open}	Opening rate of the structure protecting the N-H group from exchange
L	Leucine
LC-MS	Liquid chromatography mass spectrometry
Leu	Leucine
Lys	Lysine
m	Meter
M	Methionine
μ_0	Permittivity of free space
*m*0 to *m*9	Local model-free models
MD	Molecular dynamics
Met	Methionine
MIC	Minimum inhibitory concentration
min	Minute
MM	Molecular mechanics
mol	Mole (6.0221415 x 10^{23} atoms or molecules, or N_A atoms or molecules)
MW	Molecular weight
N	Asparagine *or* Nitrogen
ν	Resonance frequency
N_A	Avogadro constant
	(also known as Avogadro's number, 6.0221415 x 10^{23} mol^{-1})
NCBI	National center for biotechnology information
	http://www.ncbi.nlm.nih.gov
ν_{CPMG}	CPMG pulse train frequency
NMR	Nuclear Magnetic Resonance
NOE	Nuclear Overhauser effect
NOE^{inc}	Inconsistent *NOE*
$\{^1H\}^{15}N$-*NOE*	Steady-state heteronuclear *NOE*

P	Proline
p_A	Population of state *A*
p_B	Population of state *B*
PBP	Penicillin-binding protein
PDB	Protein Data Bank http://www.pdb.org/pdb/home/home.do [15]
Penicillinate ALP	2-(1-carboxy-2-hydroxy-ethyl)-5,5-dimethyl-thiazolidine-4-carboxylic acid (also known as 6α-hydroxymethylpenicillanate)
pH	Measure of acidity and basicity of a solution
Phe	Phenylalanine
pK_a	Acid dissociation constant
ppm	Parts per million
Pro	Proline
Q	Glutamine
QM	Quantum mechanics
QM/MM	Quantum mechanics / molecular mechanics
r	Bond length
R	Arginine *or* Gas constant
R_1	Longitudinal (spin-lattice) relaxation rate
R_1^{inc}	Inconsistent R_1
R_2	Transverse (spin-spin) relaxation rate
$R_{2,A}$	R_2 of state *A*
$R_{2,B}$	R_2 of state *B*
R_2^{eff}	Effective R_2 (in the context of relaxation dispersion experiments)
R_2^{inc}	Inconsistent R_2
RDC	Residual dipolar coupling
R_{ex}	Chemical exchange relaxation rate
Ref-DB	Re-referenced Protein Chemical Shift Database http://redpoll.pharmacy.ualberta.ca/RefDB/stat.html [294]
RF	Radio frequency
RMSD	Root Mean Square Deviation
RT	Room temperature
s	Second

S^2, S_f^2, and S_s^2	Model-free generalised order parameters
SD	Standard deviation
SDS-PAGE	Sodium dodecyl sulfate polyacrylamide gel electrophoresis
SF	Slowing factor for amide exchange
S/N	Signal-to-noise ratio
σ_{NOE}	Cross-relaxation rate
T	Threonine *or* Tesla
τ	Correlation time
θ	Angle between the ^{15}N-^{1}H vector and the principal axis of the ^{15}N chemical shift tensor
θ_0	Cone semi-angle
T_1	Longitudinal (spin-lattice) relaxation time
T_2	Transverse (spin-spin) relaxation time
τ_c	Effective correlation time
τ_{CPMG}	Time between the 180° pulses in a CPMG train
τ_e, τ_f, and τ_s	Model-free effective internal correlation times
τ_m	Global rotational correlation time
τ_m^{app}	Estimated isotropic global correlation time
Thr	Threonine
*tm*0 to *tm*9	Local model-free models including a local correlation time
TROSY	Transverse relaxation-optimised NMR spectroscopy [220]
Trp	Tryptophane
Tyr	Tyrosine
V	Valine
Val	Valine
V_{max}	Maximum enzyme velocity extrapolated to maximum substrate concentrations
VT	Variable temperature
W	Tryptophane
w	Weight (in the context of an Equation)
Y	Tyrosine

Constants

Boltzmann constant	k_B	1.381 x 10^{-23} J K^{-1}
Gas constant	R	8.314472 J K^{-1} mol^{-1}
Magnetogyric ratio of ^{1}H	γ_H	26.7522 x 10^{7} $T^{-1}s^{-1}$
Magnetogyric ratio of ^{15}N	γ_N	-2.7126 x 10^{7} $T^{-1}s^{-1}$
Permittivity of free space	μ_0	4 π x 10^{-7} T m A^{-1} 4 π x 10^{-7} T^2 m^3 J^{-1}
Planck's constant	h $\bar{h} = h/2\pi$	6.626 x 10^{-34} J s 1.055 x 10^{-34} J s

Part I

Improved Analysis of NMR Dynamics

Chapter 1

Improved Analysis of NMR Dynamics: Introduction

1.1 Nuclear Magnetic Resonance

Nuclear magnetic resonance (NMR) spectroscopy is a powerful technique to obtain information at an atomic resolution on structural as well as on dynamical aspects of molecules. NMR can be divided in three principal areas: imaging, solid state, and liquid state NMR. Liquid state NMR, as its name says, probes samples in the liquid state (*i.e.* in an isotropic environment). This means that macromolecules are studied in solution, a significant advantage in terms of physiological relevance compared to methods employing the crystalline form (*e.g.* X-ray crystallography).

NMR is made possible by an intrinsic property of atomic nuclei termed nuclear spin. In some circumstances, *i.e.* when the nuclear spin angular momentum quantum number I has a non zero value, the spin behaves as a dipole and can thus interact with a magnetic field. This property is at the base of NMR techniques. In protein studies, isotopic labelling is generally performed in order to obtain both observable nuclei (*i.e.* with non null I) and absence of quadrupolar effects (*i.e.* with $I < 1$, since quadrupolar nuclei with $I \geq 1$ give rise to phenomenona far more complex to analyse), hence with $I = 1/2$. As shown in Table 1.1, the ^{1}H, ^{13}C, and ^{15}N nuclei are preferred, although the ^{2}H (or D) nucleus is also used in some circumstances.

Table 1.1: Spin properties of different nuclei.†

Nucleus	I	γ ($T^{-1}s^{-1}$)	Natural abundance (%)	Relative sensitivity ‡	ν^{*} for $B_0 = 14.1$ T (MHz)
^{1}H	1/2	26.752 x 10^{7}	99.985	1.000	600
^{2}H	1	4.107 x 10^{7}	0.015	0.009	92
^{12}C	0		98.9		
^{13}C	1/2	6.728 x 10^{7}	1.1	0.016	150
^{14}N	1	1.934 x 10^{7}	99.63	0.001	43
^{15}N	1/2	-2.713 x 10^{7}	0.37	0.001	60

† Values from Cavanagh *et al.* [35] and http://www.eclipse.net/ñumare/nsinmrpt.htm.

‡ Compared to sensitivity of ^{1}H nucleus and considering an equal number of spins (*i.e.* assuming an abundance of 100 %).

* Calculated from $\nu = (\gamma B_0)/2\pi$ with γ as the gyromagnetic ratio for the observed nuclear spin, and B_0 as the strength of the static magnetic field **B**.

1.2 Dynamics in Macromolecules

Despite the apparent lack of plasticity implicit in the 2D display of 3D structures of macromolecules, they in fact undergo dynamics on many different timescales separated by many orders of magnitude. Figure 1.1 displays some of the dynamic processes present in proteins. Fast motions include bond vibration and libration. Side-chain rotations, when not constrained sterically, are a few orders of magnitude slower, on timescales similar to that of global tumbling (macromolecular Brownian rotational diffusion). Slower dynamics, on timescales spanning many orders of magnitude towards 'human' timescales (s, min, etc), include such processes as folding/unfolding, ligand binding, allosteric regulation, and catalysis.

Many different techniques offer insights into protein dynamics: X-ray and neutron scattering (reviewed in [90]), mass spectrometry (either hydrogen exchange or charge state distributions in electrospray mass spectra, reviewed in [74]), time-resolved X-ray crystallography (reviewed in [192]), time-resolved fluorescence (reviewed in [243]), molecular dynamics (MD, reviewed in [134]), and NMR (reviewed in [211]).

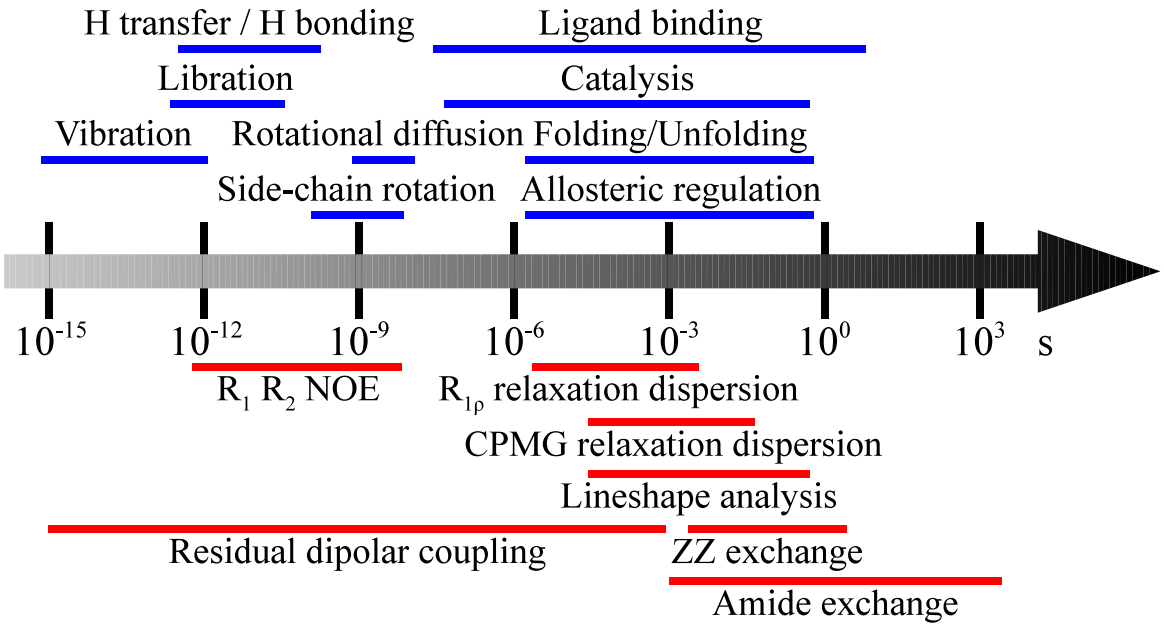

Figure 1.1: Timescales of protein dynamics (top and blue) as well as timescales probed by NMR experiments (bottom and red). Adapted from Palmer [211] with permission from the American Chemical Society.

1.3 Studying the Dynamics of Proteins with NMR

One of the most useful applications of NMR lies in the study of dynamics. Indeed, NMR is one of the most powerful tools available for the study of protein dynamics. It allows atom specific data to be gathered for movements as fast as side-chain rotations or hydrogen bond formation, and as slow as protein folding. Figure 1.1 shows some of the experiments available to probe the different timescales from fs (10^{-15} s) to Ms (10^{6} s, $\sim$ 12 days). These include RDC, relaxation dispersion (both $R_{1\rho}$ and CPMG), amide exchange, lineshape analysis, ZZ exchange, and spin relaxation experiments (reviewed in [4, 16, 71, 126, 127, 136, 137, 143, 210, 211, 213, 267, 275]).

Studying motions of N-H bonds provides a specific probe for almost all residues (except prolines and the N-terminal residue). Because degrees of freedom in the protein chain are introduced by the ϕ and ψ dihedral angles, N-H (and C=O) bond motions report on motions of the peptide plane (discussed in [23]). This thus allows characterisation of motions of the entire protein backbone. Hence, this approach is often used to characterise the dynamics of a protein. Most experiments mentioned above can allow characterisation of motions of the N-H bond vectors on different timescales. The spin relaxation rates depend mainly on the N-H bond reorientations with respect to the external magnetic field as a function of time [6] allowing the study of the information-rich ps-ns and μs-ms timescales. It is known that motions arising on the ps-ns timescale influence the thermodynamics of ligand binding, as well as the kinetics of catalysed reactions (reviewed in [273]). Indeed, changes in free energy of binding, heat capacity or conformational entropy (*i.e.* changes affecting thermodynamics) can arise from contributions of ps-ns motions [5, 162, 289, 290]. Moreover, motions on the μs-ms timescale share the same timescale as enzyme catalysis and can thus be linked to these processes [293].

1.3.1 Spin Relaxation

Spin relaxation experiments generally include three different types of measurements: longitudinal relaxation, transverse relaxation, and steady-state heteronuclear *NOE*. The magnetic field dependence of these spin relaxation parameters [1] allows quantification of both global and local dynamics within a molecular system. It is the preferred approach for studying dynamics in proteins and will be detailed below.

1.3.1.1 Longitudinal Relaxation

Longitudinal relaxation (also known as R_1, spin-lattice relaxation, or, in the case of ^{15}N relaxation, ^{15}N-R_1 or $R_N(N_z)$, see Equation 1.1 below) defines the rate with which the magnetisation, after being perturbed (*e.g.* by a RF pulse), returns to equilibrium along the direction of the static magnetic field **B**. This equilibrium is defined by the Boltzmann distribution and is caused by a coupling of spins with their environment, hence the name of spin-lattice relaxation. In other words, R_1 is the return rate of magnetisation parallel to a magnetic field and is defined as follows [1]:

$$R_1 = d\,[J(\omega_H - \omega_N) + 3J(\omega_N) + 6J(\omega_H + \omega_N)] + c\,J(\omega_N) \tag{1.1}$$

where d, the dipolar constant, is defined as:

$$d = \frac{1}{4}\left(\frac{\mu_0}{4\pi}\right)^2 \frac{(\bar{h}\,\gamma_N\,\gamma_H)^2}{r_{N\text{-}H}^6} \tag{1.2}$$

the chemical shift anisotropy (*CSA*) constant is:

$$c = \frac{(\omega_N\,\Delta\sigma)^2}{3} \tag{1.3}$$

$J(\omega)$ are values of the spectral density at different frequencies (ω), μ_0 is the permittivity of free space, $\bar{h}$ is Planck's constant divided by 2π, γ_N, and γ_H are the gyromagnetic ratios of ^{15}N and ^{1}H, respectively, the Larmor frequency of ^{15}N is:

$$\omega_N = 2\pi\,\nu_N = \gamma_N\,B_0 \tag{1.4}$$

$r_{N\text{-}H}$ is the vibrationally averaged effective N-H bond length, and $\Delta\sigma$ is the *CSA*. R_1 depends on the Larmor frequency ω and effective correlation time τ_c as shown in Figure 1.2. Historically, the reciprocal of R_1, the longitudinal relaxation time, has been used

preferentially. T_1 and R_1 are related as follows: $T_1 = 1/R_1$.

The recording of R_1 data for proteins generally proceeds through an inversion-recovery approach (discussed in [161]) implemented in a HSQC [138] pulse sequence. Figure 1.3 shows the behaviour of magnetisation in such an experiment (neglecting magnetisation transfers to the ^{15}N nucleus and evolution in the indirect dimension, hence for a simple 1D case). The experiment starts with a 180° pulse in order to get the magnetisation along -*z*. Then, after a delay, a 90° pulse brings the magnetisation into the *xy* plane for acquisition. Varying the delay between the two pulses affects the magnetisation amplitude which varies from negative to positive values under the following relation [35]:

$$A_t = A_0 \left(1 - 2e^{-R_1 t}\right) \tag{1.5}$$

where A_t is the amplitude after a delay t and A_0 the amplitude at time 0.

In the case of an R_1 experiment implemented in a 2D ^{15}N-HSQC [138] pulse sequence (*i.e.* the approach generally used for quantification of protein dynamics), the decay by longitudinal relaxation follows an exponential decay such as [35]:

$$A_t = A_0 \, e^{-R_1 t} \tag{1.6}$$

Hence, in this case, the longer the delay, the more relaxation, and the less signal at the end of the experiment.

Apart from its use in the characterisation of dynamics, R_1 has an important impact on the recording of NMR data. Indeed, R_1 defines the recovery of magnetisation on the *z* axis and, thus, the total magnetisation available at the start of the experiment. If a too high repetition rate is used for NMR signal averaging, then lower signal is obtained as a result of incomplete recovery of magnetisation. However, if a too low repetition rate is used, a lower sensitivity is obtained as a result of lower signal averaging. The Ernst angle defines the relation between the repetition rate and R_1 [35]. From this relation, near complete recovery of magnetisation will result after a delay of 3 T_1, although to maximise sensitivity per unit time, in most experiments repetition rate is adjusted to between 1 and 1.5 T_1 because a majority of the

relaxation has occurred by this time.

1.3.1.2 Transverse Relaxation

Transverse relaxation (also known as R_2, spin-spin relaxation, or, in the case of ^{15}N relaxation, ^{15}N-R_2 or $R_N(N_{x,y})$, see Equations 1.7 and 1.8 below) defines the rate with which the magnetisation, after being perturbed (*e.g.* by a RF pulse), decays in the plane perpendicular to the direction of the static magnetic field **B**. This phenomenon happens through energy exchange between spins as they precess around **B**, *i.e.* the magnetisation decays in the *xy* plane while rotating around the *z* axis. Jointly with longitudinal relaxation (the buildup of magnetisation on the *z* axis after perturbation, see above), the magnetisation can be seen as rotating around the *z* axis (along **B**) on the surface of a sphere from the equator to the pole. However, what causes transverse relaxation is not precession around **B** itself, but instead loss of coherence resulting from local magnetic field fluctuations affecting the Larmor frequency of individual spins. In other words, after a perturbing RF pulse which creates coherence among the spins, these spins evolve independently and coherence is gradually lost, a phenomenon called transverse relaxation. R_2 is defined from R_2^0, the pure transverse relaxation rate (not influenced by processes on the μs-ms timescale), as follows [1]:

$$R_2^0 = \frac{d}{2}\left[4J(0) + J(\omega_H - \omega_N) + 3J(\omega_N) + 6J(\omega_H) + 6J(\omega_H + \omega_N)\right] + \frac{c}{6}\left[4J(0) + 3J(\omega_N)\right] \tag{1.7}$$

and

$$R_2 = R_2^0 + R_{ex} \tag{1.8}$$

where R_{ex} is the contribution to R_2 accounting for slow processes occurring on the μs-ms timescale. Generally, R_2 is measured, although means of recording R_2^0 (*i.e.* R_{ex}-free R_2) have been proposed recently [109]. R_2 also depends on the Larmor frequency ω and effective correlation time τ_c as shown in Figure 1.2. Similarly to R_1, the reciprocal of R_2, known as

the transverse relaxation time, has been used in former documentation such that $T_2 = 1/R_2$.

The recording of R_2 data for amide groups in proteins generally proceeds through a spin echo [105] approach implemented in a HSQC [138] pulse sequence. Figure 1.3 shows the behaviour of magnetisation in such an experiment (neglecting magnetisation transfers to the ^{15}N nucleus and evolution in the indirect dimension, hence for a simple 1D case). The experiment starts with a 90° pulse in order to get the magnetisation in the *xy* plane. After a delay, a 180° pulse inverses the magnetisation which is allowed to evolve for a further delay (of length equal to the first delay). This way, an echo is created where signals from different chemical shifts (*i.e.* different angular frequencies) are refocused to the same position (such that coherence is recovered). Recording proceeds right after the second delay. It is during these two delays that transverse relaxation processes are active. Hence, varying the length of relaxation delays will affect signal amplitude and, in turn, allow quantification of R_2 (extracted using Equation 1.6).

Apart from its use in dynamics studies, R_2 also has an important effect on NMR line shapes. Indeed, the higher R_2, the shorter it takes for loss of magnetisation on the *xy* plane. A faster loss of magnetisation in the detection plane then means a shorter-lived FID which, after Fourier transform, yields a broader peak. On the other hand, a resonance with a small R_2 possesses a slowly decaying FID, yielding a sharper line and a higher S/N ratio.

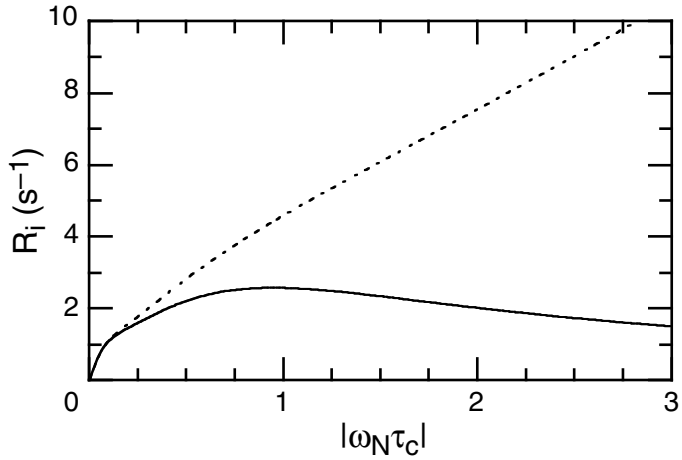

Figure 1.2: Dependence of ^{15}N-R_1 (solid line) and ^{15}N-R_2 (dashed line) on nitrogen Larmor frequency ω_N and effective correlation time τ_c. In this case, ω_N was calculated with $B_0 = 11.74$ T. The figure is a generous gift from Arthur G. Palmer. It is from [35] and is used with permission from Elsevier.

1.3.1.3 Steady-State Heteronuclear Nuclear Overhauser Effect

The steady-state heteronuclear nuclear Overhauser effect (in the case of ^{15}N relaxation, also known as $\{^1\text{H}\}^{15}\text{N}$-*NOE* or $R_N(H_z^N \rightarrow N_z)$, see Equation 1.9 below) corresponds to cross-relaxation between two dipolar-coupled spins (in this case, ^{1}H and ^{15}N) [35]. It is defined by the following Equation:

$$NOE = 1 + \frac{\gamma_H}{\gamma_N}\frac{d}{R_1}\left[6J(\omega_H + \omega_N) - J(\omega_H - \omega_N)\right] \tag{1.9}$$

and is thus dependent on the distance between the two spins (through a modulation of d) and on the relative gyromagnetic ratios of these spins.

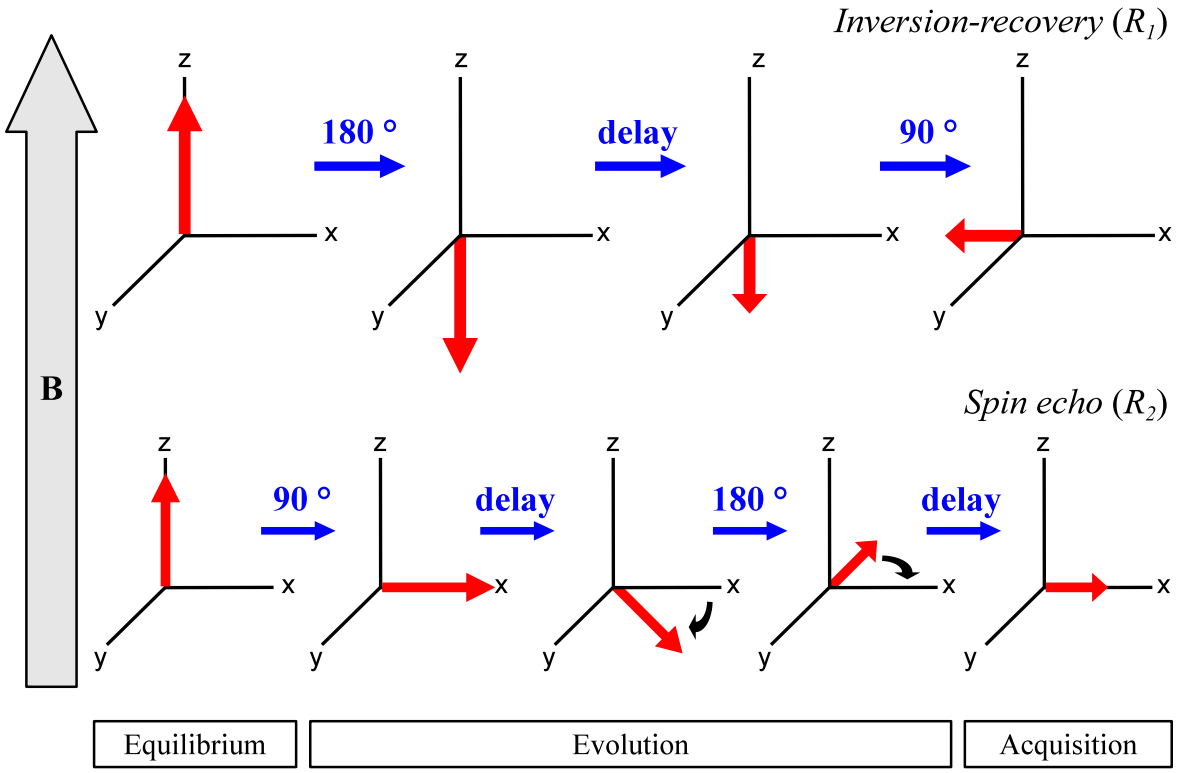

Figure 1.3: Experimental approaches to the recording of R_1 (inversion-recovery) and R_2 (spin echo). Bulk magnetisation is shown as a red arrow while the different pulses or delays are coloured blue. Varying the delays allows the recording of exponential decays for relaxation rate measurements. This figure does not take into account other details than longitudinal and transverse relaxation.

Acquisition of steady-state *NOE* data generally proceeds through the recording of two different spectra: with and without proton presaturation. Saturating the ^{1}H spin with a sufficiently long weak RF field (weak enough not to perturb the ^{15}N spin) has the effect of equalizing populations for this spin. This causes the magnetisation of the ^{15}N spin to evolve to a steady-state. Experimentally, the *NOE* is measured as the ratio of peak amplitudes in both situations (with and without proton saturation) such as:

$$NOE = \frac{A_{sat}}{A_{eq}} \tag{1.10}$$

where A denotes the peak amplitude with (A_{sat}) and without (A_{eq}) proton saturation.

1.3.1.4 Linking R_1, R_2, and *NOE* Data to Molecular Motions

As mentioned earlier, R_1, R_2, and *NOE* data are used to characterise molecular motions. This is made possible by the fact that relaxation phenomenona are non spontaneous and depend on the presence of motions. Indeed, Equations 1.1, 1.7, and 1.9 show that these observables are in fact dependent on motions on different discrete timescales. These motions are quantified by the spectral densities and, for ^{15}N-R_1, ^{15}N-R_2, and $\{^{1}\text{H}\}^{15}$N-*NOE* data, depend on the following frequencies: 0, ω_N, $\omega_H + \omega_N$, ω_H, and $\omega_H - \omega_N$. In other words, motions influencing relaxation are stochastic motions on timescales that are different combinations of the Larmor frequencies of the involved spins. Hence, spin relaxation rates and spectral densities are indissociable.

1.3.2 Reduced Spectral Density Mapping

The link between spin relaxation data and actual bond vector motions is quite complex and non trivial. Several means of analysis have been proposed to relate spin relaxation data to the spectral density function which is a description of the frequency spectrum of the stochastic processes experienced by a given bond vector.

1.3.2.1 Theory

The most simple technique for spin relaxation data analysis, beyond raw data interpretation, is known as spectral density mapping. Spectral density mapping does not introduce a possible bias related to physical models for interpretation of internal and global motions [75]. Indeed, no assumption is made on the shape of the spectral density $J(\omega)$ using this method [218], contrary to, for example, the model-free approach (see below) [167, 168] where the spectral density is assumed to possess a Lorentzian shape.

Complete spectral density mapping allows the extraction of the proton-proton dipolar relaxation rate ($\rho_{H^N\text{-}H^i}$, a relaxation phenomenon caused by surrounding protons H^i) and of the spectral densities at the five different frequencies ($J(0)$, $J(\omega_N)$, $J(\omega_H+\omega_N)$, $J(\omega_H)$ and $J(\omega_H-\omega_N)$) [218]. However, this requires the recording of six different relaxation rates (namely ^{15}N-R_1; ^{15}N-R_2; $\{^1\text{H}\}^{15}$N-*NOE*; $R_H(H_z^N)$ or ^{1}H-R_1; $R_{N\text{-}H}(2H_z^N N_z)$, the longitudinal two-spin order relaxation rate; and $R_{N\text{-}H}(2H_z^N N_{x,y})$, the antiphase ^{15}N single quantum coherence relaxation rate) in order to solve this system of six equations. The dependence of some of these rates (namely $R_H(H_z^N)$, $R_{N\text{-}H}(2H_z^N N_z)$ and $R_{N\text{-}H}(2H_z^N N_{x,y})$) on proton-proton dipolar relaxation makes them difficult to characterise [160]. This is because experiments to measure these rates can lead to non mono-exponential decays from which relaxation rates are difficult to extract with precision.

A simplified approach to the complete spectral density mapping is that of reduced spectral density mapping [160]. This is done by assuming that the spectral density does not vary much at higher frequencies, hence the possibility to equate the three spectral densities at higher frequency and centered around $J(\omega_H)$ (*i.e.* $J(\omega_H+\omega_N)$, $J(\omega_H)$, and $J(\omega_H-\omega_N)$) to a single one, namely $\langle J(\omega_H)\rangle$, the spectral density at the effective proton frequency. This corresponds to $J(0.87\omega_H)$ as described in Farrow *et al.* [75].

Thus, reduced spectral density mapping consists in determining the spectral density at three frequencies: at the zero frequency $J(0)$, at the nitrogen frequency $J(\omega_N)$, and at the effective proton frequency $\langle J(\omega_H)\rangle$ (which approximates $J(\omega_H+\omega_N)$, $J(\omega_H)$, and $J(\omega_H-\omega_N)$). These assumptions about the form of the spectral density are minimal and, because less equations are involved, less data need to be recorded. An obvious strategy is to measure only relaxation rates not influenced by proton-proton dipolar interaction, *i.e.* ^{15}N-R_1, ^{15}N-R_2, and $\{^1\text{H}\}^{15}$N-*NOE*. Equations 1.11, 1.12 and 1.13 show the dependence of the three reduced spectral densities on the measured variables R_1, R_2, and *NOE* [75, 160]:

$$J(0) = \frac{-1.5}{3d+c}\left(\frac{R_1}{2} - R_2 + 0.6\,\sigma_{NOE}\right) \tag{1.11}$$

$$J(\omega_N) = \frac{1}{3d+c}\left(R_1 - 1.4\,\sigma_{NOE}\right) \tag{1.12}$$

$$\langle J(\omega_H)\rangle = \frac{\sigma_{NOE}}{5d} \tag{1.13}$$

where the cross-relaxation rate, σ_{NOE}, is defined from both the NOE and R_1:

$$\sigma_{NOE} \;=\; (NOE - 1)\,R_1\,\frac{\gamma_N}{\gamma_H} \tag{1.14}$$

1.3.2.2 Analysis

Analysis of reduced spectral density mapping is in some ways more straightforward than analysis of raw data. However, the approach does not give rise to parameters with a clear physical meaning such as in the model-free formalism (see further below). Hence, the approach has never reached a widespread use as is the case for the model-free formalism.

Reduced spectral density mapping can serve to discriminate between motions either faster, slower or on a similar timescale than the global tumbling. Indeed, as proposed by Křížová *et al.* [154], a simple approach to analysis of reduced spectral density mapping consists in plotting either $J(\omega_N)$ or $\langle J(\omega_H)\rangle$ as a function of $J(0)$ and, then, comparing the distribution to theoretical functions. These functions describe the simple case of a single motion defined by a single Lorentzian (where $J(0) = 0.4\,\tau_m$, with τ_m as the global rotational correlation time) and are defined by:

$$J(\omega_N) = \frac{J(0)}{1+6.25(\omega_N\, J(0))^2} \tag{1.15}$$

$$\langle J(\omega_H)\rangle = \frac{J(0)}{1+6.25(\omega_H\, J(0))^2} \tag{1.16}$$

Graphical analysis of the data is performed such as in Figure 1.4. This allows qualitative separation of different residues, for example, as highly flexible on the fast ps-ns timescale, principally affected by global diffusion or involved in conformational exchange (slow μs-ms motions). Additionally, this approach allows the comparison of data acquired at different temperatures or in the presence and absence of a ligand.

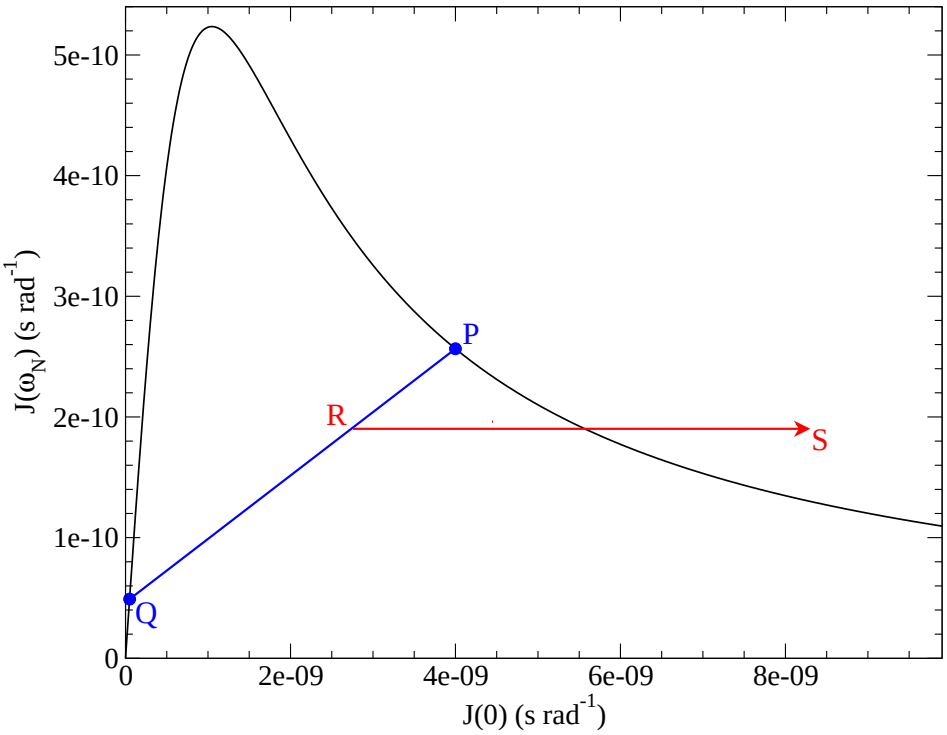

Figure 1.4: Graphical analysis of reduced spectral density mapping. The curve was generated from Equation 1.15. Points P and Q represent, respectively, motions on the global tumbling timescale (here for $\tau_m = 10$ ns, with point P at 0.4 $\tau_m = 4$ ns) and on a much faster internal correlation time (here $\tau_i = 125$ ps, with point Q at 0.4 $\tau_i = 50$ ps). In general, most relaxation data should be clustered between points P and Q (around the blue line), such as point R. However, when slow μs-ms motions are present, the data point is shifted to higher $J(0)$ values (in the direction of point S at the end of the red arrow). Adapted from Křížová *et al.* [154] with kind permission from Springer Science+Business Media.

1.3.3 Model-Free Formalism

The model-free formalism [40, 51, 167, 168] is the preferred approach for spin relaxation data analysis. It allows the extraction of parameters with physical meanings rather more concrete than the relaxation data themselves. Using this formalism, two main parameters, S^2 and τ, account respectively for the restriction of the motion for one vector (*e.g.* the N-H bond) and the effective timescale of this motion (a value influenced and normalised by S^2). Moreover, the R_{ex} parameter can account for slow motions on the μs-ms timescale contributing to the observed R_2 (see Equation 1.8). Usually, spin relaxation data is analysed by fitting 'model-free' functional forms of spectral density. In the model-free formalism [40, 51, 167, 168], functions are introduced containing a limited number of parameters, thus allowing one to get insights into the motions causing spin relaxation. The model-free formalism is preferred compared to reduced spectral density mapping, as more information can be obtained (at the price of more assumptions concerning the form of the spectral density). Hence, because of its easier interpretation, the model-free formalism is the most popular approach for spin relaxation data analysis.

1.3.3.1 Theory

The model-free formalism was introduced by Lipari and Szabo [167, 168] and further extended by Clore *et al.* [40], and d'Auvergne and Gooley [51]. Its main theorem is that internal motions can be decoupled from the global tumbling of the molecule. A correlation function, which forms a Fourier pair with the spectral density, is used to define and decouple global and internal motions. This correlation function is thus the product of the correlation function of Brownian rotational diffusion (global tumbling) and the correlation function of internal dynamics (*e.g.* N-H bond motions) [167]:

$$C(\tau) = C_O(\tau) \cdot C_I(\tau) \tag{1.17}$$

where $C(\tau)$ denotes a correlation function and the subscripts O and I stand for overall tumbling and internal motions, respectively.

This approach allows the description, with simple parameters, of the correlation function of internal dynamics independently of the overall tumbling with [39, 40, 47]:

$$C_O(\tau) = \frac{1}{5} \sum_{i=-k}^{k} w_i \cdot e^{-\tau/\tau_i} \tag{1.18}$$

and

$$C_I(\tau) = S^2 + (1 - S_f^2)e^{-\tau/\tau_f} + (S_f^2 - S^2)e^{-\tau/\tau_s} \tag{1.19}$$

where w defines a weight, τ defines a correlation time, and index i ranges over the number of exponential terms in the correlation function (*i.e.* from -k to k). In the simplest case of isotropic tumbling (also known as spherical diffusion), $k = 0$ (hence $i = 0$) and τ_i is replaced by a single term, τ_m, defined as the global correlation time and closely related to the isotropic component of diffusion $\mathfrak{D}_{iso}$ by [18]:

$$\frac{1}{\tau_m} = 6\,\mathfrak{D}_{iso} \tag{1.20}$$

At the opposite of spherical diffusion lies anisotropic diffusion (also known as the diffusion of an ellipsoid), where $k = 2$ (hence index i has five possible values and ranges from -2 to 2). When the ellipsoid diffuses with an axial symmetry, a spheroid diffusion tensor is defined (where $k = 1$ and i has three values ranging from -1 to 1). This spheroid is either prolate or oblate, depending on its shape (see Figure 1.5). For an extensive discussion on the topic of overall correlation functions in the context of model-free analysis, the reader is further directed to Edward J. d'Auvergne's Ph.D. thesis [47].

Using different combinations of internal parameters (S^2 and τ) in Equation 1.19 of local correlation, local model-free models are created [39, 40, 49, 51, 52, 87, 147, 167, 168, 206, 295]:

$$
\begin{aligned}
&m0 : \{\} \\
&m1 : \{S^2\} \\
&m2 : \{S^2, \tau_e\} \\
&m3 : \{S^2, R_{ex}\} \\
&m4 : \{S^2, \tau_e, R_{ex}\} \\
&m5 : \{S^2, S_f^2, \tau_s\} \\
&m6 : \{S^2, \tau_f, S_f^2, \tau_s\} \\
&m7 : \{S^2, S_f^2, \tau_s, R_{ex}\} \\
&m8 : \{S^2, \tau_f, S_f^2, \tau_s, R_{ex}\} \\
&m9 : \{R_{ex}\}
\end{aligned}
\tag{1.21}
$$

where S^2 is the square of the generalised order parameter [167], τ is the effective timescale of the motion characterised by S^2, and subscript e refers to the local motion characterised in models $m2$ and $m4$ whereas subscripts s and f refer to the slow (ns) and the fast (ps) motions (as compared to the global tumbling) characterised in models $m5$ to $m8$. The effective order

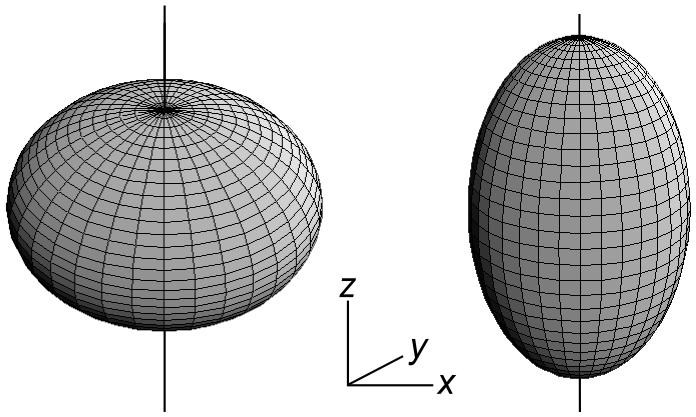

Figure 1.5: Axially symmetric diffusion tensors. The oblate (left) and prolate (right) diffusion tensors are shown as well as their axis of symmetry and a reference frame. The oblate spheroid has a component of diffusion in the z axis smaller than in both the x and y axes. The situation is reversed in the prolate spheroid. The ellipsoid diffusion tensor does not include an axis of symmetry along z (hence the components in x and y are different). In the sphere, the situation is reversed where components in the three directions (x, y, and z) are equal. The figure is adapted from Wikipedia (http://en.wikipedia.org/wiki/Spheroid).

parameter is a combination of order parameters for different timescales:

$$S^2 = S_f^2 \cdot S_s^2 \tag{1.22}$$

and is limited physically to values between 0 (unrestricted isotropic motion) and 1 (completely restricted, absence of motion). As stated by Lipari and Szabo [167], the S^2 parameter can be rationalised in terms of a semi-angle θ_0 within a cone as shown in Figure 1.6 from the following Equation:

$$S_{cone}^2 = \left[\frac{1}{2}\cos\theta_0(1+\cos\theta_0)\right]^2 \tag{1.23}$$

For parameter sets of models *m*0 to *m*9, the absence of a parameter means this parameter has a null value, *i.e.* either $S^2 = 1$, $\tau = 0$ or $R_{ex} = 0$. Moreover, even though parameter R_{ex} does not appear in Equation 1.19, it is used in the model-free formalism to compensate for the discrepancy caused between experimental and back-calculated R_2 values in cases where

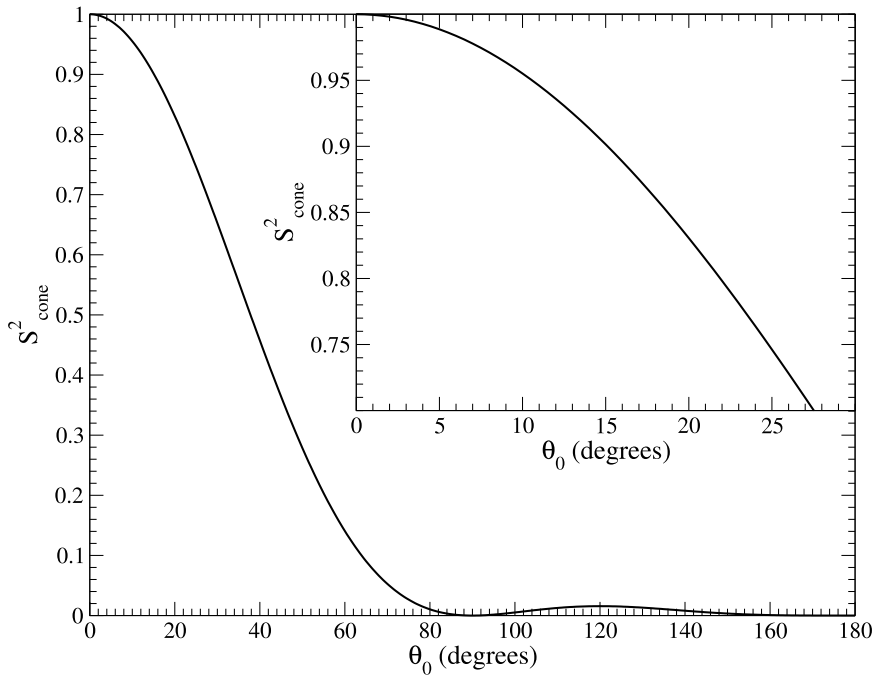

Figure 1.6: S^2 parameter as a function of cone semi-angle θ_0, calculated using Equation 1.23. The inset zooms to values around 0.85, the typical value for secondary structure elements.

slow μs-ms motions are present. In the model-free formalism, R_{ex} is assumed to be caused by motions in the fast exchange limit and is thus scaled quadratically with the magnetic field [125]. Finally, models $m9$ and $m0$ are both limit situations where a residue respectively has its relaxation dominated by conformational exchange ($m9$), or displays very limited local motions ($m0$).

By assuming a Lorentzian form of the spectral density, a model-free spectral density function can be derived from these correlation functions [47]:

$$J(\omega) = \frac{2}{5} \sum_{i=-k}^{k} w_i \cdot \tau_i \left(\frac{S^2}{1+(\omega\,\tau_i)^2} + \frac{(1-S_f^2)(\tau_f+\tau_i)\,\tau_f}{(\tau_f+\tau_i)^2+(\omega\,\tau_f\,\tau_i)^2} + \frac{(S_f^2-S^2)(\tau_s+\tau_i)\,\tau_s}{(\tau_s+\tau_i)^2+(\omega\,\tau_s\,\tau_i)^2} \right) \tag{1.24}$$

In the case of isotropic global diffusion (where $i = 0$, τ_i adopts a single value with $\tau_i = \tau_m$, and the weight w equals 1, as stated before), the function reduces to the following [51]:

$$J(\omega) = \frac{2}{5} \tau_m \left(\frac{S^2}{1+(\omega\,\tau_m)^2} + \frac{(1-S_f^2)(\tau_f+\tau_m)\,\tau_f}{(\tau_f+\tau_m)^2+(\omega\,\tau_f\,\tau_m)^2} + \frac{(S_f^2-S^2)(\tau_s+\tau_m)\,\tau_s}{(\tau_s+\tau_m)^2+(\omega\,\tau_s\,\tau_m)^2} \right) \tag{1.25}$$

Relating the correlation functions to the spectral density is possible since, as discussed before, the spectral density and correlation functions form a Fourier pair. Hence, applying a Fourier transform to the combined correlation functions (overall and internal) yields the above model-free spectral density from which R_1, R_2 and NOE (see Equations 1.1, 1.7, and 1.9) can be back-calculated. This is how model-free minimisation proceeds.

1.3.3.2 Minimisation

Algorithm

Until recently, most studies using the model-free formalism minimised data for local

model-free models by first defining a diffusion tensor externally to the model-free formalism. The process is known as the diffusion-seeded model-free optimisation and goes as follows:

1. The diffusion tensor is defined externally, generally using the R_2/R_1 ratio for vectors judged to be deprived from μs-ms motions [139, 217].
2. The local model-free models are optimised separately.
3. The best local model-free model is chosen for each vector.
4. The diffusion tensor is optimised with the chosen local model-free models.
5. Steps 2-4 are performed iteratively until convergence of all parameters.

This approach was used for several years but was recently shown to have some shortcomings and often yield incorrect characterisation of diffusion and, in turn, potentially incorrect characterisation of local dynamics. Indeed, d'Auvergne and Gooley proposed a new approach where the algorithm is as follows [52]:

1. Local model-free models including a local correlation time (local τ_m, *i.e.* an effective global correlation time for each vector, all of which are independent) are minimised. These models correspond to models *m*0 to *m*9 to which a local τ_m parameter is added and are named *tm*0 to *tm*9.
2. Model selection of these local model-free models with local τ_m proceeds.
3. The local parameters are used for separate optimisation of different diffusion tensors (sphere, oblate, prolate, and ellipsoid). For this purpose, the local τ_m is first removed from the sets of local model-free parameters (*i.e.* models *tm*0–*tm*9 reduce to *m*0–*m*9, respectively) and parameters for the diffusion tensor are determined.
4. Local model-free models (now without local τ_m, but with the diffusion tensor optimised in step 3) are minimised.
5. Model selection is performed for choosing the best local model.
6. The diffusion tensor is optimised with the chosen local parameters.

7. Steps 4-6 are performed iteratively until convergence of all parameters.

8. Model selection is performed in order to chose the optimised parameter set from the best diffusion tensor.

Model selection

There are several possible models both for overall (local τ_m, sphere, oblate, prolate, and ellipsoid) and local (models $m0$ to $m9$) description of dynamics. This means that a process called model selection needs to be applied in order to chose from the different diffusion tensors and local model-free models.

Model-free minimisation proceeds by minimising the discrepancy between the actual experimental data and the values back-calculated with the chosen parameters in the model-free equations. Generally, a function for measuring the goodness of fit between the experimental (R) and back-calculated data (R') is used such as:

$$\chi^2 = \sum_{j=1}^{n} \left[\frac{(R_j - R'_j)^2}{\sigma_j^2} \right] \tag{1.26}$$

where σ is the experimental error and j is the residue number. From this function, the best model is then chosen using a function such as the Akaike Information Criteria (*AIC*) [3]:

$$AIC = \chi^2 + 2k \tag{1.27}$$

where k is the number of parameters in a given model. This normalisation of the number of parameters in the model allows a comparison of different models in order to reach parsimony, *i.e.* choosing the simplest model which fits data well [25]. This process is also known as Occam's razor, the equilibrium between bias and variance.

Historically, approaches using *F-test* statistics (discussed in [57]) have been widely used for model selection in the context of model-free analysis such as proposed by Mandel *et al.* [174]. However, it is suggested to use frequentist methods such as *AIC* instead [48]. Moreover, it is

even best to perform model elimination [49] prior to model selection. In this additional step of model elimination, models with aberrant parameter values are excluded and not tested for model selection. This prevents the choice of models with low χ^2 and *AIC* values, although with aberrant parameters such as, for example, a local correlation time τ_e longer than the global tumbling time τ_m.

Programs for model-free calculations

Several programs have been developed for the optimisation of the model-free parameters. These include *ModelFree* [174, 214], *DASHA* [205], *Tensor2* [17, 45, 60, 268], *DYNAMICS* [87], the suite of *Mathematica* (Wolfram Research, Champaign, IL) notebooks by Leo Spyracopoulos [251], as well as several in-house programs [56, 76, 171]. Recently, an open source program coded in Python called *relax* [51, 52] has become the most advanced tool for model-free analysis of spin relaxation data. This program provides, among other things, high precision optimisation, model-free model elimination before model selection (avoiding the selection of models with non physical parameter values) [49], different model selection methods (AIC [3], AICc [120], BIC [245]), different optimisation algorithms (through the use of the minfx optimization library), and fully anisotropic diffusion tensor optimisation.

1.4 Data Consistency

In order to over-determine model-free equations, it is paramount to record data at multiple magnetic fields (discussed in [50]). However, combining multiple-field datasets is not trivial and, in some circumstances, can lead to artifacts. Indeed, this problem has previously been discussed in the literature [88, 89, 159].

Indeed, to extract high quality information from multiple field experiments, it is important that datasets share a high degree of consistency, as combining inconsistent datasets is similar to combining datasets recorded under different experimental conditions, *i.e.* potentially reporting on different motions. Inconsistencies can arise from several factors, including variations in sample viscosity (caused by changes in temperature and concentration), water saturation during acquisition (which influences N-H moieties as a function of the exchange

rate with the aqueous solvent), other differences in data acquisition between different NMR spectrometers or NMR centers, and any form of time-dependent sample modifications (*e.g.* binding state, degradation, and aggregation). If variations are present among the datasets recorded at different magnetic fields, then recorded spin relaxation parameters will be inconsistent with each other.

The effects of combining inconsistent datasets can vary depending on the source of the problem. In certain cases, incorrect characterisation of global tumbling can arise, indirectly leading to erroneous evaluation of local dynamics [244, 265]. Moreover, artifactual μs-ms motions can be falsely detected as non-null R_{ex} parameters [265]. Finally, inconsistent datasets can yield to some N-H vectors being rejected from the analytical scheme because of too high χ^2 statistics, thus reducing the information content obtained from the experiments. No matter the exact situation, however, it is clear that inconsistent datasets will lead to a mistaken description of local motions and should be avoided entirely.

1.5 Objectives of this Work

The work presented in this first part of the thesis was concerned by the improvement of spin relaxation data analysis in the context of the model-free formalism. This project was born by the need to validate the quality of spin relaxation data recorded for PSE-4 β-lactamase in the course of the study of its dynamics (see Part II, Chapter 7, and [194]). Specific objectives were as follows:

- Develop an approach to identify inconsistent transverse relaxation rates acquired at multiple magnetic fields (in order to avoid artifacts caused by the combined analysis of inconsistent data).
- Sensitise the NMR community on the importance of highly consistent multiple field spin relaxation data for extraction of reliable information on protein dynamics.

Chapter 2

Improved Analysis of NMR Dynamics: Simple Tests for the Validation of Multiple Field Spin Relaxation Data

Multiple field ^{15}N spin relaxation data is widely used within the model-free formalism to extract detailed dynamic information for protein amide N-H groups. However, severe artifacts can be introduced if inconsistencies arise between experimental setups with different magnets (or samples). Here, we propose the use of simple tests as validation tools for the assessment of consistency between different datasets recorded at multiple magnetic fields. Synthetic data are used to show the effects of inconsistencies on the proposed tests. Moreover, an analysis of data currently deposited in the BMRB is performed. Finally, two examples are presented. These tests are implemented in the open-source program *relax*, and we propose their use as a routine check-up for assessment of multiple field dataset consistency prior to any analysis such as model-free calculations. We believe this will aid in the extraction of higher quality dynamics information from ^{15}N spin relaxation data.

2.1 Context

In this study, three field independent functions are proposed to assess the consistency of transverse relaxation rates within spin relaxation datasets at multiple magnetic fields to be used for model-free analysis. The goal of these tests is similar to the self-consistency test previously proposed by Fushman *et al.* [89] or to the indirect R_1 consistency verification approach proposed by Mack *et al.* [172]. The use of the three tests, for which we show the efficiency using both synthetic and experimental data, should become routine so dataset quality is assessed prior to derivation of dynamics parameters. This additional step in ^{15}N spin relaxation studies is believed to allow more relevant data to be extracted from the information rich R_1, R_2, and NOE, avoiding experimental errors such as those arising from temperature or concentration deviations.

2.2 Methods

2.2.1 Consistency Tests

Three consistency tests can be used in the proposed approach: $J(0)$ [75], F_η, and F_{R_2} [88]. These field independent functions using R_1, R_2, and NOE as input parameters were implemented in the program *relax*, versions 1.2.14 and higher) [51, 52]. $J(0)$ was defined previously (see Equation 1.11), and F_η and F_{R_2} are defined below:

$$F_\eta = \frac{\eta}{B_0\{4+3[1+(\omega_N\,\tau_m^{app})^2]^{-1}\}} \tag{2.1}$$

$$F_{R_2} = \frac{R_2 - P_{HF}}{\{4+3[1+(\omega_N\,\tau_m^{app})^2]^{-1}\}(d+c/3)} \tag{2.2}$$

where the cross-correlation rate between the ^{15}N *CSA* and the ^{15}N-^{1}H dipolar interaction is

defined as:

$$\eta = 0.5 \sqrt{\frac{dc}{3}} \left[4J(0) + 3J(\omega_N)\right] \left[3\ (cos\theta)^2 - 1\right] \tag{2.3}$$

the spectral density at the ^{15}N frequency is calculated from Equation 1.12, θ is the angle between the ^{15}N-^{1}H vector and the principal axis of the ^{15}N chemical shift tensor, τ_m^{app} is an estimated isotropic global correlation time for the system under study (expressed in ns, and estimated from the following relation [78]:

$$\tau_m^{app} = 2.5\ J(0) \tag{2.4}$$

and the contribution to R_2 from high frequency motions is:

$$P_{HF} = -1.3\ \sigma_{NOE} \tag{2.5}$$

For the calculations presented here, θ was 15.7^o as in Fushman *et al.* [88], $r_{N\text{-}H}$ was 1.02 Å, and the ^{15}N *CSA* was assumed to be -172 ppm. Both $r_{N\text{-}H}$ and ^{15}N *CSA* were typical of spin relaxation studies analysed using the model-free formalism.

Performing these simple calculations for each residue and then comparing results obtained at different magnetic fields should, in the case of perfect consistency and assuming the absence of conformational exchange, yield equal values independently of the magnetic field.

2.2.2 Synthetic Datasets

Synthetic datasets were generated using the program *relax* (version 1.2.14) [51, 52]. R_1, R_2, and *NOE* were calculated at three magnetic fields in the case of an N-H vector with an order parameter (S^2) of either 0.6, 0.7, 0.8, 0.9 or 1.0, and with a correlation time (τ_e) of either 20 or 100 ps (model *m*2 within the model-free analysis) on a molecule tumbling isotropically with a correlation time (τ_m) of either 5, 10, 20 or 40 ns. As for consistency tests, both $r_{N\text{-}H}$

and ^{15}N *CSA* were 1.02 Å and -172 ppm, respectively.

2.2.3 Experimental Datasets

Experimental datasets were retrieved from the BMRB [269]. These datasets were recorded at two or three magnetic fields for proteins with apparent correlation times $\geq$ 5 ns (see Equation 2.4 or Table 2.5 for a description of the method used to estimate τ_m^{app}). Moreover, two test cases for homologous proteins TEM-1 [240] and PSE-4 [194] were analysed in details to show the advantage of performing consistency tests.

2.2.4 Temperature Calibrations

Temperature calibration for different NMR probes (Varian RT and cold probes) were performed using a 4 % CH_3OH / 96 % CD_3OD sample. The following relation (from Bruker Instruments VT-Calibration Manual, valid approximately between 0 and 30 °C) was used:

$$T = \frac{4.109 - \Delta\delta}{0.008708} \tag{2.6}$$

where the temperature T is expressed in K and $\Delta\delta$, the chemical shift difference between the OH and CH_3 resonances, is expressed in ppm.

2.3 Results

The magnetic field dependence of spin relaxation parameters [1] (see Equations 1.1, 1.7, and 1.9 as well as Figures 2.1, 2.2, and 2.3) allows over-determination of model-free equations for quantification of both global and local dynamics within a molecular system. Recorded data is usually taken directly as input into minimisation procedures to yield model-free parameters. A field independent function based on these dynamics parameters would be useful to assess datasets consistency prior to these analyses. This would avoid the

potential extraction of erroneous information as well as the waste of time associated to dissecting inconsistent datasets using numerous long model-free minimisations with different subsets of data.

The three tests proposed in this study are $J(0)$, F_η, and F_{R_2} (see Equations 1.11, 2.1, and 2.2). While $J(0)$ [75], the spectral density at the zero frequency, is mainly used in studies of unfolded proteins using reduced spectral density mapping, it is very well suited for assessing consistency since it is, in the absence of μs-ms motions, a field independent function. On the other hand, F_η and F_{R_2} are two functions which were previously proposed for consistency testing in the case of determining the ^{15}N *CSA* using the cross-correlation rate η and the transverse relaxation rate R_2 [88], and are also, in the absence of μs-ms motions, field independent functions. Performing these three tests for consistency testing purposes requires R_1, R_2, and *NOE* data at two magnetic fields or more. Moreover, an estimate of the global correlation time τ_m^{app} (see Equation 2.4) is required for tests F_η and F_{R_2} (see Equations 2.1 and 2.2).

Consistency testing is performed by calculating the different functions using the experimental data from each magnetic field and then comparing values obtained on a per residue basis before having a look at correlation plots and at the distribution of ratios. This global picture

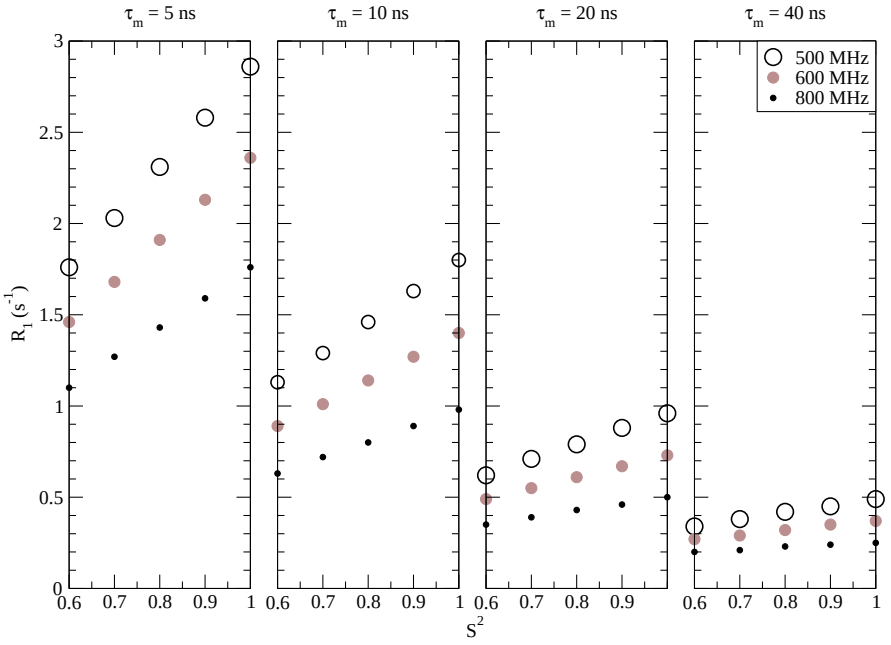

Figure 2.1: Effect of dynamics on spin relaxation: R_1 (based on synthetic data for model-free model *m2* and a local correlation time τ_e of 20 ps).

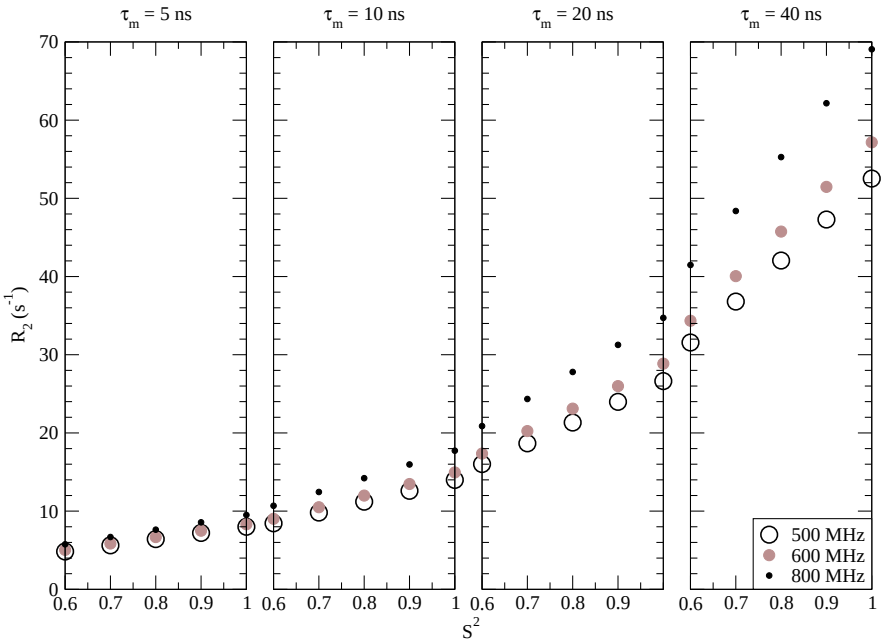

Figure 2.2: Effect of dynamics on spin relaxation: R_2 (based on synthetic data for model-free model *m*2 and a local correlation time τ_e of 20 ps).

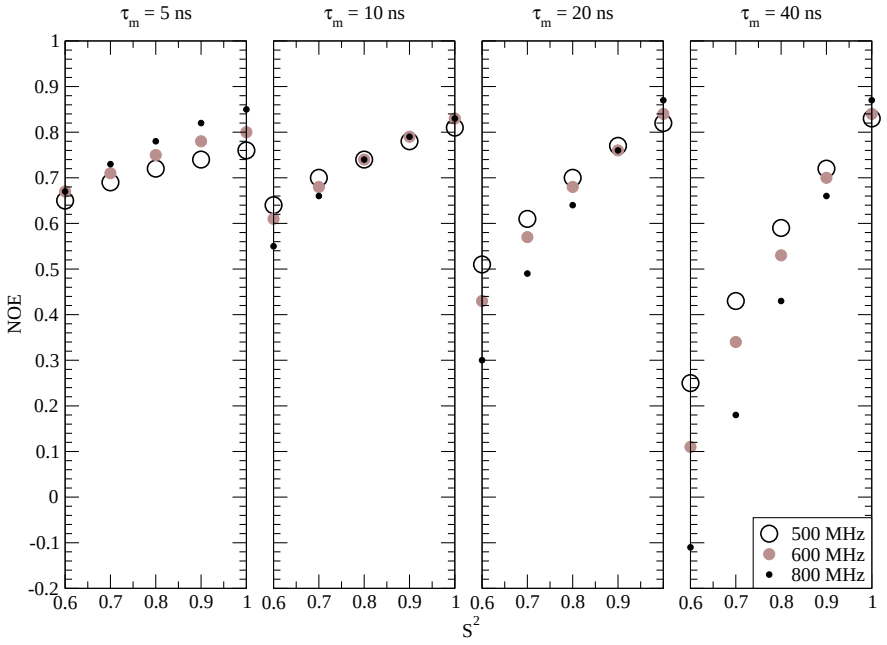

Figure 2.3: Effect of dynamics on spin relaxation: *NOE* (based on synthetic data for model-free model *m*2 and a local correlation time τ_e of 20 ps).

then indicates the level of consistency in a qualitative manner, where consistent datasets have distributions of ratios centered at one, while deviations from one are observed for inconsistent datasets.

2.3.1 Consistency Tests on Synthetic Datasets

Simulations based on synthetic data confirm the field independent nature of the $J(0)$, F_η, and F_{R_2} functions in the case of consistent datasets for spins not affected by slow μs-ms motions (Table 2.1, see also Figures 2.4, 2.5, and 2.6). This observation is valid at least for S^2 varying from 0.6 to 1 and τ_m varying from 5 to 40 ns, thus valid for most protein NMR studies. Additionally, variations in the local correlation time τ_e (from 20 to 100 ps) do not affect the field independent nature of the functions (data not shown), a prerequisite for their use as consistency tests. Contrary to the proposed tests, and even though it is sometimes used for testing global consistency of R_2 data, the normalisation of R_2 by the square root of the magnetic field ($R_2/\sqrt{B_0}$) is not a 'real' field independent function, *i.e.* it is not unaffected by local dynamics (data not shown) and, thus, should not be used for serious consistency validation of multiple field R_2 data.

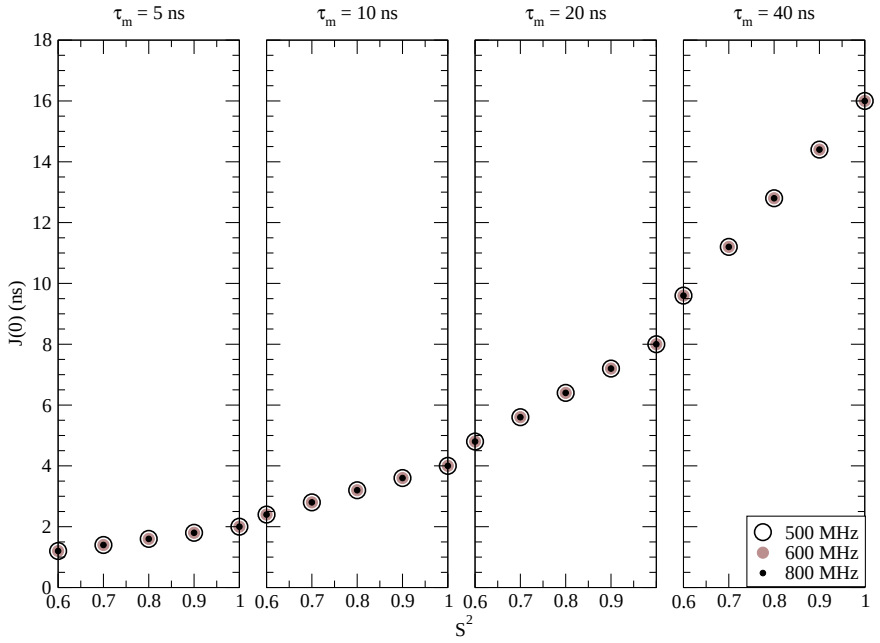

Figure 2.4: Effect of dynamics on consistency functions: $J(0)$ (based on synthetic data for model-free model *m*2 and a local correlation time τ_e of 20 ps).

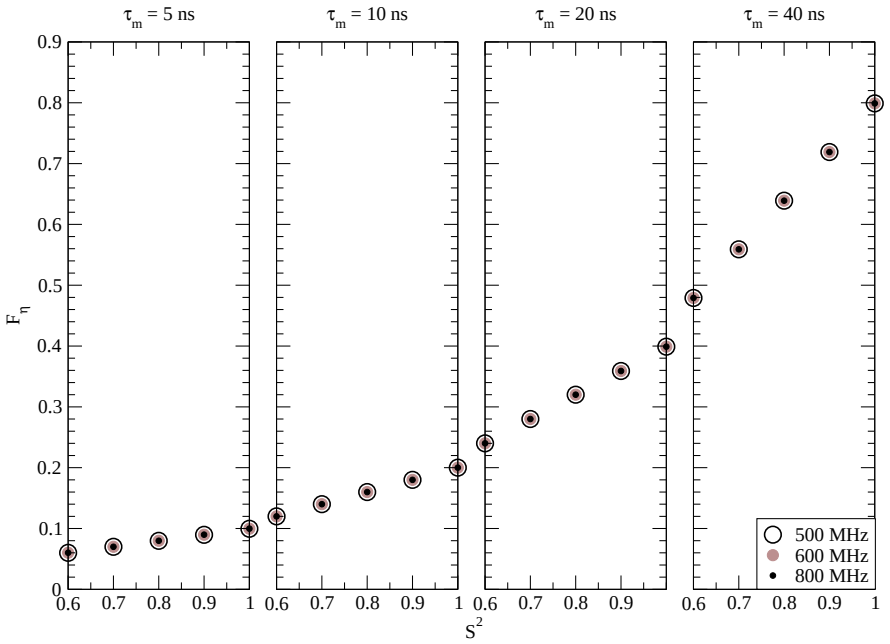

Figure 2.5: Effect of dynamics on consistency functions: F_η (based on synthetic data for model-free model *m*2 and a local correlation time τ_e of 20 ps).

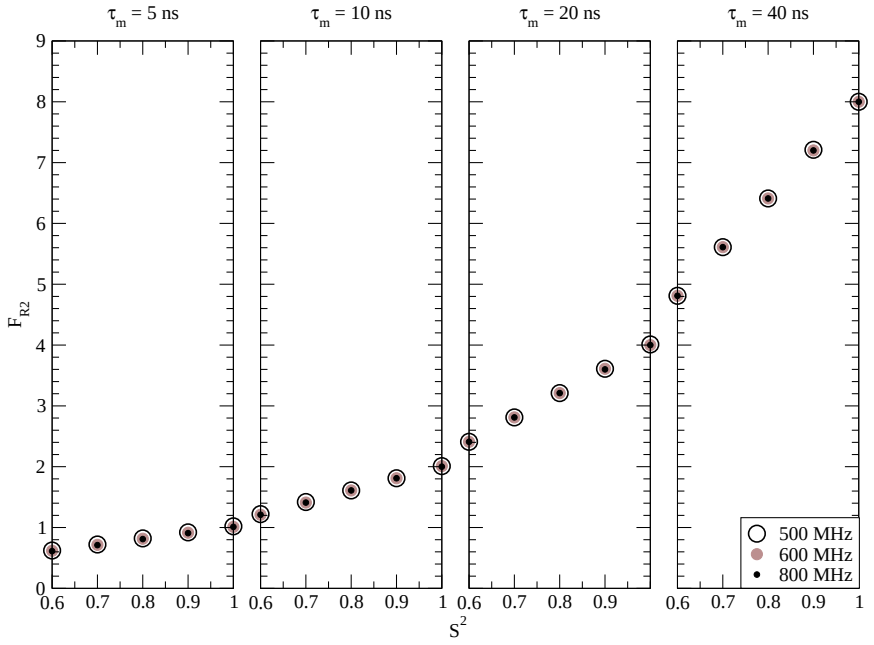

Figure 2.6: Effect of dynamics on consistency functions: F_{R_2} (based on synthetic data for model-free model *m*2 and a local correlation time τ_e of 20 ps).

A second prerequisite for the use of these functions as consistency tests is that these be affected by inconsistencies. Tables 2.2, 2.3, and 2.4 indeed show that errors in the transverse relaxation rates affect the results of consistency testing and that both R_1 and *NOE* have a negligible effect on the calculated values for the three tests (see also Figures 2.7, 2.8, 2.9, 2.10, 2.11, and 2.12). Moreover, this effect of R_2 on the consistency functions is almost quantitative, even though we propose that assessment of consistency be performed in a qualitative manner, looking at the different vectors of a macromolecule as a whole, since particular conditions could give rise to a local deviation in R_2 unrelated to consistency issues. For example, errors on the measured rates will slightly affect consistency of single spins. However, taken as a whole, a consistent dataset with a non null error on the measured rates should give rise to a distribution of ratios centered at one, but with a spread proportional to the experimental error. Indeed, most inconsistencies will arise from factors affecting all spins and thus skewing the distribution of ratios away from an average value of 1, as opposed to giving rise to a wider distribution.

Of course, the proposed tests are not strictly perfect, *i.e.* some deviations are observed in the case of perfect datasets, for example when τ_m is short ($\sim$ 5 ns) probably because $\omega_N\tau_m$ approaches 1 where some assumptions are not valid anymore. Indeed, the shape of the spectral density is characterised as an inverse quadratic function of ω_N when $\omega_N\tau_m \gg 1$ (*i.e.*

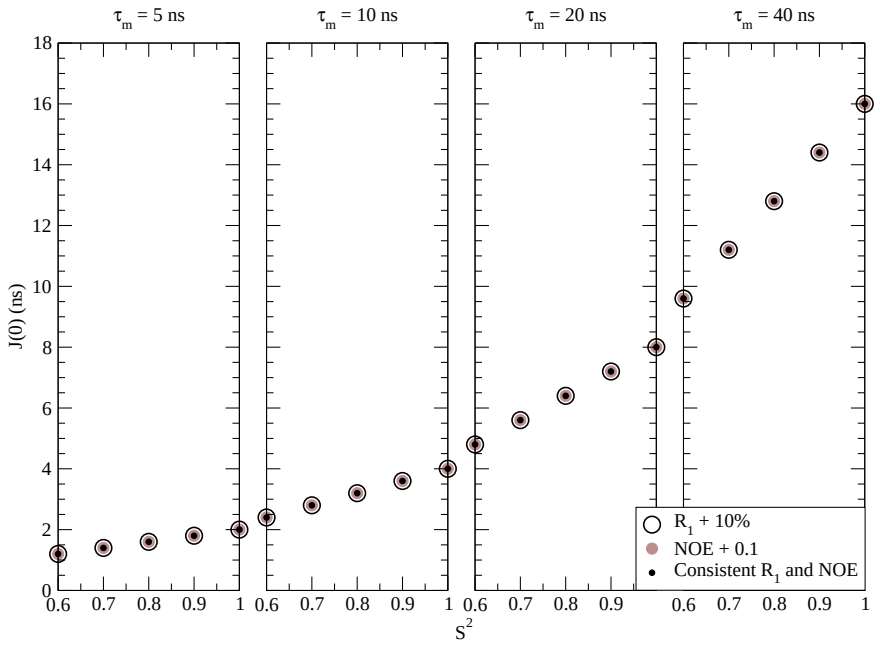

Figure 2.7: Effect of inconsistencies in *NOE* and R_1 on $J(0)$ (based on synthetic data for model-free model *m*2 and a local correlation time τ_e of 20 ps; consistency function calculated for a ^{1}H frequency of 600 MHz).

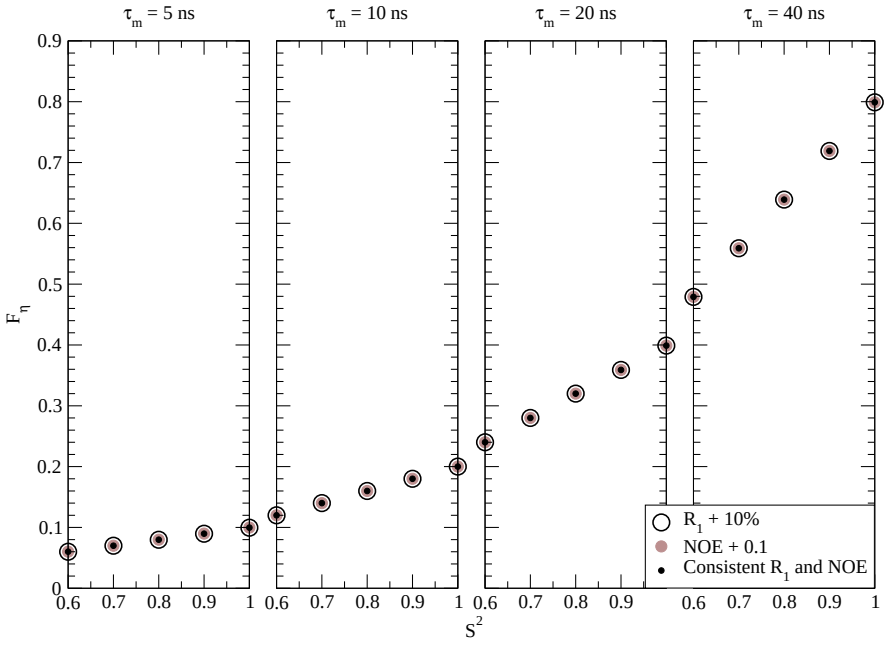

Figure 2.8: Effect of inconsistencies in *NOE* and R_1 on F_η (based on synthetic data for model-free model *m*2 and a local correlation time τ_e of 20 ps; consistency function calculated for a ^{1}H frequency of 600 MHz).

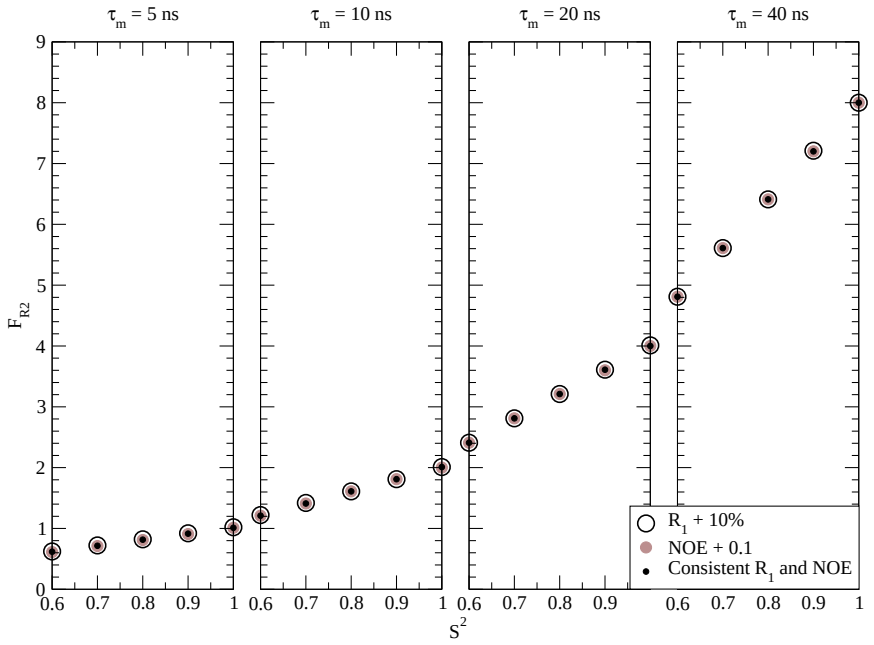

Figure 2.9: Effect of inconsistencies in *NOE* and R_1 on F_{R_2} (based on synthetic data for model-free model *m*2 and a local correlation time τ_e of 20 ps; consistency function calculated for a ^{1}H frequency of 600 MHz).

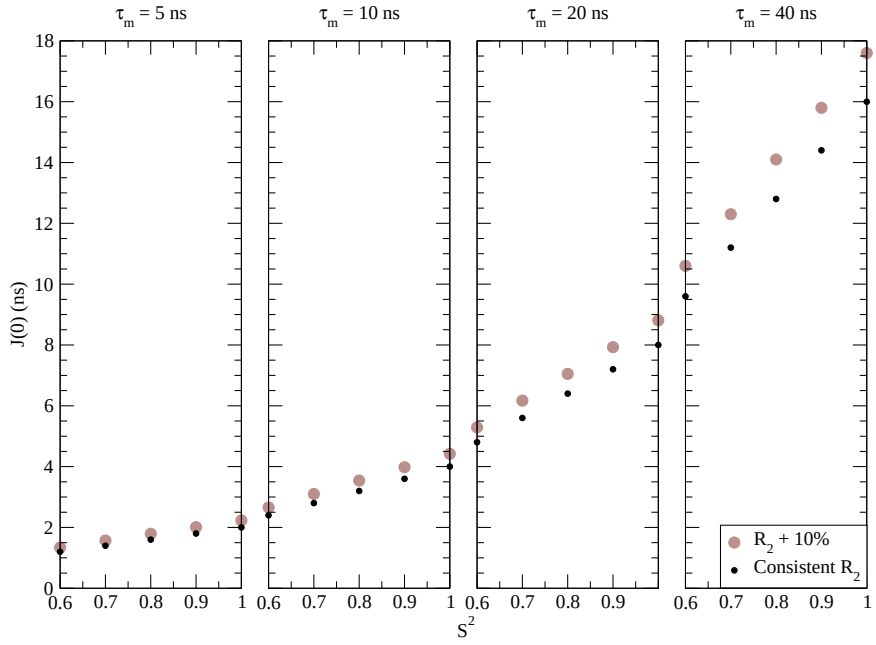

Figure 2.10: Effect of inconsistencies in R_2 on $J(0)$ (based on synthetic data for model-free model *m*2 and a local correlation time τ_e of 20 ps; consistency function calculated for a ^{1}H frequency of 600 MHz).

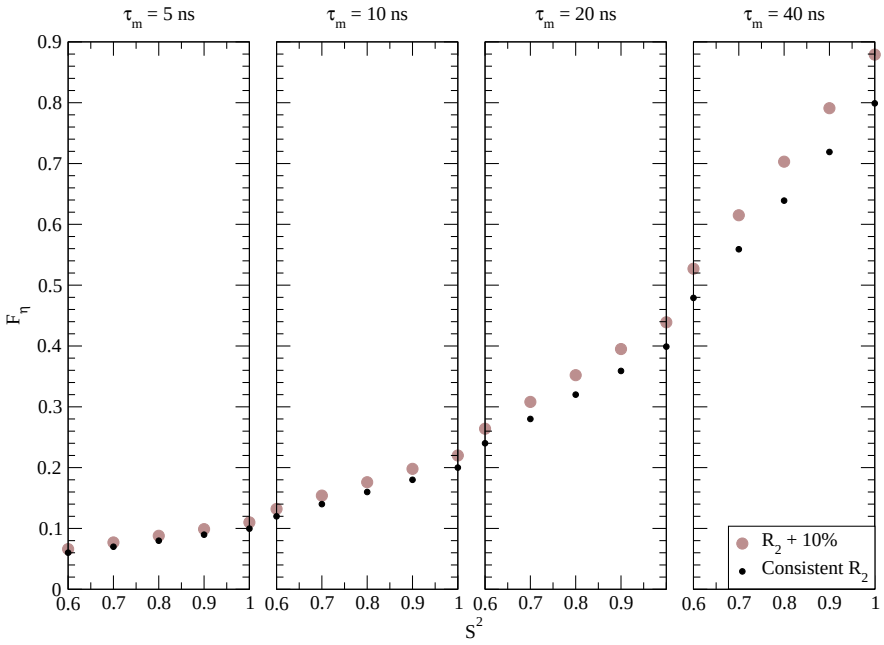

Figure 2.11: Effect of inconsistencies in R_2 on F_η (based on synthetic data for model-free model *m*2 and a local correlation time τ_e of 20 ps; consistency function calculated for a ^{1}H frequency of 600 MHz).

in the so-called slow tumbling or spin diffusion regime). On the other hand, when this condition is not met, the shape of the spectral density changes and the assumptions necessary for reduced spectral density mapping in case of the $J(0)$ test (assuming that the spectral density does not vary much at higher frequencies, see Section 1.3.2) are not valid anymore. However, these deviations are less than 1.5 % in all cases (see Table 2.1). Moreover, some effects of R_1 and *NOE* inconsistencies can also be observed, mostly lower than 2.5 % for 10 % inconsistencies, thus generally not precluding the use of these tests for consistency testing. Of course, if different inconsistencies are combined, these effects also combine in an additive way, potentially increasing or decreasing the consistency scores (depending on the combination), but again in a limited way since the effects on $J(0)$, F_η, and F_{R_2} of both R_1 and *NOE* inconsistencies are small compared to the effects of R_2 inconsistencies (see Tables 2.2 and 2.4 as well as Figures 2.7, 2.8, 2.9, 2.10, 2.11, and 2.12).

Hence, the above arguments confirm the availability of these functions for use as consistency tests. However, as all three functions report on the same inconsistency (affecting R_2), we prefer the use of the spectral density at the zero frequency, $J(0)$, alone since it does not rely on an estimation of the global correlation time (τ_m^{app}), neither on a measure of θ, the angle between the ^{15}N-^{1}H vector and the principal axis of the ^{15}N chemical shift tensor (which was shown to vary for different residues in ubiquitin, with an average value of $15.7 \pm 5.0°$, for a

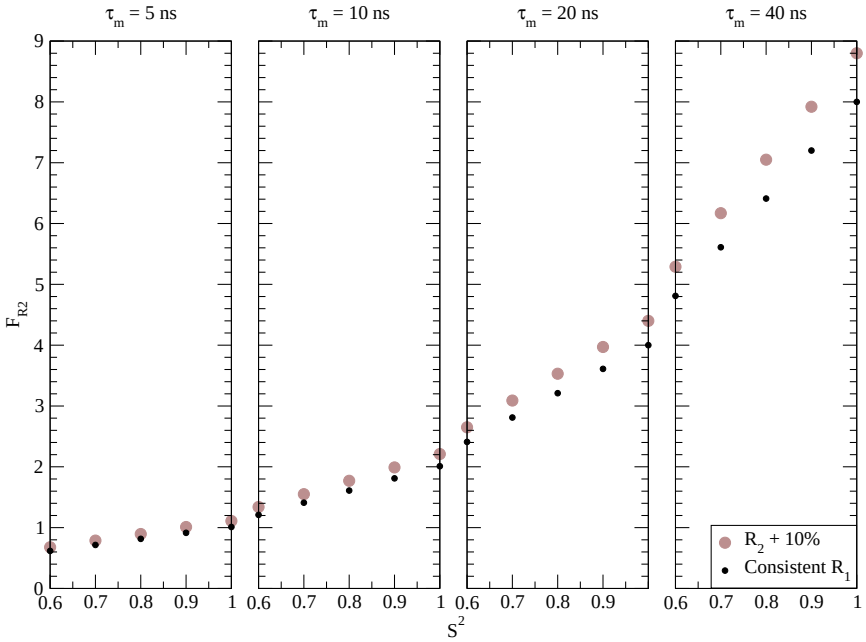

Figure 2.12: Effect of inconsistencies in R_2 on F_{R_2} (based on synthetic data for model-free model *m2* and a local correlation time τ_e of 20 ps; consistency function calculated for a ^{1}H frequency of 600 MHz).

range of 6 to 26° [88]). Hence, $J(0)$ is less likely to be affected by incorrect parametrisation of input parameters. For example, an error of 10 % in the estimation of τ_m (which certainly cannot be excluded) gives rise to an apparent inconsistency of up to 2 % for perfect data in both F_η and F_{R_2} (data not shown). For these reasons, we will focus solely on consistency assessment using $J(0)$ in the examples discussed below.

2.3.2 Consistency Tests on Experimental Datasets

Since, at short correlation times (*i.e.* $<$ 5 ns), consistency tests are less efficient (see text above), only datasets for which the correlation time was estimated to be $\geq$ 5 ns were extracted from the BMRB [269] and analysed (see Table 2.5). Among the datasets retrieved from the BMRB (17 in total), some showed apparent inconsistencies, whereas others displayed excellent multiple field consistency (see Table 2.5).

Good Consistency

Examples of very good consistency included data for the enzyme human neutrophil gelatinase-associated lipocalin (BMRB 4267, [42]), the apo-cellular retinol-binding protein type I (BMRB 5331, [84]), the enzyme adenylate kinase in complex with inhibitor Ap5A (BMRB 5746, [246]), the kinase-interacting FHA domain of KAPP protein (BMRB 5841, [58]), the protein azurin (BMRB 6243, [295]), and the class A β-lactamase TEM-1 (BMRB 16392, [240], discussed further below).

Table 2.1: Simulations for consistent synthetic data (calculated for S^2 = 0.8 and τ_e = 20 ps).

τ_m (ns)	$\frac{500-600}{600}$ (%)			$\frac{500-800}{800}$ (%)			$\frac{600-800}{800}$ (%)		
	$J(0)$	F_η	F_{R_2}	$J(0)$	F_η	F_{R_2}	$J(0)$	F_η	F_{R_2}
5	-0.1	-0.1	0.7	-0.1	-0.1	1.4	-0.1	-0.1	0.7
10	0.0	0.0	0.2	0.0	0.0	0.5	0.0	0.0	0.2
20	0.0	0.0	0.1	0.0	0.0	0.1	0.0	0.0	0.1
40	0.0	0.0	0.0	0.0	0.0	0.0	0.0	0.0	0.0

Table 2.2: Simulations for synthetic data with inconsistent $R_1^{inc} = R_1 + 10\%$ for S^2 = 0.8 and τ_e = 20 ps. †

τ_m (ns)	$\frac{500-600}{600}$ (%)			$\frac{500-800}{800}$ (%)			$\frac{600-800}{800}$ (%)		
	$J(0)$	F_η	F_{R_2}	$J(0)$	F_η	F_{R_2}	$J(0)$	F_η	F_{R_2}
5	-2.3 / 1.7	-0.2 / 0.0	0.8 / 0.6	-2.4 / 1.0	-0.3 / -0.1	1.6 / 1.4	-1.8 / 1.0	-0.2 / 0.0	0.8 / 0.7
10	-0.7 / 0.5	-0.1 / 0.0	0.3 / 0.2	-0.7 / 0.3	-0.1 / 0.0	0.5 / 0.4	-0.5 / 0.3	-0.1 / 0.0	0.3 / 0.2
20	-0.2 / 0.1	0.0 / 0.0	0.1 / 0.1	-0.2 / 0.1	0.0 / 0.0	0.2 / 0.1	-0.1 / 0.1	0.0 / 0.0	0.1 / 0.1
40	-0.1 / 0.0	0.0 / 0.0	0.0 / 0.0	-0.1 / 0.0	0.0 / 0.0	0.0 / 0.0	0.0 / 0.0	0.0 / 0.0	0.0 / 0.0

Table 2.3: Simulations for synthetic data with inconsistent $R_2^{inc} = R_2 + 10\%$ for S^2 = 0.8 and τ_e = 20 ps. †

τ_m (ns)	$\frac{500-600}{600}$ (%)			$\frac{500-800}{800}$ (%)			$\frac{600-800}{800}$ (%)		
	$J(0)$	F_η	F_{R_2}	$J(0)$	F_η	F_{R_2}	$J(0)$	F_η	F_{R_2}
5	12.2 / -10.5	10.1 / -9.2	10.6 / -8.4	12.2 / -10.1	10.0 / -9.3	11.4 / -7.7	11.7 / -10.0	10.0 / -9.2	10.7 / -8.4
10	10.7 / -9.5	10.0 / -9.1	10.2 / -8.9	10.7 / -9.4	10.0 / -9.1	10.5 / -8.7	10.5 / -9.4	10.0 / -9.1	10.2 / -8.9
20	10.2 / -9.2	10.0 / -9.1	10.1 / -9.0	10.2 / -9.2	10.0 / -9.1	10.1 / -9.0	10.1 / -9.2	10.0 / -9.1	10.1 / -9.0
40	10.1 / -9.1	10.0 / -9.1	10.0 / -9.1	10.1 / -9.1	10.0 / -9.1	10.0 / -9.1	10.0 / -9.1	10.0 / -9.1	10.0 / -9.1

Table 2.4: Simulations for synthetic data (with inconsistent $NOE^{inc} = NOE + 0.1$ for S^2 = 0.8 and τ_e = 20 ps. †

τ_m (ns)	$\frac{500-600}{600}$ (%)			$\frac{500-800}{800}$ (%)			$\frac{600-800}{800}$ (%)		
	$J(0)$	F_η	F_{R_2}	$J(0)$	F_η	F_{R_2}	$J(0)$	F_η	F_{R_2}
5	0.2 / -0.3	0.4 / -0.4	0.2 / 1.1	0.2 / -0.2	0.3 / -0.4	1.0 / 1.7	0.2 / -0.2	0.3 / -0.3	0.4 / 1.0
10	0.1 / -0.1	0.2 / -0.1	0.0 / 0.3	0.1 / -0.1	0.1 / -0.1	0.3 / 0.5	0.0 / 0.0	0.1 / 0.1	0.1 / 0.3
20	0.0 / 0.0	0.0 / 0.0	0.0 / 0.1	0.0 /0.0	0.0 / 0.0	0.1 / 0.2	0.0 / 0.0	0.0 / 0.0	0.0 / 0.1
40	0.0 / 0.0	0.0 / 0.0	0.0 / 0.0	0.0 / 0.0	0.0 / 0.0	0.0 / 0.0	0.0 / 0.0	0.0 / 0.0	0.0 / 0.0

† Results in Tables 2.2, 2.3, and 2.4 are presented for inconsistencies in both low and high field data (low field / high field).

High Inconsistency

On the contrary, some datasets displayed high apparent inconsistencies (> 5 %, see Table 2.5). These include data from the functional domain of *Paracoccus denitrificans* cytochrome c552 in the oxidised state (BMRB 5080, [232]), the *de novo* designed protein S-824 (BMRB 5687, [96]), the kinase-interacting FHA domain of KAPP protein (BMRB 6474, [58]) the *de novo* designed protein S836 monomer (BMRB 15437, [96]), and the human 15.5 kDa / NHPX protein (BMRB 15445, [250]) where inconsistencies were $>$ 5 % when comparing data acquired at 500 and 600 MHz.

Transverse relaxation data from BMRB 5080[232], with its positive $J(0)^{(500-600)/600}$ ratio (see Table 2.5) is an interesting case of inconsistency where many residues are associated with a higher R_2 at 500 MHz compared to 600 MHz. This is theoretically impossible since R_2 (in the presence or absence of conformational exchange) should get higher as the static magnetic field increases as a result of a growing importance of the *CSA* constant c which is proportional to ω^2 (see Equation 1.7 and Figure 1.2).

BMRB 5687 and 15437 both belong to the same study [96] where the two proteins display similar apparent inconsistency with either R_2 at 600 MHz being over-estimated or, inversely, R_2 at 500 MHz being under-estimated. These inconsistent R_2 values may have lead to some R_{ex} values of the same magnitude as R_2 and unusually large S^2 errors for several residues in both S-836 (BMRB 15437) and S-824 (BMRB 5687). In the case of S-836 (BMRB 15437), most residues with significant R_{ex} terms are co-localised, indicating the potential consistency of this dataset which could probe a protein with important μs-ms motions. On the contrary, model-free analysis results for protein S-824 (BMRB 5687) display more scattered R_{ex} parameters of low value. However, since the authors only analysed the details of residues affected by R_{ex} of significant values (> 2 s^{-1}), the possible effect of inconsistencies for protein S-824 (BMRB 5687) are diminished with respect to data interpretation. Hence, in this case, even though raw consistency tests show that inconsistencies are present, the authors seem to have taken the necessary precautions to minimise incorrect conclusions.

BMRB 6474 is a very interesting case since these data relate to the bound state of the protein probed in BMRB 5841, which displayed very good consistency (see above). Hence, as proposed in the study [58], this could be a very good example of conformational exchange caused by ligand binding. Hence, for BMRB 6474, the apparent inconsistency would be artificially caused by μs-ms motions (as confirmed by relaxation dispersion

experiments [58]). In other words, further investigation confirmed that these datasets are consistent with the presence of significant conformational exchange processes.

BMRB 15445 is different; in this case, the authors associated a R_{ex} term to 15 residues out of 144 [250]. Removing these residues from the consistency analysis yields a similar inconsistency score of 33.9 % (the highest inconsistency we could analyse in this study). Since the average R_2 is too high at 500 MHz compared to 600 MHz (R_2 were ∼20 % higher at 500 MHz compared to 600 MHz), it is however normal that few R_{ex} terms were introduced in the analysis. In this case, the global tumbling description may be incorrect since, for example, the τ_m^{app} (see Table 2.5 for a description of the method used to estimate τ_m) at 500 and 600 MHz were, respectively, 13.1 and 9.8 ns. It is probable that the authors did not notice this problem when looking at the details of local dynamics. In fact, the authors chose an isotropic diffusion tensor despite a $\mathfrak{D}_{ratio}$ ($\mathfrak{D}_{\parallel}/\mathfrak{D}_{\perp}$) of 1.1. It is not clear what effects this simplistic definition of the global diffusion introduced. The combination of this incorrect characterisation of global tumbling and over-estimated R_2 at the low field would be suggested to give rise to two-timescale motions, which is apparently not the case [250]. It is clear that consistency tests, in this case, could have helped to improve the analysis and may even have yielded a different picture of dynamics in this system with potentially different biological interpretation of the results.

Moderate Inconsistency

Moderate inconsistencies, on the other hand, were observed for some datasets including the functional domain of *Paracoccus denitrificans* cytochrome c552 in the reduced state (BMRB 5079, [232]), the cellular retinol-binding protein type I (BMRB 5331, [84]), the class A β-lactamase PSE-4 (BMRB 6838, [194], discussed further below), the apo chicken triosephosphate isomerase (BMRB 15064, [142]), the 2-PGA-bound chicken triosephosphate isomerase (BMRB 15065, [142]), and the apo-PGG/GGG chicken triosephosphate isomerase (BMRB 15066, [142]).

Datasets 5079 and 5080 belong to the same study and are respectively for the reduced and oxidised forms of cytochrome c_{552} [232]. For both datasets, although to a different extent, consistency tests indicate a significantly higher R_2 at 500 MHz compared to 600 MHz for many residues. As stated before, this should normally never happen. The authors, in this case, may have missed important dynamic features of their protein which could have helped

explain, for example, their hydrogen exchange data. Indeed, they noted that the R_{ex} were of no use to explain hydrogen exchange data because of their low value ($< 1.5\ s^{-1}$).

The dataset for holo-cellular retinol-binding protein type I (BMRB 5331, [84]) shows a low apparent inconsistency of 3.5 % for data recorded at 500 and 600 MHz. The apo form of the same protein (BMRB 5330, also from the same study, [84]) showed high consistency. As in the case of BMRB 5079 and 5080 [232], consistency tests indicate a higher R_2 at 500 MHz compared to that at 600 MHz which strongly prevents the appearance of R_{ex} terms in the model-free analysis (since the model-free formalism assumes that exchange processes occur in the fast exchange regime, *i.e.* that there is a quadratic dependence of conformational exchange contributions to R_2 terms with the strength of the magnetic field). This inconsistency is not caused by a few outliers as the distribution of ${}^{500MHz}J(0)/{}^{600MHz}J(0)$ ratio is narrow and generally symmetric, pointing to an overall discrepancy between data recorded at the two magnetic fields. Of course, this low inconsistency could cause other problems such as incorrect characterisation of the global tumbling or aberrant S^2 values. However, its small amplitude may not affect data analysis.

The datasets for the triosephosphate isomerase dimer (BMRB 15064, 15065, and 15066, [142]) also show apparent inconsistencies. However, BMRB 15064 and 15065 show apparent inconsistencies in opposite directions compared to BMRB 15066, consistent with the findings of the authors who assessed that the wild-type protein (BMRB 15064 and 15065) was affected by μs-ms motions (in loops 6 and 7), whereas the mutant (BMRB 15066) was not. Considering these data, the results perfectly make sense. However, for BMRB 15066, R_2 were lower than expected at 800 MHz (strongly precluding appearance of R_{ex} terms). Hence, data for the wild-type protein (BMRB 15064 and 15065) appear of high quality with μs-ms motions co-localising on the 3D structure. Hence, it is possible that data for the mutant (BMRB 15066) are slightly inconsistent and mask the underlying dynamics.

Limits

It is difficult from consistency tests alone to decide whether or not the apparently inconsistent datasets are indeed erroneous. An apparent low consistency could be caused by widespread slow μs-ms motions affecting R_2 in a field dependent manner. However, in any case, such low consistency results indicate the need for a more in-depth analysis of results obtained by

Table 2.5: Consistency results for data retrieved from the BMRB.

τ_m^{app}† (ns)	Residues	Temperature (°C)	$J(0)$ test $\frac{500-600}{600}$ (%)	$\frac{500-800}{800}$ (%)	$\frac{600-800}{800}$ (%)	BMRB
5.4	100	25.0	4.0	–	–	5079
6.4	100	25.0	8.6	–	–	5080
6.6	102	25.0	-11.6	–	–	5687
7.1	135	25.0	-1.7	–	–	5330
7.5	135	25.0	3.5	–	–	5331
7.6	102	25.0	-13.4	–	–	15437
8.2	139	25.0	-0.9	–	–	5841
8.4	128	16.0	-0.6	-2.0	-1.5	6243
10.5	214	30.0	–	–	0.2	5746
10.9	139	22.0	-9.2	–	–	6474
11.3	179	25.0	0.1	1.7	2.1	‡4267
11.4	271	31.5	0.9	-4.1	-4.8	6838
11.5	144	20.0	33.7	–	–	15445
11.6	263	30.0	0.3	2.2	2.0	16392
27.4	2 x 248	20.0	–	–	4.8	15066
29.4	2 x 248	20.0	–	–	-4.8	15065
30.1	2 x 248	20.0	–	–	-4.5	15064

† The apparent correlation time τ_m^{app} is estimated from the relation $\tau_m^{app} = 2.5\ J(0)$ using the mean value for $J(0)$ [78].

‡ Data at the highest magnetic field was from 750 MHz, not 800 MHz.

analysing other information on the system under study (see below for such an analysis for proteins TEM-1 and PSE-4). Additionally, inconsistencies can be revealed by consistency tests, but be hidden because of limitations in analytical schemes often used for model-free analysis, particularly because of model selection [48].

It should be noted that the low number of retrieved datasets highlights a gap between the publication of relaxation studies (> 400) and the deposition of the related experimental relaxation data within the BMRB [269] (< 50). We would like to encourage NMR spectroscopists to deposit their relaxation data within the BMRB for access of these data by the scientific community. Consistency tests should be performed prior to data deposition in the BMRB with notes deposited as well to explain the obtained results, either for high or low consistency.

2.3.3 β-Lactamases TEM-1 and PSE-4 as Test Cases for Inconsistent R_2

Two studies were performed on very similar systems in our laboratory. Datasets differed in their respective level of consistency, making these studies a particularly good test case for consistency tests. TEM-1 datasets [240] displayed a very high consistency leading to a straightforward analysis of relaxation data. However, PSE-4 datasets [194] were less consistent with each other, leading to the need to remove aberrant data for proper analysis in the model-free formalism. Here, we will focus on the differences between these two studies and on the value of consistency tests for PSE-4 data analysis.

2.3.3.1 TEM-1 (BMRB 16392)

β-Lactamase TEM-1 was studied by recording spin relaxation data at three magnetic fields: 500, 600, and 800 MHz [240]. The consistency of these datasets was high (see Figure 2.13 and Table 2.5), which allowed the analysis within the model-free formalism using all data recorded. From this analysis, 12 N-H vectors required a R_{ex} term in their selected model-free model. These were mostly clustered on the 3D structure, co-localising with two N-H vectors with extremely broadened resonances, which strongly supports the presence of slower timescale dynamics. Moreover, the low number of R_{ex} terms nfor this 263 residue protein was consistent with a very high quality HSQC spectrum with sharp peaks apparently not affected by broadening from conformational exchange.

Even though consistency tests should be used to assess consistency of data for single residues, they can also be useful in identifying residues for which dynamics are of particular interest or, on the contrary, for which data is erroneous, potentially from peak overlap or other reason. Such an outlier is present in the $J(0)$ correlation plots for TEM-1 (see Figure 2.13). This residue is Thr^{141} which was not assigned to any model-free model in the original work of Savard and Gagné [240] who used the analytical scheme of Mandel *et al.* [174] based on F-test statistics. However, in a recent re-analysis of these datasets [79] using *relax* [51, 52] and an analytical scheme involving small sample size Akaike information criterion (AIC_c, see Equation 7.4) [120], this residue was assigned to model $m2$. In this case, the fit was of poor quality, with a χ^2 value of 24.9, *i.e.* the second highest score within TEM-1. Hence, the $J(0)$ test would have been useful in this case for identifying this residue and either re-evaluating the data or excluding it from the analysis to avoid the extraction of

potentially aberrant information.

2.3.3.2 PSE-4 (BMRB 6838)

An NMR study on the dynamics of the class A β-lactamase PSE-4 was recently presented (see Chapter 7 and [194]) in which we discussed the inconsistency of some data among a multiple magnetic field dataset (see Figure 2.14 and Table 2.5). In summary, from this three magnetic field dataset (500, 600, and 800 MHz), the R_2 values at 800 MHz were identified as inconsistent and discarded prior to model-free analysis.

In this case, including R_2 at 800 MHz caused dozens of artifactual R_{ex} terms appearing for residues throughout the protein. Removing the inconsistent data solved the problem and high quality dynamic information could then be extracted. Removing other parts of the dataset did not result in loss of these R_{ex} artifacts (see Table 2.6). Hence, the $J(0)$ test for R_2 consistency could easily detect the inconsistent R_2 values at 800 MHz, whereas other reporters such as

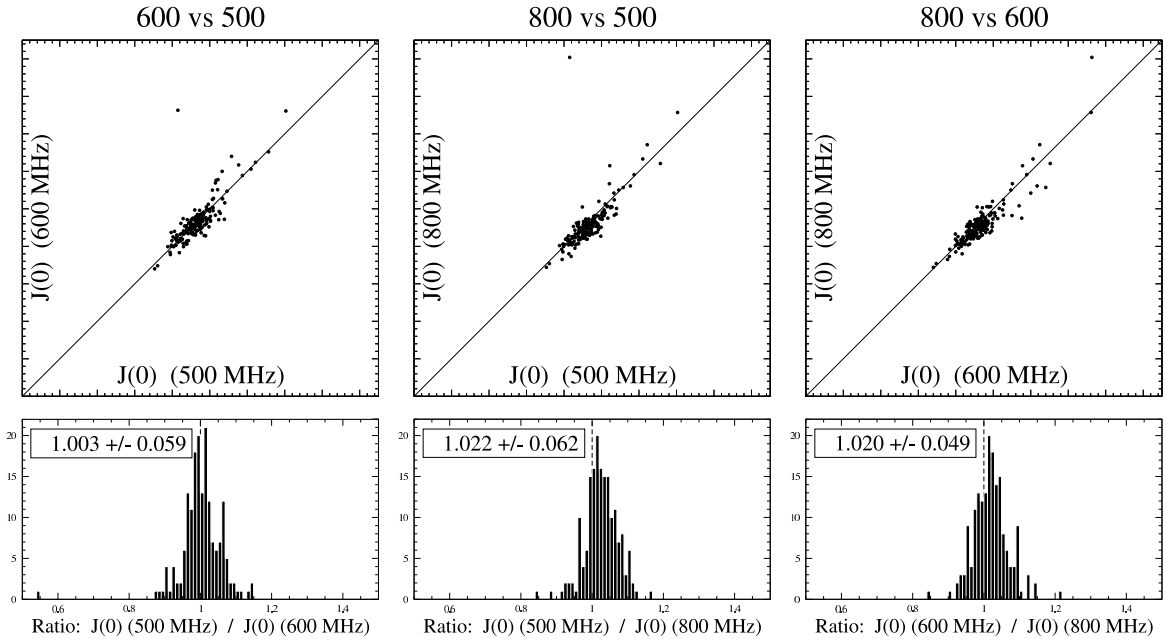

Figure 2.13: $J(0)$ consistency of datasets for TEM-1 β-lactamase (BMRB 16392). The consistency of these three magnetic field datasets is high. Since no NOEs were recorded at 800 MHz, the $J(0)$ values at 800 MHz were calculated by setting the NOEs to those at 600 MHz. As shown in the text as well as in Figure 2.7 and Table 2.4, the $J(0)$ function is quite insensitive to *NOE* inconsistencies, hence this choice is not problematic. Top: correlation plots with a diagonal at $y = x$. Bottom: distributions of the ratios with a dashed line at $x = 1$.

the χ^2 value were unable to identify the inconsistent data (see Table 2.6). In the end, the model-free analysis published for PSE-4 included 20 R_{ex} parameters, among which 5 had especially high values and co-localised in the active site where broadened resonances were also observed. This is similar to what was obtained for the homologous protein TEM-1, and very different from what would have been obtained if the aberrant data had been included in the analysis (*i.e.* if consistency tests had not been performed).

This example clearly shows the advantage of using consistency tests to avoid the time consuming step of fitting model-free parameters to different combinations of subsets of the complete dataset in order to determine if aberrant data are present (as were performed here, for test case purposes, see Table 2.6). Further discussion on PSE-4 datasets consistency is available in Part II of this thesis (in Chapter 7), and in [194].

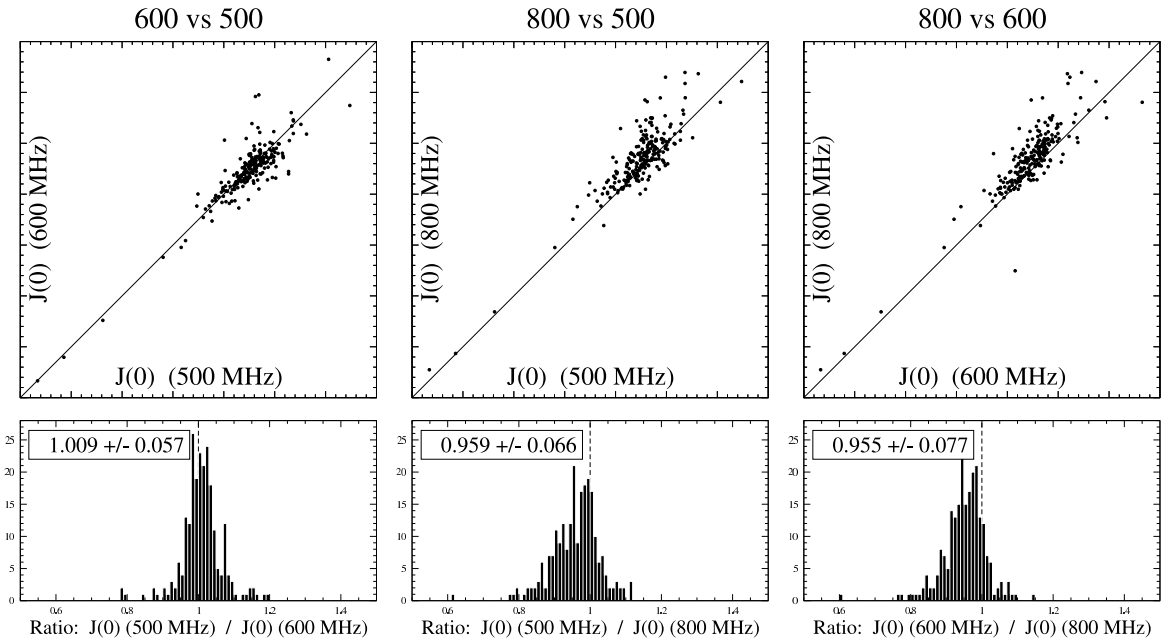

Figure 2.14: $J(0)$ consistency of datasets for PSE-4 β-lactamase (BMRB 6838). The consistency of both 500 and 600 MHz data is high, whereas the consistency of the 800 MHz data is lower. Top: correlation plots with a diagonal at $y = x$. Bottom: distributions of the ratios with a dashed line at $x = 1$.

Table 2.6: Model-free optimisation for PSE-4 β-lactamase using different datasets.†

Datasets	$< local\tau_m >$ (ns)	$< S^2 >$	$< \chi^2 >$ ‡	Number of R_{ex}
All	12.55 ± 1.16	0.86 ± 0.09	0.77 ± 0.77	46
All but 500 MHz	12.57 ± 1.69	0.84 ± 0.10	0.50 ± 0.62	42
All but 600 MHz	12.49 ± 1.28	0.86 ± 0.08	0.61 ± 0.49	49
All but 800 MHz	12.57 ± 1.24	0.86 ± 0.09	0.57 ± 0.49	9
All but $^{800\ MHz}R_1$	12.53 ± 1.19	0.86 ± 0.09	0.72 ± 0.77	45
All but $^{800\ MHz}R_2$	12.64 ± 1.11	0.86 ± 0.09	0.76 ± 0.77	8
All but $^{800\ MHz}NOE$	12.52 ± 1.23	0.86 ± 0.08	0.68 ± 0.54	46
Only 500 MHz*	12.52 ± 1.17	0.88 ± 0.07	0.15 ± 0.21	0
Only 600 MHz*	12.75 ± 1.28	0.87 ± 0.07	0.13 ± 0.20	0
Only 800 MHz*	13.11 ± 1.45	0.87 ± 0.06	0.30 ± 0.52	2

† 230 residues with data at the three magnetic fields were minimised using a local τ_m (model-free models *tm*0 to *tm*9 in *relax* [51, 52]).

‡ The χ^2 values were normalised by dividing the obtained value by the number of datasets used.

* Only model-free models *tm*0, *tm*1, *tm*2, *tm*3, and *tm*9 (*i.e.* with 3 parameters or less) were used for these small datasets.

2.3.4 Minimising Inconsistencies

Using the tests presented above, inconsistencies can be detected so they are not incorporated into a joint multiple magnetic field data analysis. However, it is best to minimise the potential for inconsistencies before actual recording of datasets, so recorded data can be used in totality in the subsequent analysis. There are three main factors one should pay attention to when recording R_1, R_2, and NOE: the sample itself, the effective temperature and pulse sequence parameters. Of course, these are inter-related.

2.3.4.1 Sample

Obviously, the sample should be in the same conditions throughout the complete experimental scheme. Concentration, in the case of using multiple samples, should be carefully matched as it affects the solvent viscosity, which in turn affects the global tumbling of the molecule (for example, in the absence of dimerisation, we observed a 5 % modulation of the apparent correlation time for PSE-4 when the protein concentration was changed from

0.125 to 0.5 mM, see Section 7.3, Figure 7.2, and [194]). Sample integrity, of course, should also be monitored as a macromolecule being degraded as a function of time will, among other problems, have its global correlation time being modulated, hence affecting dataset consistency.

In the case of the use of a single sample for the whole experimental scheme, a good way to assess sample integrity over time is to record a complete spin relaxation dataset at one magnetic field and, after data at other magnetic fields are recorded, record the first dataset again. This allows the comparison of the relaxation data at the start and end of the experimental scheme, allowing the detection of any change which could affect dynamics that may not be detected by ^{15}N-^{1}H 2D correlation spectra (*e.g.* a HSQC). Moreover, this allows a direct assessment of experimental error. This approach was adopted in our study of PSE-4 (see Chapter 7 and [194]) and helped discriminate between inconsistencies and time dependent modification of the sample.

In the case of multiple samples, special care must be taken to match both sample and salt concentrations as well as *pH*. As a check for these, relaxation data could be acquired at a common magnetic field for the different samples, allowing the comparison of datasets to assess the consistency of the samples used, prior to recording of data using other magnetic fields.

2.3.4.2 Temperature

As temperature affects the solvent viscosity, which in turn affects the diffusion of macromolecules in solution, temperature should be carefully calibrated. Indeed, the Einstein relation (or Einstein–Smoluchowski relation) [68, 249] clearly shows the dependence of the rotational diffusion constant ($\mathfrak{D}_{iso} = 1/(6\ \tau_m)$, see Equation 1.20, [18]) on both the temperature T and the viscosity η_{visc}:

$$\mathfrak{D}_{iso} = \frac{k_B\ T}{f_r} \tag{2.7}$$

where k_B is the Boltzmann constant and f_r, the rotational frictional drag coefficient for a

sphere of radius R, is defined as:

$$f_r = 8\,\pi\,\eta_{visc}\,R^3 \tag{2.8}$$

Standard procedures for measuring temperature with either methanol or ethylene glycol are well known. Typically, this involves measuring the chemical shift separation of OH and CH resonances in methanol (CH_3OH) or ethylene glycol ($HOCH_2CH_2OH$) as discussed in [35]. Temperature calibration is extremely important as temperature controllers within different probes generally behave differently depending on the probe vendor, model and/or generation, leading to differences in the effective temperature. See Figure 2.15 for an example of such differences between temperature controllers of different probes.

2.3.4.3 Pulse Sequence Parameters

Pulse sequence details should be carefully matched with special care for solvent suppression as differences can severely influence exchanging amides (*e.g.* solvent exposed amides).

Heat compensation schemes should be used when recording experiments potentially causing sample heating, such as R_2 measurements, to avoid any internal inconsistency again arising from temperature variations. These inconsistencies are also caused by duty cycle variations which affect probe tuning and lead to non-ideal RF pulses, hence causing a decrease in internal consistency and, indirectly, in overall consistency. These problems are increased at high magnetic field and/or short recycle delays. See Yip and Zuiderweg [292] for a discussion on this topic.

In the case of CPMG-based R_2 experiments, similar RF field strength during the CPMG pulse train should be used. The field strength should be high enough so that no important off-resonance effects arise within the datasets. However, the field strength should not be too high to avoid too much sample heating. A simple way to avoid such off-resonance effects could be the use of the modified phase cycling proposed by Yip and Zuiderweg [291]. Moreover, sample heating should be similar at all magnetic fields to avoid a modulation of R_2 (which would decrease as a function of temperature). Interleaving of the different delays in a scan by scan mode might help in stabilising the temperature within a single dataset and,

indirectly, minimise sample heating and stabilise temperature throughout acquisition at multiple magnetic fields [147]. Finally, unnecessary long relaxation delays (during which the CPMG pulse train is active) should be avoided also to reduce sample heating.

2.4 Discussion

As is demonstrated using synthetic datasets, the proposed consistency tests are field independent functions suitable for assessing consistency of multiple magnetic field datasets.

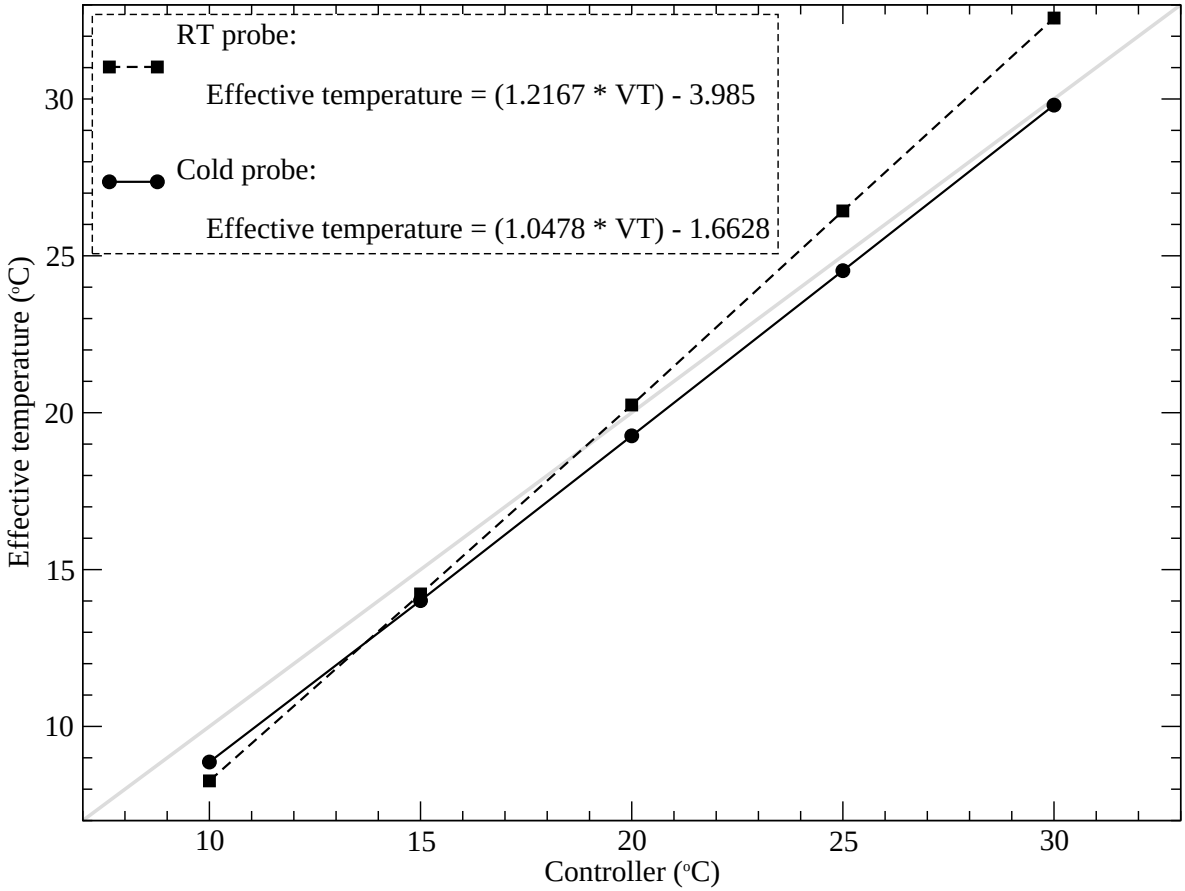

Figure 2.15: Temperature calibration for different NMR probes. Effective temperature (calibrated using methanol) as a function of the temperature set for the variable temperature (VT) controller within Varian RT (broken line and squares) and cold (solid line and circles) probes. The grey line indicates a theoretical perfect agreement between the controller temperature and the effective temperature. As can be seen, temperature on both probes is very linear ($r^2 > 0.9999$), but the slope is different, leading to potential differences in temperatures if calibration is not undertaken to assess the effective temperature in the sample.

Since local variations in R_2 caused by slow μs-ms motions are common, these tests should be used in a qualitative manner for assessing overall quality of datasets. Moreover, these tests could also be used to investigate the data for individual bond vectors.

Obviously, N-H groups affected by μs-ms motions will appear inconsistent using tests for R_2 since R_{ex} is scaled quadratically with the strength of the magnetic field. However, proteins rarely display μs-ms motions throughout their whole sequence and a majority of residues should be unaffected by such motions. Hence, once again, we point to the need for a global qualitative analysis instead of a residue focused quantitative analysis. A better option for assessing dataset consistency of such systems would be the recording of R_{ex}-free R_2 [109]. Indeed, such experiments yield the exchange-free R_2 (by quenching the effect of exchange) which should then give rise to high consistency scores in favorable conditions, irrespective of whether there are or not μs-ms motions in the particular system under study. Moreover, when such μs-ms motions are suspected because of consistency tests, experiments probing these timescales (*e.g.* CPMG or $R_{1\rho}$ relaxation dispersion experiments) should be performed.

High field effects could arise within relaxation data based on a modulation of the *CSA* constant c as a function of the magnetic field. Indeed, the *CSA* has been shown previously to vary depending on the actual N-H bond vector studied [88, 152, 264]. Assuming a value of -172 ppm for all N-H bonds, as in most spin relaxation studies, could potentially give the impression of inconsistencies at high field for some residues where the *CSA* is significantly different from -172 ppm. However, this would most probably have the effect of broadening the distribution of ratios, but not of skewing it (since the 'real' *CSA* for individual vectors should have the same chance of being lower or higher than the average value of -172 ppm), thus conserving a fairly good consistency appearance overall. Hence, we believe this should not affect consistency tests too much.

Of course, it would also be very useful to have tests for the assessment of R_1 and *NOE* data consistency. However, it turns out very difficult, if not impossible, to develop field independent functions for consistency testing purposes of R_1 and *NOE* that would also be independent of local dynamics. Indeed, contrary to R_2, R_1 and *NOE* are inter-dependent (*i.e.* they are influenced by each other) and influenced by fast motions with negligible contribution from the very slow motions probed by $J(0)$, as shown in Equations 1.1, 1.7, and 1.9. In fact, performing consistency testing on R_1 and *NOE* would require the knowledge of local dynamics which is actually why the data is recorded, hence a chicken and egg problem... However, an interesting approach to verify the approximative

consistency of R_1 and *NOE* data (as well as that of R_2 data) might be, along with consistency tests, to use the comparative approach of Reddy and Rainey [228] where synthetic data is calculated based on user variable model-free parameters. Using this approach which is implemented in a web interface, one can verify that recorded data have reasonable values for the system under study and the magnetic fields used.

We do not claim to be the first to propose ways to improve analysis of spin relaxation data. However, we think the use of these simple validation tests, in particular of $J(0)$, for the assessment of R_2 consistency within multiple field datasets will be very useful. In particular, it will reduce the extraction of erroneous μs-ms motions. Additionally, it will allow a better description of global tumbling for NMR spectroscopists using the Kay *et al.* R_2/R_1 approach [139] to determination of the isotropic correlation time τ_m, hence indirectly contributing to a better description of local motions. Overall, the use of these tests will be a valuable addition to the set of analytical tools available for spin relaxation data.

Chapter 3

Improved Analysis of NMR Dynamics: Conclusions

3.1 The Consistency of Datasets as a Pre-Requisite for the Extraction of High Quality Dynamics Information

From the limited number of published experimental datasets tested for consistency, it is clear that bias can appear in spin relaxation studies even though great care is taken to avoid such problems. This was the case in recent work on protein PSE-4 by our laboratory [194], where consistency tests helped in removing inconsistent data to allow a reliable description of protein dynamics.

Thus, we believe that the introduction of consistency tests within the analytical scheme of spin relaxation data could allow a better description of the systems studied. Indeed, when inconsistencies are seen, datasets could be excluded if other data indicates no widespread μs-ms motions are present. On the contrary, the tests could also identify when a macromolecule has widespread conformational exchange. Hence, high consistency would confirm the data is of good quality and the macromolecule is not affected by widespread conformational exchange, while low consistency would require a deeper look at the data. We propose that consistency testing should be performed prior to any joint analysis of different datasets. This includes multiple field datasets, as well as datasets recorded with different samples, such as in the case of unstable proteins.

The tests presented here apply to ^{15}N spin relaxation data (mainly R_1, R_2, and NOE) for the identification of inconsistencies within R_2. However, the same principles could apply to other spins (although large variations in the *CSA* for a given nucleus might limit their use). These tests ought to be used by anyone seelking to extract high quality data from multiple field datasets. The three consistency tests $J(0)$, F_η, and F_{R_2} are available within the program *relax* (versions 1.2.14 and higher) [51, 52].

3.2 Future Work

It will be important to encourage the community to use as much as possible these consistency tests to avoid situations where inconsistent data is analysed and gives rise to aberrant conclusions on the dynamics of the system under study.

The ease of use of this approach in the analytical scheme will certainly have a predominant role and, thus, additional work could include the semi-automation of the consistency testing procedure. Indeed, *relax* could be further improved by integrating code to handle the complete multiple field datasets, calculate $J(0)$ values, and output correlation and distribution plots of the results, along with some statistics and recommendations.

Part II

The Dynamics of Class A β-Lactamases

Chapter 4

Dynamics of Class A β-Lactamases: Introduction

4.1 Bacterial Cell Wall

One of the challenges faced by microbial organisms consists in resisting to the important osmotic pressure difference between their cytoplasm and the surrounding environment. Bacteria achieve this by synthesizing a cell wall, *i.e.* a peptidoglycan layer located outside the plasmic membrane and increasing the rigidity of the cell (see Figure 4.1). This mixed polymer is generally made of two sugar derivatives (N-acetylglucosamine and N-acetylmuramic acid) as well as different amino acids (including three amino acids not encountered in proteins: D-Ala, D-Glu, and *meso*-diaminopimelic acid) [224].

Peptidoglycan strength comes from its components forming a mesh-like structure. Many enzymes participate in the biosynthesis of this network, including DD-transpeptidases (also known as D-Ala-D-Ala carboxypeptidase-transpeptidases, or penicillin binding proteins). These enzymes participate in the last step of peptidoglycan synthesis in linking a D-Ala-D-Ala extremity from one peptidoglycan molecule to a neighbouring molecule (reviewed in [81]). This DD-transpeptidase activity is necessary throughout the cell cycle, especially during cell division when an increase in peptidoglycan synthesis is observed (reviewed in [72]). Hence, stopping (or slowing) peptidoglycan synthesis is a very efficient and specific approach to counter bacterial growth.

4.2 β-Lactam Antibiotics

Many microorganisms, in order to protect their own environment, have developed means for eliminating other organisms. β-Lactam antibiotics are molecules synthesised by fungi in order to control bacterial growth. This class of molecules was discovered more than 80 years ago by Sir Alexander Fleming in *Penicillium notatum* [82]. The molecule responsible for the activity observed by Fleming (penicillin) was purified and further investigated by Chain *et al.* [36]. A few years later (in 1945), Fleming, Chain, and Florey shared the Nobel prize for their work on penicillin. Indeed, this recent discovery had already showed its utility by saving thousands of lives during World War II. Since then, dozens of different derivatives of penicillin have been used in both medicine and agriculture.

β-Lactam antibiotics share a common structural feature: the β-lactam ring (see Figure 4.2).

This allows them to covalently bind to the active site of DD-transpeptidases and inhibit their activity, thus preventing the last step of peptidoglycan synthesis to be performed (reviewed in [44, 254, 263, 281]). This particularity gives an antimicrobial activity to β-lactams. However, there is a widespread belief in the population and among physicians that penicillin derivatives very often cause allergy. Even though penicillin derivatives cause allergic reactions, this belief of widespread allergy is exaggerated as among the 0.7–10% people with reactions to penicillin, only 10–20% are really allergic as verified by skin testing: for a total of approximately 0.07 to 2% of people allergic in the population (reviewed in [236]). Hence, with their limited number of side effects, β-lactams are very useful antibiotics for use in medicine.

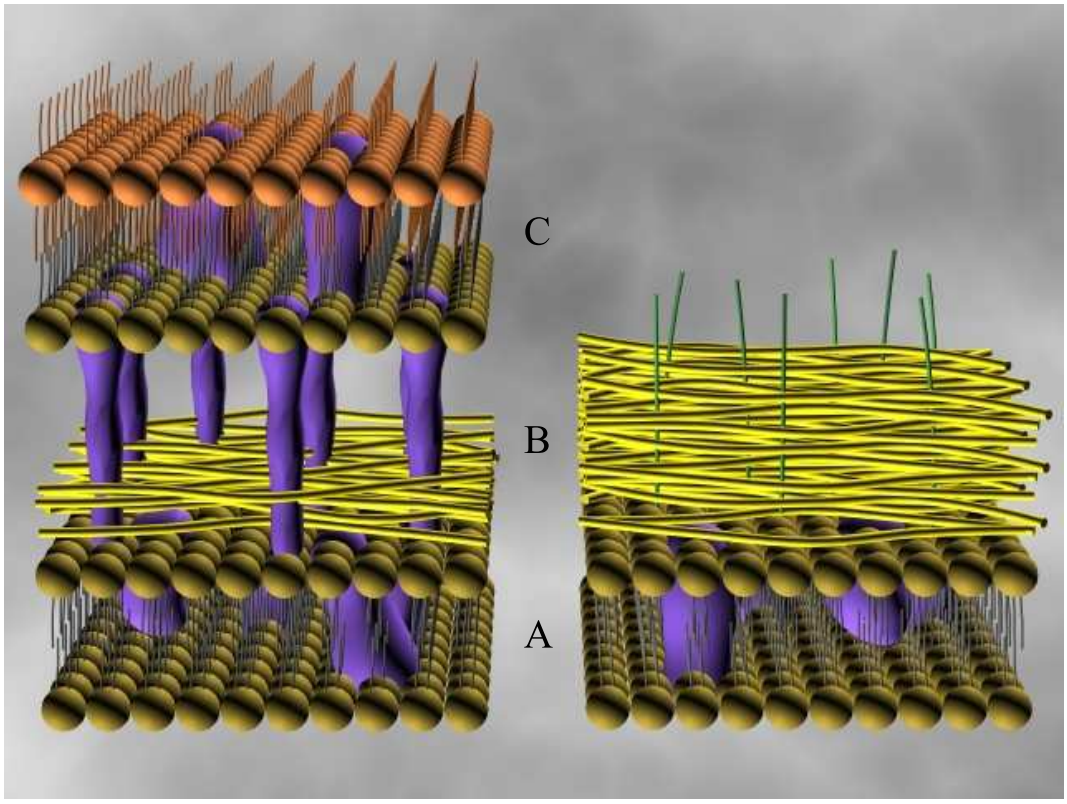

Figure 4.1: Gram$^-$ (left) and Gram$^+$ (right) bacterial cell walls. The different components are: peptidoglycan (yellow), proteins (purple), teichoic acids (green), phospholipids (brown), and lipopolysaccharides (orange). (A) The plasmic membrane is principally made of phospholipids. (B) The peptidoglycan layer gives the necessary strength to resist the high osmotic pressure from the cytoplasm. Its thickness is more important in Gram$^+$ bacteria (20–80 nm compared to 1–3 nm for Gram$^-$ bacteria) since these do not possess an external membrane. (C) The external membrane is solely present in Gram$^-$ bacteria. Different metabolic activities in Gram$^-$ bacteria take place in the periplasmic space, between the external membrane and the peptidoglycan layer. Figure from http://www.ppws.vt.edu/%7Esforza/agro/agro.html with kind permission from Peter Sforza.

4.3 Antibiotics Resistance

Antibiotics resistance was developed either by the organisms producing the β-lactams to be protected from their own weapons or by the target organisms to survive enemies producing β-lactams (reviewed in [81]). Different strategies were developed (reviewed in [81]):

- Mutations in β-lactams targets (*i.e.* the DD-transpeptidases);
- Modifications in the cell wall structure to prevent β-lactams access to their target;
- Deletion of membrane porines to prevent β-lactams entry in the cell;

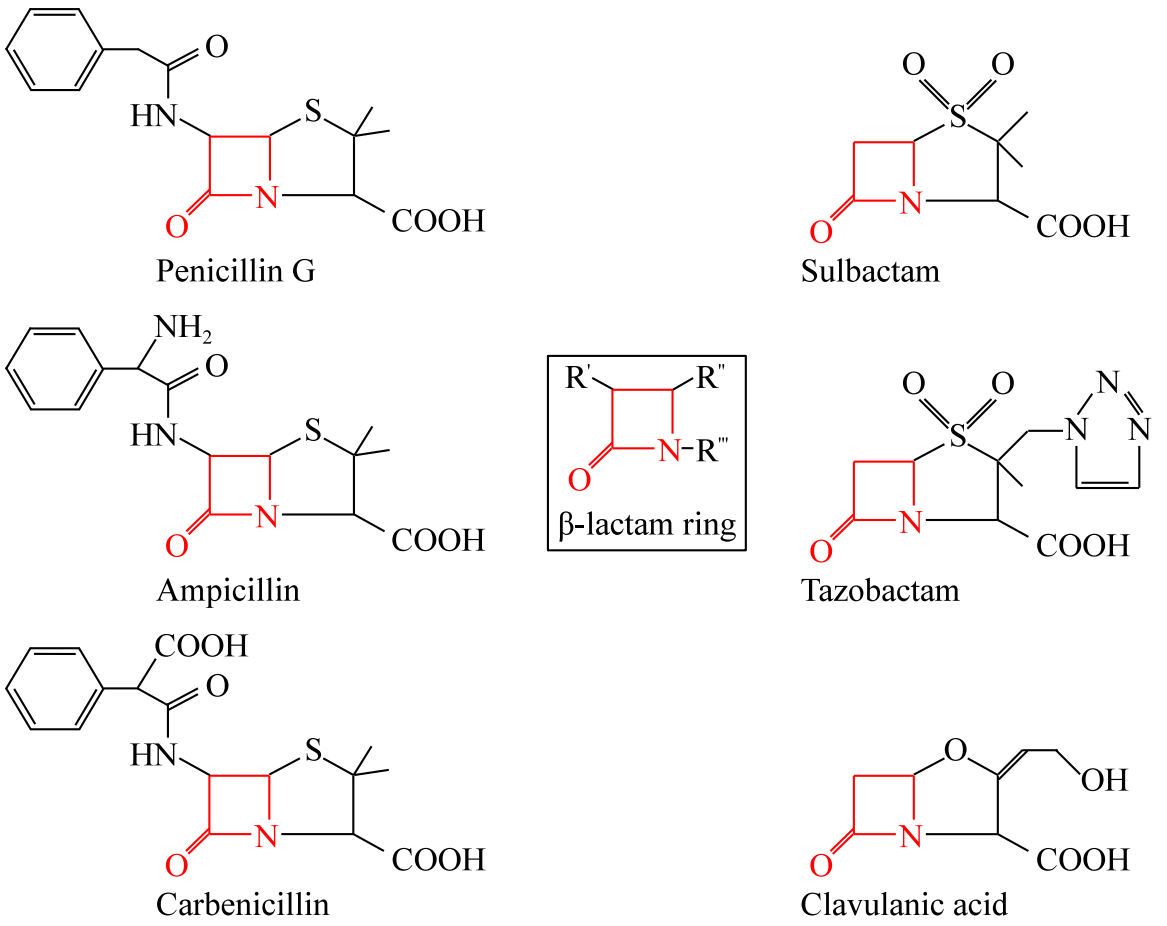

Figure 4.2: Structure of different β-lactam antibiotics (penicillin G, also known as benzylpenicillin, ampicillin, and carbenicillin) and β-lactamase inhibitors (sulbactam, tazobactam, and clavulanic acid). The β-lactam ring is shown in red with the possible substituents as R', R", and R"'.

- Production of efflux proteins to export β-lactams outside the cell wall;
- Production of proteins acting as β-lactam inhibitors;
- Production of proteins hydrolysing β-lactams (β-lactamases).

Selective pressure for resistance to β-lactam antibiotics (either natural or caused by the use of antibiotics in medicine and agriculture) has supported the widespread dissemination of these mechanisms (reviewed in [284]). This process has been extensively accelerated by the fact that the genes for many of these mechanisms are located on mobile genetic elements such as plasmids and integrons (reviewed in [53]).

4.4 β-Lactamases

The main resistance mechanism against penicillin-derived molecules (*i.e.* the β-lactams) is the production of enzymes, the β-lactamases, able to cleave the four-membered β-lactam ring [81]. β-Lactamase enzymes are divided in four classes based on their primary structure: A, B, C, and D [7, 128, 209]. Another classification scheme is based on their functional characteristics (substrate profile and inhibitor susceptibility) where β-lactamases are divided in four principal groups [27].

Classes A, C, and D are serine-catalytic, whereas enzymes from class B use (generally) one or two Zn^{2+} ions for catalysis. These β-lactamases with a catalytic serine have, as common ancestors, the DD-transpeptidases. Indeed, these different groups of enzymes are structurally and catalytically close. β-lactamases from classes A, C, and D most probably acquired the catalytic activity against β-lactams in order to avoid being irreversibly bound to these molecules, such as is the case for DD-transpeptidases (reviewed in [145]).

Enzymes from class A (which include most ESBLs) are the most often found [178]. They represent a diverse class of proteins in terms of substrate specificity. Moreover, these enzymes are highly effective catalysts. Indeed, the specific activity of several of these enzymes (*e.g.* β-lactamase I, PC1, and TEM-1) is diffusion-controlled [37].

4.4.1 Class A β-Lactamases

Class A β-lactamases have a MW of approximately 30 kDa. Their structure is made of two domains (one all α and one α/β) packed against each other and at the interface of which lies the active site (see Figures 4.3 and 4.4). This active site is constructed using different residues including Ser^{70}, Lys^{73}, Ser^{130}, Glu^{166}, and Lys/Arg^{234}.

Class A β-lactamases are closely related to DD-transpeptidases as was first observed by Tipper and Strominger back in 1965 [263]. In fact, their structures near the active site are conserved with four important motifs shared by the two groups of enzymes [129]:

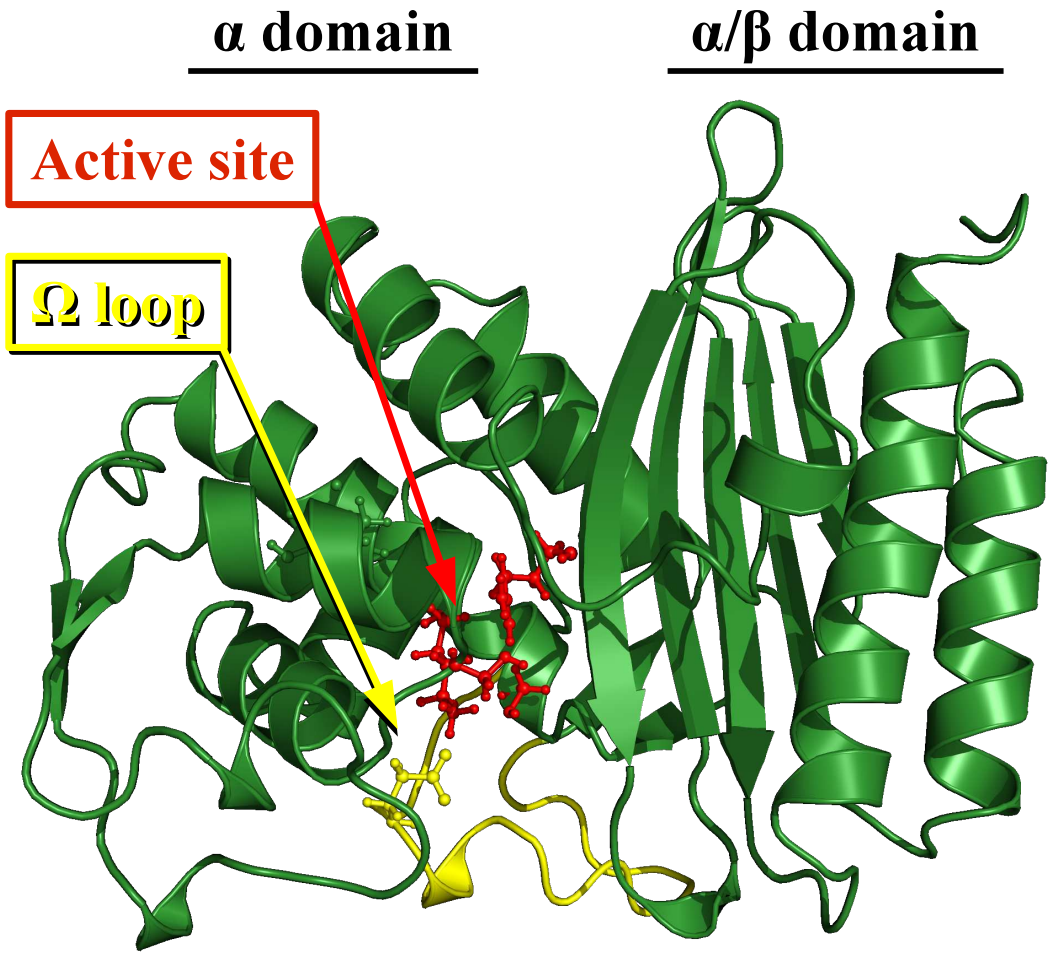

Figure 4.3: Structure of class A β-lactamases. Active site residues (Ser^{70}, Lys^{73}, Ser^{130}, Glu^{166}, and Arg^{234}), and the disulfide bond (between Cys^{77} and Cys^{123}, connecting two helices of the α domain) are shown in the stick representation on the structure of the class A β-lactamase PSE-4 (PDB 1G68, [165]).

- The strictly conserved Ser^{70}-X-X-Lys^{73} tetrad;
- The Ω loop (residues 161 to 179);
- The 'SDN' loop formed by residues Ser^{130}, Asp^{131}, and Asn^{132};
- The less conserved 'KTG' motif formed by residues Lys^{234}, Thr^{235}, and Gly^{236}, where residue 234 is replaced by an Arg in certain sub-classes of class A β-lactamases, and residue 235 is generally a Ser in class A β-lactamases.

4.4.1.1 Catalytic Mechanism of Class A β-Lactamases

The general mechanism of class A β-lactamases is composed of two steps, akin to that of serine proteinases [111]. First, catalytic Ser^{70} makes a nucleophilic attack on the carbonyl of the β-lactam ring [31, 41, 80]. This creates a tetrahedral intermediate and leads to the hydrolysis of the β-lactam ring (*i.e.* the breakage of its amide bond) [81]. The process is similar when β-lactam antibiotics inactivate their target (*i.e.* the DD-transpeptidases), ending up in an inactive acyl-enzyme complex which stops bacterial cell growth and leads to cell death. The second step, deacylation (virtually absent for DD-transpeptidases), consists in a nucleophilic attack by a H_2O molecule activated by the Ω loop conserved residue Glu^{166} [2, 32, 73, 116, 173, 191]. This leads to the hydrolysis of the acyl-enzyme complex and release

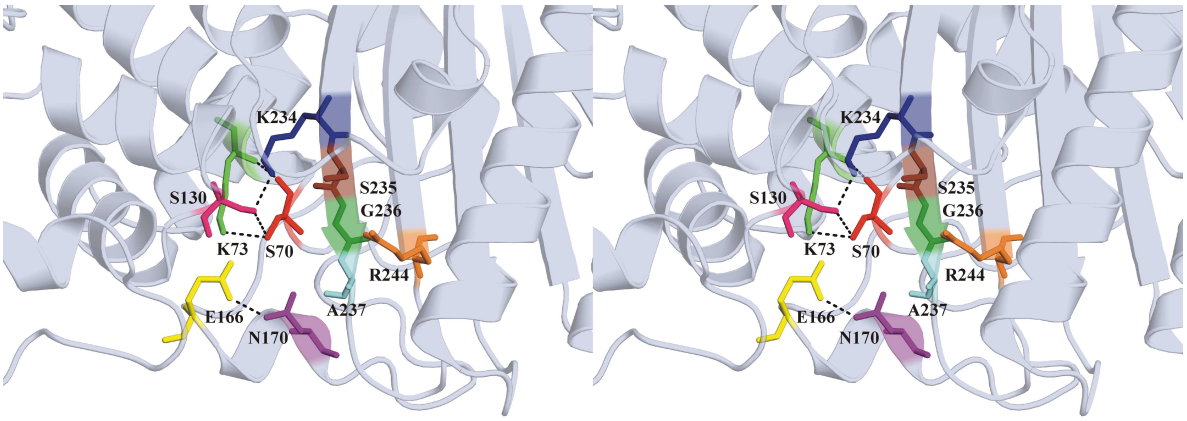

Figure 4.4: Stereoview of the active site of class A β-lactamases. Important catalytic residues are shown in the stick representation and H bonds are displayed with dashed lines using TEM-1 structure 1ERQ [199]. This figure is a generous gift from Pierre-Yves Savard and was originally published in his Ph.D. thesis [239].

of the hydrolysed β-lactam. Figure 4.5 depicts the overall general catalytic mechanism of class A β-lactamases.

However, to first attack the β-lactam ring, the catalytic Ser^{70} must have its hydroxyl proton accepted by a general base. The identity of this activator is controversial. One hypothesis involves Lys^{73} as the general base [116, 163, 173, 255]. For this hypothesis to be valid, the pK_a of the Lys would need to be under 10, *i.e.* Lys^{73} would need to be deprotonated in order to attract a proton from Ser^{70}.

Another hypothesis involves Glu^{166} [95, 155, 156] (reviewed in [81]). In this case, Glu^{166} would have a role similar to His^{57} in serine proteinases [23]. For this mechanism to be possible, Glu^{166} would need an abnormally high pK_a and would thus be protonated at physiologic *pH* (which seems to be the case from an ultrahigh resolution structure of TEM-1 [190]). Moreover, the Ω loop would need to possess a high flexibility [234, 271] or there would need a water molecule to serve as relay between Glu^{166} and Ser^{70} [9, 46, 65, 104, 112, 115, 155, 190].

Other hypotheses propose the involvement of Ser^{130} and/or the carboxyl group of the β-lactam [9, 59, 67, 203, 286].

A model has emerged recently in which a duality of mechanisms was shown for tetrahedral formation (*i.e.* acylation) [184]. In this model, the activation process depends on the

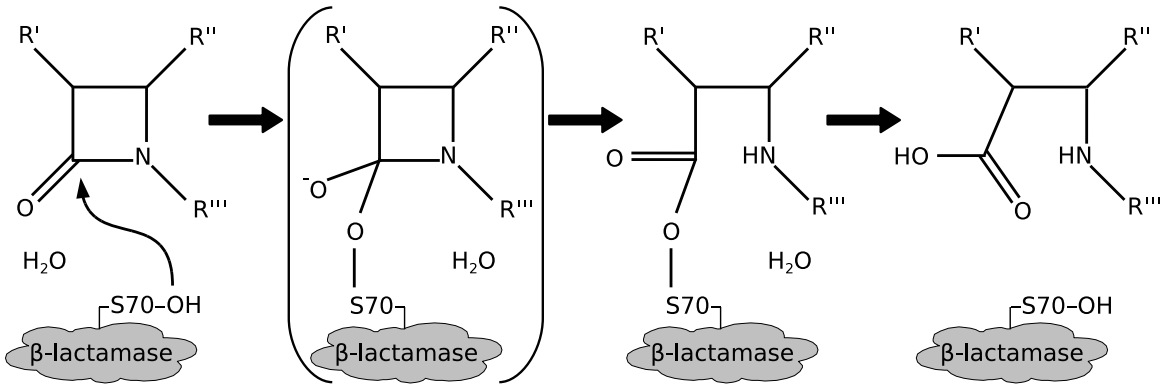

Figure 4.5: Catalytic mechanism of class A β-lactamases. Ser^{70} proceeds to the nucleophilic attack of the carbonyl on the β-lactam ring. This creates a tetrahedral intermediate which, upon the amide bond breakage, leads to an acyl-enzyme complex. Finally, after deacylation, the hydrolysed β-lactam compound is released.

β-lactamase/β-lactam combination and is a competition between mechanisms involving either Glu^{166} or Lys^{73} as the general base for activation of Ser^{70}. This kind of dual mechanism could reconcile different contradictory studies. It could also explain the high activity of class A β-lactamases where certain members, such as TEM-1 (see below) are diffusion-limited (*i.e.* their catalytic rate being limited by entry and expulsion of the substrate in and out of the active site, with $k_{cat}/K_M \sim 10^7$-10^8 $s^{-1}M^{-1}$) [165, 226].

4.4.1.2 Ambler Numbering Scheme

The numbering of residues within class A β-lactamases follows a standard numbering scheme introduced by Ambler *et al.* [8]. Using this scheme, the most important residues are numbered the same within different enzymes. A consequence of this is the presence of apparent gaps within the sequences, *i.e.* sequence numbers for which there are no residue. Additionally, since class A β-lactamases have a signal peptide (also known as leader peptide) for exportation outside the cell, the numbering of the mature proteins generally does not start at 1. The Ambler numbering scheme is very useful when comparing different class A β-lactamases and is used throughout this document.

4.4.1.3 TEM-1

The penicillinase TEM-1 is the most often found class A β-lactamase in cases of resistance to penicillins and cephalosporins (reviewed in [85, 176, 177, 278]). It is the model enzyme for class A β-lactamases and has been studied extensively, Indeed, dozens of studies have been performed on TEM-1, either using standard biochemical approaches (reviewed, among others, by [22, 26, 27, 81, 94, 106, 176–178, 221, 260]), X-ray crystallography (see Table 4.1 for an exhaustive listing), MD (including QM/MM) [29, 65, 66, 79, 112, 113, 115, 184, 185, 234], and NMR [46, 62, 240, 241].

TEM-1-like β-lactamases being the major cause for resistance against β-lactam antibiotics, a database has been launched recently in order to classify the different variants either observed clinically or designed in laboratory. This Lactamase Engineering Database [258] reconciles data from both the NCBI protein database and TEM mutation table (website hosted by Lahey Clinic).

Table 4.1: Structures of the class A β-lactamase TEM-1. †

PDB	Mutation(s)	Ligand/Complex ‡	Resolution (Å)	Year*	Reference
1BTL	$V^{84}I$, $A^{184}V$	SO_4^{2-}	1.80	1995	[129]
1XPB		SO_4^{2-}	1.90	1997	[83]
1TEM	$V^{84}I$, $A^{184}V$	Penicillate ALP	1.95	1997	[179]
1AXB	$V^{84}I$, $A^{184}V$	Inhibitor FOS	2.00	1998	[181]
1BT5	$V^{84}I$, $A^{184}V$	Imipenem, SO_4^{2-}	1.80	1999	[180]
1CK3	$V^{84}I$, $A^{184}V$, $N^{276}D$		2.28	1999	[256]
1ESU	$S^{235}A$	SO_4^{2-}	2.00	2000	[83]
1FQG	$E^{166}N$	Penicillin G	1.70	2000	[255]
1ERQ		Inhibitor BJH	1.90	2000	[199]
1ERO		Inhibitor BJP	2.10	2000	[199]
1ERM		Inhibitor BJI	1.70	2000	[199]
1HTZ[1]	$E^{104}K$, $M^{182}T$, $G^{238}S$		2.40	2001	[207]
1JTG		Ca^{2+}	1.73	2001	[164]
1JTD		BLIP-II	2.30	2001	[164]
1L19	$M^{69}V$	K^+, PO_4^{3-}	1.52	2002	[280]
1JWZ[2]	$E^{104}K$, $R^{164}S$, $M^{182}T$	Inhibitor 105	1.80	2002	[278]
1LHY[3]	$R^{241}S$	PO_4^{3-}	2.00	2002	[280]
1LI0[4]	$M^{69}I$, $M^{182}T$	CHO_3^-, K^+	1.61	2002	[280]
1LI9[5]	$M^{69}V$	K^+, PO_4^{3-}	1.52	2002	[280]
1JWV	$G^{238}A$	Inhibitor CB4, K^+	1.85	2002	[278]
1JWP	$M^{182}T$	PO_4^{3-}	1.75	2002	[278]
1M40	$M^{182}T$	Inhibitor CB4, K^+, PO_4^{3-}	0.85	2002	[190]
1JVJ	$N^{132}A$	Imipenem, K^+	1.73	2002	[279]

Table 4.1: Structures of class A β-lactamase TEM-1 (continued). †

PDB	Mutation(s)	Ligand/Complex ‡	Resolution (Å)	Year *	Reference
1NYM	$M^{182}T$	Inhibitor CXB, K^+, PO_4^{3-}	1.20	2003	[277]
1NY0	$M^{182}T$	Inhibitor NBF, K^+, PO_4^{3-}	1.75	2003	[278]
1NXY	$M^{182}T$	Inhibitor SM2, K^+	1.60	2003	[278]
1NYY	$M^{182}T$	Inhibitor 105	1.90	2003	[277]
1SOW		BLIP	2.30	2004	[230]
1PZP	$R^{100}N$	Inhibitor FTA	1.45	2004	[117]
1PZO	$M^{182}T$	Inhibitor CBT	1.90	2004	[117]
1ZG4	$V^{84}I$, $A^{184}V$		1.55	2005	[252]
1XXM	$E^{104}A$, $Y^{105}A$	BLIP, Ca^{2+}	1.90	2005	[230]
1ZG6	$S^{70}G$		2.10	2005	[252]
1YT4[6]	$S^{130}G$		1.40	2005	[262]
2B5R	$V^{84}I$, $E^{104}Y$, $Y^{105}N$	BLIP	1.65	2006	[229]
3C7U	$W^{150}A$	BLIP	2.20	2008	[276]
3C7V	$Y^{51}A$	BLIP	2.07	2008	[276]
3CMZ	$L^{201}P$	PO_4^{3-}	1.92	2008	[175]
3DTM	$P^{62}S$, $V^{80}I$, $E^{147}G$, $M^{182}T$, $L^{201}P$ $I^{208}M$, $A^{224}V$, $I^{246}V$, $L^{273}R$		2.00	2008	[135]
3GMW		BLIP-I, PO_4^{3-}	2.10	2009	[98]
3JYI	$N^{170}G$	Inhibitor EPE, PO_4^{3-}	2.70	2009	[24]

† Adapted (and updated) with permission from Pierre-Yves Savard [239].

‡ Abbreviations are defined starting at Page xvi.

* Year deposited in the PDB with structures ordered chronologically based on this date.

Mutants also known as TEM-52[1], TEM-64[2], TEM-30[3], TEM-32[4], TEM-34[5], and TEM-76[6].

The standard numbering scheme for TEM-1 starts at residue 26 and ends, after 263 residues (28.9 kDa) and two gaps (at positions 239 and 253), at residue 290.

4.4.1.4 PSE-4

PSE-4 enzyme was originally found in *Pseudomonas aeruginosa* [86, 200, 201], an opportunistic pathogen often found in cystic fibrosis patients, but was soon found in non-pseudomonal strains [231]. Its discovery closely followed the beginning of use of the penicillin derivative carbenicillin (originally marketed as Pyopen by Beecham, see Figure 4.2) [169]. PSE-4 is expressed in the periplasm of different Gram$^-$ bacteria (see Figure 4.1). It is the model enzyme for the subclass of carbenicillin hydrolysing class A β-lactamases (subgroups 2c and 2d of the Bush-Jacoby-Medeiros functional classification scheme [27]) and was, in 1990, the most widespread β-lactamase in carbenicillin resistant strains of *Pseudomonas aeruginosa* [20]. Hence, PSE-4 contributes to the multi-resistant phenotypes of *Pseudomonas aeruginosa* (reviewed in [253]).

Levesque and coworkers were the first to isolate and sequence the gene encoding PSE-4 [19, 20]. Using the Ambler numbering scheme [8], mature PSE-4 starts at residue 22 and ends, after 271 residues (29.5 kDa) and three gaps (at positions 58, 239, and 253), at residue 295. Following these advances, kinetics and mutational studies were made easier and several publications followed on PSE-4. Many of these publications are discussed below.

In order to investigate substrate specificity modulation, Therrien *et al.* [261] made mutations for residues 162–179 of the Ω loop. Indeed, it had been observed that this region of the protein was responsible for substrate specificity in TEM-1 [110, 215, 216, 222]. However, upon random mutations in its Ω loop, PSE-4 did not acquire activity toward new antibiotics or inhibitors. Nevertheless, residues 162–164 and 165–167 were shown to have a more important effect on ampicillin hydrolysis compared to carbenicillin. Similar results were obtained when the Ω loop from either TEM-1, SHV or *Streptomyces albus* G β-lactamase replaced the Ω loop in PSE-4 [238]: the mutants had MICs and kinetic properties similar to wild-type PSE-4 (*i.e.* no important effect was observed).

In one study, a library of random mutations was prepared for residues 216–218 located in a loop bordering the active site [235]. One particular mutant (Val^{216}Ser, Thr^{217}Ala, Gly^{218}Arg) showed an increase in the K_M for both carbenicillin and ampicillin (see Figure 4.2) as well

as an increase in the K_i for sulbactam and tazobactam (see Figure 4.2), both penicillanic acid sulfone inhibitors. This contrasted observations made in TEM-1 where residues Val^{216} and Ala^{217} do not tolerate substitution [118].

In 2000, Therrien *et al.* [259] characterised the inhibition of PSE-4 by the three clinically-used mechanism-based inhibitors: sulbactam, clavulanic acid, and tazobactam (see Figure 4.2). The three molecules were shown to cause irreversible inhibition of PSE-4, with tazobactam displaying the highest affinity. Moreover, the partition ratios (k_{cat}/k_{inact}) were all lower than previously observed for TEM-1 [28, 123, 124] indicating the greater susceptibility of PSE-4 against these inhibitors. These were good news.

In another study, mutations were made in the region including residues 125–129 [242]. It was observed that mutations in this region (within an α helix close to the active site, right next to the loop of residues 216–218) were sensitive to activity towards mechanism-based suicide inhibitors (*i.e.* sulbactam, clavulanic acid, and tazobactam, see Figure 4.2), with clavulanic acid as the most affected by these mutations. Moreover, residue Met^{127} was shown to be invariant, while Ala^{125} was more tolerant. This was different than in TEM-1 where mutations to Ala^{125} were not tolerated [118].

The crystal structure of PSE-4 was solved in 2001 [165] (see Table 4.2). Besides PSE-4 having a high sequence identity with TEM-1 (41.5 %), its structure (composed of two domains: an all α and an α/β domain, as in other class A β-lactamases) is also very close to that of TEM-1 with a backbone RMSD of only 1.3 Å. Figure 4.3 displays most of PSE-4 structural features. What distinguishes PSE-4 (and other carbenicillinases) from non-carbenicillinases (such as TEM-1), however, is the mutation $Lys^{234}Arg$. This change confers its enlarged specificity to PSE-4, placing it in group 2c of carbenicillin hydrolysing β-lactamases inhibited by clavulanic acid [27]. Indeed, the two structures solved for PSE-4 (PDB 1G68 and 1G6A, see Table 4.2, [165]) showed that the substitution of a Lys to an Arg residue at position 234 in PSE-4 prevents a clash between the α-carboxyl group of the carbenicillin molecule and Asn^{170} by allowing a different conformation for Ser^{130}. Indeed, the k_{cat}/K_M for carbenicillin hydrolysis is reduced by a factor of 50 in the $Arg^{234}Lys$ mutant compared to wild-type PSE-4, whereas the effect on penicillin and ampicillin hydrolysis is less than fivefold [165, 242]. Since the publication of this crystal structure in 2001, no other studies on PSE-4, prior to ours, has been released.

Table 4.2: Structures of the class A β-lactamase PSE-4.

PDB	Mutation	Ligand	Resolution (Å)	Year†	Reference
1G68		SO_4^{2-}	1.95	2000	[165]
1G6A	$R^{234}K$	SO_4^{2-}	1.75	2000	[165]

† Year deposited in the PDB.

4.4.1.5 Dynamics in Class A β-Lactamases

Several MD, QM/MM, and NMR studies have been performed to get insights into the relation between function, structure, and dynamics in the class A β-lactamase TEM-1 [29, 65, 66, 79, 112, 113, 115, 184, 185, 234]. These different studies used methods which have evolved over time to look at different aspects of TEM-1 dynamics.

To our knowledge, the first modern MD study on TEM-1 was performed by Meroueh *et al.* in 2002 [185]. Simulations were performed on wild-type TEM-1 and the inhibitor-resistant mutant $Met^{69}Leu$ (also known as TEM-33) for 2 ns. Dynamics of the two variants were very similar and differed only in short regions suggesting that the $Met^{69}Leu$ mutation would be the less destructive mutation conferring inhibitor resistance.

Following this study, Díaz *et al.* presented two MD simulations of 1 ns each for TEM-1 and its complex with benzylpenicillin [65]. These authors concluded that the Ω loop was rigid with a structural water molecule between Ser^{70} and Glu^{166} not exchanging with bulk water during the simulations. The simulation in the presence of substrate did not yield additional insights from a dynamic point of view. However, by analysing the detailed structure of TEM-1 and its bound substrate in the course of the simulation, they could propose two different hypotheses for activation of Ser^{70}: either by Glu^{166} helped with a structural water molecule, or by the substrate carboxylate helped by Ser^{130}.

An interesting QM/MM study was published in 2003 by Hermann *et al.* [115]. The authors studied the acylation step of the mechanism and concluded that Ser^{70} is activated by Glu^{166} acting as the general base via a water molecule, similarly as proposed earlier by Díaz *et al.* [65], but with further data to prove the hypothesis.

Another QM/MM study was performed to compare TEM-1 with two DD-transpeptidases [204], all in the presence of substrates. The two mechanisms proposed earlier and involving

either Glu^{166} or the carboxylate moiety of the substrate as the general base were shown consistent with the simulations. Additionally, pK_a calculations indicated that Lys^{73} would be protonated at physiological *pH*, hence contradicting the model involving this residue as the general base activating Ser^{70} prior to acylation.

Later, a MD study focused on elucidating the preference of TEM-1 for benzylpenicillin over cephalosporin [66]. It was concluded that this preference is due to the higher efficacy of benzylpenicillin to bind both the 'carboxylate pocket' (formed by residues Ser^{130}, Lys^{234}, Ser^{235}, and Arg^{244}) and 'oxyanion' hole (formed by the backbone of residues Ser^{70} and Ala^{237}) at the same time.

In 2005, Hermann *et al.* realised other QM/MM simulations in order to characterise further the acylation step for TEM-1 in the presence of benzylpenicillin [112]. Their conclusions were similar to their 2003 study [115], although with additional details. In particular, the 'oxyanion hole' (residues Ser^{70} and Ala^{237}) was observed to be especially important for stabilisation of the transition state and tetrahedral intermediate. Residue Asn^{132}, different positively charged residues close to the active site and the 'carboxylate pocket' (Ser^{130}, Lys^{234}, Ser^{235}, and Arg^{244}) were also shown as important for this stabilising effect.

The same year, in a 5 ns MD study of TEM-1, Roccatano *et al.* observed a flap-like motion of the Ω loop towards the protein core [234]. This motion would fill a cavity and potentially stabilise residue Glu^{166} of the Ω loop in a catalytically efficient position near Ser^{70}. Also, based on H bonding patterns, the authors speculated that acylation might be possible through different mechanisms. This new hypothesis would reconcile the different contradicting mutational, kinetics, structural, and *in silico* studies by allowing more than one single avenue to acylation.

As stated before in Section 4.4.1.1, Meroueh *et al.* performed a QM/MM study on TEM-1 and observed a duality of competing mechanisms for Ser^{70} activation: either through Lys^{73} or Glu^{166} [184]. These results confirmed speculations by Roccatano *et al.* [234] and were consistent with previous mutational studies, thus apparently solving the controversy concerning the acylation step within class A β-lactamases.

In 2006, Hermann *et al.* studied the deacylation step with QM/MM approaches. Their work yielded further details on the widely accepted hypothesis of Glu^{166} acting as the general base in this second step of β-lactam hydrolysis by class A β-lactamases. As they concluded from

their data, this process would happen through a conserved water molecule.

Prior to our studies of PSE-4, the dynamics of only one class A β-lactamase, again TEM-1, had been characterised by NMR. Savard and Gagné [240] demonstrated that TEM-1 is a very rigid protein on the ps-ns timescale. This rigidity is especially significant in the vicinity of the active site, suggesting that substrate binding should not trigger any important unfavorable loss in conformational entropy. In other words, if ligand binding affects ps-ns motions, it should more probably reduce order, *i.e.* induce a favorable increase in conformational entropy (as opposed to rigidify the active site). Also, *μ*s-ms motions were observed around the active site and Ω loop. Further insights into TEM-1 dynamics from NMR were obtained by a study on the comparative dynamics of the wild-type enzyme with the mutant $Tyr^{105}Asp$ [62]. It was shown that this single point mutation affected the dynamics of several active site residues and, thus, could have long-range allosteric effects on the dynamics of the protein. This suggested that motions in TEM-1 might be at least partly concerted.

Feeding the controversy on the acylation step, Hermann *et al.* published a QM/MM study of wild-type TEM-1 and the mutant $Lys^{73}Ala$ [113]. They concluded that the general base in the acylation step is Glu^{166} while Lys^{73}'s role would be limited to a stabilising effect on the transition state, as proposed earlier for other residues [115]. The authors proposed that this role, in conjunction with a proton shuttle role in later stages of the reaction [114], would explain the decreased acylation rates of mutants at position 73. Data from a similar study on a Glu^{166} mutant would have been interesting in rationalising these conclusions and assessing their validity in the context of the dual mechanism proposed by Meroueh *et al.* [184].

A MD study published the same year dealt with general dynamics as the authors extracted root mean-square fluctuations and S^2 parameters from their 50 ns (10 x 5 ns) simulation [29]. Similar to the results of Savard and Gagné [240], secondary structure elements were very ordered, as well as the Ω loop, except for residues 173–177 which moved to open and close a cavity between the Ω loop and protein core. This motion was similar to the flap-like motion of Roccatano *et al.* discussed above [234]. The absence of motion for the rest of the Ω loop was explained by a network of water molecules in the cavity between the Ω loop and residues 65–69.

The dynamic study of TEM-1 published most recently was by Fisette *et al.* in our laboratory [79]. The study included a re-analysis of NMR data from Savard and Gagné [240] in the context of a new 60 ns (3 x 20 ns) MD simulation. These are the longest MD simulations

ever performed on TEM-1. As observed earlier by NMR, MD results showed that TEM-1's active site is highly ordered on the fast timescales probed by MD. Moreover, motion of part of the Ω loop was observed, which could have impact on the catalytic mechanism of class A β-lactamases. Indeed, this motion partially fills a cavity between the Ω loop and the protein core, which could stabilise Glu^{166} in a catalytically efficient position. This is similar to the proposal by Roccatano *et al.* [234] and Bös and Pleiss [29], although the exact motion is different. Indeed, the motion observed by Fisette *et al.* is better characterised, thanks to the simulation length (3 x 20 ns), and thus more realistic. In particular, the motion is more complex compared to the simple flap-like motion proposed earlier from 5 ns simulations.

From the previous studies of the dynamics in class A β-lactamases, it is clear that insights can be obtained into the function of these important enzymes using approaches to investigate protein dynamics. Hence, a deeper understanding of structure, dynamics and function in β-lactamases, especially the knowledge of the motions near the active site, should provide additional information yielding to a better mechanistic understanding to complement the extensive, already available data.

4.5 Objectives of this Work

The work presented in this second part of the thesis concerned principally the characterisation of the dynamics of the class A β-lactamase PSE-4. Although this work was of a descriptive nature (as opposed to hypothesis-driven), the following specific objectives were pursued:

- Overexpression and purification of PSE-4;
- Assignment of backbone ^{1}H, ^{13}C, and ^{15}N chemical shifts;
- Titration of Lys^{73};
- Characterisation of fast dynamics from ^{15}N spin relaxation;
- Characterisation of slow dynamics from ^{15}N relaxation dispersion;
- Characterisation of protein stability from amide exchange experiments;
- Study of PSE-4/TEM-1 chimeras.

In the following chapters, results are presented in order to fulfill most of these different research objectives.

Chapter 5

Dynamics of Class A β-Lactamases: PSE-4 Backbone Resonance Assignments

PSE-4, the model enzyme for carbenicillinases, is an especially interesting target for NMR characterisation as it gives rise to spectra of very high quality despite its 271 residues. Here we report the overexpression, purification, and backbone resonance assignments for PSE-4. The TROSY versions of several 3D heteronuclear experiments were used, and more than 98 % of backbone nuclei (including C_β) have been assigned. Backbone ^{1}H, ^{13}C, and ^{15}N resonances have been deposited in the BMRB (under accession number 6838).

5.1 Context

In order to extract information on PSE-4 with atomic resolution using NMR, PSE-4 was overexpressed and its backbone resonances were assigned.

5.2 Methods

5.2.1 Overexpression and Purification

Recombinant PSE-4 fused to the signal peptide ompA [93] was inserted in the pEt24 plasmid (Novagen, Gibbstown, NJ) and overexpressed in *Escherichia coli* BL21 DE3 (Stratagene, La Jolla, CA) for $\sim$ 20 h under 0.4 mM IPTG at 25 °C in modified M9 minimal medium [237].

The first part of the purification involved recovering the enzyme from the cytoplasm but also, to a smaller extent, from the supernatant where a portion of the PSE-4 production was sent due to its signal peptide. However, contrary to the homologous protein TEM-1, which is completely exported outside the bacteria with the use of the ompA signal peptide, the effect was incomplete for PSE-4. The purification involved two chromatographic steps: an anion exchange (HiPrep 16/10 Q XL, GE Healthcare, Piscataway, NJ) step to enrich the sample in PSE-4 and a gel filtration (HiLoad 26/60 Superdex 75 prep grade, GE Healthcare) step to achieve optimal purity. Finally, PSE-4 was lyophilised and its identity was confirmed by electrospray ionisation mass spectrometry which also served for evaluation of the extent of isotopic labelling.

Four different samples were prepared:

- [^{15}N]-labelled,
- [^{13}C, ^{15}N]-labelled,
- [^{2}H, ^{13}C, ^{15}N]-labelled,
- [^{15}N]-Thr and [^{13}C-^{15}N]-Lys-labelled.

Table 5.1: Amino acid supplemented M9 medium (based on McIntosh and Dahlquist [182])

Amino acid	Concentration (mg/L)	Amino acid	Concentration (mg/L)
A	600	N	200
C	200	P	200
D	200	Q	380
E	550	R	380
F	80	S	500
G	500	V	100
H	200	W	200
I	100	Y	80
L	80	K (^{13}C-^{15}N)	110
M	160	T (^{15}N)	150

The specifically [^{15}N]-Thr and [^{13}C-^{15}N]-Lys-labelled sample was produced using M9 minimal medium supplemented with the different amino acids, either labelled ([^{15}N]-Thr and [^{13}C-^{15}N]-Lys) or not, with quantities based on McIntosh and Dahlquist [182]. Exact quantities were as in Table 5.1.

Throughout the purification scheme, PSE-4 was followed (qualitatively) with the use of the chromogenic cephalosporin nitrocefin (see Figure 5.1, [202]). Indeed, upon hydrolysis of this cephalosporin by a β-lactamase like PSE-4, nitrocefin color will change from yellow to red allowing hydrolysis to be monitored qualitatively. The use of nitrocefin also helped a lot in optimising purification conditions.

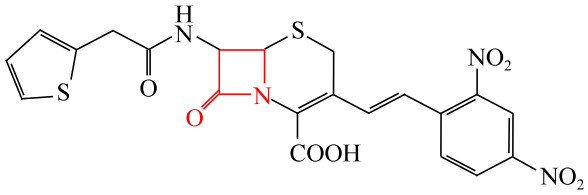

Figure 5.1: Structure of the chromogenic cephalosporin nitrocefin. As in Figure 4.2, the β-lactam ring is shown in red.

5.2.2 NMR Spectroscopy

The NMR samples contained 0.6 mM protein at *pH* 6.65 (as confirmed with imidazole chemical shifts, [12]), 0.1 mM DSS, 3 mM imidazole, 0.1% sodium azide, 10% D_2O, and a proteinase inhibitor cocktail (Complete protease inhibitor cocktail from Roche Applied Science, Laval, QC). Measurements were performed on a Varian INOVA 600 MHz spectrometer at 30 °C in normal length tubes and in Shigemi tubes. TROSY [220] versions of HSQC [138] and of several 3D experiments (HNCO [102, 122, 141, 197], HN(CA)CO [288], HNCA [102, 122, 141, 197], HN(CO)CA [288], CBCA(CO)NH (also known as HN(CO)CACB) [101], and HNCACB [141, 197, 285]) from Biopack (Varian Inc, Palo Alto, CA) were used with protonated or deuterated samples for sequential assignments. The different spectra were recorded using their sensitivity enhanced versions [138, 274]. Spectral widths were as follows for ^{1}H and ^{15}N dimensions, respectively: 10000 and 1529 Hz. For the different triple resonance spectra, the spectral widths for ^{13}C varied as follows: 4100 Hz (HNCA and HN(CO)CA), 10858 Hz (HNCACB and HN(CO)CACB), and 2200 Hz (HNCO and HN(CA)CO).

Spectra were processed with *NMRPipe* [55] and analysed within *NMRView* [131] using *Smartnotebook* [248] to facilitate handling of connectivities and speed up the process. Moreover, initial chemical shifts were predicted with the assignments for TEM-1 [241], a class A β-lactamase with 41.5% sequence identity compared to PSE-4.

5.3 Results and Discussion

5.3.1 Overexpression and Purification

Despite the fact that some protein was recovered from the supernatant, while most of the production was recovered after cell lysis, all of the purified protein was free from the fused signal peptide. This was confirmed by SDS-PAGE and mass spectrometry, the latter also serving to estimate the extent of isotopic labelling (see Table 5.2). It is possible that the protein obtained after cell lysis was located in the periplasmic space. This would explain why the signal peptide is removed, although the protein is not exported outside the cell wall as for TEM-1 [241]. Labelling used standard approaches and yielded standard results with > 95%

Table 5.2: Labelling extent for PSE-4

Sample	Theoretical MW† (Da)	Measured MW‡ (Da)	Extent of labelling (%)
[^{15}N]-labelled	29885*	29872	96.4 for ^{15}N
[^{13}C, ^{15}N]-labelled	31183 **	31140	97.7 for ^{13}C
[^{2}H, ^{13}C, ^{15}N]-labelled	32730 ***	32682	97.0 (91.4) for ^{2}H ****

† The theoretical MW of mature PSE-4 is 29527 Da, wth 32331 Da for PSE-4 with its signal peptide.
‡ As measured from LC-MS.
* Corresponding to 29527 Da + 358 ^{15}N.
** Corresponding to 29527 Da + 358 ^{15}N + 1298 ^{13}C.
*** Corresponding to 29527 Da + 358 ^{15}N + 1298 ^{13}C + 1590 ^{2}H.
**** Assuming exchangeable amides are 100 % exchanged (assuming 80 % exchange).

of nitrogen and carbon sites labelled, and > 90 % of proton site changed to deuterium (see Table 5.2). Hence, the production of PSE-4 for NMR was successful and yielded between 20 and 80 mg of > 95 % pure (see Figure 5.2) protein per liter of culture.

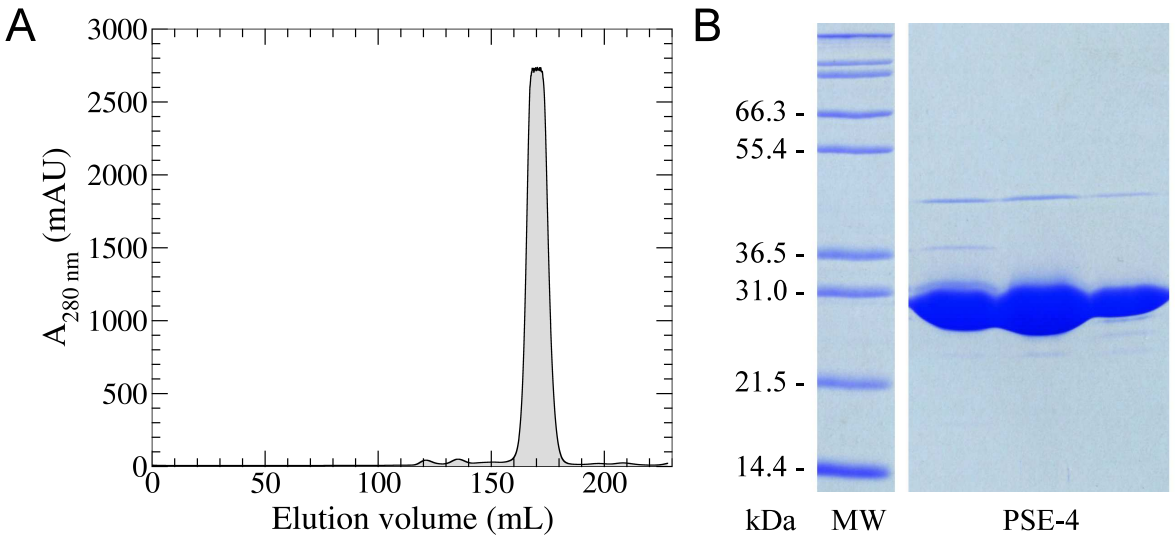

Figure 5.2: Gel filtration chromatograph and SDS-PAGE of purified [^{2}H, ^{13}C, ^{15}N]-labelled PSE-4. (A) Typical gel filtration chromatograph of purified PSE-4. (B) Corresponding SDS-PAGE. Shown are molecular weight markers as well as three fractions covering most of the gel filtration peak (around the peak center at ∼ 170 mL).

5.3.2 Assignments

PSE-4 yields a very well dispersed 2D ^{15}N-HSQC with very little overlap considering its MW (see Figure 5.4). 98.1 % of all backbone $^{1}H_N$ and ^{15}N, 99.3 % of $^{13}C_\alpha$, 96.8 % of $^{13}C_\beta$, and 98.2 % of ^{13}C' were assigned. The three last residues of PSE-4 which were not seen in the crystal structure are very intense with low, or even negative, ^{1}H^{15}N-NOEs (see Section 7.3, [194]) confirming their high mobility and explaining their absence in the crystal structure. Moreover, secondary structure predicted from the *PsiCSI* program [119] were in almost perfect agreement with secondary structures in the crystal structure 1G68 [165] (data not shown). Finally, assignments for the Thr and Lys amides were counter-verified using a [^{15}N]-Thr and [^{13}C-^{15}N]-Lys specifically-labelled sample (see Figure 5.3).

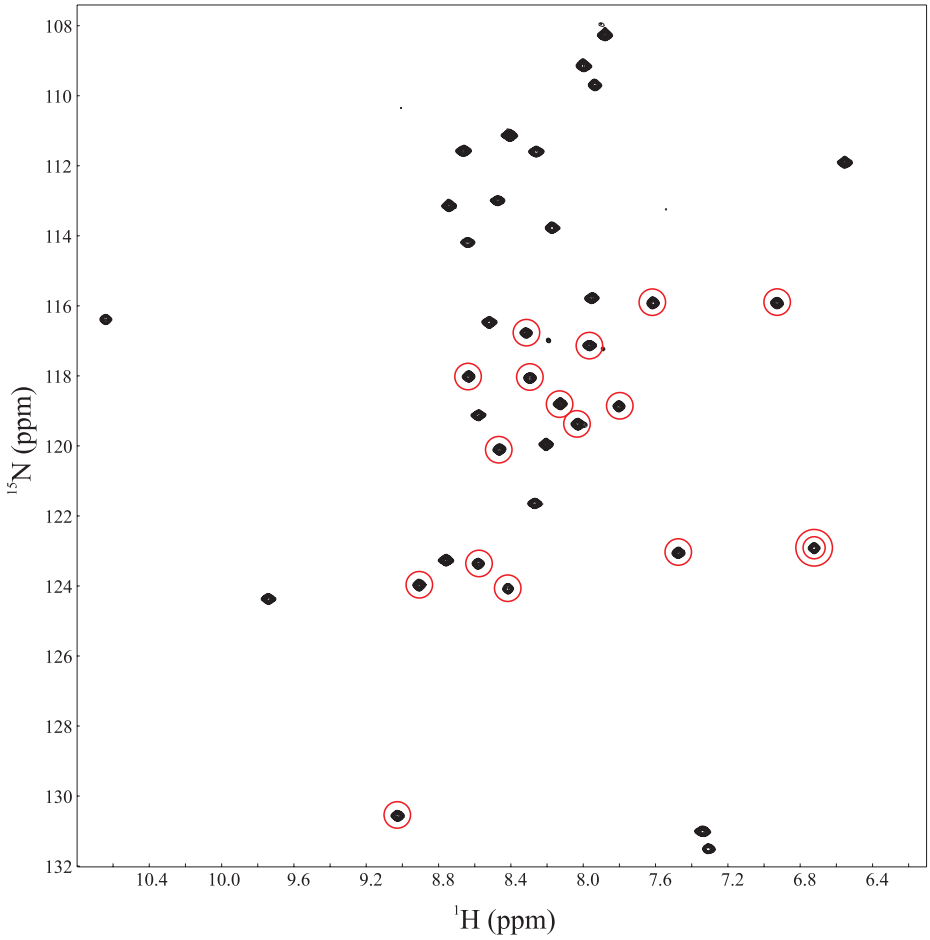

Figure 5.3: 2D ^{15}N-TROSY-HSQC for [^{15}N]-Thr and [^{13}C-^{15}N]-Lys specifically-labelled PSE-4. Lys resonances are circled in red with the resonance for active site residue Lys^{73} double-circled.

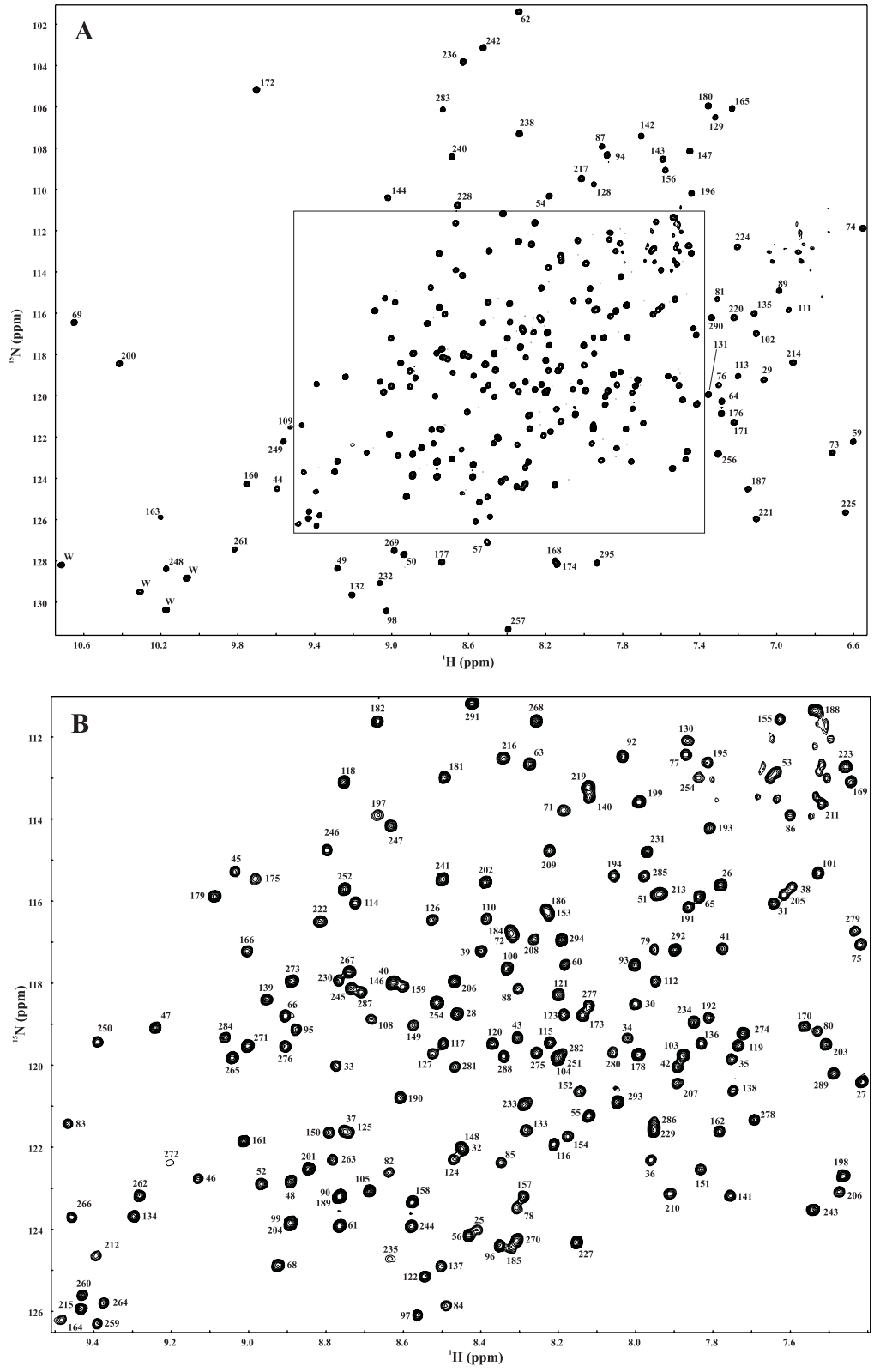

Figure 5.4: Assigned 2D ^{15}N-TROSY-HSQC spectrum (A) of deuterated PSE-4 with an enlarged view of the most crowded region of the spectrum (B).

Missing assignments (using the Ambler numbering scheme [8] in which PSE-4 is numbered 22–295 with gaps at positions 58, 239, and 253) are those of residues Ser^{22} and Ser^{23}, the amide of Ser^{24}, the $^{13}C'$-Thr^{69}, the amide and $^{13}C_{\beta}$ of Ser^{70}, the $^{13}C'$-Asn^{90}, the $^{13}C'$-Ser^{106}, the $^{13}C_{\beta}$-Thr^{149}, the $^{13}C_{\beta}$-Thr^{182}, the $^{13}C_{\beta}$-Thr^{189}, the $^{13}C_{\beta}$-Ser^{209}, the amide of Ala^{237} and the $^{13}C_{\beta}$-Ser^{285}. As in the case of TEM-1 [240], active site residue Ala^{237} was not observed, probably from extreme broadening caused by conformational exchange. Additionally, residue Ser^{70} was also not observed in PSE-4, potentially because of the same reason (as the amide resonances for this residue were weak and broadened in TEM-1 [240]). This points to the generality of potentially important dynamics going on in the active site of class A β-lactamases on the μs-ms timescale.

Backbone ^{1}H, ^{13}C, and ^{15}N chemical shifts have been deposited under accession number 6838 in the BMRB and are also available in Appendix 1 (Table 10.1).

Chapter 6

Dynamics of Class A β-Lactamases: PSE-4 Lys^{73} Titration Trial

An hypothetical involvement of Lys^{73} in the acylation step of the mechanism of class A β-lactamases implies that the pK_a of its side-chain is anormally low (*i.e.* below 10). Hence, many *in silico* and experimental studies aimed at determining this pK_a in order to validate or invalidate this hypothesis. None of these groups, however, obtained convincing results. Unfortunately, as these groups, we were not succesful in measuring the pKa of this Lys^{73}. This chapter presents the result of our endeavor to mesure this pK_a value.

6.1 Context

After the proposal by Strynadka *et al.* that the pK_a of Lys^{73} would be modulated by the proximity of the positively charged Lys^{234} [255], many research groups aimed at characterising the pK_a of Lys^{73} in order to prove or refute this hypothesis. This is indeed an important mechanistic aspect for class A β-lactamases as a lowered pK_a around 8 would be needed for the involvement of Lys^{73} in the acylation step. Several studies were thus carried out to characterise the pK_a of Lys^{73} with many of these using *in silico* approaches. These yielded contradictory results with a pK_a of either 8.0 [257] or 10.0 [157, 227]. An experimental study by Damblon *et al.* [46] reported having titrated Lys^{73} in TEM-1 using NMR. Unfortunately, the assignments used were found erroneous when compared to the (almost) complete assignments for TEM-1 [239]. Another group reported a pK_a of 8.0-8.5 for Lys^{73} using different *in silico* and experimental approaches [97]. However, the value of this study was reduced by the ambiguous assignment of $C_\varepsilon/H_\varepsilon$ resonances for Lys^{73}.

In our laboratory, using a sample labelled only for Lys residues, Savard [239] could completely observe 9 out of 11 Lys side-chains in TEM-1, except Lys^{73} and Lys^{234}, the resonances for these two residues being broadened and too weak for observation passed the $^{13}C_\beta$ resonances. Later, during further assignment of side-chain resonances, the chemical shifts for every side-chain ^{13}C atom in both Lys^{73} and Lys^{234} could be obtained, however indirectly, *i.e.* through the extrapolation of the diagonal in 3D HCCH-TOCSY spectra by observation of corresponding C_α and C_β cross-peaks (Pierre-Yves Savard, personal communication). These Lys^{73} side-chain chemical shifts were different from those reported by Damblon *et al.* [46] (data not shown). Hence, no experimental study has ever succeeded in characterising the pK_a of Lys^{73} without ambiguity.

We thus decided to see if the situation could be different in PSE-4 and if we could assign and titrate Lys^{73}'s side-chain.

6.2 Methods

The [^{15}N]-Thr and [^{13}C-^{15}N]-Lys specifically labelled sample of PSE-4 produced for verification of backbone chemical shift assignments of Thr and Lys residues (see Chapter 5,

[196]) was re-used for titration trials.

In order to assign side-chain chemical shifts from Lys^{73} using this sample, different spectra were recorded (under the same experimental conditions as for backbone chemical shift assignments, see Chapter 5): a 2D ^{13}C-HSQC [130, 138], a 3D HCCH-TOCSY [13, 140], and the TROSY [220] version of a 3D H(CCO)NH (also known as 3D HCCH-TOCSY-NNH, [100, 170]). These were all from Biopack (Varian Inc, Palo Alto, CA).

6.3 Results and Discussion

Lys^{73}'s C$_\alpha$ resonance was the weakest of all lysines C$_\alpha$ resonances in the 2D ^{13}C-HSQC (see Figure 6.1). Moreover, we were unable to see Lys^{73}'s side-chain further than the C$_\alpha$ on the 3D HCCH-TOCSY spectrum (data not shown). Finally, even in the 3D H(CCO)NH spectrum which would yield a single set of resonances for Lys^{73} on the N-H plane for residue Thr^{74} (because the segment 'KT' is present only once in PSE-4 sequence), not a single peak could be observed (data not shown). This lack of signal (from the C$_\varepsilon$, H$_\varepsilon$ and other resonances) prevented the titration of the side-chain N$_\zeta$ group.

A potential avenue to solving this S/N issue caused by potential intermediate exchange of Lys^{73}'s side-chain would have been to record the data at other temperatures (either lower or higher, not exceeding 41 °C where both TEM-1 and PSE-4 precipitate *in vitro*, data not shown). This approach would maybe have moved the exchange process from the intermediate regime to the slow or fast regime, in turn allowing observation of these resonances.

In summary, as was the case for TEM-1, assigning the side-chain resonances of Lys^{73} at 30 °C proved impossible in PSE-4. This, however, again emphasised the potential presence of important μs-ms motions in the vicinity of the active site where amides from two residues (Ser^{70} and Ala^{237}) are unobservable. Indeed, all these 'invisible' resonances could be broadened from conformational exchange arising on the catalysis timescale.

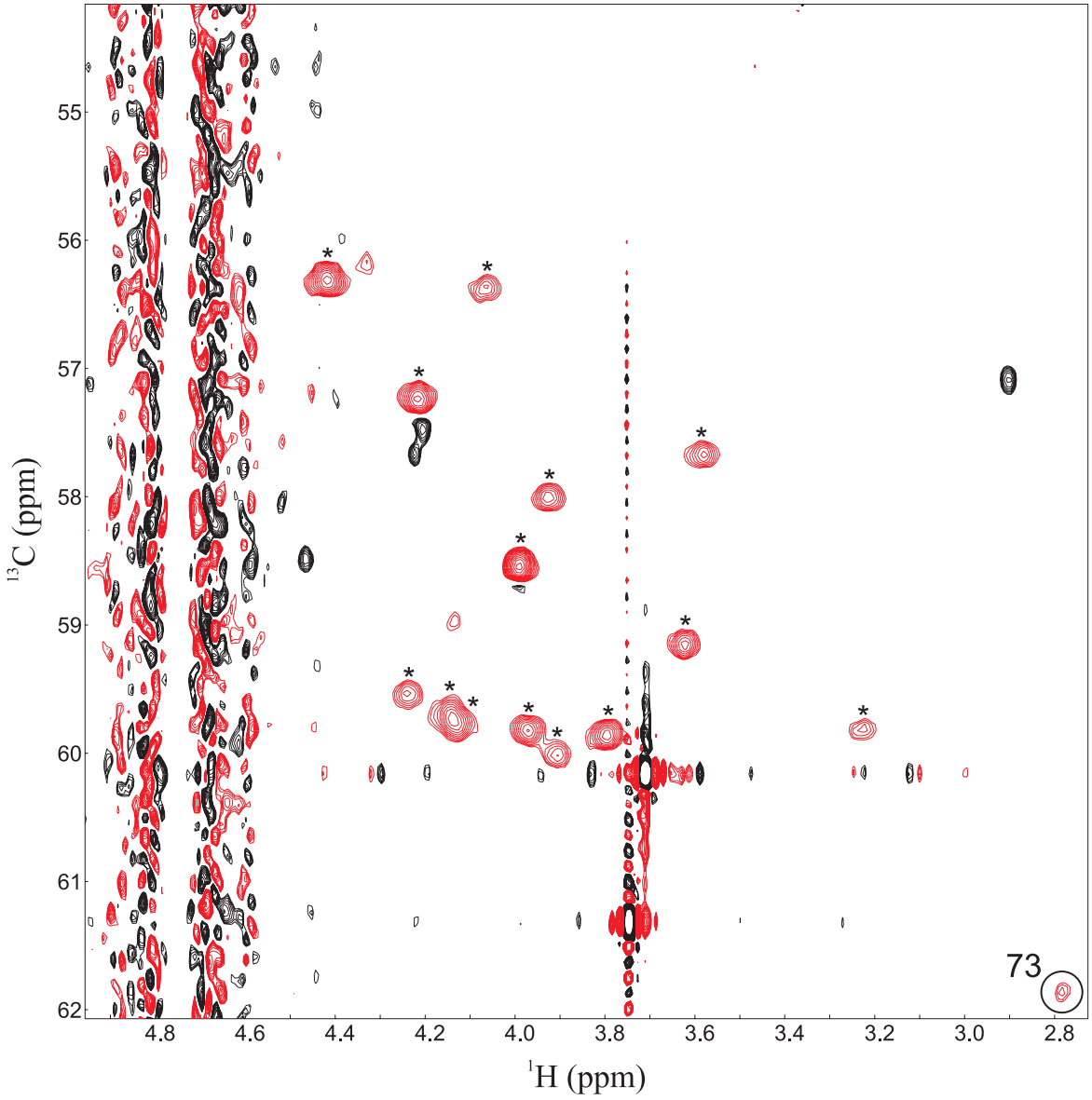

Figure 6.1: C_α resonances of Lys residues in PSE-4. The C_α region of a 2D ^{13}C-HSQC of [^{15}N]-Thr and [^{13}C-^{15}N]-Lys specifically labelled sample of PSE-4 is shown with the resonance for Lys^{73} C_α circled and 14 other Lys C_α marked by a star (*). Black and red denote positive and negative resonances, respectively. The 16th Lys C_α is overlapped by the water signal and, thus, unobservable. As can be seen, the C_α resonance for Lys^{73} is the weakest of all observed Lys C_α resonances.

Chapter 7

Dynamics of Class A β-Lactamases: PSE-4 Backbone Dynamics

The backbone dynamics for the 29.5 kDa class A β-lactamase PSE-4 is presented. This solution NMR study was performed using multiple field ^{15}N spin relaxation, ^{15}N CPMG relaxation dispersion, and amide exchange data in the EX2 regime. Analysis was carried with the *relax* program and the Lipari-Szabo model-free approach. Similar to the homologous enzyme TEM-1, PSE-4 is very rigid on the ps-ns timescale, although slower μs-ms motions are present for several residues; this is especially true in the vicinity of the active site. However, significant dynamics differences exist between the two homologs for several important residues. Moreover, our data support the presence of motion of the Ω loop first detected using MD simulations on TEM-1 but not detected when studying TEM-1 by NMR. Class A β-lactamases appear to be a class of highly ordered proteins on the ps-ns timescale despite their efficient catalytic activity and high plasticity toward several different β-lactam antibiotics. The μs-ms motions present in the active site suggest this dynamics has a potential role in catalysis.

7.1 Context

Amide backbone chemical shift assignments being missing for two important active site residues (Ser^{70} and Ala^{237}, see Chapter 5 and [196]) and being corroborated with invisible side-chain resonances for Lys^{73} (see Chapter 6), intermediate exchange processes are suspected in the vicinity of PSE-4's active site. Hence, in order to understand further these processes, the backbone dynamics of PSE-4 on different timescales were studied and compared to NMR data already available for TEM-1 [62, 79, 240].

7.2 Methods

7.2.1 NMR Data Acquisition

[^{15}N]-labelled PSE-4 was produced as described previously (see Chapter 5, [196]). NMR samples were as follows: 0.5 mM PSE-4, 10 % D_2O, 3 mM imidazole, and 0.1 % sodium azide at *pH* 6.65. Chemical shift referencing was performed externally using a sample of 0.4 mM DSS in 10 % D_2O. Spectra were acquired at a temperature of 31.5 °C (calibrated using MeOH) on a Varian INOVA 600 (in-house), and Varian INOVA 500 and 800 (Québec / Eastern Canada High Field NMR Facility, Montréal, Canada) spectrometers (corresponding to 60.8, 50.6, and 81.0 MHz nitrogen frequency, respectively) equipped with *z*-axis pulse field gradients triple resonance cold probes (except for amide exchange data at *pH* 7.85 which was acquired using a room temperature probe).

Measurement of longitudinal (R_1) and transverse (R_2) relaxation rates as well as the steady-state heteronuclear *NOE* proceeded with established pulse sequences [76, 138]. For both R_1 and R_2 experiments recorded at 500 and 800 MHz, acquisition of relaxation data was performed in an interleaved manner (interleaving the different delays) to prevent the effects of field and sample inhomogeneity as a function of time [265]. For example, if delays 1, 2, 3, 4, 5, 6 had to be recorded, the acquisition order of the different 2D spectra was as follows: 1, 3, 5, 2, 4, 6 (or, inversely, 6, 4, 2, 5, 3, 1). In the case of R_1 and R_2 data recorded at 600 MHz, interleaving proceeded as part of the recording of pseudo 3D spectra. In this case, relaxation delays were interleaved after each two FIDs (*i.e.* after the real and

imaginary parts of each indirect dimension increment). *NOE*s were collected in duplicate at 50.6 MHz. At 60.8 MHz, R_1 experiments were recorded in quadruplicate, R_2, in quintuplicate, and *NOE*, in triplicate, with some experiments recorded before and others after the recording of data at 50.6 and 81.0 MHz. This ensured that the sample was in the same state throughout the complete experimental scheme.

For the measurement of the longitudinal relaxation rate (^{15}N-R_1), the sensitivity-enhanced inversion-recovery pulse sequence from Lewis Kay's group [76] was used. Relaxation delays were of 10.9, 21.8 (60.8 MHz), 43.6, 87.2 (50.6 and 60.8 MHz), 174.4, 348.9 (50.6 and 60.8 MHz), 697.7, 1395.4 (50.6 and 60.8 MHz), and 1995.0 ms. With eight transients per FID and a recycle delay of 2 s, this acquisition scheme represented a total acquisition time of $\sim$ 13 h per magnetic field.

For the measurement of the transverse relaxation rate (^{15}N-R_2), the pulse sequence was the implementation of Lewis Kay's sequence [138] within BioPack (Varian Inc., Palo Alto, CA). Relaxation delays were of 10, 30, 50, 70, 90, 110, 130, 150, and 190 ms. Heat compensation [274] was used. An interpulse delay of 575.6, 583.2, and 574.0 μs was used in the CPMG train (at 50.6, 60.8, and 81.0 MHz, respectively). Also, the RF field strength for the ^{15}N 180° pulses in the CPMG sequence was 5.061, 5.187 (and 5.981 and 5.952), and 4.902 kHz at 50.6, 60.8, and 81.0 MHz, respectively. These spectra were recorded by accumulating eight transients per FID using a recycle delay of 3 s for a total of $\sim$ 7 h at each magnetic field.

For the measurement of the steady-state heteronuclear *NOE* ($\{^1$H$\}^{15}$N-*NOE*), the pulse sequence was again from Lewis Kay's group [76]. Spectra were recorded with and without ^{1}H saturation. A saturation time of 4 s was used and recycle delays were of 5 s for experiments with and without saturation (4 s of saturation + 1 s of blank delay, or 5 s of blank delay, respectively). *NOE* experiments being less sensitive than R_1 or R_2 experiments, every experiment (with or without saturation) took $\sim$ 14 h per magnetic field for the recording of 44 transients per FID.

^{15}N CPMG relaxation dispersion experiments proceeded also using a pulse sequence from Lewis Kay's group in which relaxation occurred during a constant-time delay T [108]. Spectra were recorded at two different magnetic fields: 500 and 800 MHz. The delay T was set to 40 ms. A reference spectrum was recorded for each dataset as well as spectra for the following CPMG pulse train frequencies (ν_{CPMG}): 67, 133, 200, 267, 333, 400, 467, 533, 600, 733, 867, and 1000 Hz. Duplicates were recorded at 800 MHz for ν_{CPMG} of 133 and

533 Hz. Every experiment took $\sim$ 8 h for the recording of either 48 (500 MHz) or 32 (800 MHz) transients.

Amide exchange experiments proceeded from TROSY-HSQC [138, 220] spectra (BioPack, Varian Inc., Palo Alto, CA) using lyophilised PSE-4 dissolved in D_2O. The TROSY [220] implementation allowed smaller phase cycling so very short spectra could be acquired with limited baseline distortions. Hence, at the beginning, more frequent short spectra (with a low number of transients) were acquired, and at the end fewer long spectra (with increasing transients) were acquired. To determine the exchange regime, amide exchange experiments were performed for 80 days at *pH* 6.65, and for six days at *pH* 7.85. In both situations, approximately 60 spectra were recorded.

Amide exchange experiments were performed with the INOVA 600 spectrometer, at a temperature of 31.5 °C as for spin relaxation experiments. At *pH* 7.85, the acquisition was at the following times (when half the acquisition had been completed): 35; 43; 51; 59; 67; 75; 83; 91; 99; 107; 119; 135; 150; 166; 182; 197; 213; 228; 244; 260; 276; 291; 307; 322; 338; 354; 369; 385; 408; 439; 470; 500; 531; 562; 593; 624; 655; 685; 717; 748; 778; 809; 840; 871; 1039; 1206; 1373; 1541; 1708; 2710; 2877; 2924; 3122; 3537; 3935; 4334; 5068; 5803; 6874, and 8974 min. Spectra up to 107 min were recorded with two transients; from 119 to 385 min, with four transients; from 408 to 2877 min, with eight transients; and from 2924 min to the end, with 16 transients. At *pH* 6.65, the acquisition was at the following times (when half the acquisition had been completed): 32; 40; 48; 56; 68; 76; 84; 92; 100; 108; 120; 136; 151; 167; 182; 198; 214; 229; 245; 260; 276; 291; 307; 323; 338; 354; 369; 385; 407; 438; 469; 500; 531; 562; 592; 623; 654; 685; 716; 746; 777; 808; 870; 1103; 1398; 1937; 2416; 3060; 3152; 5331; 6503; 8096; 12,492; 16,100; 37,334; 38,217; 44,253; 58,532; 77,293, and 115,559 min. Spectra up to 108 min were recorded with two transients; from 120 to 385 min, with four transients; from 407 to 2416 min, with eight transients; and from 3060 min to the end, with 16 transients.

7.2.2 NMR Data Processing

NMR data were processed using the program *NMRPipe* [55]. FIDs were shuffled to yield pure absorptive two-dimensional line shapes from the sensitivity-enhanced [138, 212] data with the ‘ranceY.M’ macro. Water signals were subtracted with the function ‘SOL’. Linear

prediction was performed in the indirect (^{15}N) dimension to extend the amount of data points by 50 % (70 % for amide exchange data). The baseline in each dimension was corrected using the function 'POLY -auto -ord 0'. As stated before, the number of transients was higher as time proceeded for amide exchange experiments; thus FIDs were scaled accordingly (so amplitudes were comparable between spectra with a different number of transients) using the *NMRPipe* function 'MULT -c'.

Peak deconvolution proceeded using the macro 'nlinLS' invoked from the script 'autoFit.tcl', both distributed within *NMRPipe* [55]. R_1 and R_2, as well as amide exchange rates, were obtained with the program *CurveFit* (A. G. Palmer, Columbia University, New York, NY). R_1 and R_2 relaxation rates were obtained by fitting peak amplitudes as a function of relaxation delay using a two-parameter exponential decay function of the form:

$$A_{(t)} = A_0\, e^{-Rt} \tag{7.1}$$

where A stands for amplitude, R is the relaxation rate (either R_1 or R_2), and t is the time. Amide exchange rates (k_{HX}) were obtained by fitting peak amplitudes as a function of time after dissolution in D_2O using an offset three-parameter exponential decay function of the form:

$$A_t = A_0\, e^{-k_{HX}t} + A_\infty \tag{7.2}$$

where A_∞ represents the amplitude at infinite time (*i.e.* the signal from residual protons, or the offset). Errors on these fits were obtained from either 500 Monte Carlo [186] simulations or the Jackknife [225] method, using the method that yielded the largest error. A correction was introduced for systematic errors not accounted for when a near-perfect fit was obtained from the R_1 and R_2 exponential curve-fitting. This was done only for model-free analysis where too small errors on experimental data can introduce over-complex models. Thus, parameters with unrealistically small errors (smaller than the mean value) had their error scaled to the mean value. This is similar to the approach of Savard and Gagné [240]. *NOE*s were calculated as the ratio of peak amplitude with and without proton saturation (see Equation 1.10), and error propagation was calculated from the noise. Finally, relaxation dispersion profiles were obtained by calculating R_2^{eff}, the effective R_2, for each value of ν_{CPMG} using the following

function [148]:

$$R_2^{eff} = -\frac{1}{T} \ln \left[\frac{A_{CPMG}}{A_{ref}} \right] \tag{7.3}$$

where T is the constant relaxation time during which the CPMG train with frequency ν_{CPMG} is applied (here 40 ms), A_{CPMG} is the peak amplitude in the experiment with CPMG, and A_{ref} is the peak amplitude in the reference spectrum (*i.e.* without CPMG train). T was chosen so that A_{CPMG}/A_{ref} was approximately equal to 0.5 (as proposed by Mulder *et al.* [198]). Following extraction of R_2^{eff} values, curve-fitting of dispersion profiles using a two-state exchange model was performed with either a *Matlab* script from Lewis Kay's group [149], or the program *CPMGFit* (A. G. Palmer, Columbia University, New York, NY).

7.2.3 Verification for Absence of Concentration Effects on Global Diffusion

To make sure no dimerisation was present in our sample, we assessed the effect of concentration on global rotational diffusion. Two samples of lower concentration were prepared (*i.e.* 0.25 and 0.125 mM, with 0.5 mM for the main sample).

7.2.4 Consistency Test

Consistency between datasets acquired at different magnetic fields was assessed with the use of reduced spectral density mapping [75] within the program *relax* (version 1.2.14) [51, 52]. The test, as proposed by Morin and Gagné (see Chapter 2, [195]), consisted of calculating the field independent function $J(0)$ for each residue and then comparing results obtained at different fields. For these calculations, the ^{15}N chemical shift anisotropy (*CSA*) was -172 ppm, and the vibrationally averaged effective N-H bond length ($r_{N\text{-}H}$) was 1.02 Å.

7.2.5 Model-Free Analysis

Model-free analysis of relaxation data was performed using the program *relax* (version 1.2.14) [51, 52] with a variant of the methodology for the dual optimisation of the model-free parameters and the global diffusion tensor proposed recently [52] (see experimental flowchart in Figure 7.1). To avoid any artifact (resulting from under- or over-fitting), only residues for which data was available at the three magnetic fields were analysed. N-H vectors orientations were extracted from PDB 1G68 [165]. Since this crystal structure does not include amide protons, these were added using Molmol [146]. Values for the *CSA* and $r_{N\text{-}H}$ were as for the consistency test (*i.e.* -172 ppm and 1.02 Å, respectively). The values were set to the same as in Savard and Gagné [240] to facilitate the comparison to the dynamics of the homologous protein TEM-1.

Five different diffusion models were tested (no global diffusion tensor, *i.e.* with a local τ_m parameter for each residue; sphere; prolate spheroid; oblate spheroid; and ellipsoid). These were optimised using residues from well defined secondary structures (determined using *DSSP* [133], see Table 10.3 in Appendix 3) and selected by *AIC* (see Equation 1.27 [3]). Ten model-free models (with 0 to 5 adjustable parameters, defined previously in Equation 1.21) were used to describe internal dynamics.

Local model-free models selection during iterations for diffusion tensor optimisation was also done using *AIC*. This allowed the selection of complex models for residues difficult to fit, avoiding the diffusion tensor from being biased by those residues. After convergence of the different diffusion tensors and selection of the diffusion tensor with the lowest *AIC*, local model-free models were minimised for all residues using this diffusion tensor, which was then held fixed. Then, the best model for each residue was selected using *AICc* [120]:

$$AICc = \chi^2 + 2k + \frac{2k\,(k+1)}{n-k-1} \tag{7.4}$$

where n represents the size of the dataset. This was done to minimise over-fitting which could lead to over-interpretation of relaxation data.

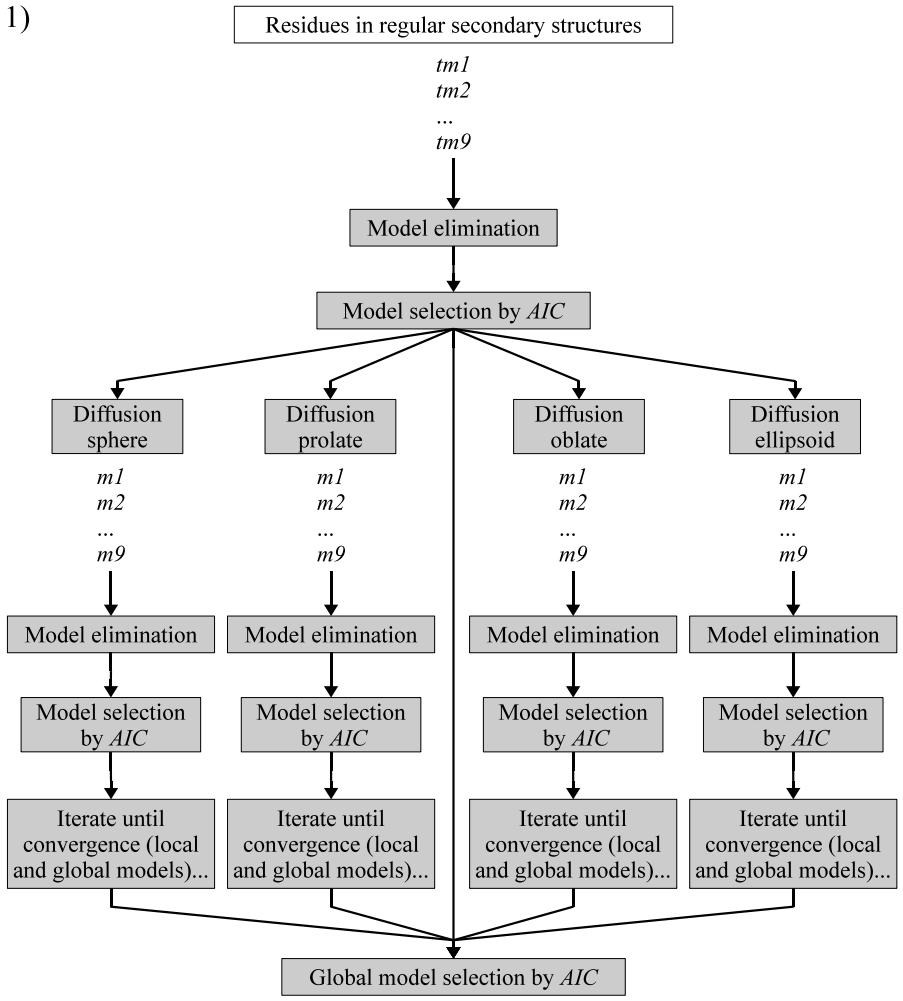

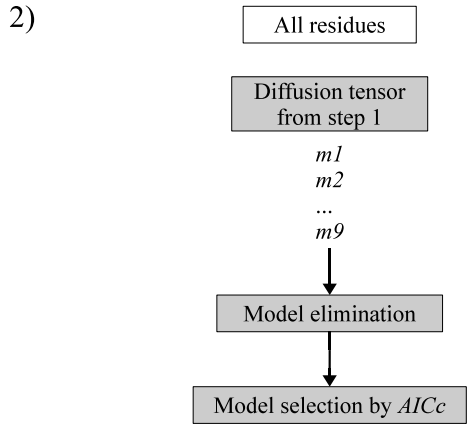

1) a) Use residues in regular secondary structures.
   b) Use the new methodological protocol as proposed by d'Auvergne and Gooley (2007, *Mol. Biosyst.*, **3**: 483–494. ; 2008, *JBNMR*, **40**:121–133). First, optimize model-free models with a local correlation time (τ_m) and perform model-free model elimination and model-free model selection using *AIC*. Second, optimize each diffusion tensor type as well as model-free models, and perform model-free model elimination and model-free model selection using *AIC*.
   c) Once convergence is reached for each different diffusion tensor, perform diffusion tensor selection using *AIC*. The diffusion tensor is now minimized.

2) a) Use the diffusion tensor selected in step 1.
   b) Optimize model-free models for each residue and perform model-free model elimination and model-free model selection using *AICc*.

Figure 7.1: Flowchart of the model-free protocol which employs the approach of d'Auvergne and Gooley [50, 52] for the first step with only residues from the core of regular secondary structures (α-helices and β-strands). In this step, model selection is performed using *AIC* (see Equation 1.27, [3]). In the second step, the optimised diffusion tensor is used for minimisation of local model-free models for all residues. The best local model for each residue is chosen using *AICc* (see Equation 7.4, [120]).

Optimising the diffusion tensor using only residues within well-defined secondary structures takes advantage of the information contained in the crystal structure concerning secondary structures and avoids any bias of the global diffusion tensor that could arise from incorrect N-H orientations in loops caused by crystal packing or intrinsic flexibility. After optimisation of the different diffusion models, the *AIC* chosen diffusion tensor was used to minimise models for every residues, except for the three C-terminus residues (which were analysed as diffusing independently of the rest of the protein, because their N-H vector orientation is unavailable). Final model selection for all residues (after the tensor had been fixed) then proceeded using *AICc* (see Equation 7.4, [120]) to minimise over-fitting. Indeed, on a per residue basis, the sample size for relaxation data is quite small ($n = 8$) compared to the complete set used for diffusion tensor optimisation ($n = 1072$), justifying the use of different statistical approaches suited for these two situations. Additionally, using *AIC* instead drastically increased the number of residues displaying non significant and isolated R_{ex} terms. In fact, *AIC* yielded 52 residues with R_{ex} terms and *AICc* yielded 32, with the 20 supplementary R_{ex} terms from *AIC* being questionable because of both their low values and isolated distribution. For these reasons, *AICc* was used for the selection of local model-free models after the global diffusion tensor had been fixed.

In the current study, minimisation of both local and global models was performed using the Newton algorithm. Finally, errors on the extracted local parameters were obtained by performing 500 Monte Carlo [186] simulations. A flowchart of the model-free protocol used in this study is shown in Figure 7.1.

7.3 Results and Discussion

Chemical shift referencing was done externally because DSS interacts weakly with PSE-4. Indeed, the DSS peak at 0 ppm was observed to lose more than 60 % of its intensity after several days in the presence of PSE-4 (data not shown). Its ^{1}H-R_1 also changed from 0.9 s^{-1} to 2.8 s^{-1} over the same period of time. These two observations pointed in the same direction with DSS MW increasing because of an interaction with PSE-4 in a slow exchange process. In addition, samples did not contain any proteinase inhibitor cocktail because we also observed that some inhibitors bind to the active site (data not shown). This was not surprising as class A β-lactamases are closely related to serine proteinases (see Chapter 4) and may thus bind similar inhibitors. Finally, no buffer was used because NMR data indicates that the

phosphate buffer interacts weakly with TEM-1's active site [239], despite its ubiquitous use in many kinetics studies of β-lactamases. Therefore, samples were prepared to minimise any unwanted interaction that could bias our study because relaxation experiments are extremely sensitive.

A slight modulation of R_1 and R_2 relaxation rates was observed by varying the protein concentration from 0.125 to 0.5 mM, The variation corresponded to a lowering of the estimated correlation time by less than 5 % for this concentration range (see Figure 7.2). This small variation is expected due to viscosity changes as a function of protein concentration and excludes the possibility of concentration driven partial dimerisation which could, if present, bias the analysis. In fact, a similar modulation of relaxation parameters was observed for ^{1}H-R_1 of imidazole as a function of protein concentration (see Figure 7.2). This variation was different than for PSE-4 because imidazole is in the fast tumbling (*i.e.* extreme narrowing) regime ($\omega_H^2\,\tau_m^2 \ll 1$) while PSE-4 is not ($\omega_N^2\,\tau_m^2 \sim 1$). Nevertheless, this showed that the apparent tumbling time of imidazole increased with increasing protein concentration, thus confirming the change in sample viscosity.

Backbone resonance assignments for PSE-4 (BMRB 6838, see also Table 10.1 of Appendix 1) [196] allowed for the extraction of atom specific data. However, no information could be extracted for residues Ser^{22}, Ser^{23}, Ser^{24}, Ser^{70}, and Ala^{237} for which amide assignments are unavailable; Ser^{22}, Ser^{23}, and Ser^{24} probably due to fast solvent exchange, and Ser^{70} and Ala^{237} because of very broad and/or highly overlapped resonances. Also, residues which overlapped severely were excluded from further analysis (see Tables 10.2, 10.3, and 10.4). Hence, a total of 230 residues out of 271 were characterised with data at the three magnetic fields ($N = 231$ at 50.6 MHz, 232 at 60.8 MHz, 238 at 81.0 MHz).

7.3.1 ^{15}N Spin Relaxation Data

^{15}N spin relaxation data consisted of three sets of experiments: ^{15}N-R_1, ^{15}N-R_2 and $\{^1\text{H}\}^{15}$N-*NOE*. Data at more than one magnetic field being required for over-determination of model-free parameters, we acquired data at 11.7, 14.1, and 18.8 T (respectively, 50.6, 60.8, and 81.0 MHz nitrogen frequency). To confirm that the sample did not change during the experimental scheme, we recorded one set of *NOE*, three complete sets of R_1, and two complete sets of R_2 at 60.8 MHz before recording data at 50.6 and 81.0 MHz. Following

data acquisition at 50.6 and 81.0 MHz, we recorded two sets of *NOE*, one complete set of R_1, and three complete sets of R_2 again at 60.8 MHz. This also allowed us to verify that error on spin relaxation data was neither under- nor over-estimated using Jackknife [225] and Monte Carlo [186] methods (data not shown). For example, the four different R_1 datasets recorded at 60.8 MHz gave rates that, within estimated errors, were reproducible for most residues. Mean relative errors for these datasets were as follows: 2.77 %, 2.91 %, 2.77 %, and 3.28 %. On the other hand, mean error for the combined datasets was 2.47 %, reflecting the improvement obtained when using more data points. Datasets recorded at 50.6 and 81.0 MHz were not repeated as for 60.8 MHz (except for *NOE* at 50.6 MHz), but displayed errors on the same range. Finally, even though R_2 values obtained at 60.8 MHz were extracted from experiments with two different RF fields (5.2 and 6.0 kHz), this difference did not affect rates, which fell within respective errors (data not shown). ^{15}N spin relaxation data for PSE-4 have been deposited in the BMRB under accession number 6838, are available in Appendix 2 (Table 10.2) and are shown in Figure 7.3.

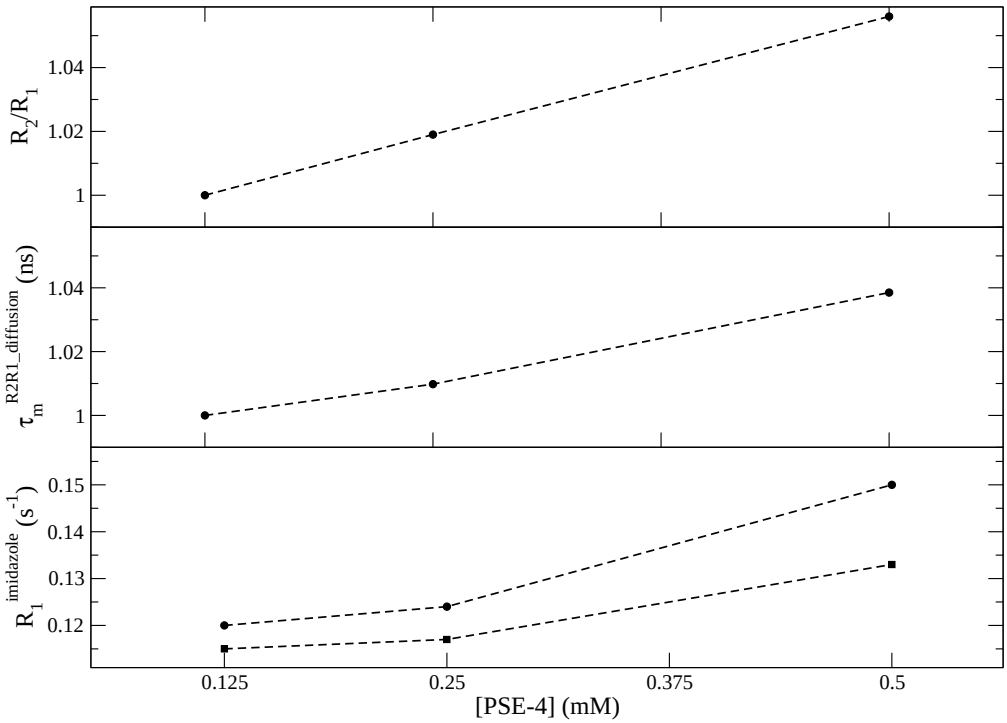

Figure 7.2: Effect of protein concentration on PSE-4 estimated global correlation time $\tau_m^{\text{R2R1\_diffusion}}$ (middle). Estimation proceeded from the R_2/R_1 ratio ([139], top) in the program R2R1_diffusion (A. G. Palmer, Columbia University, New York, NY). A trimmed set of R_2/R_1 was used such that no residue was outside $R_2/R_1 \pm 1$ SD. Moreover, an axially symmetric diffusion tensor was assumed and PDB 1G68 [165] was used for data fitting. Data is compared to R_1 for imidazole (bottom) based on both the low frequency (squares) and high frequency (circles) peaks.

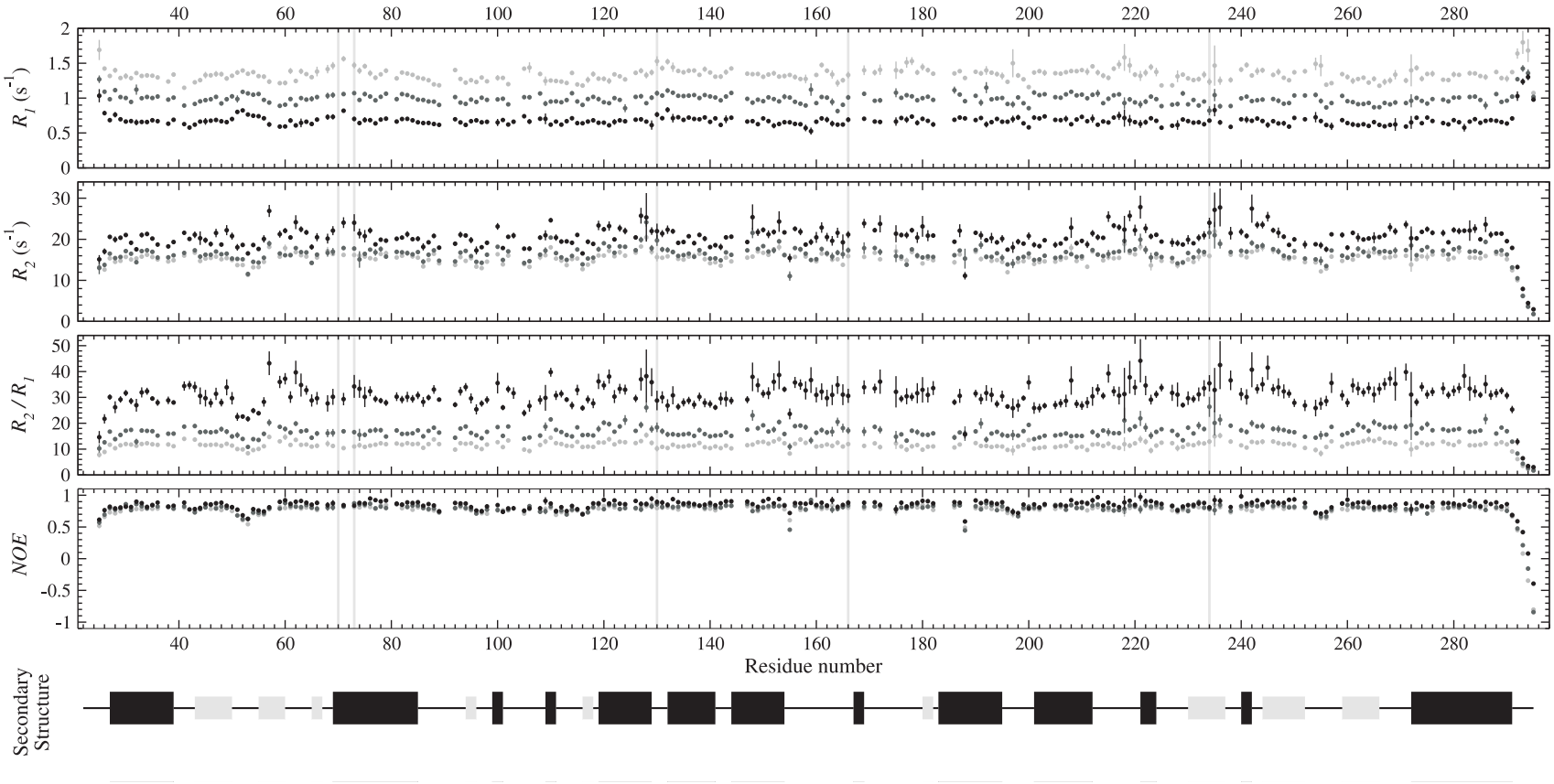

Figure 7.3: ^{15}N spin relaxation data. Shown are the longitudinal (R_1) and transverse (R_2) relaxation rates as well as the R_2/R_1 ratio and the steady-state heteronuclear *NOE* at 50.6 (*light grey*), 60.8 (*dark grey*), and 81.0 (*black*) MHz nitrogen frequency. Important active site residues are highlighted vertically in light grey. Secondary structures are shown with helices as wide black boxes, and β sheets as narrow grey boxes.

Statistics for the 2103 observables are available in Table 7.1. Mean errors for the recorded parameters vary between 2 and 4 % before scaling (see the Methods Section 7.2). Except for the five C-terminal residues, PSE-4 dynamics seems to be quite homogeneous, as is the case for TEM-1 [240]. This points to a unique diffusion core for this two-domain enzyme.

7.3.2 Dataset Consistency

To extract high quality information from multiple field experiments, it is important that datasets share a high degree of consistency. As discussed in Chapter 2 [195], inconsistencies can arise from several factors, including variations in sample viscosity (caused by changes in temperature, concentration, etc.) and water saturation during acquisition (which influences N-H moieties as a function of the exchange rate with the aqueous solvent). In this study, the field independent function $J(0)$ (the spectral density at the zero frequency) [75] was used to assess datasets consistency as proposed by Morin and Gagné (see Chapter 2, [195]).

Results from this consistency test demonstrate the good quality of the three datasets (Figure 2.14). 50.6 and 60.8 MHz data display especially high consistency, whereas 81.0 MHz consistency with 50.6 and 60.8 MHz data is good. The somehow wider distributions seen for data at 81.0 MHz were assessed further and some inconsistency was identified to be caused by R_2 data (see the following Model-Free Section 7.3.3).

On an individual basis, a few outliers from the correlation and distribution plots are observed. These can arise because of five principal reasons. First, modulation of the R_2 parameter can arise because of conformational exchange. Since this modulation is field dependent, apparent consistency will be lower (residue Arg^{234} is one of those). Second, consistency can appear lower as a result of some assumptions being erroneous. These include the assumption of

Table 7.1: ^{15}N spin relaxation statistics.

	50.6 MHz	60.8 MHz	81.0 MHz
R_1 (s^{-1})	1.34 ± 0.08	0.99 ± 0.07	0.67 ± 0.06
R_2 (s^{-1})	15.6 ± 1.4	16.5 ± 1.6	20.7 ± 2.3
R_2/R_1	11.6 ± 1.3	16.8 ± 2.2	31.0 ± 4.3
NOE	0.78 ± 0.05	0.80 ± 0.06	0.85 ± 0.06

Mean values with associated SD. The last three residues are excluded because of high mobility (hence, $N = 228$ at 50.6 MHz, 229 at 60.8 MHz, 235 at 81.0 MHz)

constant $r_{N\text{-}H}$ and *CSA* (discussed further in Section 7.3.3.3). Third, residues can possess extremely high mobility yielding negative *NOE* values, giving rise to a higher $J(0)$ value, hence giving the false impression of a overestimated R_2 (see Equation 1.11). Fourth, data for a given residue might be erroneous because of overlapping resonances. Fifth, one or more relaxation measurement at one field strength could be prone to errors (probe imperfection, environmental instability, difficulty of carrying reliable data acquisition given the available hardware, etc). This last reason may be the case for the overall R_2 inconsistency at 81.0 MHz that we observed.

To assess if datasets recorded at 81.0 MHz should be used for model-free analysis, several tests were done with optimisation of model-free models using a local correlation time (*local* τ_m) for each residue (see Table 2.6). This approach was inspired by the work of Gagné *et al.* who analysed their 500 and 600 MHz data together and separately in order to confirm their consistency [91]. When using all datasets, a high number of residues needed a R_{ex} parameter (35 residues among the 134 located in regular secondary structure elements). This number was similar when removing either of the two consistent datasets (50.6 and 60.8 MHz). However, when removing the 81.0 MHz dataset, this number decreased significantly (from 35 to 17). Not surprisingly, the number of R_{ex} parameters was still high when removing R_1 or *NOE* data at 81.0 MHz. However, when discarding R_2 at 81.0 MHz, the number of R_{ex} decreased to the low number encountered when removing all three parameters at 81.0 MHz. Thus, R_2 recorded at 81.0 MHz were excluded from the subsequent model-free analysis. This is not surprising because, for molecules of $\sim$ 30 kDa, R_2 has a high weight in the $J(0)$ consistency test function. In fact, as we proposed in Chapter 2 [195], the $J(0)$ consistency test should be used to assess consistency of multiple field transverse relaxation rates. Despite our best efforts, which involved recording a total of three datasets at 81.0 MHz over a period of two years and carrying numerous parameter optimisations, we never succeeded to record R_2 at 81.0 MHz that was flawless with the available hardware. The cause for the R_2 at 81.0 MHz to be slightly inconsistent with the rest of the data is still unknown although it could be caused by factors such as water saturation or probe stability during the CPMG pulse train. Nevertheless, the inconsistency was detected and does not affect the quality of the extracted information. On the contrary, some studies could contain artifacts resulting from a failure to recognise such inconsistent datasets. We therefore believe some consistency test should always be done as proposed before (see Chapter 2, [195]).

7.3.3 Model-Free Analysis

As stated in Chapter 1, the model-free formalism [40, 51, 167, 168] is the preferred approach for spin relaxation data analysis. Using this formalism, two main parameters, S^2 and τ, account respectively for the restriction of the motion for one vector (*e.g.* the N-H bond) and the effective upper limit for the timescale of this motion (normalised by S^2). Moreover, the R_{ex} parameter can account for slow motions on the μs-ms timescale contributing to the observed R_2. Several programs have been developed for the optimisation of the model-free parameters. We used the open source program *relax* [51, 52] with the protocol presented in Figure 7.1. As stated above, since the consistency test revealed some inconsistency in the 81.0 MHz data, an in-depth look at the data was performed and we found that the R_2 at 81.0 MHz were inconsistent. Hence, we did not use these data for model-free analysis. Fortunately, because the inconsistency was detected, high quality is anticipated for the extracted information.

A re-analysis of TEM-1's spin relaxation data [240] using the same approach as the one used here for PSE-4 has been presented recently [79]. In this recent study, data were also re-analysed using the same approach as in Savard and Gagné [240], but with *ModelFree-4.20* [174, 214] to avoid problems present in the preceding versions of the program [51]. In the following discussion, results obtained for PSE-4 will be compared to those for TEM-1 in either publication, especially when differences arise.

7.3.3.1 Description of Global Diffusion

The diffusion of PSE-4 is homogeneous. This is confirmed by the derivation of model-free parameters using a local diffusion tensor for each N-H vector. Indeed, the mean local τ_m is 12.70 ± 0.87 ns (excluding the three C-terminal residues) with only a few dispersed outsiders, thus with no region in the 3D structure showing differential diffusion (data not shown).

Table 7.2 shows a summary of the optimisation results for the different diffusion tensors tested. The best model is an ellipsoid described by the parameters in Tables 7.2 and 7.3. A representation of this diffusion tensor, and of the orientations of the N-H vectors used for its optimisation, is available in Figure 7.4. As can be seen, N-H orientations are generally well dispersed over the structure, although the axis along $\mathfrak{D}_z$ seems less sampled. However,

Table 7.2: Summary of the diffusion tensor optimisation.*

Diffusion model	*AIC*	τ_m (ns)	$\mathfrak{D}_\parallel/\mathfrak{D}_\perp$	θ (°)	ϕ (°)	ψ (°)
Local τ_m	1442.1†	12.70				
Sphere	1492.2	12.39	1			
Prolate spheroid	1391.3	12.67	1.33	147.5	50.1	
Oblate spheroid	1475.6	12.45	0.92	38.9	27.2	
Ellipsoid‡	**1385.1**	**12.68**	**1.32**	**166.2**	**146.8**	**131.6**

* Using 134 residues in regular secondary structures with relaxation data at three magnetic fields.
† Mean value excluding the three C-terminal residues.
‡ Lowest *AIC*: selected description of PSE-4 diffusion.

Table 7.3: Diffusion tensor parameters.

Isotropic component of diffusion	$\mathfrak{D}_{iso}$	13.141 ($\pm$ 0.024) x 10^6 s^{-1}
Anisotropy of diffusion	$\mathfrak{D}_a$	3.75 ($\pm$ 0.19) x 10^6 s^{-1}
Rhombicity	$\mathfrak{D}_r$	0.080 ($\pm$ 0.022) s^{-1}
Diffusion constants for the *x* axis	$\mathfrak{D}_x$	11.59 ($\pm$ 0.10) x 10^6 s^{-1}
Diffusion constants for the *y* axis	$\mathfrak{D}_y$	12.19 ($\pm$ 0.11) x 10^6 s^{-1}
Diffusion constants for the *z* axis	$\mathfrak{D}_z$	15.64 ($\pm$ 0.13) x 10^6 s^{-1}
Global correlation time	$\tau_m = 1/(6\,\mathfrak{D}_{iso})$	12.683 ($\pm$ 0.024) ns

since the shape of the diffusion tensor covers the shape of the structure, we are confident with its overall value as the description of PSE-4 rotational diffusion. Moreover, the parameters are close to the prolate description of TEM-1 presented in Savard and Gagné [240] where $\mathfrak{D}_\parallel/\mathfrak{D}_\perp$ was equal to 1.23. Indeed, using the following relation:

$$\mathfrak{D}_\parallel/\mathfrak{D}_\perp \approx \frac{\mathfrak{D}_z}{(\mathfrak{D}_x+\mathfrak{D}_y)/2} \tag{7.5}$$

a value of 1.32 is calculated for $\mathfrak{D}_\parallel/\mathfrak{D}_\perp$ in PSE-4. Also, anisotropy for PSE-4 extracted from the model-free analysis generally agrees with the shape of the crystal structure [165]. Indeed, the relative moments of inertia are 1.00, 0.89, and 0.59 as determined using *pdbinertia* (A. G. Palmer, Columbia University, New York, NY). These can be compared to the $\mathfrak{D}_\parallel/\mathfrak{D}_\perp$ ratio by the following calculation: $((1.00+0.89)/2)/0.59$, which gives an apparent ratio of ~ 1.60, slightly higher than that obtained from spin relaxation, the lower value in solution being potentially caused by some loops being flexible compared to the static view given by the crystal structure.

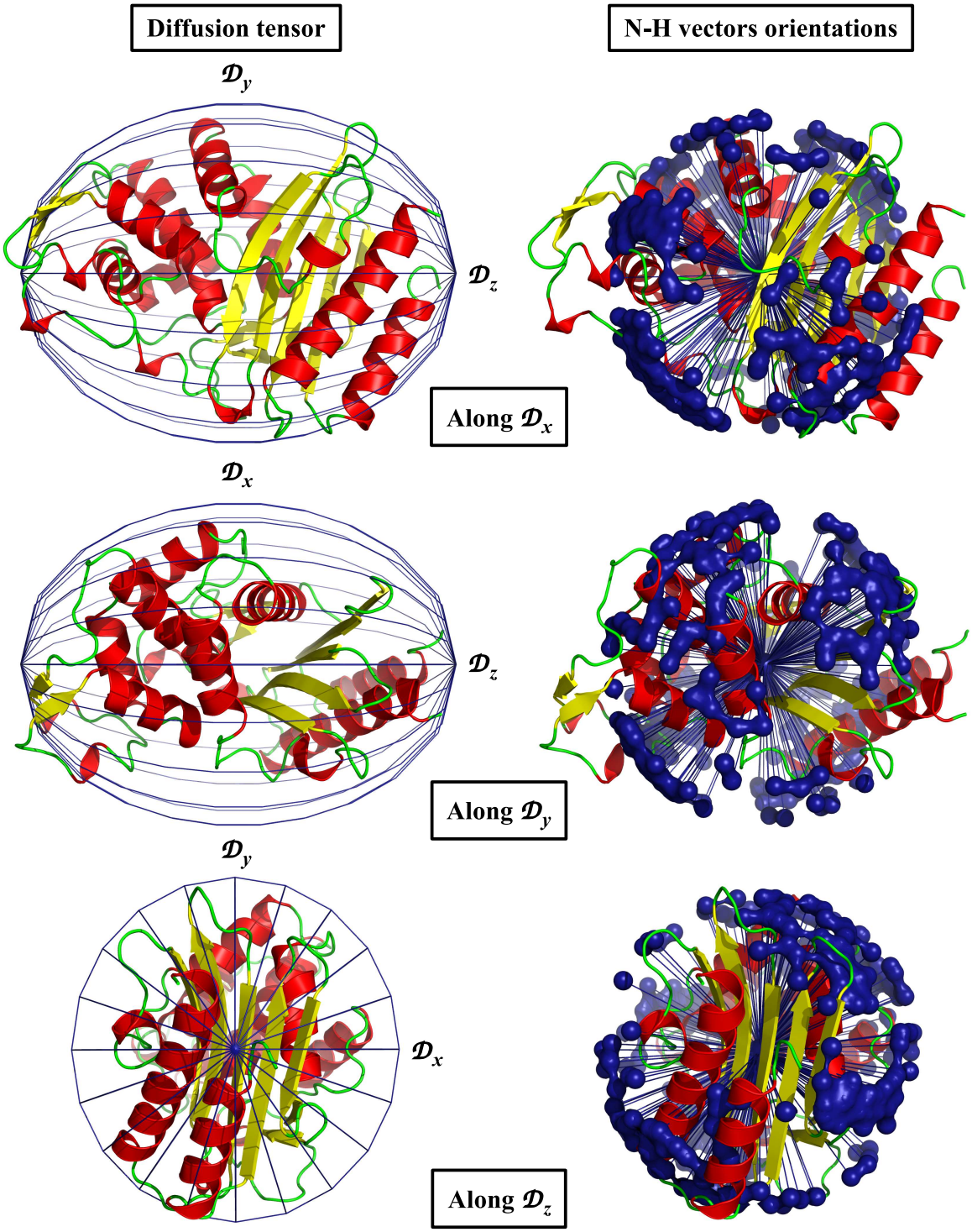

Figure 7.4: Representation of the diffusion tensor (left) and of the N-H vectors orientations (right). N-H vectors orientations are shown as surface on artificial vectors of length 20 Å placed at the center of mass of the protein. These vectors are duplicated in the opposite direction because of symmetry in the ellipsoidal diffusion tensor. Missing residues in the crystal structure (Ser^{22}, Ser^{23}, Gln^{293}, Ser^{294}, and Arg^{295}) were added for visualisation of the whole protein; their exact position being unknown.

Finally, diffusion description from model-free analysis is close to that estimated from hydrodynamics calculations using *HYDRONMR* [92] (with parameter *a*, the effective radius of the atomic element, set to 2.6 Å, as in Hall and Fushman [107]). In fact, using this approach, $\mathfrak{D}_a$ = 3.82 x 10^6 s^{-1} *i.e.* within 2 % of model-free derived $\mathfrak{D}_a$. Moreover, values of the diffusion constant for the three principal axes of the diffusion were within 4 % of the model-free derived values, with $\mathfrak{D}_{\parallel}/\mathfrak{D}_{\perp} = 1.30$. A similar analysis for TEM-1 is in agreement with PSE-4 having a higher anisotropy than TEM-1 and endorse model-free results for global tumbling.

7.3.3.2 Description of Local Motions

Figure 7.5 shows the optimised residue specific model-free parameters. Even though parameters are far more important than model listing, we can summarise PSE-4 local model-free models as follows:

*m*0	1 residue,
*m*1	129 residues,
*m*2	46 residues,
*m*3	28 residues,
*m*4	3 residues,
*m*5	19 residues,
*m*6	3 residues,
*m*7	no residue,
*m*8	no residue,
*m*9	1 residue,

for a total of 230 N-H vectors analysed. As is seen here, most residues (*i.e.* 77 %) are fitted with simple models *m*1 and *m*2. Local model-free parameters for PSE-4 have been deposited in the BMRB under accession number 6838 and are available in Appendix 3 (Table 10.3).

Order parameters

The mean order parameter (S^2) of PSE-4 backbone amides is 0.861 ± 0.087 (0.868 ± 0.051 excluding the three C-terminal flexible residues). Additionally, the mean S^2 for the secondary structure core (0.879 ± 0.035) is slightly higher and less dispersed than that for the loops and very short helices (0.834 ± 0.125; 0.852 ± 0.066 excluding the flexible C-terminus). Clearly, PSE-4 is a highly ordered protein on the ps-ns timescale, displaying $S^2 > 0.85$ (the typical value for regular secondary structures, equivalent to motion on a cone of semi-angle $\theta_0 = 19°$ [167]) for 70 % of its amides (see Figures 7.5, 7.6, and 7.7-A). The most rigid amides are located around the active site and Ω loop, as is the case for TEM-1 [240]. Only some solvent exposed loops are less rigid, with just five residues (Asn^{53}, Ser^{292}, Gln^{293}, Ser^{294}, and Arg^{295}) possessing an order parameter below 0.70, indicating the absence of high amplitude backbone motions on the ps-ns timescale in PSE-4, similar to previous observations for TEM-1. This high rigidity might be related to the low thermal stability of both TEM-1 and PSE-4, which both precipitate *in vitro* at temperatures > 41 °C (data not shown).

When comparing TEM-1's model-free order parameters with those of PSE-4, TEM-1 appears slightly more rigid than PSE-4 (Figure 7.8). Differences seem to be smaller for the Ω loop where order parameters agree more than for other loops, pointing to a conservation of order for this important part of the enzyme. This is also the case around the Ser^{70}-X-X-Lys^{73} tetrad and for the 'SDN' loop (residues 130-132) where S^2 parameters are elevated in both TEM-1 and PSE-4. This similarity of backbone dynamics on the ps-ns timescale might hide important differences for side-chain motions as is the case for calmodulin [158]. However, this is beyond the scope of the current study.

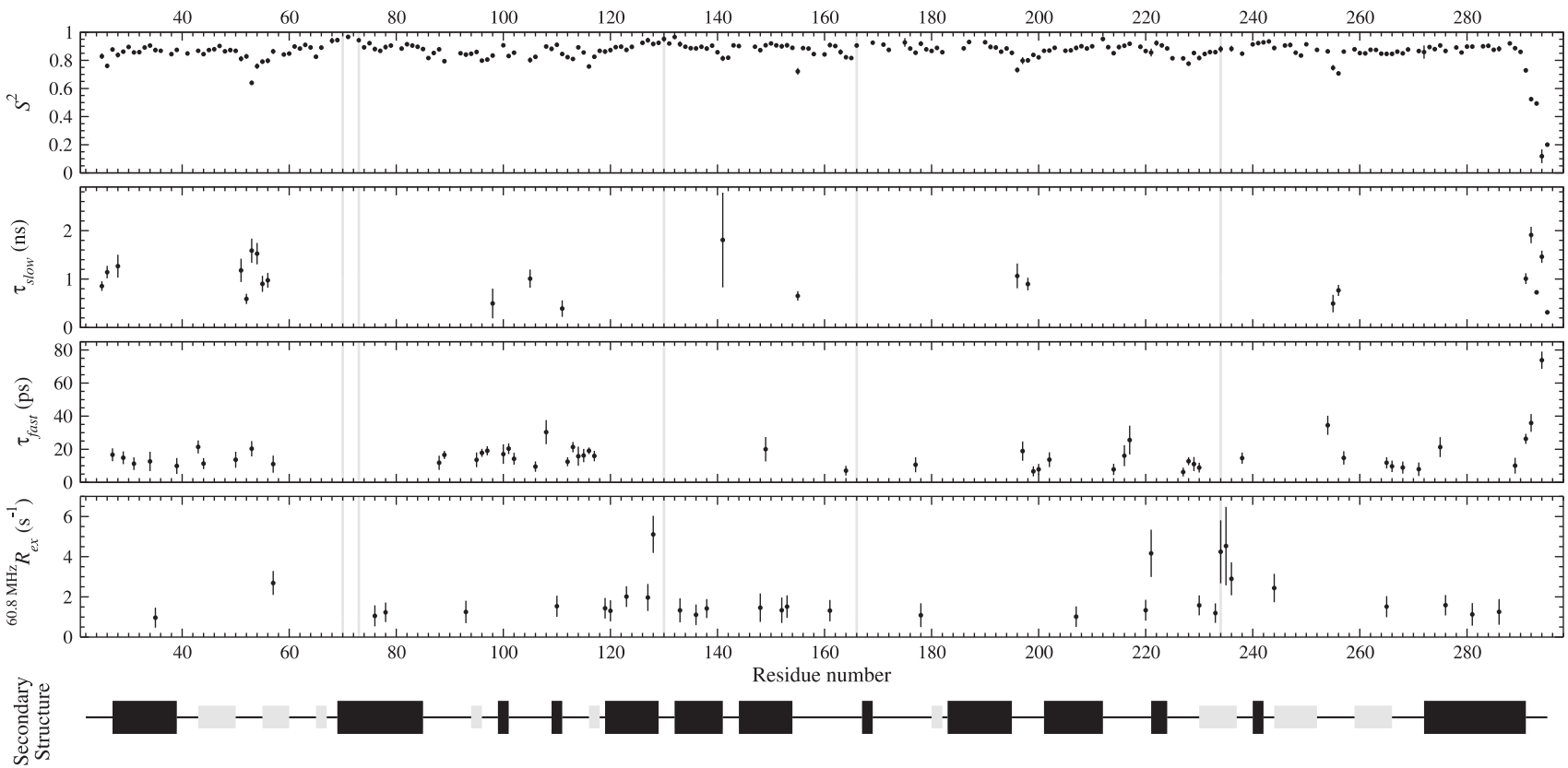

Figure 7.5: Optimised model-free parameters. Shown are the S^2, τ (on both slow, τ_s, and fast, τ_e and τ_f, timescales), and R_{ex} (at 60.8 MHz) values. Important active site residues are highlighted vertically in light grey. Secondary structures are shown with α helices as wide black boxes, and β sheets as narrow grey boxes.

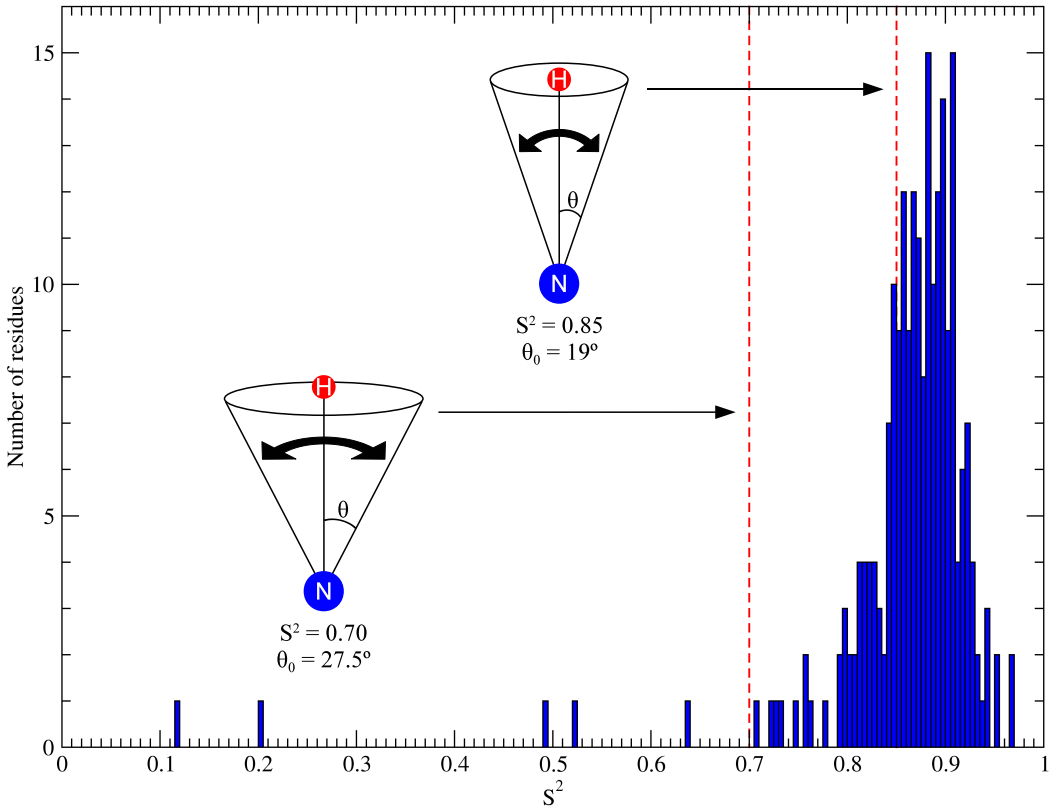

Figure 7.6: Distribution of order parameters for PSE-4. The red dashed vertical lines represent S^2 values of 0.70 and 0.85 and are shown with their equivalent representation using a 'motion in a cone' model (with θ_0, the cone semi-angle, calculated from Equation 1.23, [167]).

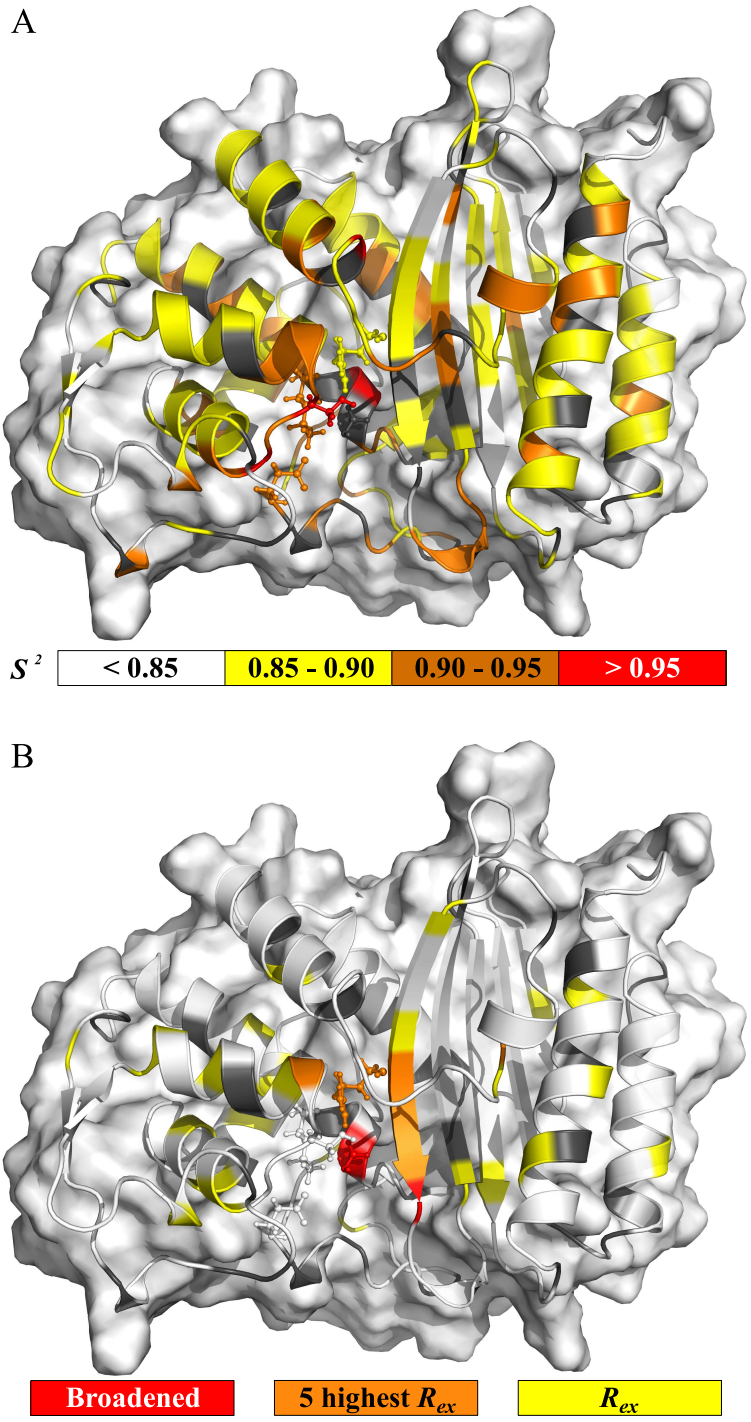

Figure 7.7: Motions extracted from model-free analysis. (A) Backbone amide ps-ns timescale generalised order parameter (S^2). (B) Residues fitted using a conformational exchange term (R_{ex}, in model-free models *m*3, *m*4, *m*7, *m*8 or *m*9). In all inserts, grey is used for residues without data (prolines, overlapped, and unassigned). In the R_{ex} insert, white is used for absence of the parameter in the model fitted. Active site residues (Ser^{70}, Lys^{73}, Ser^{130}, Glu^{166}, and Arg^{234}) are shown in the stick representation. Missing residues in the crystal structure (Ser^{22}, Ser^{23}, Gln^{293}, Ser^{294}, and Arg^{295}) were added for visualisation of their fitted parameters.

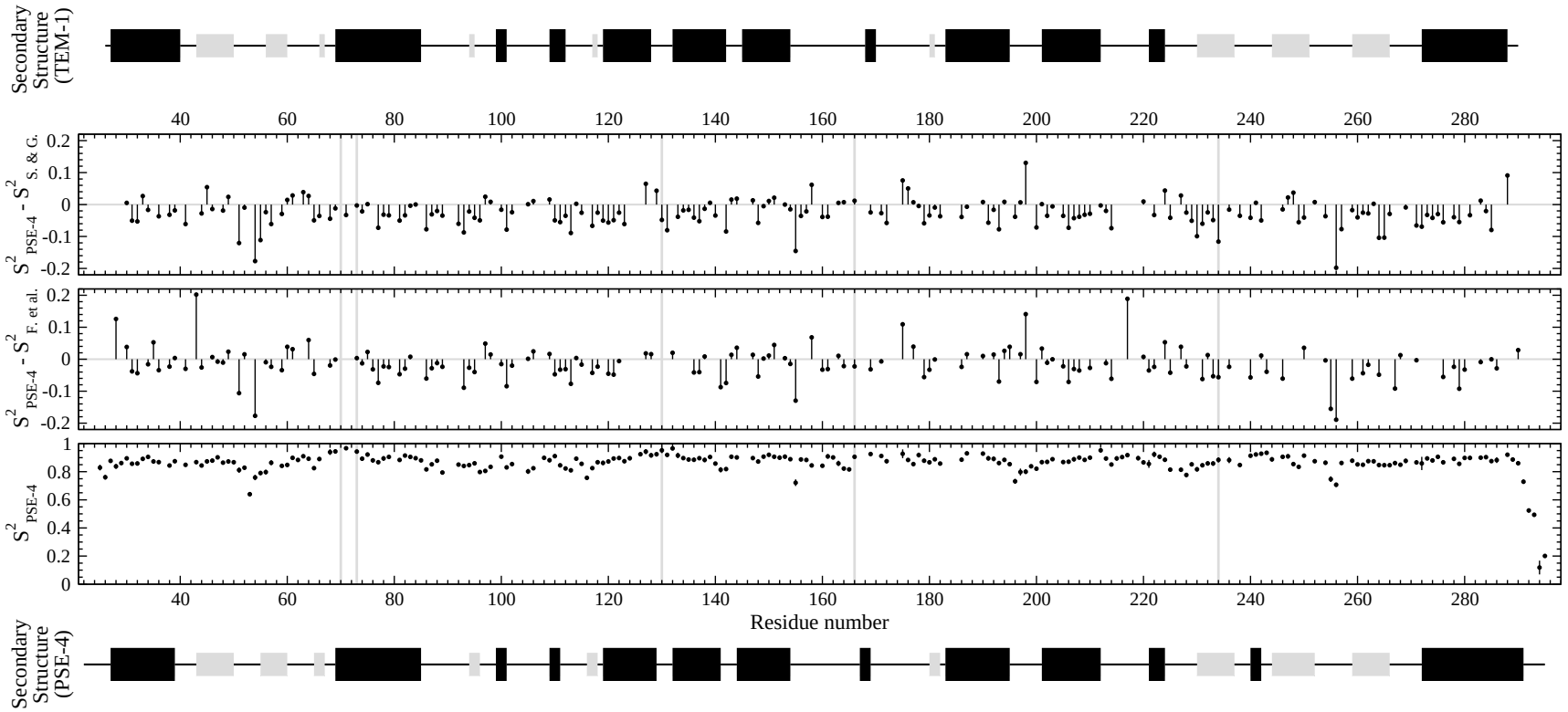

Figure 7.8: Comparison of PSE-4 and TEM-1 order parameters. Differences are shown for either the TEM-1 order parameters of Savard and Gagné ($S^2_{S.\ \&\ G.}$, [240]) or the order parameters using the same analytical approach as in the current study ($S^2_{F.\ et\ al.}$, [79]). Important active site residues are highlighted vertically in light grey. Secondary structures are shown with α helices as wide black boxes, and β sheets as narrow grey boxes.

Conformational exchange

Figure 7.7-B shows residues for which a contribution to R_2 from μs-ms motions had to be accounted for during model-free minimisation. R_{ex} parameters depend on several factors (timescale of exchange, populations of either states and chemical shift difference, see Section 7.3.4). Conformational exchange can be detected either for a moving N-H moiety or for a rigid vector with a moving neighbour modulating its chemical shift. This can also be invisible for certain combinations of timescales, populations and chemical shift changes. R_{ex} parameters from model-free analysis are considered in the fast exchange regime and thus scaled quadratically with the magnetic field. They are presented in this study for an effective magnetic field of 60.8 MHz. Thus, R_{ex} for TEM-1 [240] were rescaled from their originally associated field (50.6 MHz) for comparison purposes.

In PSE-4, 32 residues have a non null R_{ex} parameter. Of these, five are particularly important because of both their elevated R_{ex} parameter and localisation on the protein 3D structure. These are residues Thr^{128} ($R_{ex} = 5.1 \pm 0.9$ s^{-1}), Leu^{221} ($R_{ex} = 4.2 \pm 1.2$ s^{-1}), Arg^{234} ($R_{ex} = 4.2 \pm 1.6$ s^{-1}), Ser^{235} ($R_{ex} = 4.5 \pm 2.0$ s^{-1}), and Gly^{236} ($R_{ex} = 2.9 \pm 0.8$ s^{-1}) which are located 4.0–12.6 Å from the active site (N-H to N-H distance with Ser^{70}). This is consistent with two nearby residues (Ser^{70} and Ala^{237}) not being observed, probably due to extreme broadening arising from important μs-ms motions. Indeed, residue Ser^{235} even is fitted using model *m*9 (with the second largest R_{ex} in PSE-4) which means that its dynamics is dominated by conformational exchange. Since these motions are near the surface of the active site cavity, conformational exchange could arise because of a ligand moving in and out of the cavity. A potential candidate for this motion could be a structural water molecule moving slowly between residues Asn^{214}, Arg^{234}, and Ser^{235} as seen in a 5 ns MD simulation of TEM-1 [234]. Indeed, in these simulations, the network of H bonds between active site residues was frequently disrupted by water molecules. This would point to a conservation of slow motions in the active site for both TEM-1 and PSE-4. The motion of this water molecule would also affect residues Ser^{70} and Ala^{237} (extremely broadened), both being on the path which the ligand would take to possibly access residues Asn^{214}, Arg^{234}, and Ser^{235}. The R_{ex} for Gly^{236} could be explained in the same way. Another candidate for causing line broadening in the active site would be the water molecule bridging residues Ser^{70}, Glu^{166}, and Asn^{170}, also observed in the same study. The extreme broadening of N-H groups of Ser^{70} and Ala^{237} might also be explained by their proximity (N-H to N-H distance: 3.0 Å) where the movement of one N-H group would affect the other. These hypotheses are also plausible for TEM-1, where R_{ex} parameters arise near the active site and Ala^{237}'s amide could not be

observed (nor assigned).

Active site residues

TEM-1's active site has been shown to be extremely ordered on the ps-ns timescale with several residues displaying order parameters higher than 0.94 [240]. This was consistent with active site residues displaying lower than average B-factors for TEM-1 in the presence of a sulfate ion in the active site [129]. In PSE-4, the most rigid residues on the ps-ns timescale (highest S^2) are also located in the active site, pointing to a meaningful conservation of this feature which could also be foreseen from backbone amide B-factors [165] (see Figure 7.9).

Indeed, qualitative dynamics information can be extracted from crystallographic B-factors (or temperature factors). However, compared to model-free order parameters, differences can originate because B-factors are dominated by lattice disorder [153]. Moreover, these are often recorded at very low temperatures compared to NMR, as in the case of PDB 1G68 [165] for which X-ray diffraction data was recorded at 100 K. Other possible differences might also arise from crystal packing or translational motions within the crystal. Crystal packing interactions would quench motions while translational motions wihtin the crystal would affect B-factors, but be invisible to S^2 from NMR. Finally, B-factors do not report on a specific timescale and thus can be influenced by motions much slower than the ps-ns timescale probed by order parameters obtained from ^{15}N spin relaxation data. Hence, in our case, some differences are seen while some parts show better agreement (Figure 7.9). This is the case for both N- and C-termini, the Thr^{51}–Gly^{54} loop, the Leu^{225}–Trp^{229} loop, and the Glu^{254}–Pro^{258} loop. On the other hand, the Leu^{102}–Val^{108} loop, which displays fairly low order parameters (compared to the rest of the protein), possesses low nitrogen amide B-factors (*i.e.* low flexibility); these may be artifacts due to crystal packing interactions as this loop is closely packed against two helices (Leu^{221}–Val^{224} and Met^{272}–Thr^{291}) from a neighbour protein in the crystal lattice of PDB 1G68 [165]. Additionally, the region from residue Ala^{84} to Asp^{101} displays very high B-factors although the mean S^2 for this region (0.846 ± 0.034) is only slightly below average. In this case, B-factors might see a broader timescale than that probed by the model-free order parameters (*i.e.* ps-ns).

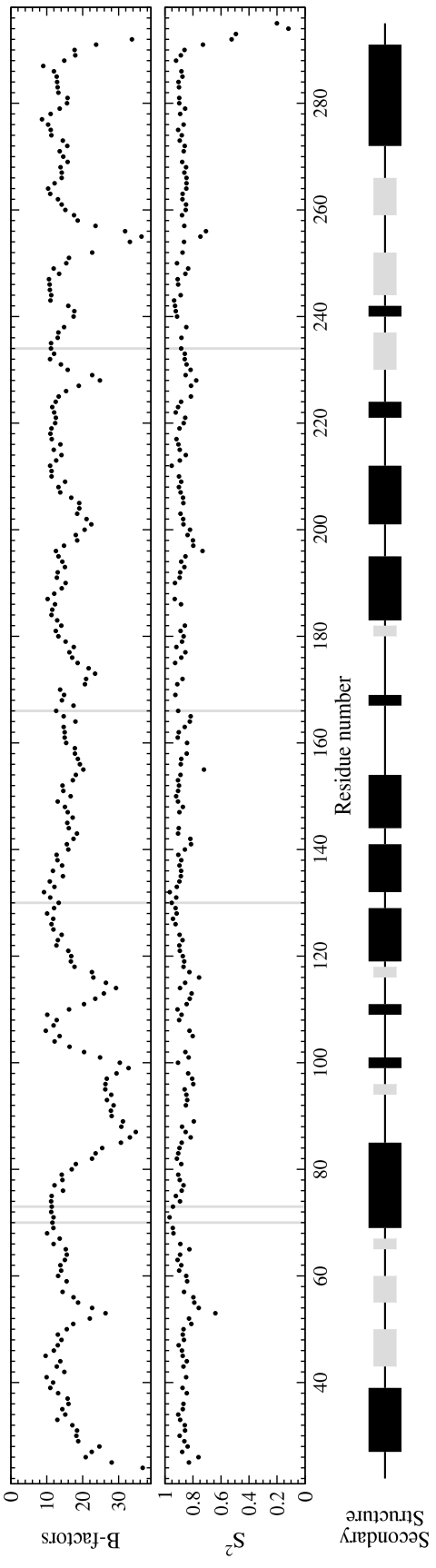

Figure 7.9: Comparison of order parameters (S^2) with amide nitrogen crystallographic B-factors from PDB 1G68 [165]. Important active site residues are highlighted vertically in light grey. Secondary structures are shown with α helices as wide black boxes, and β sheets as narrow grey boxes.

Ser^{70} N-H correlation for Ser^{70} is not observed. In TEM-1, it is severely overlapped and broadened, thus unusable. This strongly supports the existence of motions on timescales slower than global tumbling (*e.g.* μs-ms) also affecting other residues in the vicinity which display broadened backbone (Ala^{237}, see Chapter 5, [196]) or side-chain (Lys^{73}, see Chapter 6) resonances.

Lys^{73} Lys^{73} is suspected of being involved in the first catalytic step (acylation), where its side-chain N_ζ group could activate Ser^{70} by accepting a proton from the side-chain hydroxyl group (2.8 Å away, reviewed in [81]). Lys^{73} was fitted to model *m*1 with one of the highest order parameters throughout PSE-4 (0.94 $\pm$ 0.01). This contrasts with the low intensity of its N-H cross-peak which suggests that chemical exchange broadening may be present. Indeed, Lys^{73}'s C_α is the weakest of all lysines C_α (see Figure 6.1). Moreover, we were unable to see Lys^{73}'s side-chain further than the C_β, thus preventing the titration of the side-chain N_ζ group (see Chapter 6). These, again, indicate that important μs-ms motions are nearby. These motions could be similar to those presumably affecting Ser^{70}, located less than 6 Å away (N-H to N-H). If rejecting model *m*1 because of these evidences of slow motions arising nearby, the second lowest *AICc* score for Lys^{73} within PSE-4 is model *m*3 with a R_{ex} parameter of 0.7 $\pm$ 0.5 s^{-1}. Compared to the R_{ex} parameters for other residues, this R_{ex} would be the lowest and the one with the highest relative error. Hence, the possibility for Lys^{73} N-H to be fitted using a R_{ex} parameter is questionable although strong signs of conformational exchange are present, especially for the side-chain. The situation in TEM-1 was very similar and Lys^{73} fitted model *m*1 with a S^2 of 0.95 $\pm$ 0.02. These data indicate that Lys^{73}'s side-chain could be affected by motions in the slow- or intermediate-exchange regime. In these conditions, R_{ex} does not scale quadratically with the magnetic field [189]. This could explain the low R_{ex} with high error obtained for Lys^{73} when using model *m*3 where the model-free fitting procedure scales the R_{ex} quadratically for multiple field data. Incorporating the parameter α from Millet *et al.* [189] in the fitting procedure could potentially alleviate this problem. Finally, if present, these motions could explain the extreme broadening of Lys^{73}'s side-chain, as well as Ser^{70} and Ala^{237} amides.

Tyr^{105} Tyr^{105} displays a slow correlation time (τ_s) of 1008 $\pm$ 188 ps in conjunction with a S^2 of 0.80 $\pm$ 0.02 using the two-timescale model *m*5. In TEM-1, this residue was one of the most flexible [240] and the selected model did not incorporate this kind of two-timescale motion as in PSE-4. This could be of significant importance in regards to substrate

recognition and specificity. The motion detected here could however be artifactual because model *m*2 also fits relatively well PSE-4 experimental data: with a higher S^2 (0.85 $\pm$ 0.01), but with a correlation time of 26 $\pm$ 4 ps, similar to the case in TEM-1. On the other hand, model *m*5 could suit data almost as well in TEM-1, yielding a similar S^2 (0.79) but with a τ_s of $\sim$ 500 ps.

In another work, Doucet *et al.* [63] discussed the importance of this residue for substrate specificity and proposed that steric restriction of the active site by the side-chain of residue Tyr^{105} could allow the correct positioning and stabilisation of substrates within the active site, thus facilitating catalysis. This gate-keeping function was further investigated and the side-chain of Tyr^{105} was shown to adopt two conformations: one in which the side-chain points toward Val^{216} (open state, rotamer *t*) and one in which the side-chain points toward Glu^{104} (closed state, rotamer *m*, only visible in inhibitor bound TEM-1) [61]. This motion seen for TEM-1 could influence the dynamics of the backbone N-H moiety of Tyr^{105} in PSE-4 where rotamer *t* is present, with only minor electronic density toward the position of rotamer *m* (data not shown). Using *SHIFTS* (version 4.1.1) [287], chemical shifts for the two rotamers discussed in Doucet *et al.* [63] were predicted. Based on these results, only two residues would have their backbone ^{15}N chemical shift modified by such a transition between the two rotamers *t* and *m*. Of course, Tyr^{105} amide nitrogen has a different chemical shift in both rotamers, although the difference is very small (12 Hz at 60.8 MHz) and would not give rise to a significant R_{ex}. Ser^{106} would be more affected with a difference in ^{15}N chemical shift of 286 Hz at 60.8 MHz ($\sim$ 0.5 ppm) between the two rotamers. This could be expected to give rise to a R_{ex} term, although no such parameter was observed in the model-free minimisation. Indeed, even when deliberately choosing a model with a R_{ex} term (*i.e.* *m*3, *m*4, *m*7, *m*8 or *m*9), no significant R_{ex} term was fitted and values tended to 0. A possible explanation for this situation is that the timescale for this conversion from rotamer *t* to rotamer *m* would be on the sub-nanosecond timescale as proposed by the selected model for Tyr^{105}. If so, it would not influence transverse relaxation of Ser^{106} and would only be probed by Tyr^{105} itself.

Ser^{130} Residue Ser^{130} has been proposed to participate in the catalytic process [203] and was shown to be of clinical importance for enhanced resistance (see Lahey Clinic Website). In the crystal structure by Lim *et al.* [165], the hydroxyl group of Ser^{130} displays two alternative positions. Such alternative positions with a shared occupancy of 0.5 between two conformations are seen for eight other residues (Ser^{140}, Glu^{159}, Asp^{168}, Ile^{186}, Ser^{188}, Leu^{190}, Glu^{208}, and Ser^{209}) in the crystal structure [165]. From model-free

analysis, Ser^{130} fits model *m*1 (as other residues we could observe with atoms displaying shared occupancy of 0.5) with a S^2 of 0.95 ± 0.02. The movement of its side-chain might not influence the amide transverse relaxation of Ser^{130}, but, depending on the timescale, could be the cause of such conformational exchange effects seen for nearby residues Ser^{70} (not observed, broadened), Thr^{128} ($R_{ex} = 5.1 \pm 0.9$ s^{-1}), Arg^{234} ($R_{ex} = 4.2 \pm 1.6$ s^{-1}), Ser^{235} ($R_{ex} = 4.5 \pm 2.0$ s^{-1}), Gly^{236} ($R_{ex} = 2.9 \pm 0.8$ s^{-1}), and Ala^{237} (not observed, broadened), all within 5 to 8 Å from the side-chain of Ser^{130}. In TEM-1, no model-free parameter could be extracted for Ser^{130} in the original study of Savard and Gagné [240]. However, in the re-analysis using *ModelFree-4.20* [79], Ser^{130} was assigned a S^2 of 0.99 ± 0.01, exactly as Asp^{131}, indicating a high local rigidity. In PSE-4, as for Lys^{73}, Ser^{130} order parameter is very high. This is also the case for other residues of the conserved Ser^{130}-Asp^{131}-Asn^{132} (0.95 ± 0.02, 0.92 ± 0.01, and 0.97 ± 0.01, respectively) structural motif (known as the 'SDN' loop). These data in TEM-1 and PSE-4 point to a conservation of ps-ns order in the active site of class A β-lactamases.

Glu^{166} Residue Glu^{166} is directly involved in catalysis, probably for both acylation and deacylation steps (reviewed in [81]). As was the case for the two catalytic residues Lys^{73} and Ser^{130}, residue Glu^{166} fits model *m*1 with a fairly high order parameter (0.91 ± 0.02). In the re-analysis using *ModelFree-4.20* for TEM-1, Glu^{166} fitted model *m*1 with $S^2 = 0.94 \pm 0.02$, in contrast with model *m*4 in the original work [240]. Using *relax* , this residue was assigned model *m*2 with $S^2 = 0.93 \pm 0.02$ and $\tau_e = 47 \pm 24$ ps. This is not surprising as the R_{ex} first detected was of low significance and, thus, *m*4 could simplify to *m*1 or *m*2 (two similar models). Rigidity for Glu^{166} thus seems similar in TEM-1, although a bit higher as for many other residues.

Arg^{234} In carbenicillin-hydrolysing β-lactamases such as PSE-4, residue 234 is an arginine. In other class A β-lactamases, it is a lysine. Arg^{234} first fitted model *m*2 with an average S^2 of 0.88 ± 0.02. However, the value measured for R_2 at 50.6 MHz is most likely under-estimated and erroneous, because of the partial overlap with residue Lys^{192}, a result of the poorer resolution at the lower field. Indeed, Arg^{234} has one the highest R_2 at both 60.8 and 81.0 MHz, whereas at 50.6 MHz the measured R_2 is much lower than for surrounding residues. Hence, when excluding R_2 at 50.6 MHz, the selected model becomes *m*3 with an unchanged order parameter of 0.88 and a R_{ex} parameter of 4.2 ± 1.6 s^{-1}. This is much more logical for this residue because the majority of surrounding residues display signs of

conformational exchange. Indeed, residues Asp^{233}, Ser^{235}, and Gly^{236} all possess a R_{ex} term (respectively 1.2 ± 0.5, 4.5 ± 2.0, and 2.9 ± 0.8) while residue Ala^{237} is not even observed most probably because of line broadening. Moreover, for TEM-1, the presence of R_{ex} for Arg^{234} was also found using either *ModelFree-4.20* or *relax*, both with a R_{ex} of $1.9 \pm 0.4\ s^{-1}$ and a high S^2 of 0.94 ± 0.02. It should be noted here that surrounding residue Gly^{236} also possessed a R_{ex} while residue Ala^{237} was also not observed. Thus, order on the ps-ns timescale would be higher in TEM-1, but the presence of slow μs-ms motions would be similar, again indicating the presence of conserved μs-ms motions near the active site of class A β-lactamases.

Ω loop A 19 residue loop is located below the active site of class A β-lactamases (residues Arg^{161} to Asp^{179}). This loop is an Ω loop, a non regular secondary structure found in many proteins [77]. It was shown in two different studies to be flexible in TEM-1 using *in silico* approaches [234, 271]. Indeed, in a five ns simulation by Roccatano et al. [234], a flap-like motion of the Ω loop was present for TEM-1 in the absence of a ligand. The timescale was undefined in this study because this phenomenon was only seen once, the loop keeping its new position after the movement had happened. No such motion had been seen in the 1 ns simulation by Diaz *et al.* [65]; these inconsistencies could either be a result of the short simulation length in the Diaz *et al.* [65] study or of simulation artifacts in the Roccatano *et al.* [234] study. Nevertheless, in TEM-1, using NMR, the Ω loop was shown to be very rigid on the ps-ns timescale, although displaying the presence of some μs-ms motions [240]. This seems to unite short simulations results showing limited motions with longer simulations pointing to slow high amplitude motions. Indeed, movements on the μs-ms timescale are hardly defined using currently available MD simulations.

Our results for PSE-4 confirm this observation, although differently from what was seen in TEM-1 using NMR. In fact, only two residues within PSE-4 Ω loop display signs of conformational exchange (*i.e.* Arg^{161} and Arg^{178}). These residues are located at the extremities of the Ω loop, where it narrows (with N-H moieties separated by ~ 8 Å). Arg^{178} could represent the hinge of a movement similar to that stated above which could allow Gly^{175} (Asn^{175} in TEM-1) to reach Arg^{65} to form the hydrogen bond discussed by Roccatano *et al.* [234] (see Figure 7.10). This would correspond to a movement of ~ 5 Å, Arg^{65} carbonyl being 7.1 Å from Gly^{175} amide nitrogen in the steady-state crystal structure. This motion would fill the cavity between the Ω loop and the protein core present in both TEM-1 and PSE-4 (see Figure 7.10-D). With this cavity closed, the structure would be better

packed, possibly transiently stabilising Glu^{166} in a catalytically relevant position. The absence of R_{ex} for residues Asp^{176} and Leu^{177} does not counter indicate this possibility as the N-H moiety of Leu^{177} would point toward the solvent in both conformations and hydrogen bonding of Asp^{176} N-H group with the carbonyl of residue Lys^{173} would also be present in both conformations, hence not affecting the chemical shift. Unfortunately, due to overlapped resonances, no spin relaxation data is available for residues Lys^{173} and Leu^{174} which could sense this movement because they are closer to the protein core. However, these residues both display normal amplitude N, H_N, C_α, and C_β resonances, which could contradict their involvement into conformational exchange. Hence, current observations support the slow motion of the Ω loop proposed by Roccatano *et al.* [234], but are also consistent with a slightly different motion of the Ω loop observed by Fisette *et al.* in TEM-1 [79] and PSE-4 (Olivier Fisette and Stéphane M. Gagné personal communication).

Because of the implications of movements of the Ω loop in terms of catalysis, it will be very important to get more insights into this part of the enzyme. In fact, if a movement such as the one discussed above exists, it would allow Glu^{166} to stay close to Ser^{70} and potentially act during the acylation step [234].

Resistance to inhibitors and extended spectrum β-lactams

Extended spectrum β-lactams such as oxyimino-β-lactams (*e.g.* ceftizoxime, cefotaxime, ceftriaxone, and ceftazidime) and monobactams (*i.e.* beta-lactams with the ring not juxtaposed to another ring; *e.g.* aztreonam, as well as non commercially available tigemonam, nocardicin A, and tabtoxin) have allowed for a better fight against the resistance phenomenon. However, their beneficial effect was diminished by the rapid appearance of resistance to these molecules. The mutations for such resistance include those at positions 69, 237, 240, and 276 [144].

Additionally, β-lactamase inhibitors have been useful in the fight against β-lactam antibiotics resistance. However, since the introduction of β-lactamase inhibitors, several mutations appeared that provided resistance to those compounds which include the widely used clavulanic acid, sulbactam, and tazobactam. Several mutations have been documented which include those at positions 69, 130, 165, 275, and 276 (see Lahey Clinic Website).

Most of these mutations were found in TEM-like β-lactamases. However, even if the actual

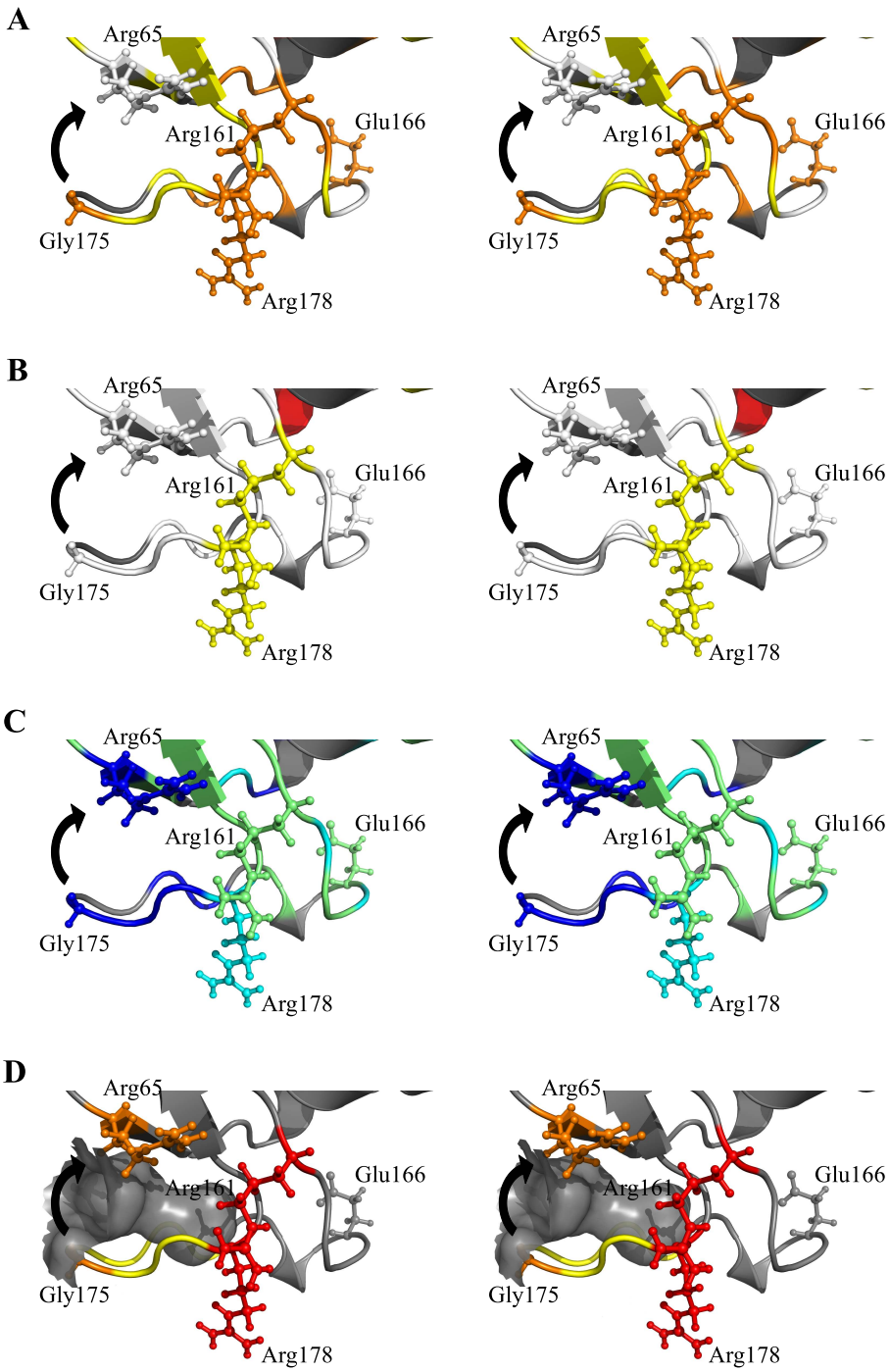

Figure 7.10: Stereoview of the cavity-filling motion for residues Glu^{171}–Leu^{177} of the Ω loop. (A) Order parameters (S^2 coloured as in Figure 7.7-A). (B) Conformational exchange (R_{ex} coloured as in Figure 7.7-B). (C) Apparent free energies of exchange (ΔG_{HX}, coloured as in Figure 7.17). (D) The cavity between the Ω loop and the protein core which the motion of residues Glu^{171}–Leu^{177} (*yellow*) would fill is shown in grey surface. Residues from the hinge (Arg^{161} and Arg^{178}) are coloured red and shown in the stick representation as well as residues Arg^{65} and Gly^{175} (orange) which would form a hydrogen bond once the motion (*black arrow*) is completed. Catalytic Glu^{166} is also shown as sticks.

effects of such mutations are unknown in PSE-4, the differential dynamics for these conserved residues in TEM-1 and PSE-4 might help understand what is happening. Here is a discussion of dynamics at positions relevant to resistance to inhibitors and extended spectrum β-lactams.

Thr^{69} In the homologous protein TEM-1, residue at position 69 (Met^{69}) was shown to be of high importance with regard to resistance against both extended-spectrum β-lactams and β-lactamase inhibitors (see Lahey Clinic Website). This is no surprise as this residue is located next to the catalytic Ser^{70}. In PSE-4, residue 69 is not a methionine, but a threonine. Thr^{69} fits model *m*1 with a very high S^2 (0.94 ± 0.02). In TEM-1, Met^{69} had also a high order parameter (0.96 ± 0.02) [240]. Given the very high S^2 at position 69 and for residues nearby, mutations at this position (in TEM-1: Met $\rightarrow$ Ile, Leu, or Val) might loosen the region around Ser^{70} so catalytic residues can reposition according to these evolved compounds.

Ser^{130} See Section 7.3.3.2 above.

Ile^{165} Inhibitor resistance was shown to be sometimes caused by mutations at position 165 (see Lahey Clinic Website) which is occupied by a tryptophan residue in TEM-1. As for position 164, N-H backbone order parameter for Ile^{165} is low relative to most residues in PSE-4 (0.82 ± 0.01). This contrasts with the catalytic Glu^{166} which displays a S^2 of 0.91 ± 0.02. The joint flexibility of residues at position 164 and 165 may allow Glu^{166} to move slightly toward Ser^{70} as could be needed for its direct activity (without help of a structural water molecule) in the acylation step of the mechanism [234, 271]. Hence, the flexibility of Trp^{165} in TEM-1 could be increased in mutants (in TEM-1: Trp $\rightarrow$ Arg, Cys or Gly) resistant to inhibitors allowing a specific positioning of Glu^{166}. However, no NMR dynamics data is available for this residue in TEM-1 [240].

Ala^{237} Mutations of residue Ala^{237} are found in resistance to extended-spectrum β-lactams (see Lahey Clinic Website). In PSE-4, this residue has not been assigned probably due to broadened resonances, thus preventing gathering of dynamic information at this position. Nevertheless, μs-ms motions could be affecting Ala^{237} and nearby residues such as Asp^{233}, Arg^{234}, Ser^{235}, and Gly^{236} which are all fitted using a R_{ex} (respectively 1.2 ± 0.5, 4.2 ± 1.6, 4.5 ± 2.0, and 2.9 ± 0.8 s^{-1}). The same situation is found in TEM-1 where no N-H cross-peak is observed for Ala^{237}, thus supporting the conservation and importance of

such slow motions. It would be interesting to see if mutants for Ala^{237} modify these slow motions affecting Ala^{237} and its neighbours.

Gly^{240} Position 240 is another position mutated in extended-spectrum β-lactamases (see Lahey Clinic Website). It is occupied by a glycine in PSE-4 (as in most carbenicillinases [165]) and is quite ordered (S^2 of 0.91 $\pm$ 0.01). However, in TEM-1, Glu^{240} is much more ordered with a S^2 of 0.97. Motions might be more released in PSE-4 as a result of Gly^{240}'s side-chain being smaller, comparatively to the situation in TEM-1 where Glu^{240} has its side-chain packed against residues 170–172 of the Ω loop. Hence, mutations in TEM-1 (Glu $\rightarrow$ Lys, but also Arg and Val) might allow more movement at this position, as is the case in PSE-4. This could also have an indirect effect on flexibility of the Ω loop.

Arg^{275} Even though it is quite far from the active site ($>$ 15 Å, Arg^{275} being located on the side of the active site entry), residue Arg^{275} is often mutated in β-lactamase inhibitor resistance cases (see Lahey Clinic Website). In PSE-4, this residue is fitted using model *m*2 with a pretty high order parameter of 0.91 $\pm$ 0.01. The situation is similar in TEM-1 where the order parameter is $\sim$ 0.93. A loosening of motional restriction might cause the augmented resistance for Arg^{275} variants by potentially allowing more motions in the periphery of the active site, hence permitting adaptation of the active site configuration in order to avoid steric clashes with bulky molecules.

Asn^{276} Mutation at position 276 is found in TEM-1 mutants resistant to extended-spectrum β-lactams and inhibitors (see Lahey Clinic Website). In PSE-4, residue Asn^{276} fits, as residue Arg^{244} (also often mutated in cases of resistance, and making side-chain contacts with Asn^{276}), model *m*3 with a S^2 of 0.87 $\pm$ 0.02 and a R_{ex} of 1.6 $\pm$ 0.5 s^{-1}. In TEM-1, where this mutation was identified as clinically relevant, model *m*1 is chosen with a fairly high order parameter of 0.92 $\pm$ 0.02. This points to a potentially important difference in TEM-1 with regards to PSE-4. Looking at the dynamics of TEM-1 mutants at this position could be of high interest for further understanding resistance to broad spectrum β-lactams.

7.3.3.3 Limits in the Analytical Approach

Many factors limit interpretation of results extracted using the model-free approach [51, 52]. Here, we will concentrate on three specific limitations: variations of the *CSA* and $r_{N\text{-}H}$ for different N-H moieties, and lack of well-defined N-H vector orientations in crystal structures used for model-free minimisation. In this study, the *CSA* was held fixed with a value of -172 ppm. This allowed comparison with dynamics data for TEM-1 [240]. The N-H bond length, $r_{N\text{-}H}$, was also held fixed with a value of 1.02 Å which also allowed comparison with dynamics data for TEM-1 [240].

Variations of the CSA Within model-free analyses, the *CSA* is generally held fixed with an assumed value of -172 ppm as in this study. However, several studies [88, 152, 264] showed that the *CSA* varies among different residues in a given protein. Variations of the *CSA*, although limited, influence results extracted using the model-free formalism. Thus, trying to optimise the *CSA* as part of the model-free analysis is a potential avenue to extracting better dynamics information because the *CSA* directly affects several parameters such as the extracted order parameters. Despite this, one needs to be really careful with such an analysis because optimising the *CSA* could lead to artifacts. We tried such an optimisation with models $m1$ to $m5$ to which the *CSA* was added as an additional parameter. After model selection using *AICc* and exclusion of outsiders ($S^2 \rightarrow 1$ and $CSA \rightarrow 0$), a value of -157.3 $\pm$ 19.3 ppm was reached, with values ranging from -237.1 to -120.0 ppm. The associated S^2 values extracted using this approach were slightly more elevated than those using the standard approach with a mean S^2 of 0.909 $\pm$ 0.061. This is certainly related to the large variation of *CSA* obtained which contrasts to published data where a narrower distribution of the *CSA* was measured (*i.e.* -170 ± 11 ppm, [264]). Results obtained by Lee and Wand [159] who also optimised the *CSA* as part of their model-free analysis of ubiquitin yielded such a narrow distribution of *CSA* values. We are thus aware that some bias and artifacts could arise in our description of the dynamics of PSE-4 by introducing a variable *CSA*. Hence, all results presented before in this study did not include such a variable parameter.

Variations of the N-H bond length Similarly to the the *CSA*, $r_{N\text{-}H}$ is generally assumed constant throughout the sequence. In the current study, a value of 1.02 Å was used. The order parameters extracted with such a value will incorporate contributions from bond vibration and libration, hence the proposal by Ottiger and Bax [208] of a value of 1.04 Å for

extraction of pure angular motions from spin relaxation data within the model-free framework. These different $r_{N\text{-}H}$ values have been equivalently proposed (1.02 Å [33], and 1.04 Å [208], respectively). Using the first value, S^2 values are $\sim$ 12 % lower than with the second (0.85 vs 0.95, respectively, for residues within rigid secondary structures) [210]. This is due to the fact that the value of 1.04 Å is an effective bond length which incorporates quantum mechanical zero-point motions of the proton. Hence, S^2 parameters extracted using this value only report on motions of the peptide plane. However, the difference between both values is only a matter of scaling and doesn't influence the conclusions resulting from the corresponding model-free analysis. Moreover, dynamics of two different proteins analysed with the same N-H bond length (either 1.02 or 1.04 Å) will compare equivalently, irrespective of whether $r_{N\text{-}H}$ is 1.02 or 1.04 Å [33], as behaviours of vectors with S^2 of 0.85 (from $r_{N\text{-}H} = 1.02$ Å) and 0.95 (from $r_{N\text{-}H} = 1.04$ Å) are indistinguishable [34]. As stated in Section 7.2, the 1.02 Å value is widely used in the community with most model-free studies using it and many programs having it as default parameter. Moreover, the study of TEM-1 dynamics was performed using this value [240]. Hence, for comparison purposes, we chose to set $r_{N\text{-}H}$ to 1.02 Å.

Absence of protons in crystal structures Crystal structure 1G68 [165] has a 1.95 Å resolution, which does not allow the visualisation of protons. Hence, derived N-H vector orientations may be erroneous from their actual average position, potentially having an effect on the model-free models selected because, because for non isotopic diffusion tensors, goodness of fit depends on N-H vector orientation compared to the diffusion tensor orientation. Moreover, for residues potentially involved in crystal contacts, orientations might be slightly off, which could also bias model-free analysis. This situation could be assessed by allowing variation of N-H bond orientations during model-free minimisation. However, we chose not to introduce such a variable into our analysis.

7.3.4 ^{15}N CPMG Relaxation Dispersion

CPMG relaxation dispersion experiments were performed to probe the ms timescale and quantitatively characterise the slow motions observed from model-free analysis in PSE-4's active site (see Section 7.3.3.2). Data were recorded at two magnetic fields (500 and 800 MHz) as Millet *et al.* showed that this is essential in order to fully characterise potentially observable motions [189].

Considering a two-state exchange process between states *A* and *B*:

$$A \underset{k_B}{\overset{k_A}{\rightleftharpoons}} B \tag{7.6}$$

dispersion experiments can potentially yield quantitative information including p_A (with $p_A = 1 - p_B$, where p_A and p_B are populations for states *A* and *B*, respectively), k_{ex} (the apparent exchange rate between both states where $k_{ex} = k_A + k_B$), and $\Delta\omega$ (the chemical shift difference between resonances in both states). Indeed, assuming $p_A \gg p_B$ and $R_{2,A} = R_{2,B}$ (respectively, the transverse relaxation rate for the resonances in sites A and B), R_{ex}, the contribution on R_2 from conformational exchange processes, is approximated as follows [189]:

$$R_{ex} \approx \frac{p_A\,(1 - p_A)\,k_{ex}}{1 + (k_{ex}/\Delta\omega)^2} \tag{7.7}$$

The exchange can either be slow, intermediate or fast on the NMR timescale. This nomenclature defines the observable resonances and their characteristics and is a function of both k_{ex} and $\Delta\omega$. A parameter, α, can be calculated to establish the exchange regime [189]:

$$\alpha = \frac{2(k_{ex}/\Delta\omega)^2}{1 + (k_{ex}/\Delta\omega)^2} \tag{7.8}$$

Slow exchange is defined when α is between 0 and 1, intermediate when $\alpha = 1$, and fast when α has a value between 1 and 2. In other words, exchange is generally slow when $k_{ex} \ll \Delta\omega$ and fast when $k_{ex} \gg \Delta\omega$. The limiting values for R_{ex} are then either [189]:

$$R_{ex} = (1 - p_A)\,k_{ex} \tag{7.9}$$

or

$$R_{ex} = \frac{p_A\,(1 - p_A)\,\Delta\omega^2}{k_{ex}} \tag{7.10}$$

for the cases of extremely slow ($kex/\Delta\omega \to 0$) or fast ($kex/\Delta\omega \to \infty$) exchange, respectively.

In the extremely slow exchange limit, R_{ex} is independent of the magnetic field [75, 219, 223]. On the contrary, in the extremely fast exchange limit, R_{ex} depends quadratically on the magnetic field [125].

When slow exchange is present, peaks from both states A and B can theoretically be observed. However, when populations are highly skewed, the low-populated resonances are hardly observable (because of S/N issues). Slow exchange can be probed by observation of the major resonance (from state A). In this case, a relaxation dispersion profile is defined by the exchange rate from state A to state B (k_A), the transverse relaxation rate in state A ($R_{2,A}$), the chemical shift difference between resonances in both states ($\Delta\omega$), and either the CPMG pulsing frequency (ν_{CPMG}) or the time between the 180° pulses in the CPMG train (τ_{CPMG}, with $\tau_{CPMG} = 1/\nu_{CPMG}$, [150]) as [266]:

$$R_2^{eff} = R_{2,A} + k_A - k_A \left[\frac{\sin\left(\frac{\Delta\omega}{\nu_{CPMG}}\right)}{\frac{\Delta\omega}{\nu_{CPMG}}} \right] \tag{7.11}$$

where R_2^{eff} is the effective transverse relaxation rate.

In the intermediate exchange regime, resonances are usually severely broadened such that they are no longer observable.

In the fast exchange regime, different information can be extracted from the single observable resonance for which the chemical shift is averaged depending on the different populations p_A and p_B and their respective chemical shifts (ω_A and ω_B). The corresponding relaxation rate then depends on R_{ex} (see Equation 7.7 above), k_{ex}, and ν_{CPMG} [150, 189]:

$$R_2^{eff} = R_2 + R_{ex} \left[1 - 2\tanh\left(\frac{k_{ex}}{2\,\nu_{CPMG}} \right) \frac{\nu_{CPMG}}{k_{ex}} \right] \tag{7.12}$$

In order to characterise conformational exchange, relaxation dispersion experiments are recorded where R_2^{eff} is measured as a function of varying ν_{CPMG} (see Equation 7.3) in order to obtain dispersion profiles. These are then fitted using Equation 7.11 or 7.12, depending on the exchange regime. Figure 7.11 shows examples of dispersion profiles in the slow and fast exchange limits, as well as in a case where dispersion is unobservable.

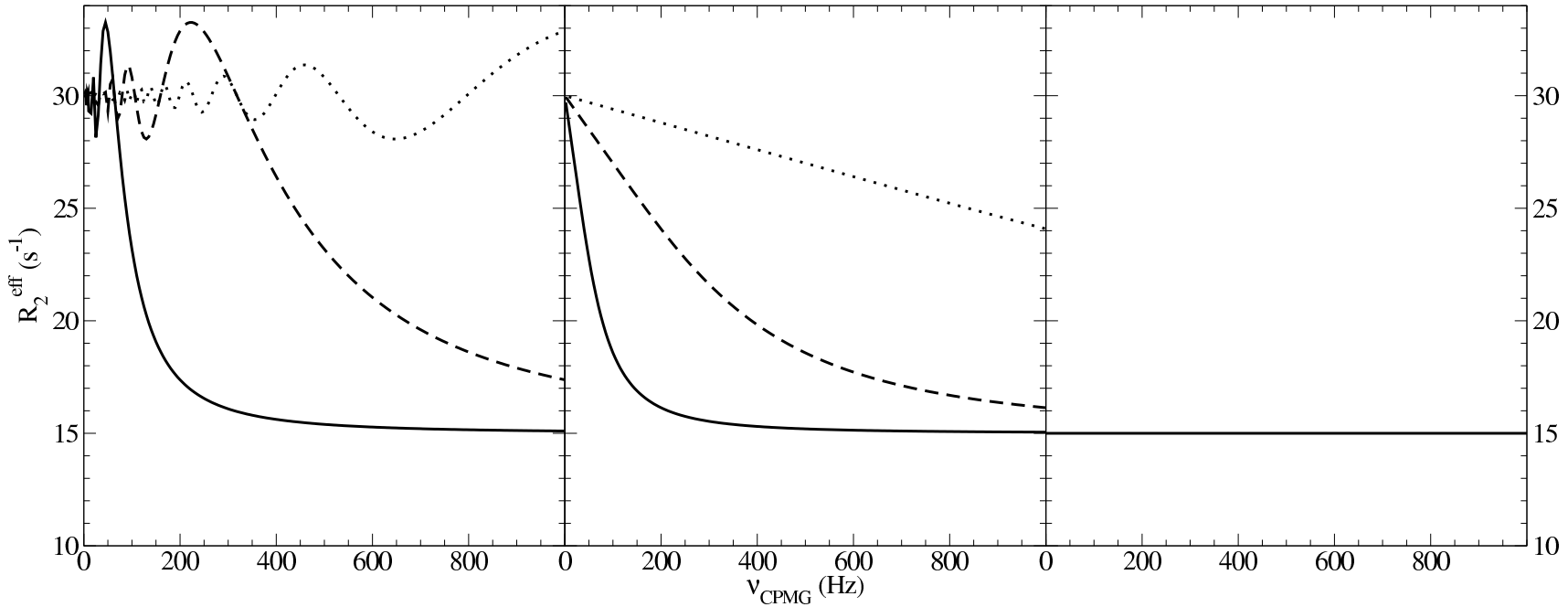

Figure 7.11: Theoretical dispersion profiles for different exchange regimes as a function of the pulsing rate ν_{CPMG}. Left: Slow exchange dispersion profiles calculated from Equation 7.11 using $R_{2,A} = 15\ s^{-1}$, $k_A = 15\ s^{-1}$, and $\Delta\omega = 200$ (solid line), 1000 (dashed line), or 5000 (dotted line) Hz. Middle: Fast exchange dispersion profiles calculated from Equation 7.12 using $R_2 = 15\ s^{-1}$, $R_{ex} = 15\ s^{-1}$, and $k_{ex} = 200$ (solid line), 1000 (dashed line), or 5000 (dotted line) s^{-1}. Right: Absence of dispersion with $R_2^{eff} = R_2 = 15\ s^{-1}$.

Unfortunately, although dispersion was perceptible for some residues based on a visual inspection of data (not shown), both curve-fitting approaches (*i.e.* Lewis Kay's group *Matlab* script [149] and *CPMGFit* — A. G. Palmer, Columbia University, New York, NY) failed to provide reliable fits. Hence, no dispersion was quantified using this approach. Figure 7.12 shows two examples of the recorded data. Ala^{135} represents a typical profile with no effect of the CPMG pulse train on the effective transverse relaxation rate (*i.e.* a flat profile), whereas Ser^{235} represents a residue with apparent dispersion, although giving rise to a poor quality fit because of noise in the data.

There are different possible reasons for such absence of detectable and quantifiable dispersion from our ^{15}N CPMG relaxation dispersion datasets:

- The population of state *B* could be very low (*e.g.* below 1 %). This would affect parameter p_A in Equation 7.7, yielding a very low R_{ex} which would be unobserved in the profile because of S/N issues.
- The chemical shift difference between states *A* and *B* could be very small (potentially because of only a small structural change between both states, *i.e.* a small change in electronic environment). This would affect parameter $\Delta\omega$ in Equation 7.7, also yielding a small R_{ex} term.
- Slow motions detected from model-free analysis of spin relaxation data could happen on a timescale faster than that probed by CPMG relaxation dispersion, *i.e.* on the μs-ms timescale, as is generally the case for R_{ex} terms obtained from model-free analysis. It is possible that such motions could not be quenched by the CPMG pulse train and, as a consequence, no variation in R_2^{eff} would be observed. An experimental approach to solve this issue would be to perform relaxation dispersion experiments in the presence of a spin lock field instead of a CPMG pulse train. This kind of experiment is known as $R_{1\rho}$ relaxation dispersion and can probe slightly faster motions than conventional CPMG relaxation dispersion experiments (see Figure 1.1). However, this approach is more difficult technically as the different spin lock fields used are usually calibrated based on measurements of scalar couplings (*e.g.* $^1J_{NH}$) in the presence and absence of the spin lock field (reviewed in [213]).

One of the above reasons (or a combination of many) could give rise to small R_{ex} terms which would not be observed because of S/N issues. Indeed, the S/N ratio of recorded data could be

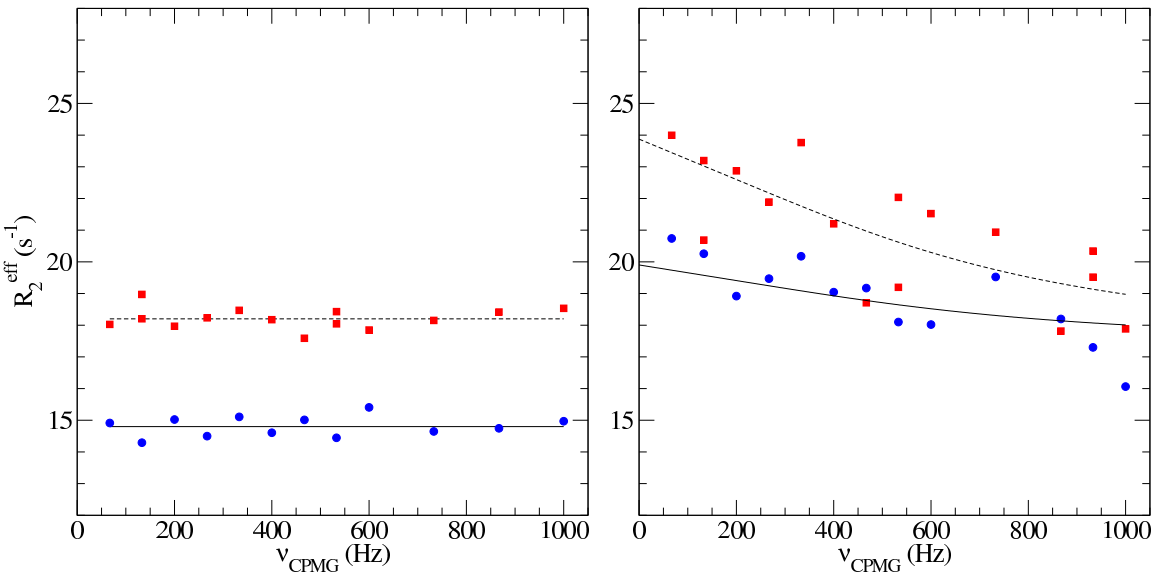

Figure 7.12: Representative relaxation dispersion profiles for residues Ala^{135} (left) and Ser^{235} (right). CPMG relaxation dispersion data are shown at 500 (circles and solid line for the proposed fit) and 800 (squares and dashed line for the proposed fit) MHz. No dispersion is detected for Ala^{235}. At 500 MHz, the equation $R_2^{eff} = 14.81$ represents the data with a low RMSD of 0.31. At 800 MHz, the equation, $R_2^{eff} = 18.22$ represents the data also with a low RMSD of 0.33. For residue Ser^{235}, dispersion is visible, although the fit (with $R_2 = 17.39 \pm 0.49$ s^{-1}, $^{600MHz}R_{ex} = 3.61 \pm 0.57$ s^{-1}, and $k_{ex} = 2029 \pm 535$ s^{-1}; the proposed R_{ex} being close to the model-free derived value of 4.53 ± 1.95) is of poor quality with a χ^2 value of 36.6 for the dual fit of 500 and 800 MHz together within *CPMGFit*. Residue Ser^{235} is the only residue for which the *Matlab* script from Lewis Kay's group [149] detected dispersion.

too low (*i.e.* recorded data could be too noisy compared to the amplitude of these R_{ex}) such that there is a masking effect on potential low amplitude dispersion. This might be the case as the dispersion profile of many residues possesses a slightly scattered appearance (*i.e.* R_2^{eff} varies randomly with an amplitude ≥ 1 s^{-1}, see Figure 7.12). Indeed, considering the modest values of model-free derived R_{ex} parameters (with a mean value of 1.88 ± 1.12 s^{-1}, where the highest R_{ex} is 5.11 s^{-1}, see Appendix 3, Table 10.3), the effect of noise on the curve-fitting process cannot be excluded.

7.3.5 Amide Exchange

Protein backbone amide protons can exchange with surrounding water molecules. Hence, dissolving lyophilysed protein in D_2O causes exchange of amide protons from N-H to N-D,

giving rise to a signal decay in 2D ^{15}N-HSQC [138] spectra (see Figure 7.13). The process is as follows:

$$\text{N-H}_{protected} \underset{k_{close}}{\overset{k_{open}}{\rightleftharpoons}} \text{N-H}_{exposed} \overset{k_{int}}{\rightarrow} \text{N-D}_{exposed} \tag{7.13}$$

with k_{open} and k_{close} respectively as the opening and closing rate of the structure protecting the N-H group from exchange with the solvent, and k_{int} as the intrinsic rate of exchange for an isolated residue (*i.e.* in absence of protection from the solvent).

Steady-state amide exchange experiments allow the study of higher energy states difficult to detect with techniques reporting on ensembles [38]. In other words, they allow the study of very slow movements of relatively high amplitude by which solvent access to N-H moieties is allowed [166]. Not requiring denaturing conditions, they can probe the presence of partially unfolded states, intermediates of which can be of importance for catalysis. Additionally, they provide helpful information on the long-term stability of tertiary and secondary structures, including hydrogen bond networks [69, 70].

Two limiting cases for amide exchange exist: EX1 and EX2 [151]. In the EX1 regime, exchange rates are *pH* independent, whereas in the EX2 limit, they are affected by *pH* variations (see Figure 7.14).

Depending on the exchange regime, different information can be extracted. In the EX1 regime, insights into the kinetics of exchange can be obtained since then $k_{HX} = k_{open}$, the opening rate of the structure protecting the N-H group from access by the solvent. In the EX2 regime, insights into the thermodynamics of the opening reaction for the structure protecting the N-H group from exchange (transient unfolding processes) can be obtained. The equilibrium constant of exchanging sites K_{op} is then defined as follows:

$$K_{op} = \frac{1}{SF} = \frac{k_{open}}{k_{close}} \tag{7.14}$$

where SF is the slowing factor (or protection factor), and k_{open} and k_{close} the opening and

closing rates, respectively. Experimentally, it can be calculated from:

$$K_{op} = \frac{k_{HX}}{k_c} \tag{7.15}$$

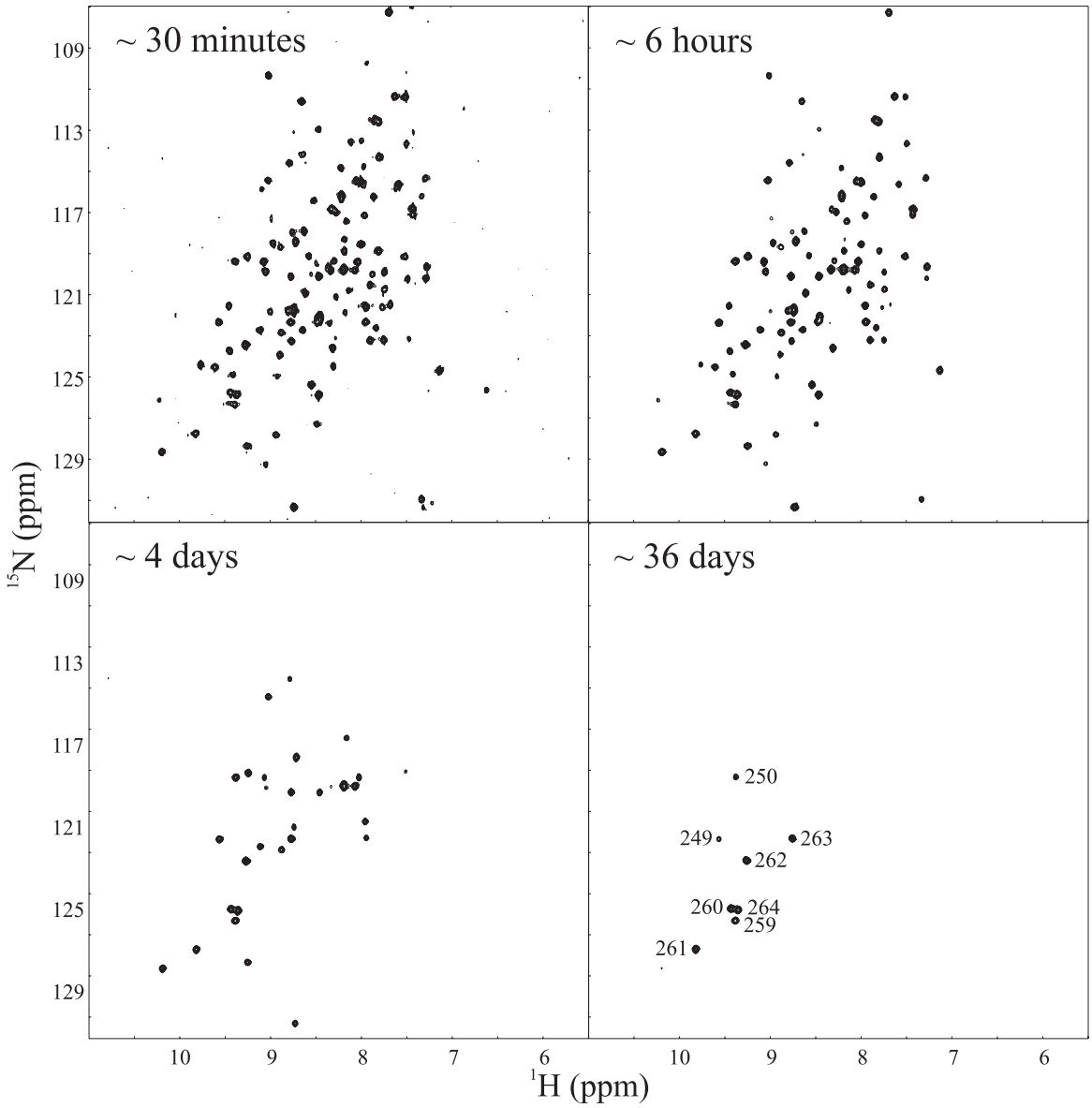

Figure 7.13: Amide resonance signal decay as a function of time. HSQC snapshots are shown for PSE-4 at *pH* 6.65 with time after dissolution in D_2O shown for each spectrum. At time 36 days, remaining resonances are identified and correspond to residues with $\Delta G_{HX} > 9$ kcal/mol, all located in the β sheet of the α/β domain.

where k_{HX} is the exchange rate; and k_c, the expected unprotected exchange rate (intrinsic rate) [11, 43]. Moreover, ΔG_{HX}, the apparent stabilisation free energy of the protecting structure is obtained as usual [10] from:

$$\Delta G_{HX} = -RT \ln K_{op} = -RT \ln \left(\frac{k_{HX}}{k_{int}} \right) \tag{7.16}$$

Information on local stability derived from this parameter can be rationalised from amide exchange data in the EX2 regime.

In our experiments, since some residual water prevented the signals from completely vanishing (to an amplitude $A_\infty = 0$), better fits were obtained using an exponential decay function including an offset ($A_\infty > 0$, see Figure 7.15). In fact, the offset was between 5 and 10 % for most residues. This value is in the expected range considering the experimental scheme.

Exchange was faster at *pH* 7.85 for all residues for which data were available, hence confirming the EX2 regime at *pH* 6.65 (see Table 10.4 and Figure 7.16). A change of *pH*

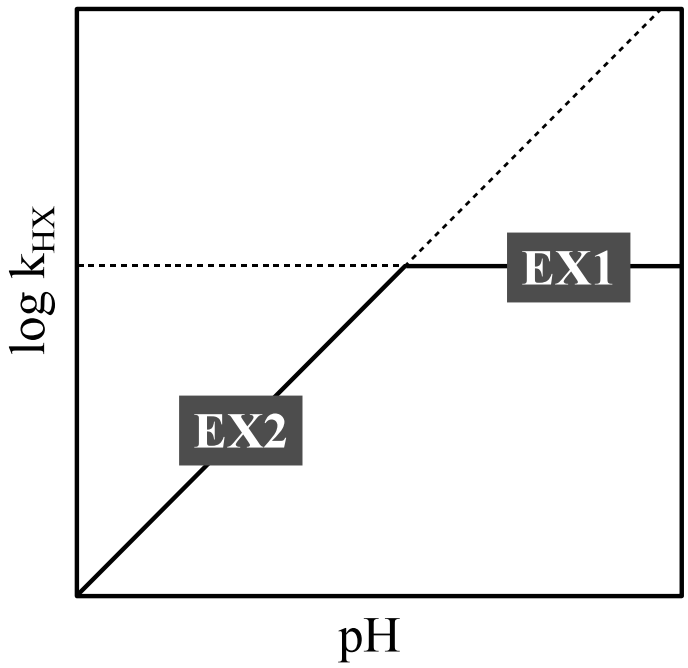

Figure 7.14: Amide exchange regimes EX1 and EX2. Rates are shown as a function of *pH*.

from 6.65 to 7.85 would theoretically cause effective rates to increase by a factor of approximately 16 ($10^{1.2} \approx 15.85$). The mean increase of k_{HX}, in our case, was of 11 ± 7 (not including amides exchanging too fast for observation at *pH* 7.85). This lower value (compared to the theoretical value of 16) could be a result of some amides entering the EX1 regime at a *pH* below 7.85.

Of the 226 residues with available data at *pH* 6.65, 101 exchanged very rapidly and were already unobservable in the first time point (*i.e.* after only 32 min, with $k_{HX} > 1 \text{ x } 10^{-3}$ s^{-1}). Therefore, 125 residues had a measurable exchange rate ranging from $2 \text{ x } 10^{-3}$ s^{-1} to $3 \text{ x } 10^{-8}$ s^{-1}. ΔG_{HX}, as well as K_{op} and SF, were calculated using an Excel spreadsheet from S. W. Englander (University of Pennsylvania, Philadelphia, PA, [11, 43]) and are displayed in Table 10.4 and Figure 7.16. Moreover, ΔG_{HX} values are shown in

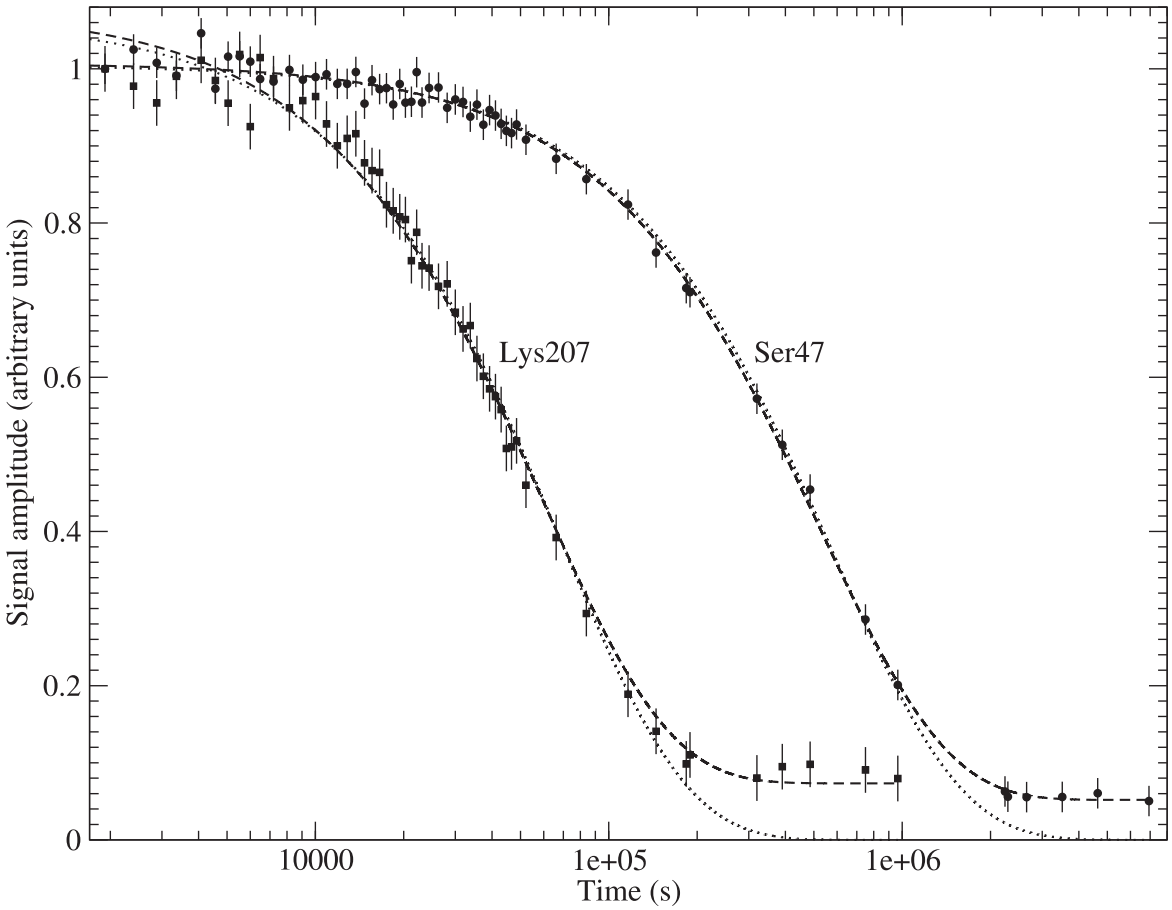

Figure 7.15: Amide exchange data for residues Ser^{47} (circles) and Leu^{207} (squares). Fits are shown with both a 2-parameter function (dotted line) and a 3-parameter function (dashed line). For both residues, the best fit is obtained with the 3-parameter function, which allows A_∞, the contribution from residual protons, to also be fitted.

Figure 7.17. These data have been deposited in the BMRB under accession number 6838 and are available in Appendix 4 (Table 10.4).

Globally, free energies of opening are on the order of 6–11 kcal mol^{-1} for most residues within secondary structures, and are slightly higher in the α/β domain where many residues have $\Delta G_{HX} > 8$ kcal mol^{-1}. Hence, this domain is more stable than the all α domain. This is contrary to what was proposed for TEM-1 [240] that the α domain might be the most stable. This hypothesis was speculative as no amide exchange rates have been determined, nor was exchange in the EX2 regime verified. For TEM-1, the slowest exchanging amides were those from the all α domain and the authors concluded that this domain is more stable than the α/β domain due to the presence of the disulfide bond between Cys^{77} and Cys^{123}, as proposed by Vanhove *et al.* [270]. Here, we postulate the contrary for PSE-4 based on EX2 exchange data. In PSE-4, though the disulfide bond between Cys^{77} and Cys^{123} stabilises the local structure (surrounding residues with ΔG_{HX} between 4 and 8 kcal mol^{-1}), the protection from the solvent in the α domain is globally lower than in the α/β domain. One might argue that the disulfide bond in the PSE-4 sample is not formed. However, this is ruled out by C_β chemical shifts [247] for Cys^{77} (41.6 ppm) and Cys^{123} (42.0 ppm) [196], which show that both Cys residues are oxidised. The most stable domain in PSE-4 is the α/β domain whereas it could be the α domain in TEM-1. Indeed, the theoretical free energies of folding calculated using *VADAR* [282] shows that the all α domain in TEM-1 would be more stable than in PSE-4, while the inverse is predicted for the α/β domain (data not shown). This could indicate some thermodynamic differences between the two domains of these homologs. However, to confirm this hypothesis, analysis of data in the EX2 regime would be required for TEM-1.

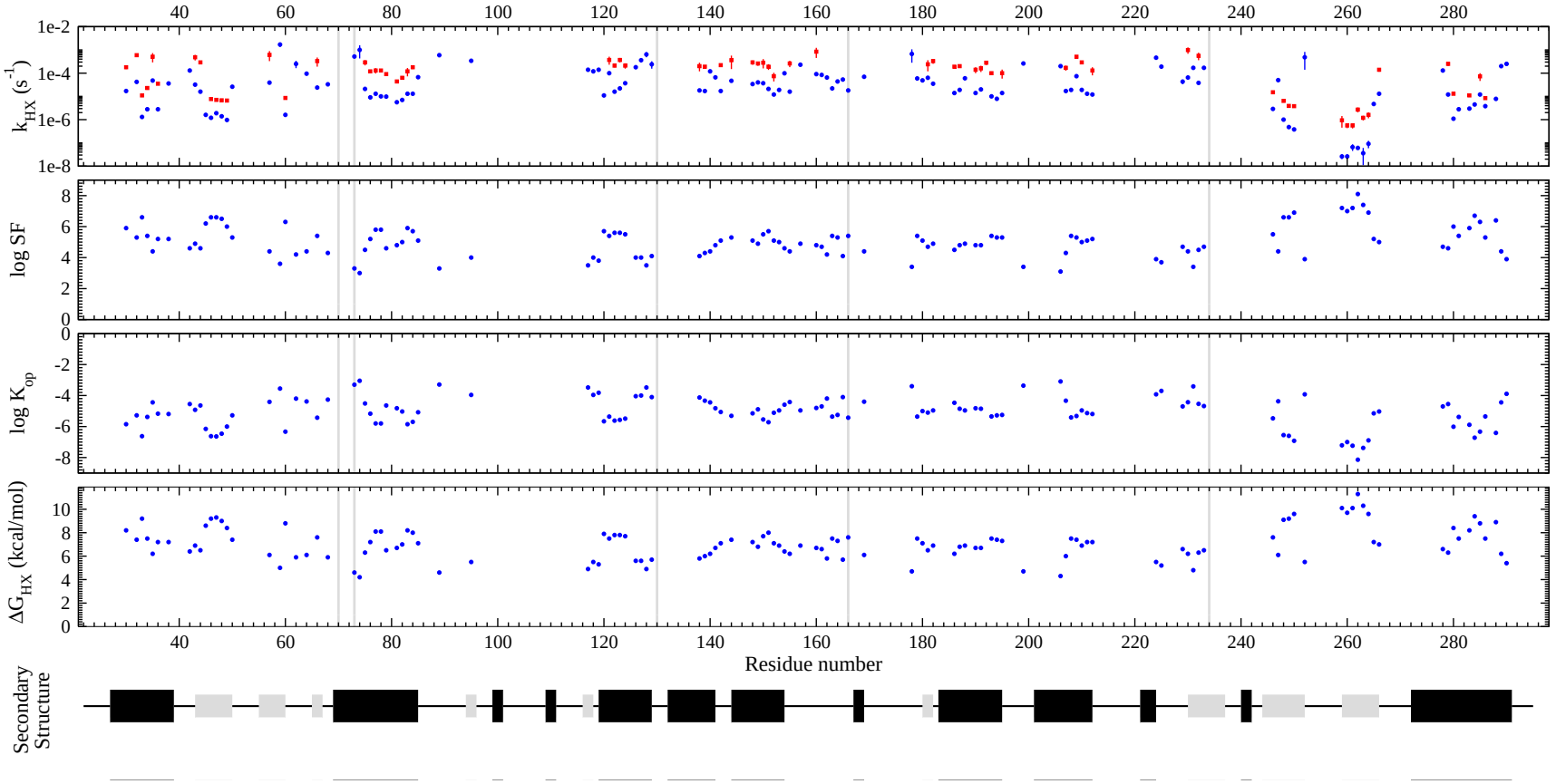

Figure 7.16: Amide exchange results. Shown are amide exchange rates (k_{HX}) at *pH* 6.65 (blue circles) and 7.85 (red squares). Slowing factors (*SF*), equilibrium constants (K_{op}) and apparent free energies for the opening of the protecting structure (ΔG_{HX}) are also shown for *pH* 6.65 (*i.e.* in the EX2 regime). Important active site residues are highlighted vertically in light grey. Secondary structures are shown with α helices as wide black boxes, and β sheets as narrow grey boxes.

As expected, the first protons to exchange with the solvent were those within loops as well as most key residues from the active site (see Figure 7.17). Moreover, all glutamine and asparagine side-chains were exchanged rapidly. These N-H moieties being all located at or near the protein surface, their exchange is too fast for steady-state exchange experiments and would require approaches such as pulse labelling [151]. It is interesting to note that all residues from the Ile^{97} to Gln^{115} region exchange fast, as well as residues Asn^{132} to Ile^{137} from the adjacent α-helix (Figure 7.18). This region of PSE-4 could have a non negligible population existing as a partially unfolded state (probably with $\Delta G_{HX} < 4$ kcal mol^{-1}, k_{HX} values all being > 1 x 10^{-3} s^{-1}, despite 17 amide groups out of 24 having null ASA, and 15 out of 24 being involved in H bonds, as calculated using *VADAR* [282]). Indeed, ΔG_{HX} below 4 kcal mol^{-1} would correspond to populations of partially unfolded states for > 0.1 %, according to the following relation [10]:

$$\frac{p_U}{p_F} = \frac{k_{F\rightarrow U}}{k_{U\rightarrow F}} = e^{-\Delta G_{F\rightarrow U}/RT} \equiv e^{-\Delta G_{HX}/RT} = K_{op} = \frac{k_{HX}}{k_{int}} \tag{7.17}$$

Thus, the sub-domain formed by residues Ile^{97} to Gln^{115} and Asn^{132} to Ile^{137} could be the driving force for the lower stability of the close by α domain. Also, local unfolding could arise near the active site, including residue Tyr^{105} for which motions were discussed above. These local unfolding events, from both their population, possible timescale and location could have a profound impact on PSE-4 catalysis and might be the cause of some of the observed R_{ex}.

The fact that the amide of Glu^{166} and a few other amides from the Ω loop are protected from exchange with ΔG_{HX} between 6 and 8 kcal mol^{-1} points toward some motional restriction of this long loop, preventing the disruption of the network of hydrogen bonds and the exposure of amide moieties to solvent. This argues against μs-ms motions proposed for TEM-1 in Savard and Gagné [240] where residues Arg^{164}, Glu^{166}, and Leu^{169} possessed a R_{ex} parameter, these three residues displaying ΔG_{HX} of 7.3, 7.6, and 6.1 kcal mol^{-1}, respectively, within PSE-4. However, this is in agreement with the motion proposed by Roccatano *et al.* [234] and discussed in the model-free section (7.3.3) where residues Glu^{171}–Leu^{177} (with $k_{HX} > 1$ x 10^{-3} s^{-1}) could move toward the protein core without affecting residues Arg^{161}–Glu^{170} (with mean $\Delta G_{HX} \sim 6.7$ kcal mol^{-1}) as shown in Figure 7.10. Indeed, this motion could transiently position the Ω loop so Glu^{166} is in the vicinity of Ser^{70} for its activation [234]. Moreover, the loop could be protected against

complete hydration. In fact, as stated before, at the location where residues Glu^{171}–Leu^{177} are proposed to translate by this motion, a cavity is present (see Figure 7.10-D). This available space would be filled in the 'closed' state. The same cavity being also present in TEM-1, the conservation of this motion among class A β-lactamases is plausible, in agreement with observations from Roccatano *et al.* [234], as well as with recent simulations of both TEM-1 and PSE-4 which show motions of a different nature for the Ω loop, also consistent with our experimental data (TEM-1: [79], PSE-4: Olivier Fisette and Stéphane M. Gagné personal communication). Finally, the fact that this motion was only seen once during the 5 ns simulation is consistent with a much slower effective timescale. It is thus tempting to relate this rare motion observed from a 5 ns MD simulation to those *μ*s-ms motions suggested by R_{ex} parameters extracted from model-free analysis.

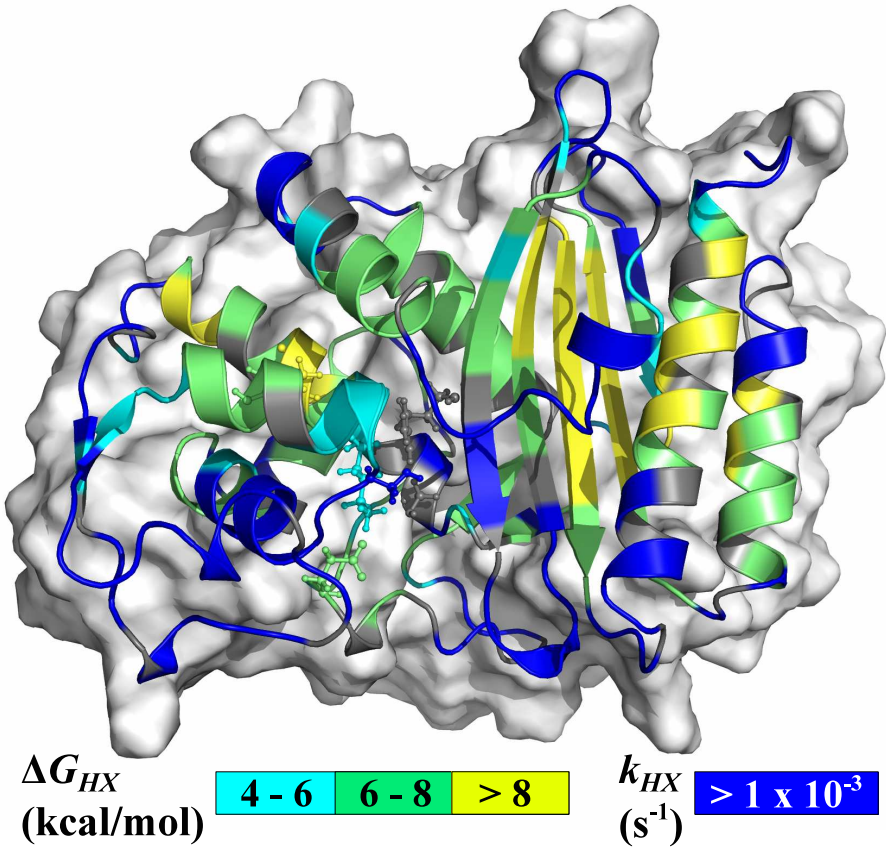

Figure 7.17: Apparent stabilisation free energies of the protecting structures (ΔG_{HX}). k_{HX} is shown for residues for which exchange was too fast for being quantified ($k_{HX} > 1 \times 10^{-3}$ s^{-1}). Important active site residues (Ser^{70}, Lys^{73}, Ser^{130}, Glu^{166}, and Arg^{234}), and the disulfide bond (between Cys^{77} and Cys^{123}, connecting two helices of the α domain) are shown in the stick representation. Missing residues in the crystal structure (Ser^{22}, Ser^{23}, Gln^{293}, Ser^{294}, and Arg^{295}) were added for visualisation of their parameters.

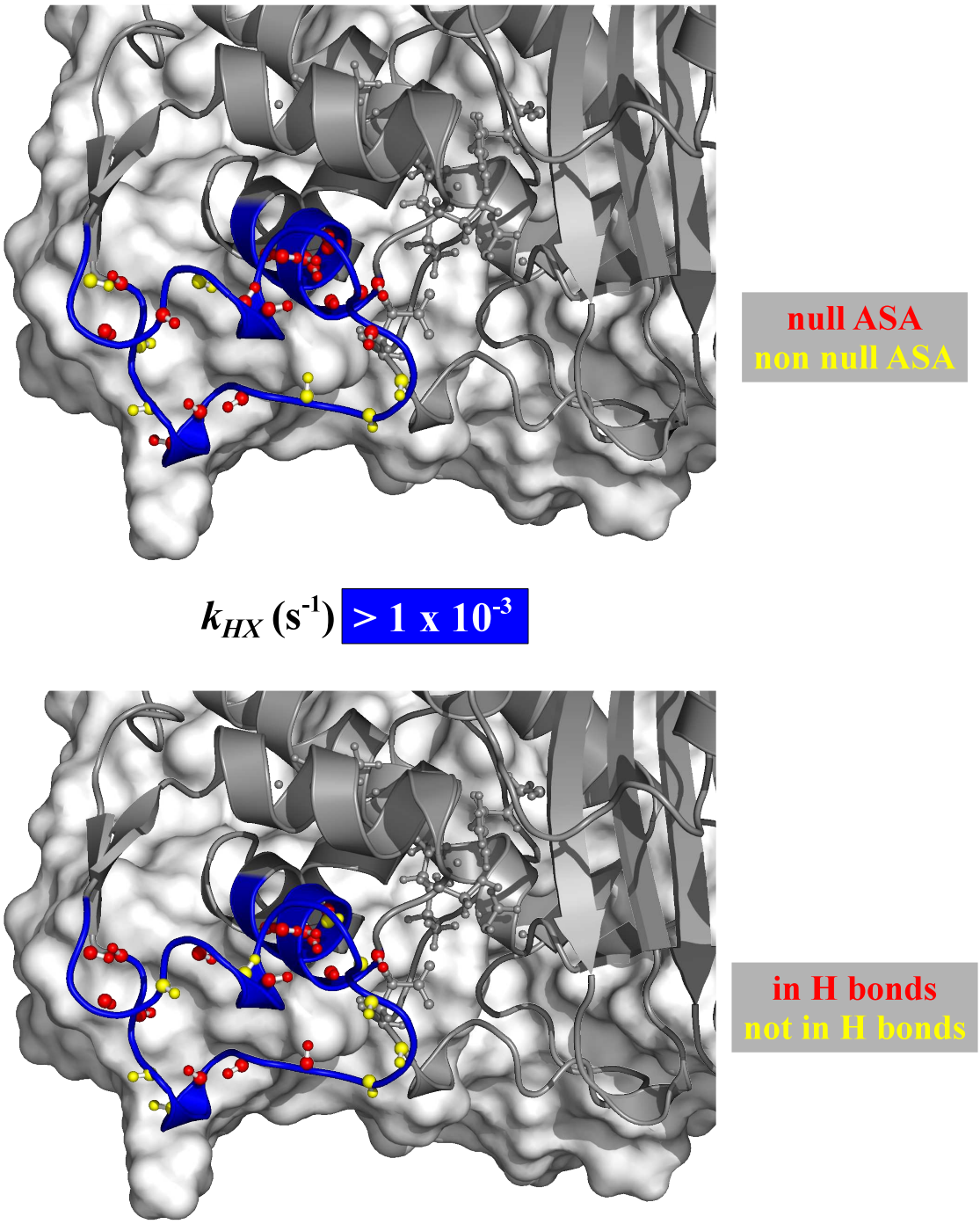

Figure 7.18: Amide exchange of the 97–115/132–137 sub-domain. These amide groups all exchange with $k_{HX} \geq 10^{-3}$ s^{-1}. Top: Amide groups with no ASA are coloured red, while those with non null ASA are yellow. Bottom: Amide groups involved in H bonds are coloured red while those not involved in such bonding are yellow. Important active site residues (Ser^{70}, Lys^{73}, Ser^{130}, Glu^{166}, and Arg^{234}), and the disulfide bond (between Cys^{77} and Cys^{123}, connecting two helices of the α domain) are shown in the stick representation.

Finally, during model-free analysis, Ser^{235} and Gly^{236}, which both exchange with rates faster than 1 x 10^{-3} s^{-1}, were fitted with high R_{ex} parameters (7.5 and 4.5 s^{-1}, respectively). These data, in addition to null ASA for these amides, support the presence of μs-ms motions near the active site, potentially severely broadening amide cross-peaks of residues Ser^{70} and Ala^{237}, as discussed before. Once again, these motions might be important for catalysis since k_{cat} for hydrolysis of β-lactams by β-lactamases is on the order of 1 $(ms)^{-1}$.

7.4 Conclusions

This work is the first NMR characterisation of the dynamics of a class A carbenicillin hydrolysing β-lactamase. It follows the study of Savard and Gagné [240] which explored the dynamics of another class A β-lactamase, TEM-1.

Linking results from the different techniques used here to PSE-4 catalytic activity is not straightforward [127]. From the available experimental data, PSE-4 appears as highly ordered on different timescales. Indeed, ps-ns timescale order parameters are elevated, almost as much as in the case of the homologous TEM-1. Moreover, overall stability is also quite elevated with apparent free energies of opening (from amide exchange experiments) reaching 11 kcal mol^{-1} for several residues in the β sheet of the α/β domain. Theses results contrast with the low thermal stability of both TEM-1 and PSE-4 and with the presence of slow μs-ms motions as indicated by model-free analysis.

Rigidity on the ps-ns timescale could be a characteristic of all class A β-lactamases. As stated before, the catalytic efficiency of some of the class A β-lactamases is diffusion-controlled [37]. This high efficiency supplemented by a high plasticity toward different types of β-lactams contrasts with the restricted motions in the catalytic site, at least on the ps-ns timescale. Longer timescales might be populated by important conserved motions as shown for many active site residues displaying conformational exchange terms (R_{ex}) reporting on the μs-ms timescale, the timescale of enzyme catalysis (*e.g.* the k_{cat} against ampicillin and carbenicillin is $\sim$ 1.2 $(ms)^{-1}$ for PSE-4 [235]). Moreover, the absence of detectable high amplitude motions on the faster ps-ns timescales might show that the active site of class A β-lactamases adapts its shape on substrate approach, thus pointing to motions present during some steps of the catalytic process (although such data in the presence of a substrate is currently not available). However, CPMG relaxation dispersion

experiments failed to quantify accurately these slow motions. It is possible that $R_{1\rho}$ relaxation dispersion experiments would have yielded better data for these motions since they probe slightly different (*i.e.* faster) timescales (reviewed in [211], see Figure 1.1). Nevertheless, the fit for residue Ser^{235} (although of poor quality) is very exciting as the fitted k_{ex} (2029 ± 535 s^{-1}, see Figure 7.12) is close to the k_{cat} against ampicillin and carbenicillin for PSE-4 ($\sim$ 1.2 $(ms)^{-1}$, [235]). To further understand these motions potentially linked to catalysis, it will be interesting to get more insights into the μs-ms timescales and to study dynamics of TEM-1 and PSE-4 mutants. Moreover, it will be critical to obtain data regarding dynamics during catalysis (see below).

We are aware that backbone dynamics can be decoupled from side-chain motions [158]. The apparent lack of motions seen for backbone N-H moieties on the ps-ns timescale could be coupled to important side-chain motions on the same timescale as observed by Lee *et al.* [158]. Also, the apparent dynamics similarity between TEM-1 and PSE-4 might also prove limited to backbone amides with side-chains potentially displaying different motional patterns. Hence, a side-chain dynamics study might prove very insightful. Moreover, we are mindful about the lack of data for a bound form of wild-type PSE-4 either with a β-lactam or an inhibitor. However, as highlighted by Savard and Gagné [239, 240], this proves to be very difficult considering the high catalytic efficiency of these enzymes (in the case of β-lactams), or the high partition ratio for turnover and inhibition (k_{cat}/k_{inact}, in the case of inhibitors). For β-lactams, this means that after only a short period of time (shorter than the time needed for recording of NMR experiments), all substrate would be hydrolysed. For inhibitors, this means that very high concentrations of ligands would be needed in the NMR tube, concentrations potentially limited by solubility of the compound. Indeed, k_{cat}/k_{inact} for clavulanic acid and tazobactam are 80 and 1000, respectively [235]. Finally, we are aware that indications of conformational exchange shown here are qualitative and extracted from the variations of the transverse relaxation rate (R_2) over a restricted range of magnetic field strengths. Indeed, despite the highly convincing model-free data showing the presence of R_{ex} around the active site, CPMG relaxation dispersion experiments failed to give new insights by supplying quantitative data. Hence, the μs-ms timescale will be an interesting target for further studies to better quantify the slow motions detected here, especially for what concerns motions around the Ω loop and active site cavity. This will be very interesting as this timescale corresponds to that of the cleavage of the β-lactam ring. Thus, the recording of $R_{1\rho}$ relaxation dispersion data will certainly shed light onto the conformational exchange processes suspected to arise near the active site where some residues (*e.g.* Lys^{73}), although rigid on the ps-ns timescale, display broadened resonances, in

addition to some resonances being even invisible as a result of peak broadening (*e.g.* Ser^{70} and Ala^{237}).

Finally, the detailed backbone dynamics data gathered for PSE-4 will join those from TEM-1 in enabling in-depth comparative MD simulations. Such a comparative study of PSE-4 backbone dynamics characterised by MD and NMR is currently underway by Olivier Fisette in our laboratory. This will permit better *in silico* studies of the dynamics of class A wild type and mutant β-lactamases in the presence of substrate, experiments which are impossible using NMR because the turnover rate of relevant β-lactams is tremendously fast with respect to NMR experiments being quite long.

Chapter 8

Dynamics of Class A β-Lactamases: cTEM-17m Backbone Resonance Assignments

The rapid evolution of class A β-lactamases, which procure resistance to an increasingly broad panel of β-lactam antibiotics, underscores the urgency to better understand the relation between their sequence variation and their structural and functional features. To date, more than 300 clinically-relevant β-lactamase variants have been reported, and this number continues to increase. With the aim of obtaining insights into the evolutionary potential of β-lactamases, an artificially engineered, catalytically active chimera of the class A TEM-1 and PSE4 β-lactamases is under study by kinetics and NMR. Here we report the ^{1}H, ^{13}C, and ^{15}N backbone resonance assignments for the 30 kDa chimera cTEM-17m. Despite its high molecular weight, the data provide evidence that this artificially-evolved chimeric enzyme is well folded. The hydrolytic activity of cTEM-17m was determined using the chromogenic substrate CENTA, with $K_M = 160 \pm 35$ μM and $k_{cat} = 20 \pm 4$ s^{-1}, which is in the same range as the values for TEM-1 and PSE-4 β-lactamases.

8.1 Context

Hundreds of β-lactamase variants have been clinically isolated (see Lahey Clinic Website, visited in November 2009). Their rapidly increasing numbers underscore the urgency to better understand their swift evolution, which is severely undermining the clinical effectiveness of β-lactam drugs.

Series of functional, 'chimeric' β-lactamases have previously been obtained, where fragments of different class-A β-lactamases were blended [64, 187, 272]. The novel protein engineering algorithm SCHEMA was applied to recombine TEM-1 and PSE-4 β-lactamases with the least amount of disruption of native residue contacts. Their high topological homology (backbone RMSD = 1.3 Å) was offset by their moderate sequence identity (41 %). Application of the SCHEMA algorithm resulted in orders of magnitude better success in generating functional TEM-1/PSE-4 chimeras relative to random sequence shuffling [64]. Nonetheless, greater recombination resulted in less functional chimeras, underscoring the negative impact toward function of disrupting specific contacts within the protein. Indeed, it was not possible to predict which among the greater sample of designed chimeras would fold, or be functional.

To further understand the evolutionary potential of β-lactamases, we must gain insight into the structure of such artificially evolved yet functional enzymes. We cannot predict how closely matched the functional chimeras may be to either of the TEM-1 and PSE-4 'parent' structures. As a first step toward this goal, we report the backbone assignment of a functional chimera produced by blending eight sequence blocks (A: residues 26–65, B: 66–73, C: 74–149, D: 150–161, E: 162–176, F: 177–190, G: 191–218, H: 219–290) of TEM-1 and PSE-4 [272], according to the standard Ambler numbering scheme for which cTEM-17m is numbered from 26 to 290, with gaps at positions 239 and 253 [8]. The chimera cTEM-17m is the blend of segments 26–149 (A-B-C) and 191–290 (G-H) from the TEM-1 parent, with segment 150–190 (D-E-F, encompassing the conserved Ω loop) from PSE-4. The chimera cTEM-17m was selected according to its capacity to hydrolyse ampicillin (personal communication from Michelle M. Meyer and Frances H. Arnold, California Institute of Technology). cTEM-17m has 17 mutations relative to TEM-1 (hence its name) and 133 mutations relative to PSE-4 (Figure 8.1-A); other residues are identical between the two parents. This results in a chimeric active site (see Figure 8.1-B).

A

```
cTEM-17m   26 HPETLVKVKDAEDQLGARVGYIELDLNSGKILESFRPEERFPMMSTFKVLLCGAVLSRVD
TEM-1      26 HPETLVKVKDAEDQLGARVGYIELDLNSGKILESFRPEERFPMMSTFKVLLCGAVLSRVD

cTEM-17m   86 AGQEQLGRRIHYSQNDLVEYSPVTEKHLTDGMTVRELCSAAITMSDNTAANLLLTTIGGP
TEM-1      85 AGQEQLGRRIHYSQNDLVEYSPVTEKHLTDGMTVRELCSAAITMSDNTAANLLLTTIGGP

cTEM-17m  146 KELTDFLRQIGDKETRLDRIEPDLNEGKLGDLRDTTTPKAIASTLRKLLTGELLTLASRQ
TEM-1     146 KELTAFLHNMGDHVTRLDRWEPELNEAIPNDERDTTMPAAMATTLRKLLTGELLTLASRQ

cTEM-17m  206 QLIDWMEADKVAGPLLRSALPAGWFIADKSGAGERGSRGIIAALGPDGKPSRIVVIYTTG
TEM-1     206 QLIDWMEADKVAGPLLRSALPAGWFIADKSGAGERGSRGIIAALGPDGKPSRIVVIYTTG

cTEM-17m  268 SQATMDERNRQIAEIGASLIKHW 290
TEM-1     268 SQATMDERNRQIAEIGASLIKHW 290
```

B

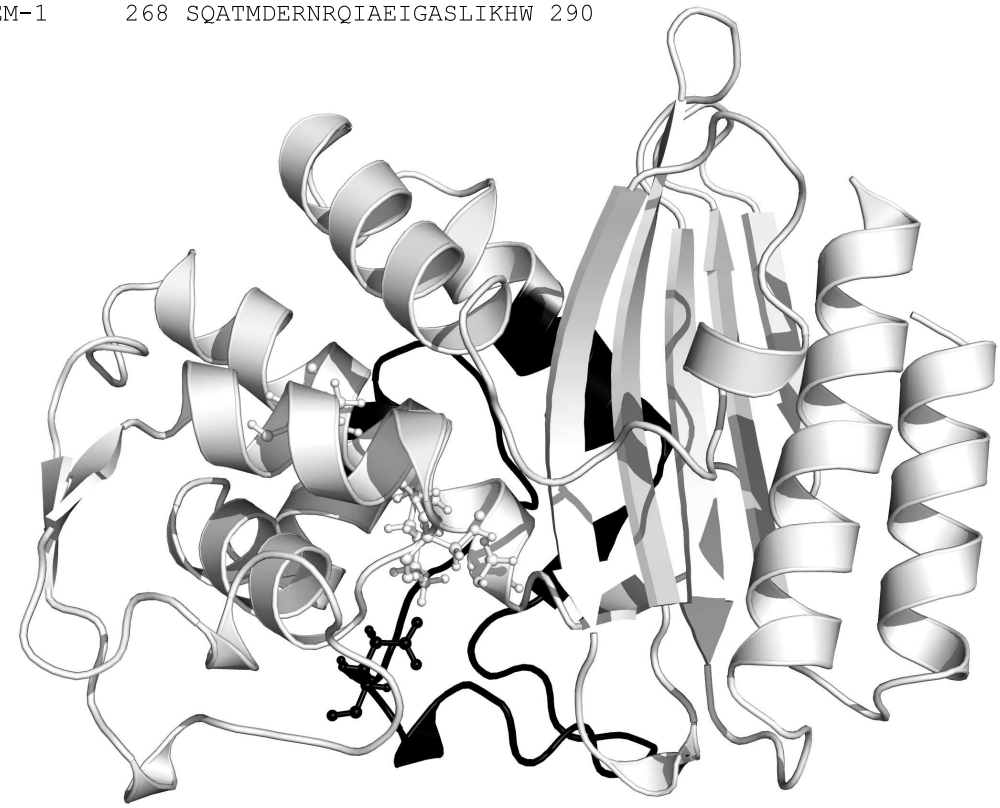

Figure 8.1: Building blocks for cTEM-17m. (A) Primary sequence alignment of cTEM-17m with the parental TEM-1. Mutations relative to TEM-1 (17 in total) are underlined and bold while the segment from PSE-4 is in bold. (B) cTEM-17m recombination blocks from TEM-1 and PSE-4 β-lactamases displayed on PSE-4 structure (PDB 1G68, [165]). White: segments from TEM-1 (residues 26–149 and 191–290); black: segment from PSE-4 (residues 150–190). Active site residues (Ser^{70}, Lys^{73}, Ser^{130}, and Glu^{166}) and the disulfide bond (between Cys^{77} and Cys^{123}) are shown as balls and sticks.

8.2 Methods

8.2.1 Cloning

The original construct for cTEM-17m was produced as reported by Voigt *et al.* [272] and was a generous gift from Michelle M. Meyer and Frances H. Arnold (California Institute of Technology). The DNA sequence encoding the mature chimeric β-lactamase was fused 3' to the OmpA signal peptide and inserted into the plasmid pET-24 (Novagen, Gibbstown, NJ) as previously described for PSE-4 [196].

8.2.2 Unlabelled TEM-1, PSE-4 and cTEM-17m

The expression of unlabelled TEM-1, PSE-4, and cTEM-17m were undertaken in *Escherichia coli* using previously described procedures [54]. Purifications were performed according to a two-step protocol using an Äkta FPLC (GE Healthcare, Piscataway, NJ) as previously described [21, 54].

8.2.3 [^{15}N]- and [^{13}C, ^{15}N]-Labelled cTEM-17m

Uniformly [^{15}N]- and [^{13}C, ^{15}N]-labelled cTEM-17m was overexpressed and purified as previously described for PSE-4 [196]. Activity was qualitatively monitored during purification using the chromogenic cephalosporin substrate nitrocefin (see Figure 5.1, [202]) and purity was assessed by Coomassie blue staining following SDS-PAGE. Typical yields were of 65 mg/L of > 98 % pure protein.

8.2.4 Enzyme Kinetics

K_M and k_{cat} values for hydrolysis of CENTA (see Figure 8.2, [132]) by TEM-1, PSE4, and cTEM-17m were determined at room temperature in 50 mM sodium phosphate buffer *pH* 7.0 using a molar extinction coefficient at 405 nm $\Delta\varepsilon_{405nm}$ = 6400 $M^{-1}cm^{-1}$ [132] over

a concentration range of 35-1000 μM. Substrate hydrolysis was monitored according to initial steady-state velocities for six substrate concentrations which flanked the K_M values for TEM-1, using a Cary 100 Bio UV-visible spectrophotometer (Varian Canada Inc., Montréal, QC). The kinetic parameters were calculated from the initial linear portion (corresponding to the first 10 % of substrate hydrolysis) of the curve and analysed using non-linear regression and the Michaelis-Menten equation [188] using the software *GraphPad Prism* (GraphPad Software, San Diego, CA). The k_{cat} parameter was thus determined according to [188]:

$$k_{cat} = \frac{V_{max}}{[E]} \tag{8.1}$$

where k_{cat} is the catalytic turnover constant, V_{max} is the maximum enzyme velocity extrapolated to maximum substrate concentrations, and the enzyme concentration $[E]$ was determined using the BioRad protein assay (Biorad, Hercules, CA) taking into account its estimated purity via SDS-PAGE analysis using *Scion Image analysis software* (*NIH Image*). The values obtained are in general agreement with previously reported values for the same, or similar, systems [14].

8.2.5 NMR Spectroscopy

NMR samples were prepared from lyophilised protein in 0.1 % azide, 3 mM imidazole, 10 % D_2O, *pH* 6.7 at a protein concentration of 0.4 mM. No additional buffer was added to minimise interactions with the chimera, as had been previously observed in the case of phosphate buffer interacting with TEM-1's active site [239]. Chemical shift referencing was performed externally since it was previously shown that DSS can interact with PSE-4 (see

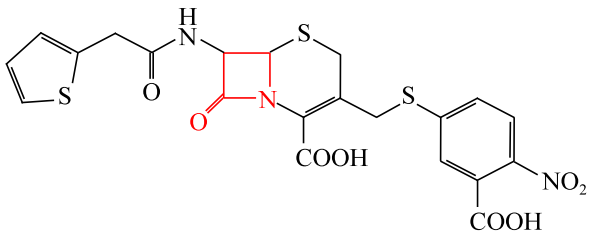

Figure 8.2: Structure of the chromogenic cephalosporin CENTA. As in Figure 4.2, the β-lactam ring is shown in red.

Chapter 7 and [194]). NMR spectra were recorded at 31.5 °C (calibrated using MeOH as described before in Section 2.2.4) on a Varian INOVA 600 MHz equipped with a *z*-axis pulsed field gradient triple resonance cold probe. Backbone assignments were obtained from ^{15}N-HSQC [138] and TROSY [220] versions of HNCA [102, 122, 141, 197], HN(CO)CA [288], HNCACB [141, 197, 285], HN(CO)CACB [101], HNCO [102, 122, 141, 197], and (HN)CO(CO)NH [103] experiments in Varian Biopack (Varian Inc, Palo Alto, CA). The different spectra were recorded using their sensitivity enhanced versions [138, 274]. Spectral widths were as follows for ^{1}H and ^{15}N dimensions, respectively: 11990 and 1534 Hz. For the different triple resonance spectra, the spectral widths for ^{13}C varied as follows: 3920 Hz (HNCA and HN(CO)CA), 9049 Hz (HNCACB and HN(CO)CACB), and 1750 Hz (HNCO and (HN)CO(CO)NH).

Processing of NMR data proceeded using *NMRPipe* [55]. FIDs were shuffled to yield pure absorptive two-dimensional line shapes from the sensitivity-enhanced data with the 'ranceY.M' macro. Water signals were subtracted with the function 'SOL'. Linear prediction was performed in the indirect (^{13}C and ^{15}N) dimensions to extend the amount of data points by 100 %. Finally, the baseline in each dimension was corrected using the function 'POLY -auto ord 0'.

Analysis of spectra was performed using *Smartnotebook* [248] within *NMRView* [131]. Chemical shifts for cTEM-17m were predicted based on assignments for TEM-1 (BMRB 6024, 6357, and 7238) and PSE-4 (BMRB 6838) using the program *ORB* [99] to guide the assignment within *Smartnotebook*. Secondary structures were inferred from the C_α / C_β / C' chemical shift index (CSI) [283] with coil reference chemical shifts taken from Ref-DB [294].

8.3 Results and Discussion

The cTEM-17m chimera gives rise to spectra of high quality (Figure 8.3-A), as do its parental β-lactamases TEM-1 [241] and PSE-4 [196], despite their molecular weight being near 30 kDa. The ^{15}N-HSQC for cTEM-17m is closely related to that of TEM-1 and PSE-4 such that some well-resolved peaks could be assigned directly (*e.g.* Glu^{28}, Val^{44}, Met^{69}, Gly^{172}, Gly^{255}, and Trp^{290}), based solely on the 2D ^{15}N-HSQC. However, for the vast majority of residues, assignment required the use of triple resonance backbone experiments

and was guided from predicted chemical shifts based on the chemical shifts for TEM-1 and PSE-4.

Assigned amide resonances are shown on Figures 8.3-A,B. 90.8 % (228/251) of backbone $^{1}H_{N}$ and ^{15}N, 92.4 % (243/263) of $^{13}C_{\alpha}$, 87.5 % (210/240) of $^{13}C_{\beta}$, and 86.3 % (227/263) of $^{13}C'$ were assigned. Missing assignments are the following: C_{α}-His^{26}, C_{β}-His^{26}, C'-His^{26}, C'-Arg^{61}, C_{α}-Pro^{67}, C_{β}-Pro^{67}, C_{β}-Met^{68}, C_{β}-Met^{69}, C'-Met^{69}, H_{N}-Ser^{70}, N-Ser^{70}, C_{β}-Ser^{70}, C_{β}-Thr^{71}, C'-Ser^{106}, C_{β}-Thr^{128}, C_{β}-Ser^{130}, C'-Ser^{130}, H_{N}-Asp^{131}, N-Asp^{131}, C_{α}-Asp^{131}, C_{β}-Asp^{131}, C'-Asp^{131}, H_{N}-Asn^{132}, N-Asn^{132}, C'-Gly^{144}, C_{β}-Thr^{149}, C_{β}-Glu^{166}, C'-Glu^{166}, C'-Gly^{172}, H_{N}-Lys^{173}, N-Lys^{173}, C'-Thr^{182}, C'-Ala^{213}, H_{N}-Asp^{214}, N-Asp^{214}, C_{α}-Asp^{214}, C_{β}-Asp^{214}, C'-Asp^{214}, C'-Lys^{215}, H_{N}-Val^{216}, N-Val^{216}, C_{α}-Val^{216}, C_{β}-Val^{216}, C'-Val^{216}, H_{N}-Ala^{217}, N-Ala^{217}, C_{α}-Ala^{217}, C_{β}-Ala^{217}, C'-Ala^{217}, H_{N}-Gly^{218}, N-Gly^{218}, C_{α}-Gly^{218}, C'-Gly^{218}, C_{α}-Pro^{219}, C_{β}-Pro^{219}, C'-Pro^{219}, H_{N}-Leu^{220}, N-Leu^{220}, C_{α}-Leu^{220}, C_{β}-Leu^{220}, C'-Leu^{220}, H_{N}-Leu^{221}, N-Leu^{221}, C_{α}-Leu^{221}, C_{β}-Leu^{221}, C'-Leu^{225}, C'-Asp^{233}, H_{N}-Lys^{234}, N-Lys^{234}, C_{α}-Lys^{234}, C_{β}-Lys^{234}, C'-Lys^{234}, H_{N}-Ser^{235}, N-Ser^{235}, C_{α}-Ser^{235}, C_{β}-Ser^{235}, C'-Ser^{235}, H_{N}-Gly^{236}, N-Gly^{236}, C_{α}-Gly^{236}, C'-Gly^{236}, H_{N}-Ala^{237}, N-Ala^{237}, C_{α}-Ala^{237}, C_{β}-Ala^{237}, C'-Ala^{237}, H_{N}-Gly^{238}, N-Gly^{238}, C_{α}-Gly^{238}, C'-Gly^{238}, H_{N}-Glu^{240}, N-Glu^{240}, C_{α}-Glu^{240}, C_{β}-Glu^{240}, C'-Glu^{240}, H_{N}-Arg^{241}, N-Arg^{241}, C_{α}-Arg^{241}, C_{β}-Arg^{241}, C'-Arg^{241}, H_{N}-Gly^{242}, N-Gly^{242}, C_{α}-Gly^{242}, C'-Gly^{242}, H_{N}-Ser^{243}, N-Ser^{243}, C_{α}-Ser^{243}, C_{β}-Ser^{243}, C'-Ser^{243}, H_{N}-Arg^{244}, N-Arg^{244}, C_{β}-Arg^{244}, C_{β}-Ile^{246}, C_{β}-Ile^{247}, C'-Gly^{251}, C'-Lys^{256}, C_{β}-Pro^{257}, C'-Thr^{265}, H_{N}-Thr^{266}, N-Thr^{266}, C_{α}-Thr^{266}, C_{β}-Thr^{266}, C'-Thr^{266}, H_{N}-Gly^{267}, N-Gly^{267}, C'-Thr^{271}, H_{N}-Met^{272}, N-Met^{272}, C_{β}-Ile^{279}, and C'-Trp^{290}.

Backbone ^{1}H, ^{13}C, and ^{15}N resonance assignments have been deposited in the BMRB under accession number 16598 and are also available in Appendix 5 (Table 10.5).

Spin relaxation studies on both TEM-1 [240] and PSE-4 (see Chapter 7) [194] have shown that conformational exchange is present in the vicinity of the active site of class A β-lactamases, broadening backbone resonances of Ser^{70} and Ala^{237}, in particular. Those resonances were also broadened for cTEM-17m. The additional unassigned resonances that are clustered around the chimeric active site (Figure 8.4) may be the result of a similar line broadening effect. Indeed, unassigned resonances in the HSQC are either very weak (with S/N five times lower than for assigned resonances on average) or absent in the different 3D spectra (data not shown), precluding their assignment. Taking this observation into consideration, the proportion of assigned chemical shifts (when compared to the number of 'really' assignable resonances) is then much closer to 100 %. Potential slow motions

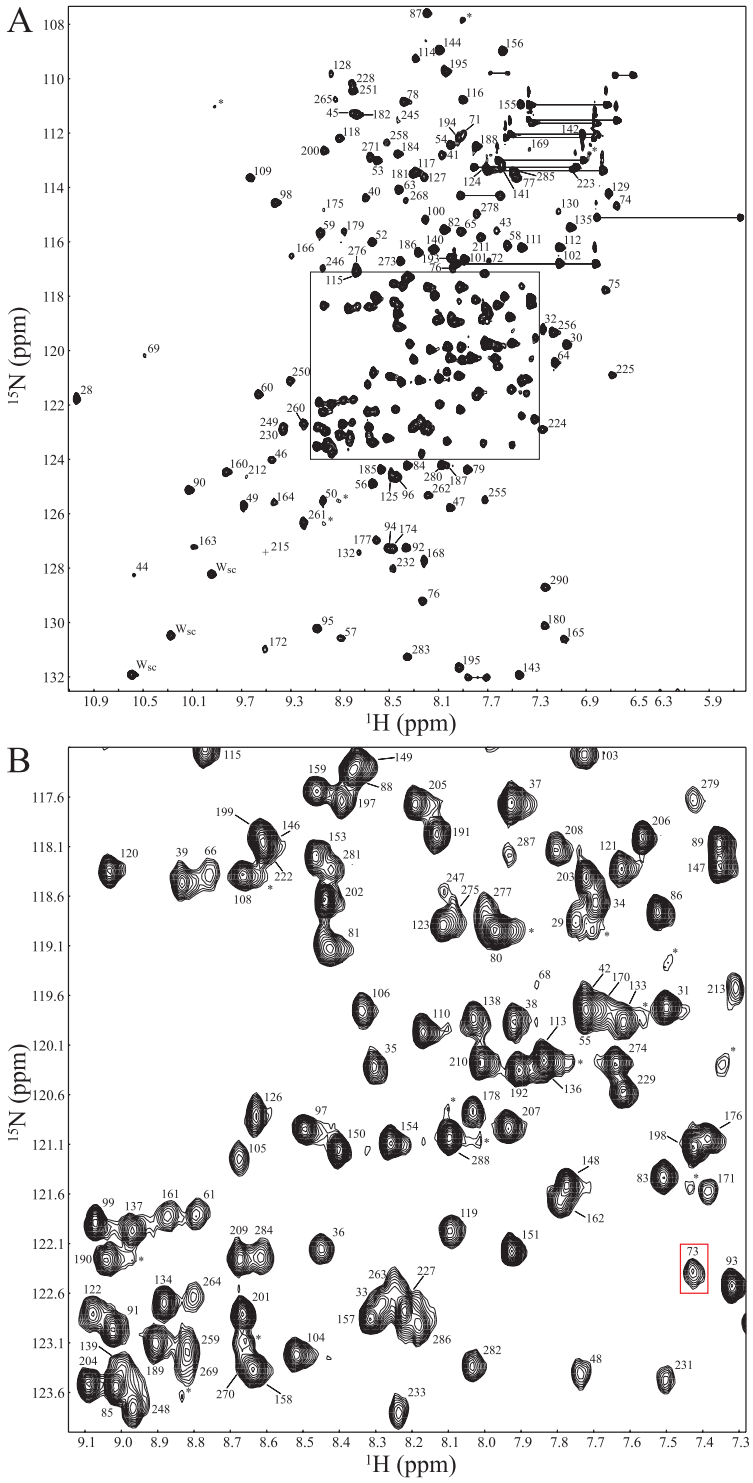

Figure 8.3: Backbone chemical shift assignments for cTEM-17m. (A) 2D ^{15}N-HSQC of [^{15}N]-labelled cTEM-17m with an enlarged view of the most crowded region of the spectrum (B). Active site residue Lys^{73} is highlighted with a red box. Side-chains are either marked by W_{SC} (for Trp side-chains) or linked by a line for Arg, Asn, and Gln side-chain doublets. Unassigned peaks are marked by an asterisk. The peak from residue Gln^{215} being too weak for observation at the current level, its position is marked by '+'.

causing this line broadening are currently under investigation and will be presented in detail elsewhere.

The class A β-lactamase-like 3D structure of cTEM-17m chimera is inferred from different observations. First, the $^{1}H_{N}$ resonances are well dispersed (see Figure 8.3-A), proving the folded nature of the protein. Second, the protein was found to be active in hydrolysing the β-lactam chromogenic substrate CENTA (see Figure 8.2, [132]). Indeed, we determined the cTEM-17m chimera to possess a K_M of 160 $\pm$ 35 μM and a k_{cat} of 20 $\pm$ 4 s^{-1} for CENTA hydrolysis, which is in the same range as the values obtained for TEM-1 and PSE-4 [14, 132] (see Table 8.1). Third, the conserved disulfide bridge between Cys^{77} and Cys^{123} is present. Indeed, C_β shifts for Cys^{77} and Cys^{123} are 44.9 and 42.5 ppm, respectively, indicating they are oxidised [247]. Finally, CSI [283] predicted secondary structures are in almost perfect agreement with TEM-1 and PSE-4 secondary structures extracted from a *DSSP* analysis [133] of the crystal structures PDB 1BTL [129] and 1G68 [165], respectively (see Figure 8.5). Together, these observations confirm that cTEM-17m is a functional class A β-lactamase, although it originates from artificial recombination.

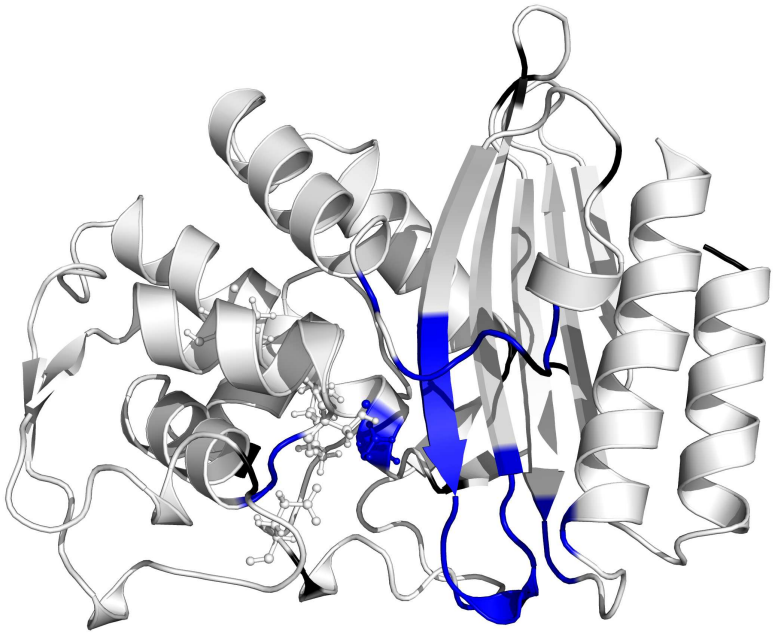

Figure 8.4: Unassigned backbone resonances for cTEM-17m are shown on the 3D structure for PSE-4 (PDB 1G68, [165]). Black denotes residues with no amide (prolines and N-terminus) whereas blue denotes missing assignments. Active site residues (Ser^{70}, Lys^{73}, Ser^{130}, and Glu^{166}) and the disulfide bond (between Cys^{77} and Cys^{123}) are shown as balls and sticks.

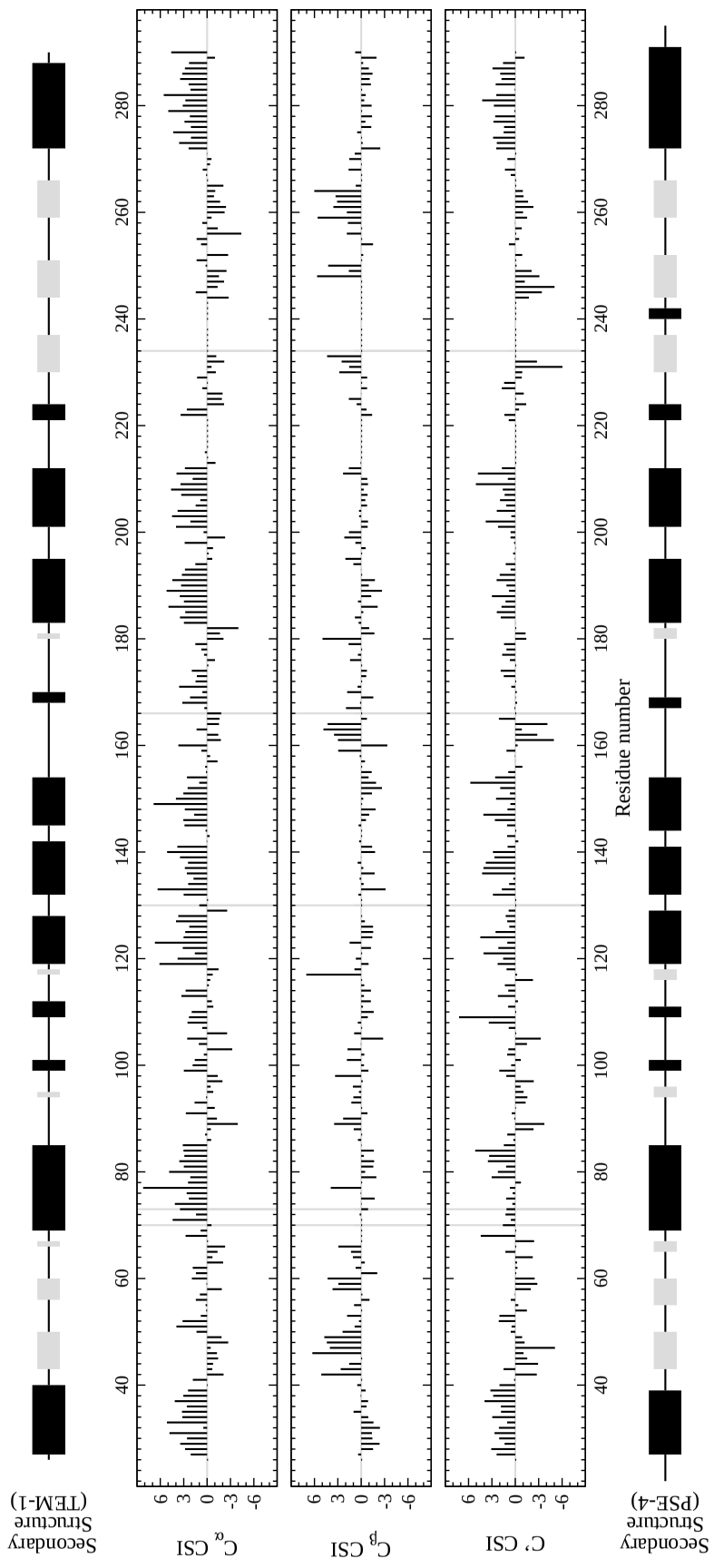

Figure 8.5: Secondary structure predictions for cTEM-17m from C_α / C_β / C' CSI [283]. The secondary structures of TEM-1 and PSE-4 are shown (based on a *DSSP* [133] analysis of PDB 1BTL [129] and 1G68 [165], respectively) with α helices and β strands as large black and small grey boxes, respectively. Active site residues (Ser^{70}, Lys^{73}, Ser^{130}, Glu^{166}, and Lys^{234}) are highlighted vertically in light grey. For C_α and C' CSI, positive values indicate an α helical propensity, while negative values indicate a propensity for the formation of β sheets. C_β CSI behave inversely.

Table 8.1: Kinetics for hydrolysis of CENTA by TEM-1, PSE-4, and cTEM-17m.

Enzyme	[Enzyme] (nM)	k_{cat} (s^{-1})	K_M (μM)	k_{cat}/K_M ($\mu M^{-1}s^{-1}$)
TEM-1	1.3	17 ± 1	120 ± 4	0.14 ± 0.01
PSE-4	2.2	7.5 ± 2	46 ± 8	0.16 ± 0.04
cTEM-17m	1.7	20 ± 4	160 ± 35	0.12 ± 0.03

† Values are the average of triplicate assays ± SD.

8.4 Conclusions

In summary, we present the backbone chemical shift assignments for cTEM-17m, a chimeric β-lactamase consisting of segments from TEM-1 and PSE-4 β-lactamases. According to both kinetics and chemical shift data, the functional and structural features of this chimera are generally conserved relative to the parental proteins. Since the main difference with TEM-1's active site is the presence of the Ω loop of PSE-4, it is not surprising that the chimera is active. Indeed, it has been observed that such Ω loops are often removed, added or moved during evolution [233]. Moreover, data suggest that the slow dynamics detected in the active sites of TEM-1 and PSE-4 could be exacerbated in cTEM-17m. Forthcoming work including kinetics toward a range of β-lactam substrates, ^{15}N spin relaxation, and relaxation dispersion data will soon complement these preliminary results.

Chapter 9

Dynamics of Class A β-Lactamases: Conclusions

9.1 Class A β-Lactamases as Highly Ordered Enzymes with Active Site Subjected to *μs*-ms Motions

In summary, the work performed in this second part of the thesis includes the backbone chemical shift assignments of PSE-4 and the chimera cTEM-17m, as well as the characterisation of PSE-4 backbone dynamics using ^{15}N spin relaxation (analysed within the model-free formalism), ^{15}N CPMG relaxation dispersion, and amide exchange experiments.

Previous NMR studies on a class A β-lactamase performed by Savard and Gagné [240] revealed two striking features in TEM-1 concerning the N-H bonds (and thus the peptide plane). First, the enzyme was shown to be highly rigid on the fast ps-ns timescale. Second, data pointed to the presence of slower (*μs-ms*) motions near the active site where ps-ns order was higher. This was the data available when the studies on PSE-4 begun.

Our studies in PSE-4 lead to no different conclusions than for TEM-1: this interplay of ps-ns order and *μs*-ms motions in the active site was also observed. Model-free data pointed to an ordered active site where R_{ex} terms also clustered. Additionally, the active site was where two residues (Ser^{70} and Ala^{237}: residues forming the 'oxyanion' hole with their backbone atoms) could not be observed, most probably because of extreme line broadening. Finally, the active site residue Lys^{73} also suffered from conformational exchange line broadening with its side-chain resonances being broadened to the noise, precluding the titration of this important residue. In fact, this duality of order and motions might be present in all class A β-lactamases as we also have clues for a similar phenomenon in the TEM-1/PSE-4 chimera cTEM-17m.

9.2 Future Work

With the data collected so far, it is now possible to take this project (the study of the dynamics of class A β-lactamases) from discovery-driven to hypothesis-driven science. Our hypothesis would then be the following:

> *A link exists between the apparently conserved slow motions in the active site of class A β-lactamases and their catalytic mechanism.*

In order to verify this hypothesis, four different aspects of the dynamics of class A β-lactamases will need further insights in the future:

1. The μs-ms timescale should be quantitatively analysed. The amplitude of R_{ex} parameters in PSE-4 could be quantified by comparing R_2 with R_2^0, the R_{ex}-free R_2, with the approach proposed by Hansen *et al.* [109]. R_{ex} parameters derived this way would be more quantitative than model-free derived R_{ex} parameters and would potentially allow the detection of more exchange. Additionally, CPMG relaxation dispersion experiments could be optimised in order to improve the S/N ratio of extracted R_2^{eff}. This would potentially allow the quantification of exchange for other residues than Ser^{235}. In the case where optimised CPMG experiments would 'really' yield no additional information on exchange processes, other types of experiments could be performed to broaden the timescale probed and include faster motions such as those assumed by the model-free formalism (*i.e.* μs-ms motions). As shown in Figure 1.1, this could be done using $R_{1\rho}$ relaxation dispersion (reviewed in [211]) and/or RDC (reviewed in [267]) experiments.

2. The dynamics should be characterised in the presence of ligands, either β-lactam antibiotics or β-lactamase inhibitors (or both). Characterisation of changes in dynamics upon ligand binding would further help the understanding of this important class of enzymes. Indeed, the binding of ligands might quench slow motions in the 'oxyanion' hole by which the amide resonances of residues Ser^{70} and Ala^{237} are broadened to the noise. This could also affect side-chain resonances of Lys^{73} and, eventually, allow its titration. In the case where characterisation of a ligand bound wild-type class A β-lactamase using NMR would be unfeasible experimentally, mutants or non-hydrolysable substrate analogs could be tried. If none of these approaches turned successful, *in silico* approaches might prove useful. Such characterisation of dynamics in the presence of ligands using MD simulations is currently performed for both TEM-1 and PSE-4 by Olivier Fisette.

3. The dynamics of mutants and chimera with different substrate profiles or different kinetics parameters should also be characterised. As a first step in this direction, the chimera cTEM-17m, for which the backbone chemical shifts are now available, is currently under study by NMR using ^{15}N spin relaxation and CPMG relaxation dispersion experiments.

4. Side-chain dynamics should also be characterised as they might be quite different

from backbone dynamics. As different side-chain groups are involved in ligand binding and/or hydrolysis, their dynamics might prove of high importance and might shed new light on the mechanism. To achieve characterisation of side-chain dynamics, two approaches could be used. As usual, NMR would be very powerful (reviewed in [121, 143]), but would rely on assignment of side-chain chemical shifts. In this case, TEM-1 might be a better target for such studies than PSE-4 since assignment of its side-chain resonances is completed [239]. On the other hand, MD simulations of TEM-1 [79] and PSE-4 (Olivier Fisette, unpublished results) which were directed toward analysis of backbone dynamics could be used for exploring also side-chain dynamics and, thus, provide novel information potentially non available from *in vitro* experiments.

Together, these new data will help further understand the relation between motions and activity in class A β-lactamases, and might serve for improvement of these invaluable β-lactam antibiotic drugs.

Appendices

Appendix 1:
PSE-4 Backbone Chemical Shift Assignments

Table 10.1: PSE-4 backbone chemical shifts

Residue		H_N	N	H_α	C_α	C_β	C'
#	aa	(ppm)	(ppm)	(ppm)	(ppm)	(ppm)	(ppm)
22	Ser	n-ter	n-ter	–	–	–	–
23	Ser	–	–	–	–	–	–
24	Ser	–	–	–	58.942	63.619	176.424
25	Lys	8.415	124.016	3.995	58.626	32.307	176.749
26	Phe	7.777	115.596	4.018	58.669	37.036	175.354
27	Gln	7.418	120.401	–	59.836	28.489	177.743
28	Gln	8.470	118.709	3.939	58.036	28.002	177.629
29	Val	7.065	119.159	–	65.689	30.905	177.747
30	Glu	8.008	118.536	–	60.832	30.109	177.754
31	Gln	7.649	116.069	4.009	58.969	28.337	178.993
32	Asp	8.444	122.143	4.422	57.718	39.853	178.793
33	Val	8.777	119.998	–	67.056	31.271	177.553
34	Lys	8.033	119.373	–	59.785	32.275	179.183
35	Ala	7.752	119.905	4.238	54.963	18.006	181.118
36	Ile	7.962	122.267	3.805	64.534	37.961	177.594
37	Glu	8.750	121.715	–	61.296	30.939	179.816
38	Val	7.600	115.614	3.914	65.632	32.234	179.445
39	Ser	8.403	117.241	4.170	61.882	62.913	176.812
40	Leu	8.632	117.977	–	54.858	42.411	177.433
41	Ser	7.781	117.176	4.214	58.849	61.618	172.828
42	Ala	7.884	120.054	5.050	49.938	23.978	176.164
43	Arg	8.301	119.340	4.993	55.651	31.936	175.861
44	Ile	9.594	124.437	5.335	60.173	40.739	173.488
45	Gly	9.038	115.339	–	44.694	–	171.643
46	Val	9.127	122.675	5.519	59.171	36.865	174.937
47	Ser	9.247	119.145	4.952	57.492	66.765	172.204
48	Val	8.891	122.823	5.052	61.471	35.621	173.719
49	Leu	9.279	128.364	5.035	53.651	45.550	174.182
50	Asp	8.935	127.713	4.828	53.575	41.877	177.128
51	Thr	7.948	115.766	–	64.611	69.027	175.960
52	Gln	8.973	122.886	4.115	58.234	29.221	176.975
53	Asn	7.624	112.828	4.862	52.011	39.325	176.853
54	Gly	8.192	110.306	–	46.235	–	174.193
55	Glu	8.119	121.234	4.332	57.526	30.782	175.023
56	Tyr	8.435	124.160	5.665	56.808	42.035	175.165
57	Trp	8.502	127.131	4.260	57.902	31.518	172.556
59	Asp	6.603	122.260	4.159	52.675	44.740	171.710
60	Tyr	8.179	117.511	4.171	57.728	41.727	175.095
61	Asn	8.764	123.962	4.301	53.926	36.107	177.017
62	Gly	8.338	101.370	–	47.244	–	173.020
63	Asn	8.268	112.637	5.002	51.783	38.948	175.339
64	Gln	7.285	120.237	4.133	55.106	29.407	173.558
65	Arg	7.837	115.935	4.805	55.092	31.818	177.238
66	Phe	8.900	118.748	–	55.635	43.286	172.500
67	Pro	–	–	–	63.005	32.414	177.748
68	Leu	8.926	124.920	–	58.413	44.746	181.532
69	Thr	10.648	116.392	–	63.087	69.354	–
70	**Ser**	**–**	**–**	**–**	**63.752**	**66.065**	**176.723**
71	Thr	8.177	113.743	–	65.016	69.673	176.275

Table 10.1: PSE-4 backbone chemical shifts (continued)

Residue		H_N	N	H_α	C_α	C_β	C'
#	aa	(ppm)	(ppm)	(ppm)	(ppm)	(ppm)	(ppm)
72	Phe	8.315	116.862	–	59.169	38.524	176.934
73	**Lys**	**6.721**	**122.814**	**2.782**	**61.821**	**30.694**	**175.016**
74	Thr	6.554	111.876	–	65.289	69.667	175.551
75	Ile	7.427	117.026	–	64.080	38.619	177.192
76	Ala	7.299	119.588	–	55.491	17.268	177.740
77	Cys	7.864	112.442	–	61.629	41.617	175.540
78	Ala	8.315	123.539	3.907	55.562	16.367	178.700
79	Lys	7.965	117.148	–	59.727	31.291	177.185
80	Leu	7.532	119.169	–	59.011	40.933	177.348
81	Leu	7.307	115.340	–	57.460	40.527	178.144
82	Tyr	8.642	122.615	–	61.971	39.462	177.953
83	Asp	9.465	121.451	–	57.266	39.438	179.981
84	Ala	8.488	125.893	4.728	54.919	18.056	182.376
85	Glu	8.350	122.397	–	59.841	29.198	179.130
86	Gln	7.600	113.914	4.248	55.024	28.983	176.344
87	Gly	7.911	107.912	–	45.817	–	174.963
88	Lys	8.302	118.089	4.211	57.330	33.868	175.797
89	Val	6.993	114.844	4.261	59.689	35.426	172.574
90	Asn	8.762	123.205	–	48.846	39.156	–
91	Pro	–	–	–	64.571	32.069	174.562
92	Asn	8.024	112.480	4.839	53.162	38.746	175.378
93	Ser	8.005	117.605	4.350	59.744	63.975	172.826
94	Thr	7.881	108.284	5.283	59.407	72.329	175.685
95	Val	8.875	119.094	4.269	60.610	35.165	174.499
96	Glu	8.356	124.433	4.477	55.721	30.524	176.285
97	Ile	8.566	126.059	4.054	60.049	35.971	176.456
98	Lys	9.032	130.468	4.727	54.267	33.449	177.032
99	Lys	8.904	123.916	–	59.851	32.240	178.802
100	Ala	8.331	117.690	–	53.852	18.692	177.816
101	Asp	7.525	115.322	4.526	55.001	41.576	176.009
102	Leu	7.106	116.970	–	55.859	41.978	177.887
103	Val	7.876	119.704	4.602	59.331	34.416	176.558
104	Thr	8.201	119.846	–	64.038	69.066	172.709
105	**Tyr**	**8.690**	**123.039**	**3.954**	**60.412**	**36.037**	**172.273**
106	Ser	8.475	117.957	4.719	55.246	64.734	–
107	Pro	–	–	–	64.065	32.405	178.030
108	Val	8.690	118.870	3.971	64.611	33.250	178.644
109	Ile	9.529	121.487	–	61.734	34.904	178.674
110	Glu	8.391	116.407	–	58.849	28.230	177.333
111	Lys	6.938	115.873	4.408	56.327	32.555	177.067
112	Gln	7.953	117.930	4.508	54.737	30.199	174.432
113	Val	7.207	119.020	3.338	65.334	31.009	177.573
114	Gly	8.723	116.085	–	45.112	–	173.971
115	Gln	8.219	119.384	4.600	54.090	30.131	173.446
116	Ala	8.212	121.990	5.302	50.577	20.065	177.086
117	Ile	8.499	119.429	4.850	58.803	41.531	174.748
118	Thr	8.749	113.075	5.205	60.165	71.305	176.400
119	Leu	7.733	119.577	–	57.803	40.838	179.199
120	Asp	8.370	119.496	–	58.638	42.383	178.118

Table 10.1: PSE-4 backbone chemical shifts (continued)

Residue		H_N	N	H_α	C_α	C_β	C'
#	aa	(ppm)	(ppm)	(ppm)	(ppm)	(ppm)	(ppm)
121	Asp	8.195	118.328	–	57.122	39.832	179.919
122	Ala	8.545	125.224	–	55.496	16.063	179.848
123	Cys	8.185	118.807	–	63.731	42.002	175.844
124	Phe	8.473	122.259	–	62.287	38.282	179.322
125	Ala	8.750	121.660	–	55.371	17.678	180.773
126	Thr	8.524	116.397	4.161	67.170	68.350	175.816
127	Met	8.529	119.761	–	55.580	29.888	180.632
128	Thr	7.942	109.673	–	64.382	70.760	176.232
129	Thr	7.318	106.338	5.227	62.562	73.853	175.187
130	**Ser**	**7.867**	**112.041**	**–**	**60.233**	**62.722**	**173.715**
131	Asp	7.355	119.962	–	57.107	43.907	177.532
132	Asn	9.196	129.696	–	56.571	39.011	177.536
133	Thr	8.277	121.569	–	68.410	67.978	176.939
134	Ala	9.293	123.763	–	55.189	18.290	178.292
135	Ala	7.113	116.050	–	55.522	18.994	178.386
136	Asn	7.828	119.507	4.763	55.498	36.857	179.686
137	Ile	8.508	124.865	–	65.508	37.824	178.764
138	Ile	7.752	120.623	–	62.282	35.357	178.538
139	Leu	8.959	118.438	–	58.154	42.402	179.489
140	Ser	8.122	113.521	4.210	61.609	62.851	176.306
141	Ala	7.755	123.228	4.421	53.721	20.147	179.260
142	Val	7.703	107.340	4.730	59.726	32.034	176.251
143	Gly	7.602	108.553	–	45.642	–	176.167
144	Gly	9.017	110.339	–	45.378	–	170.357
145	Pro	–	–	–	66.234	31.922	178.357
146	Lys	8.632	117.965	–	59.659	32.466	178.319
147	Gly	7.458	108.148	–	46.940	–	177.516
148	Val	8.454	121.963	–	67.288	31.307	177.023
149	Thr	8.581	119.015	–	68.661	–	175.408
150	Asp	8.797	121.680	–	57.834	40.156	179.147
151	Phe	7.836	122.521	–	59.305	39.133	176.086
152	Leu	8.146	120.683	–	57.865	40.581	178.586
153	Arg	8.221	116.379	–	57.332	28.324	181.353
154	Gln	8.180	121.756	–	58.922	28.135	178.480
155	Ile	7.629	111.451	4.342	60.940	37.775	176.430
156	Gly	7.585	109.064	–	45.669	–	172.968
157	Asp	8.286	123.162	4.612	52.917	39.961	176.293
158	Lys	8.582	123.329	–	56.375	32.948	176.372
159	Glu	8.598	118.061	4.479	57.478	33.032	177.409
160	Thr	9.746	124.272	–	64.706	66.406	173.854
161	Arg	9.010	121.833	4.594	54.903	33.601	170.666
162	Leu	7.781	121.592	–	53.539	45.872	174.210
163	Asp	10.211	125.956	–	55.872	45.521	175.234
164	Arg	9.469	126.224	4.664	54.905	35.027	172.009
165	Ile	7.232	106.006	–	59.427	37.984	177.903
166	**Glu**	**9.002**	**117.273**	**–**	**55.542**	**28.971**	**178.300**
167	Pro	–	–	–	63.825	32.670	177.540
168	Asp	8.142	128.115	4.378	57.418	40.881	176.478
169	Leu	7.441	113.108	–	57.204	40.749	176.971

Table 10.1: PSE-4 backbone chemical shifts (continued)

Residue		H_N	N	H_α	C_α	C_β	C'
#	aa	(ppm)	(ppm)	(ppm)	(ppm)	(ppm)	(ppm)
170	Asn	7.555	119.088	–	54.511	40.501	174.076
171	Glu	7.221	121.302	–	60.818	30.185	177.940
172	Gly	9.714	105.157	–	46.362	–	174.714
173	Lys	8.135	118.750	3.579	57.694	33.196	177.473
174	Leu	8.151	128.201	–	56.881	41.370	177.926
175	Gly	8.993	115.489	–	45.120	–	172.817
176	Asp	7.282	120.820	4.490	52.937	42.031	177.233
177	Leu	8.747	128.110	–	55.561	42.902	178.347
178	Arg	7.990	119.789	–	57.032	30.597	177.178
179	Asp	9.087	115.855	–	55.508	42.721	178.240
180	Thr	7.349	105.853	–	59.782	75.089	173.184
181	Thr	8.485	112.982	4.266	59.606	69.030	173.029
182	Thr	8.666	111.560	5.582	57.591	67.712	174.388
183	Pro	–	–	–	65.539	31.640	179.026
184	Lys	8.324	116.746	–	59.493	33.306	178.493
185	Ala	8.317	124.469	–	55.275	18.424	180.478
186	Ile	8.226	116.117	–	61.671	36.920	176.939
187	Ala	7.146	124.603	–	55.616	18.075	178.966
188	Ser	7.538	111.410	–	61.192	62.889	177.499
189	Thr	8.763	123.201	–	67.074	67.953	174.560
190	Leu	8.608	120.811	–	58.812	41.369	178.646
191	Asn	7.860	116.161	–	56.977	39.190	177.317
192	Lys	7.810	118.848	–	60.026	32.019	179.058
193	Phe	7.810	114.255	4.510	57.725	38.735	176.771
194	Leu	8.053	115.430	3.965	56.785	42.701	176.611
195	Phe	7.811	112.603	4.967	56.578	40.494	176.975
196	Gly	7.437	110.211	–	45.345	–	174.202
197	Ser	8.681	113.923	–	57.978	63.988	175.242
198	Ala	7.459	122.778	4.270	55.268	19.223	176.187
199	Leu	7.998	113.573	5.083	52.205	46.823	176.143
200	Ser	10.430	118.541	–	57.822	64.749	175.215
201	Glu	8.852	122.560	–	59.970	29.344	178.894
202	Met	8.388	115.546	4.115	58.625	32.027	178.992
203	Asn	7.501	119.525	4.845	54.595	38.559	177.236
204	Gln	8.895	123.828	–	60.033	27.617	178.577
205	Lys	7.621	115.884	3.935	57.962	31.486	179.565
206	Lys	7.475	123.079	3.626	59.214	31.906	177.551
207	Leu	7.892	120.470	–	57.826	41.668	178.259
208	Glu	8.272	117.011	–	60.200	30.452	178.448
209	Ser	8.220	114.758	–	61.965	–	177.622
210	Trp	7.915	123.170	–	58.358	28.793	176.308
211	Met	7.528	113.622	6.823	58.576	36.327	180.738
212	Val	9.409	124.675	–	66.357	32.790	178.741
213	Asn	7.930	115.795	4.821	54.132	38.621	173.259
214	Asn	6.902	118.361	–	55.365	39.231	177.400
215	Gln	9.439	125.964	4.558	56.262	30.792	178.982
216	Val	8.339	112.363	4.864	61.624	31.950	176.607
217	Thr	8.010	109.307	4.559	60.691	67.845	177.411
218	Gly	9.142	116.142	–	47.812	–	172.784

Table 10.1: PSE-4 backbone chemical shifts (continued)

Residue		H_N	N	H_α	C_α	C_β	C'
#	aa	(ppm)	(ppm)	(ppm)	(ppm)	(ppm)	(ppm)
219	Asn	8.116	113.176	4.691	52.381	36.926	174.642
220	Leu	7.211	116.186	–	51.979	40.807	177.449
221	Leu	7.097	126.059	–	57.992	41.608	178.274
222	Arg	8.821	116.534	–	60.128	30.135	176.891
223	Ser	7.466	112.791	–	61.187	63.901	174.764
224	Val	7.208	112.690	4.528	59.676	32.045	173.681
225	Leu	6.639	125.629	–	52.823	44.000	174.609
226	Pro	–	–	–	62.300	30.633	175.613
227	Ala	8.157	124.396	–	53.558	17.991	179.259
228	Gly	8.664	110.769	–	45.478	–	174.820
229	Trp	7.945	121.645	4.647	57.294	28.949	174.331
230	Asn	8.767	117.944	4.502	51.738	40.844	172.176
231	Ile	7.973	114.767	5.480	58.881	40.414	170.395
232	Ala	9.058	129.143	–	50.084	21.863	175.974
233	Asp	8.287	120.976	5.659	53.719	44.474	174.577
234	**Arg**	**7.840**	**118.962**	**–**	**57.930**	**34.023**	**172.791**
235	Ser	8.667	124.927	–	57.490	67.931	172.472
236	Gly	8.628	103.858	–	45.932	–	173.000
237	Ala	–	–	–	51.964	22.953	176.039
238	Gly	8.342	107.395	–	46.028	–	172.658
240	Gly	8.691	108.384	–	45.650	–	173.759
241	Phe	8.503	115.423	4.162	59.366	36.393	175.329
242	Gly	8.531	103.084	–	45.648	–	174.611
243	Ala	7.543	123.571	–	53.098	17.291	179.200
244	Arg	8.569	123.928	–	55.241	33.633	173.796
245	Ser	8.738	118.223	5.269	56.595	67.305	174.070
246	Ile	8.801	114.673	–	60.796	41.735	171.242
247	Thr	8.636	114.143	–	57.504	71.733	174.921
248	Ala	10.175	128.472	5.548	49.896	24.358	173.474
249	Val	9.562	122.233	5.404	61.017	33.839	175.684
250	Val	9.389	119.382	5.843	58.908	35.358	174.559
251	Trp	8.200	119.854	–	57.221	31.311	171.788
252	Ser	8.763	115.795	4.387	56.162	66.395	173.706
254	Glu	8.520	118.500	–	59.012	29.336	176.780
255	His	7.835	113.003	–	54.947	30.674	173.190
256	Gln	7.304	122.786	4.382	54.054	29.702	173.289
257	Ala	8.393	131.358	–	50.924	17.165	174.582
258	Pro	–	–	–	63.617	31.717	176.066
259	Ile	9.394	126.230	5.014	59.124	40.832	175.461
260	Ile	9.432	125.626	5.093	60.816	39.259	175.122
261	Val	9.818	127.483	5.085	60.884	35.279	174.375
262	Ser	9.283	123.275	5.491	56.935	65.607	172.891
263	Ile	8.783	122.273	4.781	61.053	41.832	172.931
264	Tyr	9.373	125.838	–	57.412	42.074	172.458
265	Leu	9.045	119.848	5.582	54.140	45.531	177.099
266	Ala	9.454	123.758	4.599	52.033	23.690	174.309
267	Gln	8.746	117.744	–	56.570	25.650	173.549
268	Thr	8.258	111.557	5.226	59.293	69.179	173.634
269	Gln	8.991	127.509	–	55.727	28.977	175.478

Table 10.1: PSE-4 backbone chemical shifts (continued)

Residue		**H_N**	**N**	**H_α**	**C_α**	**C_β**	**C'**
#	**aa**	**(ppm)**	**(ppm)**	**(ppm)**	**(ppm)**	**(ppm)**	**(ppm)**
270	Ala	8.307	124.327	4.261	52.714	20.808	177.795
271	Ser	9.010	119.609	–	58.067	65.170	175.405
272	Met	9.210	122.412	–	58.024	30.670	177.558
273	Glu	8.895	117.980	–	60.888	28.670	179.057
274	Glu	7.723	119.220	–	59.264	30.389	180.262
275	Arg	8.253	119.759	–	60.457	30.633	177.264
276	Asn	8.906	119.606	–	55.635	36.943	177.138
277	Asp	8.125	118.576	–	57.062	40.824	177.953
278	Ala	7.693	121.416	4.032	55.224	19.373	178.867
279	Ile	7.435	116.736	–	65.602	36.626	177.349
280	Val	8.063	119.683	–	67.850	31.570	177.364
281	Lys	8.468	120.062	–	59.734	32.459	179.840
282	Ile	8.195	119.653	–	65.917	38.210	177.963
283	Gly	8.737	106.146	–	47.174	–	173.267
284	His	9.066	119.342	–	59.039	28.579	176.922
285	Ser	7.989	115.444	4.050	62.302	67.298	177.124
286	Ile	7.957	121.418	–	66.117	38.122	177.941
287	Phe	8.713	118.242	4.521	59.230	36.509	179.121
288	Asp	8.344	119.809	4.413	56.927	40.475	178.827
289	Val	7.492	120.157	3.347	65.969	30.878	177.805
290	Tyr	7.339	116.209	4.300	61.300	40.274	177.868
291	Thr	8.418	111.123	4.582	62.933	69.610	175.895
292	Ser	7.900	117.211	4.421	59.368	63.620	174.805
293	Gln	8.051	120.900	4.381	55.979	29.276	175.920
294	Ser	8.195	116.984	4.467	58.425	63.727	173.526
295	Arg	7.930	128.122	4.200	57.475	31.396	180.933

- Important active site residues (Ser^{70}, Lys^{73}, Tyr^{105}, Ser^{130}, Glu^{166}, and Arg^{234}) are shown in bold red while residues from the Ω loop (residues 161–179) are coloured blue.
- Chemical shifts have been deposited in the BMRB (under accession number 6838).
- n-ter: N-terminus amine (not observable).

Appendix 2:
PSE-4 ^{15}N Spin Relaxation Data

Table 10.2: PSE-4 ^{15}N spin relaxation data

Residue		**50.6 MHz**						**60.8 MHz**						**81.0 MHz**					
#	**aa**	R_1	ΔR_1	R_2	ΔR_2	*NOE*	ΔNOE	R_1	ΔR_1	R_2	ΔR_2	*NOE*	ΔNOE	R_1	ΔR_1	R_2	ΔR_2	*NOE*	ΔNOE
		(s^{-1})	**(s^{-1})**	**(s^{-1})**	**(s^{-1})**			**(s^{-1})**	**(s^{-1})**	**(s^{-1})**	**(s^{-1})**			**(s^{-1})**	**(s^{-1})**	**(s^{-1})**	**(s^{-1})**		
22	Ser	n-ter	n-ter	n-ter	n-ter	n-ter	n-ter	n-ter	n-ter	n-ter	n-ter	n-ter	n-ter	n-ter	n-ter	n-ter	n-ter	n-ter	n-ter
23	Ser	n.o.	n.o.	n.o.	n.o.	n.o.	n.o.	n.o.	n.o.	n.o.	n.o.	n.o.	n.o.	n.o.	n.o.	n.o.	n.o.	n.o.	n.o.
24	Ser	n.o.	n.o.	n.o.	n.o.	n.o.	n.o.	n.o.	n.o.	n.o.	n.o.	n.o.	n.o.	n.o.	n.o.	n.o.	n.o.	n.o.	n.o.
25	Lys	1.690	0.144	13.203	0.601	0.518	0.037	1.269	0.054	13.027	1.513	0.572	0.043	1.034	0.095	15.113	1.050	0.614	0.026
26	Phe	1.423	0.019	12.630	0.296	0.660	0.016	1.091	0.014	13.767	0.180	0.693	0.019	0.785	0.032	17.039	0.728	0.764	0.018
27	Gln	1.317	0.024	15.382	0.271	0.730	0.015	0.984	0.012	16.511	0.234	0.798	0.020	0.683	0.014	20.580	0.298	0.819	0.020
28	Gln	1.399	0.036	14.498	0.347	0.715	0.016	1.115	0.022	15.421	0.301	0.773	0.022	0.762	0.038	19.950	0.750	0.792	0.018
29	Val	1.289	0.017	14.777	0.347	0.748	0.018	1.015	0.016	15.686	0.250	0.793	0.022	0.697	0.014	20.372	0.472	0.807	0.020
30	Glu	1.315	0.043	15.721	0.348	0.841	0.020	1.001	0.017	17.132	0.318	0.858	0.026	0.664	0.013	21.054	0.368	0.819	0.020
31	Gln	1.286	0.032	15.085	0.372	0.790	0.018	0.945	0.013	16.479	0.223	0.765	0.020	0.670	0.011	19.159	0.486	0.814	0.019
32	Asp	1.360	0.019	15.341	0.535	0.783	0.016	1.122	0.073	14.426	0.344	0.859	0.021	0.652	0.043	17.571	0.461	0.899	0.019
33	Val	1.318	0.024	15.786	0.229	0.780	0.020	0.998	0.018	17.145	0.329	0.828	0.026	0.659	0.022	21.044	0.588	0.875	0.026
34	Lys	1.326	0.029	16.232	0.369	0.810	0.018	1.016	0.015	17.337	0.263	0.791	0.022	0.658	0.013	21.296	0.466	0.816	0.020
35	Ala	1.321	0.017	15.679	0.364	0.787	0.015	1.001	0.014	16.943	0.249	0.844	0.021	0.683	0.010	20.186	0.251	0.844	0.018
36	Ile	1.296	0.025	15.088	0.401	0.789	0.020	1.023	0.019	15.564	0.303	0.823	0.025	0.669	0.014	18.734	0.436	0.885	0.022
37	Glu	o.l.	o.l.	o.l.	o.l.	o.l.	o.l.	o.l.	o.l.	o.l.	o.l.	o.l.	o.l.	o.l.	o.l.	o.l.	o.l.	o.l.	o.l.
38	Val	1.237	0.015	14.600	0.156	0.809	0.020	0.979	0.016	15.614	0.226	0.821	0.023	0.634	0.023	18.275	0.248	0.818	0.020
39	Ser	1.337	0.025	14.898	0.407	0.786	0.016	1.006	0.013	16.101	0.277	0.791	0.019	0.689	0.011	19.336	0.228	0.834	0.016
40	Leu	o.l.	o.l.	o.l.	o.l.	o.l.	o.l.	o.l.	o.l.	o.l.	o.l.	o.l.	o.l.	o.l.	o.l.	o.l.	o.l.	o.l.	o.l.
41	Ser	1.148	0.018	16.036	0.207	0.805	0.019	0.892	0.014	16.695	0.285	0.826	0.024	0.628	0.019	21.590	0.469	0.883	0.022
42	Ala	o.l.	o.l.	o.l.	o.l.	o.l.	o.l.	o.l.	o.l.	o.l.	o.l.	o.l.	o.l.	0.578	0.018	20.097	0.314	0.777	0.021
43	Arg	1.226	0.018	16.753	0.354	0.743	0.020	0.916	0.016	17.314	0.384	0.730	0.025	0.620	0.013	21.107	0.812	0.782	0.021
44	Ile	1.257	0.022	14.702	0.218	0.792	0.024	0.954	0.021	15.796	0.384	0.780	0.030	0.664	0.017	20.280	1.647	0.800	0.026
45	Gly	1.329	0.047	15.295	0.266	0.831	0.027	0.971	0.022	16.232	0.442	0.808	0.032	0.666	0.049	19.780	0.683	0.864	0.036
46	Val	1.326	0.027	15.458	0.218	0.785	0.024	0.983	0.021	16.241	0.416	0.847	0.031	0.677	0.019	18.842	0.617	0.856	0.029
47	Ser	1.346	0.042	15.799	0.238	0.813	0.023	1.017	0.021	17.021	0.361	0.791	0.027	0.687	0.019	21.547	1.037	0.875	0.028
48	Val	1.343	0.034	15.135	0.242	0.766	0.025	0.923	0.027	16.355	0.409	0.823	0.030	0.668	0.020	18.722	0.450	0.883	0.033
49	Leu	1.282	0.030	15.431	0.352	0.796	0.027	0.984	0.026	16.507	0.507	0.798	0.033	0.655	0.023	22.224	1.241	0.835	0.031
50	Asp	1.319	0.028	14.969	0.271	0.752	0.027	1.026	0.027	15.305	0.435	0.813	0.034	0.700	0.028	20.782	0.856	0.813	0.032
51	Thr	1.366	0.035	13.713	0.424	0.776	0.019	0.987	0.051	15.210	0.353	0.681	0.027	0.803	0.019	18.053	0.817	0.772	0.023
52	Gln	1.395	0.015	13.736	0.133	0.606	0.014	1.089	0.014	15.144	0.201	0.625	0.016	0.824	0.018	18.621	0.278	0.684	0.018
53	Asn	1.348	0.027	11.319	0.194	0.545	0.016	1.068	0.018	11.550	0.370	0.626	0.021	0.764	0.016	16.566	0.468	0.627	0.019
54	Gly	1.372	0.017	13.207	0.431	0.718	0.018	1.048	0.018	14.503	0.212	0.730	0.022	0.747	0.013	18.612	0.438	0.781	0.018
55	Glu	1.315	0.017	13.238	0.234	0.691	0.014	1.059	0.014	14.324	0.218	0.721	0.019	0.740	0.011	17.651	0.329	0.761	0.017
56	Tyr	1.307	0.032	14.495	0.169	0.693	0.019	0.974	0.021	15.500	0.482	0.714	0.024	0.711	0.014	20.102	0.902	0.745	0.021
57	Trp	1.236	0.034	18.162	0.513	0.780	0.029	0.936	0.026	18.965	0.682	0.791	0.035	0.623	0.032	26.914	1.467	0.811	0.032
59	Asp	1.214	0.012	15.773	0.165	0.815	0.014	0.889	0.010	16.541	0.191	0.790	0.016	0.591	0.015	21.260	0.861	0.896	0.015
60	Tyr	1.217	0.034	17.850	0.886	0.799	0.026	0.906	0.024	16.114	0.398	0.876	0.036	0.594	0.018	22.093	0.642	0.921	0.029
61	Asn	1.389	0.042	16.111	0.324	0.803	0.024	0.988	0.024	16.165	0.395	0.830	0.029	0.679	0.033	20.461	0.545	0.865	0.028
62	Gly	1.246	0.026	16.883	0.566	0.835	0.023	0.900	0.021	17.875	0.443	0.819	0.029	0.610	0.027	24.174	1.700	0.896	0.031

Table 10.2: PSE-4 ^{15}N spin relaxation data (continued)

Residue		50.6 MHz						60.8 MHz						81.0 MHz					
#	aa	R_1	ΔR_1	R_2	ΔR_2	*NOE*	ΔNOE	R_1	ΔR_1	R_2	ΔR_2	*NOE*	ΔNOE	R_1	ΔR_1	R_2	ΔR_2	*NOE*	ΔNOE
		(s^{-1})	(s^{-1})	(s^{-1})	(s^{-1})			(s^{-1})	(s^{-1})	(s^{-1})	(s^{-1})			(s^{-1})	(s^{-1})	(s^{-1})	(s^{-1})		
63	Asn	1.385	0.041	16.116	0.183	0.790	0.019	1.000	0.017	16.884	0.322	0.813	0.023	0.645	0.062	22.440	0.741	0.910	0.021
64	Gln	1.343	0.020	15.807	0.381	0.807	0.020	0.978	0.018	16.809	0.345	0.846	0.027	0.661	0.018	21.693	0.578	0.882	0.025
65	Arg	1.301	0.017	14.246	0.237	0.796	0.022	0.990	0.039	14.258	0.360	0.807	0.023	0.629	0.029	18.131	0.665	0.853	0.022
66	Phe	1.381	0.069	15.593	0.469	0.768	0.028	1.014	0.028	16.264	0.512	0.790	0.034	0.692	0.024	20.508	0.984	0.880	0.035
67	Pro	-	-	-	-	-	-	-	-	-	-	-	-	-	-	-	-	-	-
68	Leu	1.415	0.060	17.141	1.008	0.814	0.042	1.034	0.044	16.694	0.926	0.803	0.047	0.729	0.040	20.167	1.200	0.846	0.046
69	Thr	1.465	0.052	16.422	0.475	0.843	0.037	1.043	0.041	16.994	0.889	0.805	0.046	0.732	0.039	22.120	1.100	0.876	0.047
70	**Ser**	**n.o.**	**n.o.**	**n.o.**	**n.o.**	**n.o.**	**n.o.**	**n.o.**	**n.o.**	**n.o.**	**n.o.**	**n.o.**	**n.o.**	**n.o.**	**n.o.**	**n.o.**	**n.o.**	**n.o.**	**n.o.**
71	Thr	1.563	0.039	16.200	0.395	0.848	0.027	1.058	0.026	17.875	0.500	0.820	0.031	0.820	0.022	24.059	1.315	0.842	0.027
72	Phe	o.l.	o.l.	o.l.	o.l.	o.l.	o.l.	o.l.	o.l.	o.l.	o.l.	o.l.	o.l.	o.l.	o.l.	o.l.	o.l.	o.l.	o.l.
73	**Lys**	**1.470**	**0.047**	**16.174**	**0.233**	**0.813**	**0.023**	**1.072**	**0.023**	**17.740**	**0.478**	**0.873**	**0.028**	**0.702**	**0.030**	**24.036**	**2.090**	**0.836**	**0.024**
74	Thr	1.393	0.045	16.032	0.831	0.808	0.021	0.972	0.017	15.097	2.019	0.856	0.024	0.643	0.031	21.407	1.210	0.880	0.022
75	Ile	1.457	0.036	15.809	0.473	0.832	0.029	1.058	0.031	16.437	0.518	0.853	0.039	0.688	0.040	20.771	1.508	0.873	0.033
76	Ala	1.357	0.044	15.394	0.255	0.815	0.023	1.023	0.022	17.473	0.407	0.866	0.030	0.684	0.018	22.149	0.749	0.949	0.030
77	Cys	1.292	0.032	15.132	0.269	0.790	0.019	0.968	0.016	16.811	0.795	0.794	0.022	0.638	0.014	18.763	0.386	0.924	0.023
78	Ala	1.340	0.021	16.414	0.287	0.841	0.018	1.019	0.015	17.620	0.625	0.820	0.020	0.692	0.011	19.901	0.432	0.903	0.019
79	Lys	1.393	0.034	16.577	0.660	0.845	0.019	1.063	0.016	15.782	0.249	0.799	0.021	0.705	0.014	19.677	0.478	0.917	0.021
80	Leu	o.l.	o.l.	o.l.	o.l.	o.l.	o.l.	o.l.	o.l.	o.l.	o.l.	o.l.	o.l.	o.l.	o.l.	o.l.	o.l.	o.l.	o.l.
81	Leu	1.283	0.030	15.583	0.296	0.857	0.031	0.985	0.024	16.951	0.434	0.863	0.034	0.665	0.021	20.129	0.473	0.867	0.030
82	Tyr	1.366	0.025	15.998	0.279	0.795	0.024	1.058	0.023	16.823	0.406	0.850	0.029	0.701	0.019	20.430	0.468	0.852	0.026
83	Asp	1.353	0.021	16.602	0.686	0.808	0.021	1.044	0.020	16.657	0.366	0.817	0.025	0.703	0.022	21.233	0.741	0.887	0.024
84	Ala	1.332	0.017	15.845	0.551	0.771	0.018	1.015	0.016	16.345	0.242	0.838	0.022	0.681	0.024	20.032	0.308	0.879	0.021
85	Glu	1.293	0.018	15.547	0.257	0.809	0.019	0.979	0.015	16.889	0.334	0.838	0.023	0.654	0.012	20.142	0.600	0.891	0.019
86	Gln	1.278	0.028	13.406	0.166	0.792	0.019	0.973	0.015	14.562	0.560	0.802	0.023	0.643	0.013	18.162	0.864	0.834	0.021
87	Gly	1.256	0.015	14.998	0.212	0.770	0.017	0.952	0.015	16.246	0.383	0.783	0.021	0.644	0.013	19.283	0.333	0.861	0.021
88	Lys	1.197	0.017	16.458	0.311	0.759	0.019	0.949	0.016	17.311	0.276	0.791	0.025	0.630	0.016	20.832	0.541	0.838	0.021
89	Val	1.184	0.011	14.145	0.245	0.726	0.014	0.902	0.009	14.780	0.146	0.735	0.015	0.617	0.009	17.977	0.152	0.748	0.014
90	Asn	o.l.	o.l.	o.l.	o.l.	o.l.	o.l.	o.l.	o.l.	o.l.	o.l.	o.l.	o.l.	o.l.	o.l.	o.l.	o.l.	o.l.	o.l.
91	Pro	-	-	-	-	-	-	-	-	-	-	-	-	-	-	-	-	-	-
92	Asn	1.403	0.019	13.761	0.252	0.792	0.016	1.014	0.013	14.611	0.190	0.798	0.019	0.697	0.011	18.929	0.380	0.878	0.017
93	Ser	1.275	0.024	15.691	0.518	0.813	0.016	0.935	0.013	16.774	0.231	0.833	0.021	0.652	0.011	21.121	0.748	0.870	0.017
94	Thr	1.222	0.029	14.751	0.368	0.786	0.016	0.918	0.011	17.187	0.234	0.800	0.019	0.616	0.018	20.936	0.353	0.869	0.019
95	Val	1.257	0.021	15.400	0.343	0.760	0.023	0.979	0.020	15.922	0.341	0.778	0.029	0.669	0.018	19.813	0.757	0.813	0.029
96	Glu	1.230	0.016	13.351	0.137	0.729	0.014	0.945	0.012	14.503	0.190	0.712	0.017	0.681	0.014	17.286	0.989	0.759	0.015
97	Ile	1.295	0.021	12.999	0.204	0.717	0.023	1.005	0.021	14.283	0.287	0.741	0.029	0.654	0.016	18.068	0.334	0.750	0.025
98	Lys	1.240	0.018	14.556	0.179	0.710	0.021	0.975	0.018	16.241	0.320	0.774	0.026	0.659	0.018	19.151	0.429	0.824	0.029
99	Lys	o.l.	o.l.	o.l.	o.l.	o.l.	o.l.	o.l.	o.l.	o.l.	o.l.	o.l.	o.l.	o.l.	o.l.	o.l.	o.l.	o.l.	o.l.
100	Ala	1.289	0.040	16.366	0.142	0.760	0.016	0.982	0.018	18.179	0.242	0.767	0.020	0.651	0.051	23.134	0.807	0.844	0.018
101	Asp	1.289	0.021	13.891	0.213	0.761	0.018	0.991	0.014	14.974	0.198	0.746	0.020	0.686	0.011	17.879	0.416	0.738	0.019
102	Leu	1.200	0.013	16.026	0.437	0.762	0.018	0.911	0.014	17.052	0.238	0.774	0.021	0.621	0.011	20.603	0.473	0.792	0.019

Table 10.2: PSE-4 ^{15}N spin relaxation data (continued)

Residue		50.6 MHz						60.8 MHz						81.0 MHz					
#	aa	R_1	ΔR_1	R_2	ΔR_2	*NOE*	ΔNOE	R_1	ΔR_1	R_2	ΔR_2	*NOE*	ΔNOE	R_1	ΔR_1	R_2	ΔR_2	*NOE*	ΔNOE
		(s^{-1})	(s^{-1})	(s^{-1})	(s^{-1})			(s^{-1})	(s^{-1})	(s^{-1})	(s^{-1})			(s^{-1})	(s^{-1})	(s^{-1})	(s^{-1})		
103	Val	o.l.	o.l.	o.l.	o.l.	o.l.	o.l.	o.l.	o.l.	o.l.	o.l.	o.l.	o.l.	0.661	0.024	20.911	0.708	0.794	0.037
104	Thr	o.l.	o.l.	o.l.	o.l.	o.l.	o.l.	o.l.	o.l.	o.l.	o.l.	o.l.	o.l.	o.l.	o.l.	o.l.	o.l.	o.l.	o.l.
105	**Tyr**	**1.421**	**0.025**	**13.941**	**0.412**	**0.711**	**0.022**	**1.014**	**0.020**	**14.237**	**0.369**	**0.750**	**0.027**	**0.740**	**0.023**	**17.726**	**0.413**	**0.758**	**0.025**
106	Ser	1.438	0.075	13.287	0.413	0.781	0.022	1.013	0.031	14.665	0.293	0.828	0.028	0.664	0.034	17.731	0.582	0.792	0.023
107	Pro	-	-	-	-	-	-	-	-	-	-	-	-	-	-	-	-	-	-
108	Val	1.345	0.029	15.629	0.712	0.741	0.026	1.066	0.027	16.249	0.418	0.741	0.033	0.704	0.024	20.415	0.542	0.794	0.031
109	Ile	1.245	0.066	16.122	0.447	0.784	0.040	0.921	0.038	17.242	0.790	0.746	0.045	0.703	0.077	20.962	1.218	0.911	0.058
110	Glu	1.252	0.022	18.033	0.260	0.798	0.021	0.950	0.016	20.426	0.373	0.821	0.025	0.620	0.014	24.653	0.531	0.870	0.023
111	Lys	1.245	0.026	15.305	0.156	0.691	0.018	0.954	0.015	16.623	0.251	0.738	0.022	0.664	0.013	20.423	0.785	0.752	0.020
112	Gln	1.237	0.029	14.825	0.538	0.734	0.018	0.940	0.016	15.598	0.230	0.759	0.025	0.620	0.012	19.458	0.506	0.812	0.021
113	Val	1.217	0.027	13.718	0.137	0.716	0.015	0.972	0.012	14.989	0.177	0.697	0.018	0.669	0.011	19.498	0.295	0.750	0.018
114	Gly	1.360	0.026	15.188	0.305	0.759	0.029	1.070	0.027	15.959	0.409	0.776	0.033	0.712	0.022	19.146	0.463	0.830	0.032
115	Gln	1.196	0.013	15.300	0.327	0.759	0.016	0.953	0.012	17.526	0.252	0.774	0.019	0.641	0.029	21.079	0.369	0.780	0.017
116	Ala	1.179	0.010	12.739	0.175	0.695	0.013	0.902	0.014	13.890	0.175	0.700	0.016	0.639	0.021	16.557	0.165	0.703	0.013
117	Ile	1.262	0.045	13.822	0.192	0.730	0.023	0.987	0.021	15.311	0.322	0.732	0.029	0.665	0.016	19.409	0.536	0.798	0.024
118	Thr	1.344	0.039	14.581	0.277	0.800	0.024	1.017	0.019	15.527	0.326	0.815	0.027	0.682	0.033	18.891	0.370	0.872	0.027
119	Leu	1.279	0.028	16.056	0.377	0.791	0.026	0.987	0.033	17.571	0.646	0.857	0.044	0.646	0.022	23.382	1.150	0.873	0.032
120	Asp	1.277	0.035	16.024	0.261	0.830	0.023	0.941	0.018	19.042	0.483	0.781	0.028	0.648	0.016	22.441	0.582	0.926	0.026
121	Asp	1.246	0.044	17.199	0.483	0.833	0.022	0.927	0.018	18.241	0.534	0.852	0.030	0.610	0.014	23.233	1.145	0.870	0.023
122	Ala	1.340	0.020	15.880	0.406	0.808	0.020	1.000	0.016	16.738	0.271	0.845	0.024	0.659	0.042	19.969	0.384	0.918	0.023
123	Cys	1.313	0.021	16.850	0.660	0.782	0.019	0.974	0.020	18.282	0.441	0.783	0.027	0.681	0.015	22.706	0.836	0.867	0.022
124	Phe	1.268	0.026	16.020	0.572	0.841	0.024	0.855	0.058	18.179	0.388	0.796	0.026	0.668	0.014	22.038	0.817	0.858	0.021
125	Ala	o.l.	o.l.	o.l.	o.l.	o.l.	o.l.	o.l.	o.l.	o.l.	o.l.	o.l.	o.l.	o.l.	o.l.	o.l.	o.l.	o.l.	o.l.
126	Thr	1.361	0.033	16.778	0.352	0.788	0.024	1.018	0.020	17.346	0.373	0.800	0.027	0.691	0.019	20.459	0.409	0.910	0.025
127	Met	1.392	0.039	18.249	0.351	0.817	0.032	1.027	0.031	19.891	0.714	0.775	0.040	0.695	0.030	25.743	1.913	0.864	0.040
128	Thr	1.328	0.047	20.473	0.697	0.829	0.029	0.927	0.024	24.149	1.048	0.855	0.034	0.663	0.024	25.346	5.928	0.863	0.032
129	Thr	1.368	0.042	16.970	0.728	0.853	0.037	1.007	0.034	17.822	0.786	0.824	0.044	0.613	0.067	22.006	0.933	0.944	0.041
130	**Ser**	**1.530**	**0.069**	**15.653**	**1.019**	**0.799**	**0.032**	**1.070**	**0.035**	**19.723**	**1.338**	**0.859**	**0.042**	**0.764**	**0.036**	**21.992**	**1.828**	**0.894**	**0.038**
131	Asp	1.429	0.039	15.514	0.372	0.802	0.029	1.037	0.032	17.535	0.650	0.818	0.041	0.713	0.028	21.390	0.857	0.885	0.040
132	Asn	1.523	0.042	15.857	0.344	0.814	0.030	1.108	0.032	17.399	0.646	0.841	0.035	0.832	0.038	22.338	1.014	0.851	0.036
133	Thr	1.442	0.067	16.827	0.280	0.795	0.025	1.077	0.027	16.932	0.523	0.815	0.034	0.712	0.061	21.945	0.616	0.940	0.028
134	Ala	1.388	0.029	15.241	0.226	0.775	0.021	1.032	0.018	15.949	0.316	0.818	0.024	0.725	0.016	19.142	0.491	0.892	0.025
135	Ala	1.370	0.029	15.057	0.201	0.849	0.020	1.030	0.016	16.165	0.266	0.849	0.022	0.689	0.022	19.341	0.472	0.870	0.020
136	Asn	1.393	0.033	15.787	0.288	0.830	0.018	1.035	0.018	16.523	0.322	0.828	0.024	0.721	0.025	20.743	0.352	0.876	0.022
137	Ile	1.395	0.028	15.953	0.740	0.821	0.026	1.043	0.025	15.756	0.396	0.847	0.032	0.702	0.021	19.084	0.549	0.861	0.030
138	Ile	1.333	0.027	16.461	0.259	0.833	0.026	1.002	0.026	17.368	0.459	0.838	0.035	0.697	0.020	21.079	0.524	0.835	0.029
139	Leu	1.415	0.039	15.184	0.469	0.780	0.023	1.044	0.022	16.504	0.356	0.803	0.028	0.723	0.021	20.184	0.650	0.851	0.030
140	Ser	1.367	0.026	14.175	0.194	0.788	0.014	1.024	0.012	15.304	0.220	0.844	0.018	0.660	0.027	18.111	0.211	0.878	0.016
141	Ala	1.306	0.020	14.411	0.233	0.763	0.015	1.009	0.012	15.368	0.183	0.805	0.018	0.710	0.009	18.560	0.494	0.843	0.017
142	Val	1.308	0.033	13.580	0.229	0.813	0.021	0.968	0.018	14.879	0.270	0.804	0.025	0.615	0.023	18.141	0.787	0.874	0.023

Table 10.2: PSE-4 ^{15}N spin relaxation data (continued)

Residue		50.6 MHz						60.8 MHz						81.0 MHz					
#	aa	R_1	ΔR_1	R_2	ΔR_2	*NOE*	Δ*NOE*	R_1	ΔR_1	R_2	ΔR_2	*NOE*	Δ*NOE*	R_1	ΔR_1	R_2	ΔR_2	*NOE*	Δ*NOE*
		(s^{-1})	(s^{-1})	(s^{-1})	(s^{-1})			(s^{-1})	(s^{-1})	(s^{-1})	(s^{-1})			(s^{-1})	(s^{-1})	(s^{-1})	(s^{-1})		
143	Gly	1.373	0.038	15.529	0.201	0.830	0.021	1.024	0.024	16.818	0.318	0.840	0.024	0.697	0.056	20.488	0.446	0.904	0.025
144	Gly	1.425	0.028	14.629	0.254	0.830	0.020	1.073	0.018	16.223	0.293	0.835	0.022	0.719	0.023	20.649	0.397	0.904	0.024
145	Pro	-	-	-	-	-	-	-	-	-	-	-	-	-	-	-	-	-	-
146	Lys	o.l.	o.l.	o.l.	o.l.	o.l.	o.l.	o.l.	o.l.	o.l.	o.l.	o.l.	o.l.	o.l.	o.l.	o.l.	o.l.	o.l.	o.l.
147	Gly	1.349	0.021	15.547	0.197	0.829	0.021	0.989	0.018	17.314	0.322	0.863	0.025	0.664	0.018	19.343	0.397	0.901	0.025
148	Val	1.343	0.025	15.785	0.418	0.822	0.025	0.935	0.029	21.554	1.269	0.751	0.027	0.669	0.015	25.394	3.133	0.859	0.021
149	Thr	1.347	0.025	17.043	0.325	0.751	0.024	0.977	0.021	17.671	0.424	0.772	0.028	0.626	0.023	21.716	0.907	0.818	0.026
150	Asp	1.306	0.029	16.702	0.275	0.816	0.018	0.956	0.014	18.349	0.334	0.805	0.021	0.709	0.015	22.287	0.619	0.907	0.022
151	Phe	1.338	0.033	16.211	0.368	0.803	0.020	1.012	0.018	17.023	0.350	0.829	0.025	0.671	0.019	21.219	0.949	0.942	0.024
152	Leu	1.355	0.035	17.573	0.313	0.830	0.026	0.986	0.026	17.293	0.721	0.823	0.034	0.605	0.038	21.782	0.647	0.871	0.027
153	Arg	1.307	0.028	18.101	0.814	0.835	0.025	0.954	0.020	19.494	0.511	0.830	0.028	0.629	0.025	24.322	2.497	0.940	0.026
154	Gln	1.316	0.032	16.136	0.253	0.779	0.017	1.020	0.039	16.175	0.289	0.845	0.021	0.654	0.011	21.687	0.342	0.835	0.017
155	Ile	1.331	0.023	11.025	0.656	0.606	0.018	1.007	0.016	11.050	1.129	0.457	0.019	0.654	0.015	15.441	1.020	0.720	0.020
156	Gly	1.301	0.036	15.714	0.410	0.835	0.023	0.946	0.018	17.852	0.397	0.833	0.027	0.630	0.022	22.560	0.579	0.877	0.027
157	Asp	1.274	0.031	17.481	0.742	0.767	0.019	0.920	0.015	17.577	0.356	0.803	0.024	0.625	0.012	21.847	0.841	0.871	0.022
158	Lys	1.274	0.063	15.813	0.255	0.768	0.027	0.895	0.024	16.519	0.485	0.775	0.032	0.573	0.047	18.734	0.484	0.865	0.031
159	Glu	o.l.	o.l.	o.l.	o.l.	o.l.	o.l.	1.122	0.090	14.968	0.290	0.926	0.030	0.527	0.051	19.339	0.753	0.879	0.030
160	Thr	1.332	0.026	14.647	0.223	0.811	0.023	0.929	0.021	15.162	0.390	0.833	0.030	0.661	0.019	20.473	1.341	0.847	0.027
161	Arg	1.474	0.034	16.526	0.317	0.783	0.024	1.016	0.023	17.619	0.566	0.815	0.030	0.710	0.031	22.866	1.287	0.882	0.028
162	Leu	1.393	0.033	16.393	0.661	0.796	0.027	1.006	0.028	16.575	0.536	0.841	0.035	0.691	0.041	20.543	1.018	0.833	0.029
163	Asp	1.339	0.060	15.058	0.583	0.839	0.044	0.946	0.050	15.808	0.943	0.773	0.055	0.634	0.043	19.626	1.157	0.920	0.056
164	Arg	1.215	0.051	15.163	0.446	0.795	0.027	0.815	0.033	16.757	0.657	0.786	0.038	0.620	0.026	21.584	1.234	0.817	0.034
165	Ile	1.256	0.033	13.789	0.261	0.826	0.031	0.903	0.028	16.355	1.041	0.813	0.038	0.621	0.020	19.279	1.890	0.848	0.028
166	**Glu**	**1.331**	**0.048**	**15.901**	**0.400**	**0.804**	**0.034**	**1.010**	**0.036**	**17.338**	**0.679**	**0.840**	**0.042**	**0.691**	**0.034**	**21.157**	**0.855**	**0.883**	**0.042**
167	Pro	-	-	-	-	-	-	-	-	-	-	-	-	-	-	-	-	-	-
168	Asp	o.l.	o.l.	o.l.	o.l.	o.l.	o.l.	o.l.	o.l.	o.l.	o.l.	o.l.	o.l.	o.l.	o.l.	o.l.	o.l.	o.l.	o.l.
169	Leu	1.399	0.070	15.729	0.284	0.790	0.026	1.061	0.024	17.852	1.433	0.819	0.030	0.704	0.022	23.866	1.115	0.882	0.033
170	Asn	o.l.	o.l.	o.l.	o.l.	o.l.	o.l.	o.l.	o.l.	o.l.	o.l.	o.l.	o.l.	o.l.	o.l.	o.l.	o.l.	o.l.	o.l.
171	Glu	1.366	0.043	16.701	0.248	0.825	0.023	0.962	0.019	17.879	0.522	0.822	0.028	0.664	0.021	22.224	0.545	0.888	0.027
172	Gly	1.406	0.074	15.141	0.381	0.786	0.029	0.968	0.034	16.923	0.785	0.833	0.045	0.659	0.028	23.774	2.081	0.849	0.035
173	Lys	o.l.	o.l.	o.l.	o.l.	o.l.	o.l.	o.l.	o.l.	o.l.	o.l.	o.l.	o.l.	o.l.	o.l.	o.l.	o.l.	o.l.	o.l.
174	Leu	o.l.	o.l.	o.l.	o.l.	o.l.	o.l.	o.l.	o.l.	o.l.	o.l.	o.l.	o.l.	o.l.	o.l.	o.l.	o.l.	o.l.	o.l.
175	Gly	1.399	0.125	17.122	1.585	0.735	0.057	1.077	0.064	15.914	1.461	0.784	0.064	0.664	0.060	21.354	2.081	0.776	0.063
176	Asp	1.386	0.036	15.253	0.312	0.808	0.016	1.004	0.014	15.765	0.307	0.805	0.021	0.715	0.013	21.043	0.540	0.882	0.021
177	Leu	1.512	0.077	14.803	0.693	0.792	0.028	1.041	0.027	13.807	0.494	0.793	0.032	0.691	0.045	21.011	0.789	0.823	0.031
178	Arg	1.530	0.057	16.930	0.607	0.817	0.020	1.025	0.019	17.539	0.452	0.828	0.026	0.736	0.018	22.224	0.595	0.867	0.024
179	Asp	1.368	0.039	15.838	0.606	0.807	0.029	0.970	0.027	16.050	0.606	0.860	0.036	0.646	0.038	20.433	1.323	0.881	0.038
180	Thr	1.446	0.051	14.120	0.412	0.844	0.024	0.999	0.022	15.587	0.459	0.804	0.030	0.703	0.028	23.138	2.542	0.912	0.025
181	Thr	1.401	0.036	15.325	0.284	0.822	0.029	1.020	0.026	15.835	0.490	0.821	0.033	0.675	0.021	20.890	1.343	0.906	0.030
182	Thr	1.350	0.024	14.882	0.306	0.769	0.021	0.976	0.017	15.689	0.326	0.831	0.025	0.623	0.033	20.916	0.566	0.871	0.023

Table 10.2: PSE-4 ^{15}N spin relaxation data (continued)

Residue		50.6 MHz						60.8 MHz						81.0 MHz					
#	aa	R_1	ΔR_1	R_2	ΔR_2	*NOE*	Δ*NOE*	R_1	ΔR_1	R_2	ΔR_2	*NOE*	Δ*NOE*	R_1	ΔR_1	R_2	ΔR_2	*NOE*	Δ*NOE*
		(s^{-1})	(s^{-1})	(s^{-1})	(s^{-1})			(s^{-1})	(s^{-1})	(s^{-1})	(s^{-1})			(s^{-1})	(s^{-1})	(s^{-1})	(s^{-1})		
183	Pro	-	-	-	-	-	-	-	-	-	-	-	-	-	-	-	-	-	-
184	Lys	o.l.	o.l.	o.l.	o.l.	o.l.	o.l.	o.l.	o.l.	o.l.	o.l.	o.l.	o.l.	o.l.	o.l.	o.l.	o.l.	o.l.	o.l.
185	Ala	o.l.	o.l.	o.l.	o.l.	o.l.	o.l.	o.l.	o.l.	o.l.	o.l.	o.l.	o.l.	o.l.	o.l.	o.l.	o.l.	o.l.	o.l.
186	Ile	1.353	0.027	14.393	0.569	0.809	0.020	1.114	0.051	16.139	0.383	0.846	0.034	0.690	0.017	19.410	0.328	0.892	0.021
187	Ala	1.386	0.018	16.324	0.272	0.850	0.019	1.051	0.015	17.277	0.283	0.840	0.022	0.722	0.013	22.097	1.572	0.882	0.021
188	Ser	1.288	0.021	o.l.	o.l.	0.489	0.013	0.957	0.017	15.299	2.434	0.445	0.017	0.710	0.012	11.112	0.917	0.586	0.017
189	Thr	o.l.	o.l.	o.l.	o.l.	o.l.	o.l.	o.l.	o.l.	o.l.	o.l.	o.l.	o.l.	o.l.	o.l.	o.l.	o.l.	o.l.	o.l.
190	Leu	1.376	0.022	16.981	0.409	0.795	0.022	1.032	0.020	17.402	0.421	0.826	0.028	0.685	0.018	21.576	0.468	0.917	0.026
191	Asn	1.354	0.034	15.195	0.569	0.805	0.020	0.934	0.047	18.613	0.942	0.778	0.027	0.715	0.015	20.969	1.010	0.876	0.022
192	Lys	1.396	0.061	15.677	0.535	0.811	0.021	1.150	0.079	15.749	0.276	0.873	0.028	0.623	0.044	19.761	0.479	0.910	0.023
193	Phe	1.364	0.029	14.779	0.505	0.786	0.018	0.983	0.014	15.724	0.237	0.843	0.021	0.655	0.018	20.305	1.262	0.879	0.020
194	Leu	1.344	0.034	14.937	0.223	0.832	0.024	0.995	0.020	16.596	0.356	0.765	0.025	0.701	0.016	19.250	0.530	0.865	0.024
195	Phe	1.317	0.050	14.492	0.333	0.778	0.023	1.002	0.022	15.528	0.771	0.827	0.029	0.661	0.017	20.147	0.889	0.890	0.026
196	Gly	1.233	0.018	11.971	0.487	0.720	0.019	0.916	0.016	13.876	0.231	0.762	0.023	0.660	0.012	17.489	0.267	0.789	0.020
197	Ser	1.500	0.201	14.198	0.963	0.701	0.050	0.910	0.046	14.063	1.109	0.738	0.056	0.698	0.051	18.038	1.341	0.740	0.047
198	Ala	1.325	0.035	14.502	0.230	0.670	0.015	1.010	0.022	15.410	0.216	0.670	0.018	0.723	0.038	19.423	0.696	0.719	0.017
199	Leu	1.269	0.022	14.672	0.277	0.782	0.016	0.926	0.012	15.720	0.211	0.802	0.020	0.638	0.010	18.946	0.359	0.854	0.018
200	Ser	1.158	0.025	15.634	0.198	0.778	0.022	0.855	0.019	16.547	0.372	0.820	0.031	0.581	0.019	20.811	0.891	0.792	0.029
201	Glu	1.366	0.031	13.997	0.125	0.784	0.018	1.080	0.030	14.984	0.231	0.804	0.020	0.721	0.036	18.672	0.671	0.856	0.021
202	Met	1.386	0.027	14.473	0.270	0.772	0.015	1.043	0.011	15.108	0.156	0.798	0.017	0.710	0.026	18.339	0.530	0.810	0.015
203	Asn	1.361	0.044	14.633	0.239	0.844	0.022	1.055	0.021	15.997	0.294	0.847	0.028	0.738	0.018	19.765	0.350	0.859	0.025
204	Gln	o.l.	o.l.	o.l.	o.l.	o.l.	o.l.	o.l.	o.l.	o.l.	o.l.	o.l.	o.l.	o.l.	o.l.	o.l.	o.l.	o.l.	o.l.
205	Lys	1.357	0.021	14.564	0.177	0.786	0.020	1.014	0.018	15.470	0.248	0.845	0.025	0.689	0.014	18.647	0.728	0.831	0.022
206	Lys	1.350	0.018	15.025	0.152	0.809	0.020	1.005	0.018	15.677	0.320	0.833	0.023	0.684	0.026	18.965	0.394	0.851	0.022
207	Leu	1.371	0.026	15.481	0.452	0.828	0.020	1.053	0.021	16.902	0.346	0.773	0.026	0.703	0.045	20.134	0.408	0.833	0.024
208	Glu	1.387	0.027	17.930	0.933	0.844	0.029	1.091	0.018	16.382	0.274	0.844	0.025	0.625	0.026	22.854	2.507	0.922	0.024
209	Ser	1.386	0.019	14.718	0.216	0.795	0.017	1.039	0.013	15.727	0.197	0.801	0.019	0.694	0.020	19.063	0.568	0.874	0.017
210	Trp	1.401	0.025	15.325	0.315	0.812	0.017	1.050	0.015	15.820	0.217	0.801	0.019	0.731	0.027	19.609	0.514	0.888	0.019
211	Met	1.379	0.051	13.306	0.406	0.762	0.027	0.998	0.025	o.l.	o.l.	0.864	0.034	0.669	0.021	18.748	0.866	0.876	0.032
212	Val	1.455	0.033	17.011	0.326	0.794	0.027	1.047	0.029	17.380	0.529	0.836	0.035	0.706	0.059	21.457	0.798	0.919	0.039
213	Asn	1.367	0.042	16.257	0.267	0.815	0.036	1.068	0.052	16.287	0.296	0.853	0.028	0.619	0.016	20.498	0.732	0.969	0.036
214	Asn	1.322	0.038	14.863	0.361	0.807	0.018	0.927	0.015	15.940	0.348	0.769	0.022	0.665	0.015	20.366	0.401	0.838	0.022
215	Gln	1.291	0.033	15.617	0.699	0.767	0.028	0.991	0.030	16.419	1.000	0.804	0.038	0.650	0.026	25.529	1.298	0.882	0.037
216	Val	1.421	0.033	15.373	0.264	0.763	0.023	1.040	0.021	16.809	0.381	0.758	0.028	0.721	0.023	23.332	0.643	0.846	0.025
217	Thr	1.483	0.061	15.484	0.178	0.766	0.018	1.053	0.016	17.031	0.297	0.766	0.021	0.747	0.059	22.934	0.738	0.814	0.019
218	Gly	1.583	0.193	18.832	1.975	0.739	0.076	0.930	0.082	19.602	2.873	0.784	0.081	0.715	0.124	22.362	3.368	0.887	0.106
219	Asn	1.469	0.106	16.691	0.212	0.800	0.019	0.982	0.035	17.204	0.393	0.841	0.024	0.681	0.079	25.720	1.309	0.914	0.022
220	Leu	1.336	0.036	16.346	0.231	0.813	0.023	0.938	0.019	17.564	0.508	0.828	0.028	0.656	0.017	22.217	1.356	0.849	0.027
221	Leu	1.319	0.073	18.198	0.858	0.797	0.052	0.909	0.054	19.905	1.468	0.772	0.061	0.630	0.057	27.843	2.792	0.974	0.066
222	Arg	1.363	0.049	17.557	0.895	0.835	0.040	0.949	0.035	17.401	0.949	0.851	0.047	0.655	0.038	22.658	1.132	0.903	0.046

Table 10.2: PSE-4 ^{15}N spin relaxation data (continued)

Residue		50.6 MHz						60.8 MHz						81.0 MHz					
#	aa	R_1	ΔR_1	R_2	ΔR_2	*NOE*	Δ*NOE*	R_1	ΔR_1	R_2	ΔR_2	*NOE*	Δ*NOE*	R_1	ΔR_1	R_2	ΔR_2	*NOE*	Δ*NOE*
		(s^{-1})	(s^{-1})	(s^{-1})	(s^{-1})			(s^{-1})	(s^{-1})	(s^{-1})	(s^{-1})			(s^{-1})	(s^{-1})	(s^{-1})	(s^{-1})		
223	Ser	1.445	0.045	13.637	1.218	0.791	0.019	1.022	0.017	15.579	1.151	0.820	0.022	0.711	0.022	20.701	0.702	0.908	0.025
224	Val	1.374	0.061	15.607	0.424	0.808	0.024	0.985	0.020	16.420	0.407	0.845	0.029	0.675	0.016	21.087	0.456	0.885	0.026
225	Leu	1.181	0.016	14.767	0.156	0.828	0.019	0.886	0.014	15.669	0.270	0.800	0.021	0.576	0.016	19.450	0.332	0.863	0.020
226	Pro	-	-	-	-	-	-	-	-	-	-	-	-	-	-	-	-	-	-
227	Ala	1.183	0.031	14.551	0.102	0.762	0.013	0.905	0.009	15.433	0.171	0.825	0.016	0.605	0.026	19.214	1.067	0.834	0.015
228	Gly	1.312	0.084	13.626	0.743	0.732	0.024	0.916	0.036	14.134	0.379	0.773	0.027	0.614	0.068	19.064	0.759	0.757	0.023
229	Trp	1.337	0.025	14.470	0.261	0.769	0.014	1.067	0.032	14.323	0.256	0.797	0.018	0.693	0.017	18.733	0.248	0.823	0.016
230	Asn	1.283	0.027	15.073	0.477	0.775	0.023	0.910	0.024	16.654	0.443	0.750	0.028	0.670	0.021	19.901	1.128	0.844	0.031
231	Ile	1.259	0.031	14.483	0.275	0.855	0.019	0.973	0.015	15.609	0.249	0.824	0.021	0.648	0.022	19.029	0.256	0.845	0.019
232	Ala	1.272	0.037	15.679	0.993	0.812	0.035	0.895	0.029	17.124	0.746	0.891	0.041	0.654	0.029	20.384	0.825	0.871	0.041
233	Asp	1.337	0.048	16.284	0.392	0.795	0.020	0.952	0.019	16.915	0.440	0.805	0.027	0.625	0.028	20.958	1.017	0.879	0.023
234	**Arg**	**1.235**	**0.048**	**15.949**	**0.550**	**0.805**	**0.030**	**0.820**	**0.064**	**21.608**	**1.495**	**0.785**	**0.039**	**0.678**	**0.026**	**24.033**	**1.217**	**0.808**	**0.030**
235	Ser	1.466	0.289	21.903	1.580	0.846	0.073	1.043	0.088	20.983	3.235	0.764	0.080	0.827	0.088	27.182	4.184	0.924	0.076
236	Gly	1.250	0.059	19.017	0.445	0.814	0.032	0.884	0.034	18.893	1.135	0.849	0.051	0.653	0.034	27.756	4.630	0.911	0.046
237	Ala	n.o.	n.o.	n.o.	n.o.	n.o.	n.o.	n.o.	n.o.	n.o.	n.o.	n.o.	n.o.	n.o.	n.o.	n.o.	n.o.	n.o.	n.o.
238	Gly	1.260	0.039	16.250	0.509	0.730	0.020	0.886	0.016	16.894	0.418	0.752	0.025	0.588	0.019	21.495	1.536	0.814	0.024
240	Gly	1.408	0.035	16.109	0.425	0.791	0.027	0.997	0.025	17.195	0.559	0.828	0.032	0.697	0.026	21.822	0.843	0.982	0.040
241	Phe	1.474	0.039	15.627	0.436	0.771	0.027	1.021	0.026	16.996	0.553	0.830	0.033	0.691	0.048	20.834	0.610	0.867	0.029
242	Gly	1.324	0.028	16.957	0.388	0.751	0.024	0.957	0.028	19.104	0.689	0.841	0.039	0.675	0.027	27.471	3.444	0.883	0.039
243	Ala	1.385	0.054	17.324	0.387	0.836	0.019	0.970	0.014	18.242	0.378	0.826	0.021	0.706	0.014	23.506	0.833	0.919	0.023
244	Arg	1.399	0.038	17.994	0.899	0.789	0.030	0.979	0.027	18.486	0.689	0.835	0.037	0.671	0.028	23.535	0.898	0.857	0.034
245	Ser	o.l.	o.l.	o.l.	o.l.	o.l.	o.l.	o.l.	o.l.	o.l.	o.l.	o.l.	o.l.	0.615	0.041	25.514	1.198	0.892	0.037
246	Ile	1.333	0.031	17.231	0.811	0.804	0.027	0.988	0.023	17.596	0.502	0.831	0.031	0.669	0.022	22.203	0.640	0.898	0.034
247	Thr	1.375	0.047	16.966	0.620	0.836	0.037	0.962	0.034	17.078	0.742	0.872	0.047	0.637	0.028	21.598	1.274	0.875	0.040
248	Ala	1.291	0.022	15.367	0.399	0.787	0.021	0.920	0.019	15.998	0.403	0.831	0.031	0.639	0.037	20.639	0.541	0.879	0.028
249	Val	1.256	0.028	15.200	0.220	0.820	0.025	0.930	0.020	15.615	0.418	0.806	0.030	0.592	0.017	18.623	0.420	0.929	0.029
250	Val	1.370	0.029	15.594	0.352	0.801	0.027	1.038	0.025	17.145	0.457	0.817	0.033	0.716	0.023	19.977	0.523	0.934	0.032
251	Trp	o.l.	o.l.	o.l.	o.l.	o.l.	o.l.	o.l.	o.l.	o.l.	o.l.	o.l.	o.l.	o.l.	o.l.	o.l.	o.l.	o.l.	o.l.
252	Ser	1.384	0.032	14.446	0.244	0.802	0.021	1.038	0.018	15.304	0.295	0.816	0.024	0.697	0.021	18.726	0.954	0.879	0.024
254	Glu	1.490	0.090	14.386	0.401	0.709	0.022	1.046	0.032	15.103	0.399	0.718	0.027	0.726	0.074	18.789	0.437	0.728	0.023
255	His	1.466	0.153	12.171	0.436	0.640	0.030	0.958	0.037	14.746	1.065	0.664	0.038	0.672	0.029	18.542	0.797	0.711	0.032
256	Gln	1.191	0.024	12.842	0.136	0.637	0.014	0.866	0.010	13.484	0.204	0.666	0.017	0.614	0.019	17.565	0.694	0.736	0.016
257	Ala	1.214	0.018	15.782	0.414	0.748	0.018	0.930	0.015	17.276	0.314	0.774	0.022	0.596	0.053	21.214	0.446	0.809	0.022
258	Pro	-	-	-	-	-	-	-	-	-	-	-	-	-	-	-	-	-	-
259	Ile	1.344	0.029	14.759	0.301	0.783	0.027	1.032	0.028	16.024	0.456	0.867	0.035	0.684	0.023	21.068	0.659	0.872	0.030
260	Ile	1.302	0.037	15.655	0.565	0.769	0.021	0.956	0.021	15.494	0.444	0.846	0.034	0.643	0.017	17.968	0.600	0.930	0.027
261	Val	1.246	0.045	15.050	0.227	0.804	0.024	0.943	0.022	16.200	0.458	0.820	0.032	0.622	0.034	21.556	0.572	0.864	0.027
262	Ser	1.274	0.028	15.994	0.330	0.813	0.023	0.913	0.017	17.712	0.631	0.812	0.027	0.611	0.015	20.434	1.062	0.885	0.027
263	Ile	1.292	0.027	16.919	0.718	0.810	0.025	0.915	0.020	16.947	0.523	0.792	0.030	0.625	0.018	19.958	0.463	0.892	0.028
264	Tyr	1.223	0.031	16.808	0.944	0.812	0.024	0.931	0.023	15.881	0.405	0.893	0.031	0.601	0.025	20.200	0.501	0.874	0.028

Table 10.2: PSE-4 ^{15}N spin relaxation data (continued)

Residue		50.6 MHz						60.8 MHz						81.0 MHz					
#	aa	R_1	ΔR_1	R_2	ΔR_2	*NOE*	Δ*NOE*	R_1	ΔR_1	R_2	ΔR_2	*NOE*	Δ*NOE*	R_1	ΔR_1	R_2	ΔR_2	*NOE*	Δ*NOE*
		(s^{-1})	(s^{-1})	(s^{-1})	(s^{-1})			(s^{-1})	(s^{-1})	(s^{-1})	(s^{-1})			(s^{-1})	(s^{-1})	(s^{-1})	(s^{-1})		
265	Leu	1.276	0.038	16.783	0.419	0.765	0.026	0.869	0.024	17.709	0.611	0.777	0.034	0.655	0.023	20.394	1.323	0.811	0.034
266	Ala	1.177	0.018	16.457	0.351	0.767	0.021	0.870	0.015	16.942	0.367	0.788	0.024	0.617	0.029	20.535	0.453	0.816	0.024
267	Gln	1.232	0.047	15.520	0.544	0.813	0.029	0.931	0.024	17.121	0.530	0.823	0.035	0.597	0.021	20.988	0.629	0.806	0.033
268	Thr	1.254	0.045	15.632	0.271	0.797	0.020	0.910	0.015	16.848	0.350	0.765	0.024	0.616	0.019	22.937	1.032	0.821	0.021
269	Gln	1.336	0.068	15.913	0.375	0.756	0.031	0.937	0.030	17.287	0.769	0.796	0.036	0.623	0.091	21.929	0.817	0.850	0.038
270	Ala	o.l.	o.l.	o.l.	o.l.	o.l.	o.l.	o.l.	o.l.	o.l.	o.l.	o.l.	o.l.	o.l.	o.l.	o.l.	o.l.	o.l.	o.l.
271	Ser	1.252	0.039	15.992	0.263	0.759	0.022	0.929	0.023	17.364	0.495	0.780	0.027	0.593	0.026	23.598	0.937	0.868	0.029
272	Met	1.398	0.229	13.826	1.738	0.790	0.090	0.960	0.094	18.512	3.733	0.760	0.084	0.652	0.092	20.277	2.860	0.783	0.076
273	Glu	1.433	0.039	15.140	0.215	0.773	0.017	1.003	0.014	16.128	0.293	0.780	0.021	0.718	0.015	20.232	0.588	0.878	0.024
274	Glu	1.278	0.042	15.855	0.271	0.810	0.023	0.960	0.022	17.364	0.508	0.824	0.031	0.640	0.017	21.813	0.542	0.837	0.026
275	Arg	1.346	0.028	15.694	0.971	0.822	0.026	0.923	0.029	18.091	0.446	0.712	0.027	0.721	0.017	22.469	0.673	0.817	0.026
276	Asn	1.349	0.043	16.285	0.389	0.763	0.019	0.987	0.017	17.052	0.374	0.818	0.025	0.671	0.015	21.591	0.624	0.882	0.026
277	Asp	o.l.	o.l.	o.l.	o.l.	o.l.	o.l.	o.l.	o.l.	o.l.	o.l.	o.l.	o.l.	o.l.	o.l.	o.l.	o.l.	o.l.	o.l.
278	Ala	1.263	0.023	16.244	0.145	0.790	0.016	0.978	0.013	17.272	0.280	0.863	0.021	0.643	0.021	21.525	0.803	0.880	0.020
279	Ile	1.259	0.023	15.100	0.236	0.803	0.024	0.953	0.019	16.314	0.363	0.806	0.029	0.624	0.015	19.288	0.431	0.876	0.027
280	Val	1.339	0.042	15.467	0.291	0.808	0.020	1.007	0.018	17.579	0.328	0.834	0.025	0.684	0.021	22.270	0.696	0.869	0.024
281	Lys	1.332	0.027	17.121	0.790	0.797	0.021	1.009	0.018	17.969	0.341	0.814	0.027	0.654	0.015	21.986	0.781	0.846	0.026
282	Ile	o.l.	o.l.	o.l.	o.l.	o.l.	o.l.	o.l.	o.l.	o.l.	o.l.	o.l.	o.l.	0.577	0.056	22.099	0.531	0.852	0.022
283	Gly	1.357	0.032	15.565	0.261	0.822	0.026	1.016	0.024	16.992	0.438	0.821	0.032	0.663	0.018	22.129	2.502	0.914	0.031
284	His	1.353	0.019	15.545	0.176	0.812	0.020	1.022	0.017	17.103	0.307	0.828	0.024	0.698	0.018	22.598	1.059	0.876	0.026
285	Ser	1.316	0.024	15.373	0.142	0.793	0.017	0.973	0.012	16.713	0.218	0.830	0.019	0.646	0.014	19.990	0.341	0.821	0.016
286	Ile	1.301	0.042	15.923	0.386	0.831	0.025	0.895	0.056	19.354	0.593	0.767	0.030	0.673	0.016	23.627	1.850	0.894	0.030
287	Phe	o.l.	o.l.	o.l.	o.l.	o.l.	o.l.	o.l.	o.l.	o.l.	o.l.	o.l.	o.l.	0.684	0.015	21.124	0.798	0.862	0.026
288	Asp	1.374	0.029	16.439	0.131	0.789	0.017	1.058	0.017	16.958	0.250	0.809	0.021	0.676	0.025	21.404	0.339	0.887	0.020
289	Val	1.287	0.033	16.263	0.190	0.778	0.019	0.945	0.016	17.312	0.325	0.821	0.027	0.656	0.015	21.371	0.408	0.823	0.026
290	Tyr	1.279	0.046	15.153	0.387	0.805	0.026	0.963	0.023	16.288	0.370	0.754	0.029	0.636	0.016	19.536	0.388	0.859	0.026
291	Thr	1.373	0.024	12.462	0.254	0.666	0.013	1.022	0.013	13.138	0.165	0.687	0.018	0.708	0.024	17.907	0.420	0.687	0.015
292	Ser	1.639	0.074	10.042	0.191	0.449	0.008	1.270	0.024	10.496	0.083	0.476	0.010	1.028	0.068	13.249	0.452	0.589	0.009
293	Gln	1.799	0.165	6.299	0.217	0.080	0.006	1.425	0.048	6.187	0.094	0.212	0.008	1.235	0.046	7.925	0.448	0.419	0.007
294	Ser	1.682	0.164	3.776	0.235	-0.347	0.006	1.357	0.056	3.600	0.095	-0.157	0.006	1.302	0.044	4.464	0.415	0.081	0.005
295	Arg	1.072	0.011	1.764	0.095	-0.802	0.004	1.017	0.013	1.799	0.029	-0.843	0.005	0.979	0.015	2.937	0.091	-0.393	0.003

- Exact magnetic fields (reported here as nitrogen Larmour frequencies) were as follows: 50.641893 (50.6), 60.777824 (60.8), and 81.046603 (81.0) MHz.
- Values presented here are rounded to three decimals. Exact values can be obtained from the BMRB (accession number 6838).
- Important active site residues (Ser^{70}, Lys^{73}, Tyr^{105}, Ser^{130}, Glu^{166}, and Arg^{234}) are shown in bold red while residues from the Ω loop (residues 161–179) are coloured blue.
- $^{81.0}R_2$ were not used for model-free analysis.
- n-ter: N-terminus amine (not observable).
- n.o.: non-observed N-H resonances (not assigned).
- o.l.: overlapped N-H resonances.

Appendix 3:
PSE-4 Model-Free Analysis Parameters

Table 10.3: PSE-4 model-free parameters

Residue		**Model**	**Parameters**	**Diffusion**	S^2	ΔS^2	S_f^2	ΔS_f^2	S_s^2	ΔS_s^2	τ_e	$\Delta\tau_e$	τ_f	$\Delta\tau_f$	τ_s	$\Delta\tau_s$	$^{60.8}R_{ex}$	$\Delta^{60.8}R_{ex}$
#	**aa**			**core ?**							**ps**	**ps**	**ps**	**ps**	**ps**	**ps**	$\mathbf{s}^{-1}$	$\mathbf{s}^{-1}$
22	Ser	n-ter.	n-ter.	-	n-ter	n-ter	n-ter	n-ter	n-ter	n-ter	n-ter	n-ter	n-ter	n-ter	n-ter	n-ter	n-ter	n-ter
23	Ser	n.o.	n.o.	-	n.o.	n.o.	n.o.	n.o.	n.o.	n.o.	n.o.	n.o.	n.o.	n.o.	n.o.	n.o.	n.o.	n.o.
24	Ser	n.o.	n.o.	-	n.o.	n.o.	n.o.	n.o.	n.o.	n.o.	n.o.	n.o.	n.o.	n.o.	n.o.	n.o.	n.o.	n.o.
25	Lys	$m2$	S^2,τ_e	-	0.829	0.020	-	-	-	-	856.178	99.801	-	-	-	-	-	-
26	Phe	$m5$	S_f^2,S^2,τ_s	-	0.761	0.017	0.846	0.012	0.899	0.011	-	-	-	-	1143.569	127.978	-	-
27	Gln	$m2$	S^2,τ_e	yes	0.877	0.012	-	-	-	-	16.682	3.897	-	-	-	-	-	-
28	Gln	$m5$	S_f^2,S^2,τ_s	yes	0.838	0.017	0.896	0.013	0.935	0.010	-	-	-	-	1267.107	236.493	-	-
29	Val	$m2$	S^2,τ_e	yes	0.861	0.010	-	-	-	-	14.841	3.878	-	-	-	-	-	-
30	Glu	$m1$	S^2	yes	0.895	0.012	-	-	-	-	-	-	-	-	-	-	-	-
31	Gln	$m2$	S^2,τ_e	yes	0.857	0.011	-	-	-	-	11.268	3.783	-	-	-	-	-	-
32	Asp	$m1$	S^2	yes	0.858	0.014	-	-	-	-	-	-	-	-	-	-	-	-
33	Val	$m1$	S^2	yes	0.891	0.010	-	-	-	-	-	-	-	-	-	-	-	-
34	Lys	$m2$	S^2,τ_e	yes	0.905	0.012	-	-	-	-	12.647	5.907	-	-	-	-	-	-
35	Ala	$m3$	S^2,R_{ex}	yes	0.873	0.016	-	-	-	-	-	-	-	-	-	-	0.965	0.498
36	Ile	$m1$	S^2	yes	0.868	0.010	-	-	-	-	-	-	-	-	-	-	-	-
37	Glu	o.l.	o.l.	yes	o.l.	o.l.	o.l.	o.l.	o.l.	o.l.	o.l.	o.l.	o.l.	o.l.	o.l.	o.l.	o.l.	o.l.
38	Val	$m1$	S^2	yes	0.844	0.010	-	-	-	-	-	-	-	-	-	-	-	-
39	Ser	$m2$	S^2,τ_e	yes	0.875	0.013	-	-	-	-	9.908	4.818	-	-	-	-	-	-
40	Leu	o.l.	o.l.	-	o.l.	o.l.	o.l.	o.l.	o.l.	o.l.	o.l.	o.l.	o.l.	o.l.	o.l.	o.l.	o.l.	o.l.
41	Ser	$m1$	S^2	-	0.849	0.011	-	-	-	-	-	-	-	-	-	-	-	-
42	Ala	o.l.	o.l.	-	o.l.	o.l.	o.l.	o.l.	o.l.	o.l.	o.l.	o.l.	o.l.	o.l.	o.l.	o.l.	o.l.	o.l.
43	Arg	$m2$	S^2,τ_e	yes	0.868	0.012	-	-	-	-	21.376	3.934	-	-	-	-	-	-
44	Ile	$m2$	S^2,τ_e	yes	0.844	0.011	-	-	-	-	11.349	3.329	-	-	-	-	-	-
45	Gly	$m1$	S^2	yes	0.873	0.011	-	-	-	-	-	-	-	-	-	-	-	-
46	Val	$m1$	S^2	yes	0.879	0.011	-	-	-	-	-	-	-	-	-	-	-	-
47	Ser	$m1$	S^2	yes	0.902	0.012	-	-	-	-	-	-	-	-	-	-	-	-
48	Val	$m1$	S^2	yes	0.864	0.012	-	-	-	-	-	-	-	-	-	-	-	-
49	Leu	$m1$	S^2	yes	0.873	0.012	-	-	-	-	-	-	-	-	-	-	-	-
50	Asp	$m2$	S^2,τ_e	yes	0.867	0.011	-	-	-	-	13.680	4.855	-	-	-	-	-	-
51	Thr	$m5$	S_f^2,S^2,τ_s	-	0.811	0.019	0.868	0.014	0.934	0.012	-	-	-	-	1180.373	239.759	-	-
52	Gln	$m5$	S_f^2,S^2,τ_s	-	0.829	0.015	0.904	0.012	0.917	0.009	-	-	-	-	591.971	106.323	-	-
53	Asn	$m6$	S_f^2,τ_f,S^2,τ_s	-	0.640	0.015	0.749	0.013	0.854	0.013	-	-	20.329	4.640	1586.108	250.112	-	-
54	Gly	$m5$	S_f^2,S^2,τ_s	-	0.759	0.019	0.837	0.014	0.907	0.012	-	-	-	-	1524.367	221.604	-	-
55	Glu	$m5$	S_f^2,S^2,τ_s	yes	0.791	0.015	0.846	0.012	0.935	0.010	-	-	-	-	902.180	166.434	-	-
56	Tyr	$m5$	S_f^2,S^2,τ_s	yes	0.797	0.017	0.857	0.012	0.930	0.011	-	-	-	-	975.830	153.656	-	-
57	Trp	$m4$	S^2,τ_e,R_{ex}	yes	0.864	0.018	-	-	-	-	11.022	5.169	-	-	-	-	2.691	0.594
59	Asp	$m1$	S^2	yes	0.842	0.011	-	-	-	-	-	-	-	-	-	-	-	-
60	Tyr	$m1$	S^2	yes	0.848	0.012	-	-	-	-	-	-	-	-	-	-	-	-
61	Asn	$m1$	S^2	-	0.898	0.012	-	-	-	-	-	-	-	-	-	-	-	-
62	Gly	$m1$	S^2	-	0.883	0.012	-	-	-	-	-	-	-	-	-	-	-	-

Table 10.3: PSE-4 model-free analysis results (continued)

#	aa	Model	Parameters	Diffusion core ?	S^2	ΔS^2	S_f^2	ΔS_f^2	S_s^2	ΔS_s^2	τ_e ps	$\Delta\tau_e$ ps	τ_f ps	$\Delta\tau_f$ ps	τ_s ps	$\Delta\tau_s$ ps	$^{60.8}R_{ex}$ s^{-1}	$\Delta^{60.8}R_{ex}$ s^{-1}
63	Asn	*m*1	S^2	-	0.910	0.013	-	-	-	-	-	-	-	-	-	-	-	-
64	Gln	*m*1	S^2	-	0.892	0.012	-	-	-	-	-	-	-	-	-	-	-	-
65	Arg	*m*1	S^2	yes	0.826	0.011	-	-	-	-	-	-	-	-	-	-	-	-
66	Phe	*m*1	S^2	yes	0.890	0.013	-	-	-	-	-	-	-	-	-	-	-	-
67	Pro	-	-	yes	-	-	-	-	-	-	-	-	-	-	-	-	-	-
68	Leu	*m*1	S^2	-	0.940	0.020	-	-	-	-	-	-	-	-	-	-	-	-
69	Thr	*m*1	S^2	yes	0.944	0.015	-	-	-	-	-	-	-	-	-	-	-	-
70	**Ser**	**n.o.**	**n.o.**	**yes**	**n.o.**	**n.o.**	**n.o.**	**n.o.**	**n.o.**	**n.o.**	**n.o.**	**n.o.**	**n.o.**	**n.o.**	**n.o.**	**n.o.**	**n.o.**	**n.o.**
71	Thr	*m*1	S^2	yes	0.967	0.013	-	-	-	-	-	-	-	-	-	-	-	-
72	Phe	o.l.	o.l.	yes	o.l.	o.l.	o.l.	o.l.	o.l.	o.l.	o.l.	o.l.	o.l.	o.l.	o.l.	o.l.	o.l.	o.l.
73	**Lys**	*m*1	S^2	**yes**	**0.943**	**0.012**	-	-	-	-	-	-	-	-	-	-	-	-
74	Thr	*m*1	S^2	yes	0.892	0.015	-	-	-	-	-	-	-	-	-	-	-	-
75	Ile	*m*1	S^2	yes	0.922	0.014	-	-	-	-	-	-	-	-	-	-	-	-
76	Ala	*m*3	S^2,R_{ex}	yes	0.881	0.015	-	-	-	-	-	-	-	-	-	-	1.054	0.523
77	Cys	*m*1	S^2	yes	0.867	0.012	-	-	-	-	-	-	-	-	-	-	-	-
78	Ala	*m*3	S^2,R_{ex}	yes	0.894	0.016	-	-	-	-	-	-	-	-	-	-	1.235	0.484
79	Lys	*m*1	S^2	yes	0.905	0.012	-	-	-	-	-	-	-	-	-	-	-	-
80	Leu	o.l.	o.l.	yes	o.l.	o.l.	o.l.	o.l.	o.l.	o.l.	o.l.	o.l.	o.l.	o.l.	o.l.	o.l.	o.l.	o.l.
81	Leu	*m*1	S^2	yes	0.884	0.011	-	-	-	-	-	-	-	-	-	-	-	-
82	Tyr	*m*1	S^2	yes	0.915	0.010	-	-	-	-	-	-	-	-	-	-	-	-
83	Asp	*m*1	S^2	yes	0.905	0.012	-	-	-	-	-	-	-	-	-	-	-	-
84	Ala	*m*1	S^2	yes	0.896	0.013	-	-	-	-	-	-	-	-	-	-	-	-
85	Glu	*m*1	S^2	yes	0.880	0.010	-	-	-	-	-	-	-	-	-	-	-	-
86	Gln	*m*1	S^2	-	0.817	0.010	-	-	-	-	-	-	-	-	-	-	-	-
87	Gly	*m*1	S^2	-	0.852	0.010	-	-	-	-	-	-	-	-	-	-	-	-
88	Lys	*m*2	S^2,τ_e	-	0.878	0.012	-	-	-	-	11.827	4.325	-	-	-	-	-	-
89	Val	*m*2	S^2,τ_e	-	0.794	0.010	-	-	-	-	16.578	2.420	-	-	-	-	-	-
90	Asn	o.l.	o.l.	-	o.l.	o.l.	o.l.	o.l.	o.l.	o.l.	o.l.	o.l.	o.l.	o.l.	o.l.	o.l.	o.l.	o.l.
91	Pro	-	-	-	-	-	-	-	-	-	-	-	-	-	-	-	-	-
92	Asn	*m*1	S^2	-	0.851	0.010	-	-	-	-	-	-	-	-	-	-	-	-
93	Ser	*m*3	S^2,R_{ex}	-	0.841	0.015	-	-	-	-	-	-	-	-	-	-	1.251	0.558
94	Thr	*m*1	S^2	yes	0.847	0.011	-	-	-	-	-	-	-	-	-	-	-	-
95	Val	*m*2	S^2,τ_e	yes	0.859	0.011	-	-	-	-	13.605	4.456	-	-	-	-	-	-
96	Glu	*m*2	S^2,τ_e	yes	0.798	0.010	-	-	-	-	17.800	2.452	-	-	-	-	-	-
97	Ile	*m*2	S^2,τ_e	-	0.805	0.010	-	-	-	-	19.071	2.739	-	-	-	-	-	-
98	Lys	*m*5	S_f^2,S^2,τ_s	-	0.834	0.015	0.856	0.039	0.974	0.033	-	-	-	-	498.332	307.728	-	-
99	Lys	o.l.	o.l.	-	o.l.	o.l.	o.l.	o.l.	o.l.	o.l.	o.l.	o.l.	o.l.	o.l.	o.l.	o.l.	o.l.	o.l.
100	Ala	*m*2	S^2,τ_e	-	0.907	0.012	-	-	-	-	17.027	5.876	-	-	-	-	-	-
101	Asp	*m*2	S^2,τ_e	-	0.831	0.011	-	-	-	-	20.344	3.220	-	-	-	-	-	-
102	Leu	*m*2	S^2,τ_e	-	0.854	0.011	-	-	-	-	14.236	3.606	-	-	-	-	-	-

Table 10.3: PSE-4 model-free analysis results (continued)

#	aa	Model	Parameters	Diffusion core ?	S^2	ΔS^2	S_f^2	ΔS_f^2	S_s^2	ΔS_s^2	τ_e ps	$\Delta\tau_e$ ps	τ_f ps	$\Delta\tau_f$ ps	τ_s ps	$\Delta\tau_s$ ps	$^{60.8}R_{ex}$ s^{-1}	$\Delta^{60.8}R_{ex}$ s^{-1}
103	Val	o.l.	o.l.	-	o.l.	o.l.	o.l.	o.l.	o.l.	o.l.	o.l.	o.l.	o.l.	o.l.	o.l.	o.l.	o.l.	
104	Thr	o.l.	o.l.	-	o.l.	o.l.	o.l.	o.l.	o.l.	o.l.	o.l.	o.l.	o.l.	o.l.	o.l.	o.l.	o.l.	o.l.
105	**Tyr**	*m*5	S_f^2,S^2,τ_s	-	**0.802**	**0.018**	**0.855**	**0.013**	**0.938**	**0.011**	-	-	-	-	**1008.489**	**187.762**	-	-
106	Ser	*m*2	S^2,τ_e	-	0.825	0.013	-	-	-	-	9.508	3.100	-	-	-	-	-	-
107	Pro	-	-	-	-	-	-	-	-	-	-	-	-	-	-	-	-	-
108	Val	*m*2	S^2,τ_e	-	0.899	0.012	-	-	-	-	30.362	7.297	-	-	-	-	-	-
109	Ile	*m*1	S^2	-	0.882	0.015	-	-	-	-	-	-	-	-	-	-	-	-
110	Glu	*m*3	S^2,R_{ex}	-	0.911	0.014	-	-	-	-	-	-	-	-	-	-	1.535	0.523
111	Lys	*m*5	S_f^2,S^2,τ_s	-	0.845	0.014	0.876	0.022	0.965	0.016	-	-	-	-	392.691	170.001	-	-
112	Gln	*m*2	S^2,τ_e	-	0.823	0.012	-	-	-	-	12.455	2.700	-	-	-	-	-	-
113	Val	*m*2	S^2,τ_e	-	0.810	0.010	-	-	-	-	21.316	3.136	-	-	-	-	-	-
114	Gly	*m*2	S^2,τ_e	-	0.892	0.011	-	-	-	-	15.791	5.774	-	-	-	-	-	-
115	Gln	*m*2	S^2,τ_e	-	0.856	0.012	-	-	-	-	16.211	4.024	-	-	-	-	-	-
116	Ala	*m*2	S^2,τ_e	yes	0.756	0.010	-	-	-	-	19.077	1.995	-	-	-	-	-	-
117	Ile	*m*2	S^2,τ_e	yes	0.825	0.011	-	-	-	-	15.916	3.149	-	-	-	-	-	-
118	Thr	*m*1	S^2	yes	0.868	0.012	-	-	-	-	-	-	-	-	-	-	-	-
119	Leu	*m*3	S^2,R_{ex}	yes	0.863	0.016	-	-	-	-	-	-	-	-	-	-	1.434	0.513
120	Asp	*m*3	S^2,R_{ex}	yes	0.873	0.015	-	-	-	-	-	-	-	-	-	-	1.305	0.525
121	Asp	*m*1	S^2	yes	0.894	0.012	-	-	-	-	-	-	-	-	-	-	-	-
122	Ala	*m*1	S^2	yes	0.898	0.012	-	-	-	-	-	-	-	-	-	-	-	-
123	Cys	*m*3	S^2,R_{ex}	yes	0.875	0.014	-	-	-	-	-	-	-	-	-	-	2.014	0.516
124	Phe	*m*1	S^2	yes	0.896	0.014	-	-	-	-	-	-	-	-	-	-	-	-
125	Ala	o.l.	o.l.	yes	o.l.	o.l.	o.l.	o.l.	o.l.	o.l.	o.l.	o.l.	o.l.	o.l.	o.l.	o.l.	o.l.	o.l.
126	Thr	*m*1	S^2	yes	0.925	0.011	-	-	-	-	-	-	-	-	-	-	-	-
127	Met	*m*3	S^2,R_{ex}	yes	0.943	0.018	-	-	-	-	-	-	-	-	-	-	1.970	0.674
128	Thr	*m*3	S^2,R_{ex}	yes	0.917	0.017	-	-	-	-	-	-	-	-	-	-	5.112	0.920
129	Thr	*m*1	S^2	yes	0.924	0.017	-	-	-	-	-	-	-	-	-	-	-	-
130	**Ser**	*m*1	S^2	-	**0.952**	**0.020**	-	-	-	-	-	-	-	-	-	-	-	-
131	Asp	*m*1	S^2	-	0.920	0.012	-	-	-	-	-	-	-	-	-	-	-	-
132	Asn	*m*1	S^2	yes	0.966	0.013	-	-	-	-	-	-	-	-	-	-	-	-
133	Thr	*m*3	S^2,R_{ex}	yes	0.916	0.020	-	-	-	-	-	-	-	-	-	-	1.332	0.597
134	Ala	*m*1	S^2	yes	0.897	0.011	-	-	-	-	-	-	-	-	-	-	-	-
135	Ala	*m*1	S^2	yes	0.886	0.011	-	-	-	-	-	-	-	-	-	-	-	-
136	Asn	*m*3	S^2,R_{ex}	yes	0.885	0.014	-	-	-	-	-	-	-	-	-	-	1.108	0.511
137	Ile	*m*1	S^2	yes	0.896	0.013	-	-	-	-	-	-	-	-	-	-	-	-
138	Ile	*m*3	S^2,R_{ex}	yes	0.884	0.016	-	-	-	-	-	-	-	-	-	-	1.421	0.468
139	Leu	*m*1	S^2	yes	0.905	0.012	-	-	-	-	-	-	-	-	-	-	-	-
140	Ser	*m*1	S^2	yes	0.858	0.012	-	-	-	-	-	-	-	-	-	-	-	-
141	Ala	*m*5	S_f^2,S^2,τ_s	yes	0.814	0.019	0.850	0.014	0.957	0.010	-	-	-	-	1806.494	976.523	-	-
142	Val	*m*1	S^2	-	0.819	0.011	-	-	-	-	-	-	-	-	-	-	-	-

Table 10.3: PSE-4 model-free analysis results (continued)

#	aa	Model	Parameters	Diffusion core ?	S^2	ΔS^2	S_f^2	ΔS_f^2	S_s^2	ΔS_s^2	τ_e ps	$\Delta\tau_e$ ps	τ_f ps	$\Delta\tau_f$ ps	τ_s ps	$\Delta\tau_s$ ps	$^{60.8}R_{ex}$ s^{-1}	$\Delta^{60.8}R_{ex}$ s^{-1}
143	Gly	*m*1	S^2	-	0.907	0.012	-	-	-	-	-	-	-	-	-	-	-	-
144	Gly	*m*1	S^2	yes	0.902	0.012	-	-	-	-	-	-	-	-	-	-	-	-
145	Pro	-	-	yes	-	-	-	-	-	-	-	-	-	-	-	-	-	-
146	Lys	o.l.	o.l.	yes	o.l.	o.l.	o.l.	o.l.	o.l.	o.l.	o.l.	o.l.	o.l.	o.l.	o.l.	o.l.	o.l.	o.l.
147	Gly	*m*1	S^2	yes	0.897	0.012	-	-	-	-	-	-	-	-	-	-	-	-
148	Val	*m*3	S^2,R_{ex}	yes	0.872	0.014	-	-	-	-	-	-	-	-	-	-	1.462	0.709
149	Thr	*m*2	S^2,τ_e	yes	0.907	0.011	-	-	-	-	20.010	7.396	-	-	-	-	-	-
150	Asp	*m*1	S^2	yes	0.920	0.012	-	-	-	-	-	-	-	-	-	-	-	-
151	Phe	*m*1	S^2	yes	0.906	0.011	-	-	-	-	-	-	-	-	-	-	-	-
152	Leu	*m*3	S^2,R_{ex}	yes	0.900	0.017	-	-	-	-	-	-	-	-	-	-	1.336	0.634
153	Arg	*m*3	S^2,R_{ex}	yes	0.907	0.015	-	-	-	-	-	-	-	-	-	-	1.517	0.559
154	Gln	*m*1	S^2	yes	0.889	0.012	-	-	-	-	-	-	-	-	-	-	-	-
155	Ile	*m*5	S_f^2,S^2,τ_s	-	0.722	0.024	0.812	0.017	0.888	0.014	-	-	-	-	654.180	96.647	-	-
156	Gly	*m*1	S^2	-	0.887	0.012	-	-	-	-	-	-	-	-	-	-	-	-
157	Asp	*m*1	S^2	-	0.884	0.013	-	-	-	-	-	-	-	-	-	-	-	-
158	Lys	*m*1	S^2	-	0.845	0.013	-	-	-	-	-	-	-	-	-	-	-	-
159	Glu	o.l.	o.l.	-	o.l.	o.l.	o.l.	o.l.	o.l.	o.l.	o.l.	o.l.	o.l.	o.l.	o.l.	o.l.	o.l.	o.l.
160	Thr	*m*1	S^2	-	0.842	0.011	-	-	-	-	-	-	-	-	-	-	-	-
161	Arg	*m*3	S^2,R_{ex}	-	0.909	0.016	-	-	-	-	-	-	-	-	-	-	1.318	0.529
162	Leu	*m*1	S^2	-	0.902	0.013	-	-	-	-	-	-	-	-	-	-	-	-
163	Asp	*m*1	S^2	-	0.859	0.019	-	-	-	-	-	-	-	-	-	-	-	-
164	Arg	*m*2	S^2,τ_e	-	0.822	0.014	-	-	-	-	7.048	2.900	-	-	-	-	-	-
165	Ile	*m*1	S^2	-	0.817	0.013	-	-	-	-	-	-	-	-	-	-	-	-
166	**Glu**	*m*1	S^2	-	**0.906**	**0.015**	-	-	-	-	-	-	-	-	-	-	-	-
167	Pro	-	-	-	-	-	-	-	-	-	-	-	-	-	-	-	-	-
168	Asp	o.l.	o.l.	-	o.l.	o.l.	o.l.	o.l.	o.l.	o.l.	o.l.	o.l.	o.l.	o.l.	o.l.	o.l.	o.l.	o.l.
169	Leu	*m*1	S^2	-	0.925	0.014	-	-	-	-	-	-	-	-	-	-	-	-
170	Asn	o.l.	o.l.	-	o.l.	o.l.	o.l.	o.l.	o.l.	o.l.	o.l.	o.l.	o.l.	o.l.	o.l.	o.l.	o.l.	o.l.
171	Glu	*m*1	S^2	-	0.912	0.011	-	-	-	-	-	-	-	-	-	-	-	-
172	Gly	*m*1	S^2	-	0.874	0.014	-	-	-	-	-	-	-	-	-	-	-	-
173	Lys	o.l.	o.l.	-	o.l.	o.l.	o.l.	o.l.	o.l.	o.l.	o.l.	o.l.	o.l.	o.l.	o.l.	o.l.	o.l.	o.l.
174	Leu	o.l.	o.l.	-	o.l.	o.l.	o.l.	o.l.	o.l.	o.l.	o.l.	o.l.	o.l.	o.l.	o.l.	o.l.	o.l.	o.l.
175	Gly	*m*1	S^2	-	0.927	0.031	-	-	-	-	-	-	-	-	-	-	-	-
176	Asp	*m*1	S^2	-	0.883	0.012	-	-	-	-	-	-	-	-	-	-	-	-
177	Leu	*m*2	S^2,τ_e	-	0.854	0.014	-	-	-	-	10.618	4.523	-	-	-	-	-	-
178	Arg	*m*3	S^2,R_{ex}	-	0.918	0.017	-	-	-	-	-	-	-	-	-	-	1.088	0.594
179	Asp	*m*1	S^2	-	0.878	0.013	-	-	-	-	-	-	-	-	-	-	-	-
180	Thr	*m*1	S^2	yes	0.867	0.012	-	-	-	-	-	-	-	-	-	-	-	-
181	Thr	*m*1	S^2	yes	0.889	0.012	-	-	-	-	-	-	-	-	-	-	-	-
182	Thr	*m*1	S^2	yes	0.858	0.012	-	-	-	-	-	-	-	-	-	-	-	-

Table 10.3: PSE-4 model-free analysis results (continued)

#	aa	Model	Parameters	Diffusion core ?	S^2	ΔS^2	S_f^2	ΔS_f^2	S_s^2	ΔS_s^2	τ_e ps	$\Delta\tau_e$ ps	τ_f ps	$\Delta\tau_f$ ps	τ_s ps	$\Delta\tau_s$ ps	$^{60.8}R_{ex}$ s^{-1}	$\Delta^{60.8}R_{ex}$ s^{-1}
183	Pro	-	-	yes	-	-	-	-	-	-	-	-	-	-	-	-	-	-
184	Lys	o.l.	o.l.	yes	o.l.	o.l.	o.l.	o.l.	o.l.	o.l.	o.l.	o.l.	o.l.	o.l.	o.l.	o.l.	o.l.	o.l.
185	Ala	o.l.	o.l.	yes	o.l.	o.l.	o.l.	o.l.	o.l.	o.l.	o.l.	o.l.	o.l.	o.l.	o.l.	o.l.	o.l.	o.l.
186	Ile	*m*1	S^2	yes	0.885	0.015	-	-	-	-	-	-	-	-	-	-	-	-
187	Ala	*m*1	S^2	yes	0.930	0.012	-	-	-	-	-	-	-	-	-	-	-	-
188	Ser	o.l.	o.l.	yes	o.l.	o.l.	o.l.	o.l.	o.l.	o.l.	o.l.	o.l.	o.l.	o.l.	o.l.	o.l.	o.l.	o.l.
189	Thr	o.l.	o.l.	yes	o.l.	o.l.	o.l.	o.l.	o.l.	o.l.	o.l.	o.l.	o.l.	o.l.	o.l.	o.l.	o.l.	o.l.
190	Leu	*m*1	S^2	yes	0.929	0.012	-	-	-	-	-	-	-	-	-	-	-	-
191	Asn	*m*1	S^2	yes	0.895	0.016	-	-	-	-	-	-	-	-	-	-	-	-
192	Lys	*m*1	S^2	yes	0.892	0.017	-	-	-	-	-	-	-	-	-	-	-	-
193	Phe	*m*1	S^2	yes	0.862	0.012	-	-	-	-	-	-	-	-	-	-	-	-
194	Leu	*m*1	S^2	yes	0.884	0.012	-	-	-	-	-	-	-	-	-	-	-	-
195	Phe	*m*1	S^2	yes	0.853	0.014	-	-	-	-	-	-	-	-	-	-	-	-
196	Gly	*m*5	S_f^2,S^2,τ_s	-	0.732	0.017	0.774	0.012	0.946	0.011	-	-	-	-	1065.649	254.605	-	-
197	Ser	*m*2	S^2,τ_e	-	0.798	0.025	-	-	-	-	18.865	5.836	-	-	-	-	-	-
198	Ala	*m*5	S_f^2,S^2,τ_s	-	0.800	0.017	0.872	0.013	0.918	0.011	-	-	-	-	898.306	130.471	-	-
199	Leu	*m*2	S^2,τ_e	-	0.838	0.011	-	-	-	-	6.647	3.053	-	-	-	-	-	-
200	Ser	*m*2	S^2,τ_e	-	0.821	0.011	-	-	-	-	7.860	3.290	-	-	-	-	-	-
201	Glu	*m*1	S^2	yes	0.868	0.012	-	-	-	-	-	-	-	-	-	-	-	-
202	Met	*m*2	S^2,τ_e	yes	0.870	0.011	-	-	-	-	13.715	4.465	-	-	-	-	-	-
203	Asn	*m*1	S^2	yes	0.889	0.011	-	-	-	-	-	-	-	-	-	-	-	-
204	Gln	o.l.	o.l.	yes	o.l.	o.l.	o.l.	o.l.	o.l.	o.l.	o.l.	o.l.	o.l.	o.l.	o.l.	o.l.	o.l.	o.l.
205	Lys	*m*1	S^2	yes	0.869	0.011	-	-	-	-	-	-	-	-	-	-	-	-
206	Lys	*m*1	S^2	yes	0.871	0.012	-	-	-	-	-	-	-	-	-	-	-	-
207	Leu	*m*3	S^2,R_{ex}	yes	0.888	0.016	-	-	-	-	-	-	-	-	-	-	1.017	0.512
208	Glu	*m*1	S^2	yes	0.901	0.013	-	-	-	-	-	-	-	-	-	-	-	-
209	Ser	*m*1	S^2	yes	0.884	0.011	-	-	-	-	-	-	-	-	-	-	-	-
210	Trp	*m*1	S^2	yes	0.900	0.011	-	-	-	-	-	-	-	-	-	-	-	-
211	Met	o.l.	o.l.	yes	o.l.	o.l.	o.l.	o.l.	o.l.	o.l.	o.l.	o.l.	o.l.	o.l.	o.l.	o.l.	o.l.	o.l.
212	Val	*m*1	S^2	yes	0.952	0.014	-	-	-	-	-	-	-	-	-	-	-	-
213	Asn	*m*1	S^2	-	0.894	0.013	-	-	-	-	-	-	-	-	-	-	-	-
214	Asn	*m*2	S^2,τ_e	-	0.851	0.010	-	-	-	-	7.839	3.414	-	-	-	-	-	-
215	Gln	*m*1	S^2	-	0.895	0.015	-	-	-	-	-	-	-	-	-	-	-	-
216	Val	*m*2	S^2,τ_e	-	0.904	0.011	-	-	-	-	16.096	6.297	-	-	-	-	-	-
217	Thr	*m*2	S^2,τ_e	-	0.918	0.012	-	-	-	-	25.549	8.683	-	-	-	-	-	-
218	Gly	*m*0	-	-	-	-	-	-	-	-	-	-	-	-	-	-	-	-
219	Asn	*m*1	S^2	-	0.896	0.016	-	-	-	-	-	-	-	-	-	-	-	-
220	Leu	*m*3	S^2,R_{ex}	-	0.866	0.014	-	-	-	-	-	-	-	-	-	-	1.336	0.520
221	Leu	*m*3	S^2,R_{ex}	-	0.855	0.028	-	-	-	-	-	-	-	-	-	-	4.163	1.176
222	Arg	*m*1	S^2	-	0.923	0.020	-	-	-	-	-	-	-	-	-	-	-	-

Table 10.3: PSE-4 model-free analysis results (continued)

#	aa	Model	Parameters	Diffusion core ?	S^2	ΔS^2	S_f^2	ΔS_f^2	S_s^2	ΔS_s^2	τ_e ps	$\Delta\tau_e$ ps	τ_f ps	$\Delta\tau_f$ ps	τ_s ps	$\Delta\tau_s$ ps	$^{60.8}R_{ex}$ s^{-1}	$\Delta^{60.8}R_{ex}$ s^{-1}
223	Ser	*m*1	S^2	-	0.907	0.014	-	-	-	-	-	-	-	-	-	-	-	-
224	Val	*m*1	S^2	-	0.885	0.012	-	-	-	-	-	-	-	-	-	-	-	-
225	Leu	*m*1	S^2	-	0.814	0.010	-	-	-	-	-	-	-	-	-	-	-	-
226	Pro	-	-	-	-	-	-	-	-	-	-	-	-	-	-	-	-	-
227	Ala	*m*2	S^2,τ_e	-	0.814	0.012	-	-	-	-	6.241	2.638	-	-	-	-	-	-
228	Gly	*m*2	S^2,τ_e	-	0.777	0.015	-	-	-	-	12.801	2.424	-	-	-	-	-	-
229	Trp	*m*2	S^2,τ_e	-	0.852	0.011	-	-	-	-	11.011	4.232	-	-	-	-	-	-
230	Asn	*m*4	S^2,τ_e,R_{ex}	yes	0.817	0.015	-	-	-	-	8.872	2.953	-	-	-	-	1.577	0.496
231	Ile	*m*1	S^2	yes	0.846	0.011	-	-	-	-	-	-	-	-	-	-	-	-
232	Ala	*m*1	S^2	yes	0.859	0.016	-	-	-	-	-	-	-	-	-	-	-	-
233	Asp	*m*3	S^2,R_{ex}	yes	0.858	0.016	-	-	-	-	-	-	-	-	-	-	1.194	0.485
234	**Arg**	*m*3	S^2,R_{ex}	**yes**	**0.881**	**0.023**	-	-	-	-	-	-	-	-	-	-	**4.244**	**1.568**
235	Ser	*m*9	R_{ex}	yes	-	-	-	-	-	-	-	-	-	-	-	-	4.529	1.951
236	Gly	*m*3	S^2,R_{ex}	yes	0.882	0.022	-	-	-	-	-	-	-	-	-	-	2.901	0.818
237	Ala	n.o.	n.o.	yes	n.o.	n.o.	n.o.	n.o.	n.o.	n.o.	n.o.	n.o.	n.o.	n.o.	n.o.	n.o.	n.o.	n.o.
238	Gly	*m*2	S^2,τ_e	-	0.848	0.011	-	-	-	-	14.654	3.426	-	-	-	-	-	-
240	Gly	*m*1	S^2	-	0.914	0.012	-	-	-	-	-	-	-	-	-	-	-	-
241	Phe	*m*1	S^2	-	0.922	0.013	-	-	-	-	-	-	-	-	-	-	-	-
242	Gly	*m*1	S^2	-	0.928	0.013	-	-	-	-	-	-	-	-	-	-	-	-
243	Ala	*m*1	S^2	-	0.934	0.013	-	-	-	-	-	-	-	-	-	-	-	-
244	Arg	*m*3	S^2,R_{ex}	yes	0.888	0.016	-	-	-	-	-	-	-	-	-	-	2.440	0.706
245	Ser	o.l.	o.l.	yes	o.l.	o.l.	o.l.	o.l.	o.l.	o.l.	o.l.	o.l.	o.l.	o.l.	o.l.	o.l.	o.l.	o.l.
246	Ile	*m*1	S^2	yes	0.906	0.013	-	-	-	-	-	-	-	-	-	-	-	-
247	Thr	*m*1	S^2	yes	0.909	0.015	-	-	-	-	-	-	-	-	-	-	-	-
248	Ala	*m*1	S^2	yes	0.854	0.012	-	-	-	-	-	-	-	-	-	-	-	-
249	Val	*m*1	S^2	yes	0.835	0.010	-	-	-	-	-	-	-	-	-	-	-	-
250	Val	*m*1	S^2	yes	0.914	0.011	-	-	-	-	-	-	-	-	-	-	-	-
251	Trp	o.l.	o.l.	yes	o.l.	o.l.	o.l.	o.l.	o.l.	o.l.	o.l.	o.l.	o.l.	o.l.	o.l.	o.l.	o.l.	o.l.
252	Ser	*m*1	S^2	yes	0.874	0.012	-	-	-	-	-	-	-	-	-	-	-	-
254	Glu	*m*2	S^2,τ_e	-	0.864	0.015	-	-	-	-	34.480	5.795	-	-	-	-	-	-
255	His	*m*5	S_f^2,S^2,τ_s	-	0.747	0.020	0.796	0.029	0.938	0.022	-	-	-	-	495.106	180.752	-	-
256	Gln	*m*5	S_f^2,S^2,τ_s	-	0.707	0.015	0.765	0.011	0.924	0.010	-	-	-	-	766.669	114.559	-	-
257	Ala	*m*2	S^2,τ_e	-	0.862	0.012	-	-	-	-	14.766	4.017	-	-	-	-	-	-
258	Pro	-	-	-	-	-	-	-	-	-	-	-	-	-	-	-	-	-
259	Ile	*m*1	S^2	yes	0.878	0.012	-	-	-	-	-	-	-	-	-	-	-	-
260	Ile	*m*1	S^2	yes	0.852	0.012	-	-	-	-	-	-	-	-	-	-	-	-
261	Val	*m*1	S^2	yes	0.850	0.011	-	-	-	-	-	-	-	-	-	-	-	-
262	Ser	*m*1	S^2	yes	0.875	0.012	-	-	-	-	-	-	-	-	-	-	-	-
263	Ile	*m*1	S^2	yes	0.874	0.013	-	-	-	-	-	-	-	-	-	-	-	-
264	Tyr	*m*1	S^2	yes	0.848	0.013	-	-	-	-	-	-	-	-	-	-	-	-

Table 10.3: PSE-4 model-free analysis results (continued)

#	aa	Model	Parameters	Diffusion core ?	S^2	ΔS^2	S_f^2	ΔS_f^2	S_s^2	ΔS_s^2	τ_e ps	$\Delta\tau_e$ ps	τ_f ps	$\Delta\tau_f$ ps	τ_s ps	$\Delta\tau_s$ ps	$^{60.8}R_{ex}$ s^{-1}	$\Delta^{60.8}R_{ex}$ s^{-1}
265	Leu	*m*4	S^2,τ_e,R_{ex}	yes	0.846	0.016	-	-	-	-	11.828	3.379	-	-	-	-	1.513	0.524
266	Ala	*m*2	S^2,τ_e	yes	0.847	0.011	-	-	-	-	9.686	3.503	-	-	-	-	-	-
267	Gln	*m*1	S^2	-	0.861	0.012	-	-	-	-	-	-	-	-	-	-	-	-
268	Thr	*m*2	S^2,τ_e	-	0.849	0.012	-	-	-	-	8.957	3.626	-	-	-	-	-	-
269	Gln	*m*1	S^2	-	0.877	0.015	-	-	-	-	-	-	-	-	-	-	-	-
270	Ala	o.l.	o.l.	-	o.l.	o.l.	o.l.	o.l.	o.l.	o.l.	o.l.	o.l.	o.l.	o.l.	o.l.	o.l.	o.l.	o.l.
271	Ser	*m*2	S^2,τ_e	-	0.866	0.013	-	-	-	-	7.956	4.062	-	-	-	-	-	-
272	Met	*m*1	S^2	yes	0.859	0.047	-	-	-	-	-	-	-	-	-	-	-	-
273	Glu	*m*1	S^2	yes	0.895	0.011	-	-	-	-	-	-	-	-	-	-	-	-
274	Glu	*m*1	S^2	yes	0.880	0.011	-	-	-	-	-	-	-	-	-	-	-	-
275	Arg	*m*2	S^2,τ_e	yes	0.906	0.013	-	-	-	-	21.302	6.038	-	-	-	-	-	-
276	Asn	*m*3	S^2,R_{ex}	yes	0.867	0.015	-	-	-	-	-	-	-	-	-	-	1.585	0.508
277	Asp	o.l.	o.l.	yes	o.l.	o.l.	o.l.	o.l.	o.l.	o.l.	o.l.	o.l.	o.l.	o.l.	o.l.	o.l.	o.l.	o.l.
278	Ala	*m*1	S^2	yes	0.891	0.011	-	-	-	-	-	-	-	-	-	-	-	-
279	Ile	*m*1	S^2	yes	0.856	0.011	-	-	-	-	-	-	-	-	-	-	-	-
280	Val	*m*1	S^2	yes	0.898	0.011	-	-	-	-	-	-	-	-	-	-	-	-
281	Lys	*m*3	S^2,R_{ex}	yes	0.898	0.015	-	-	-	-	-	-	-	-	-	-	1.127	0.563
282	Ile	o.l.	o.l.	yes	o.l.	o.l.	o.l.	o.l.	o.l.	o.l.	o.l.	o.l.	o.l.	o.l.	o.l.	o.l.	o.l.	o.l.
283	Gly	*m*1	S^2	yes	0.900	0.011	-	-	-	-	-	-	-	-	-	-	-	-
284	His	*m*1	S^2	yes	0.903	0.013	-	-	-	-	-	-	-	-	-	-	-	-
285	Ser	*m*1	S^2	yes	0.875	0.011	-	-	-	-	-	-	-	-	-	-	-	-
286	Ile	*m*3	S^2,R_{ex}	yes	0.882	0.020	-	-	-	-	-	-	-	-	-	-	1.254	0.640
287	Phe	o.l.	o.l.	yes	o.l.	o.l.	o.l.	o.l.	o.l.	o.l.	o.l.	o.l.	o.l.	o.l.	o.l.	o.l.	o.l.	o.l.
288	Asp	*m*1	S^2	yes	0.921	0.011	-	-	-	-	-	-	-	-	-	-	-	-
289	Val	*m*2	S^2,τ_e	yes	0.886	0.011	-	-	-	-	10.056	4.798	-	-	-	-	-	-
290	Tyr	*m*1	S^2	yes	0.860	0.012	-	-	-	-	-	-	-	-	-	-	-	-
291	Thr	*m*5	S_f^2,S^2,τ_s	yes	0.729	0.015	0.810	0.011	0.899	0.010	-	-	-	-	1008.582	111.115	-	-
292	Ser	*m*6	S_f^2,τ_f,S^2,τ_s	-	0.524	0.013	0.761	0.013	0.688	0.013	-	-	35.875	5.380	1911.024	169.023	-	-
293	Gln	*tm*5	τ_m,S_f^2,S^2,τ_s	-	0.494	0.013	0.828	0.015	0.596	0.011	-	-	-	-	727.014	30.186	-	-
294	Ser	*tm*6	τ_m,S_f^2,τ_f,S^2,τ_s	-	0.119	0.049	0.539	0.036	0.220	0.075	-	-	73.828	5.213	1460.971	126.183	-	-
295	Arg	*tm*5	τ_m,S_f^2,S^2,τ_s	-	0.201	0.005	0.611	0.010	0.329	0.006	-	-	-	-	315.594	12.998	-	-

- Exact magnetic fields (reported here as nitrogen Larmour frequencies) were as follows: 50.641893 (50.6), 60.777824 (60.8), and 81.046603 (81.0) MHz.
- Values presented here are rounded to three decimals. Exact values can be obtained from the BMRB (accession number 6838).
- R_{ex} parameters are calculated for a magnetic field of 60.8 MHz.
- The diffusion tensor associated with these local model-free parameters is an ellipsoid with the following characteristics [47]:

  - Correlation time: τ_m = 12.683 ($\pm$ 0.024) ns;
  - Anisotropy: $\mathfrak{D}_a = \mathfrak{D}_z - (\mathfrak{D}_x + \mathfrak{D}_y)/2$ = 3.75 ($\pm$ 0.19) x 10^6 s^{-1};
  - Asymmetry (or rhombicity): $\mathfrak{D}_r = (\mathfrak{D}_y - \mathfrak{D}_x)/(2\mathfrak{D}_a)$ = 0.080 ($\pm$ 0.022) s^{-1};
  - Isotropic component of diffusion: $\mathfrak{D}_{iso} = 1/(6\tau_m) = (\mathfrak{D}_x + \mathfrak{D}_y + \mathfrak{D}_z)/3$ = 13.1 ($\pm$ 2.4) x 10^6 s^{-1};
  - Diffusion constants for the three principal diffusion axes: $\mathfrak{D}_x$ = 11.59 ($\pm$ 0.10) x $10^6 s^{-1}$, $\mathfrak{D}_y$ = 12.19 ($\pm$ 0.11) x 10^6 s^{-1}, $\mathfrak{D}_z$ = 15.64 ($\pm$ 0.13) x 10^6 s^{-1};
  - Orientations (relative to PDB 1G68 [165]): $\theta = 166.2\ (\pm\ 8.4)^\circ$, $\phi = 146.8\ (\pm\ 1.1)^\circ$, and $\psi = 131.6\ (\pm\ 2.6)^\circ$.

- This diffusion tensor was minimised using residues in secondary structures (*i.e.* with 'Diffusion core $\rightarrow$ yes', *N*=134). Other residues (*N*=96) were excluded from diffusion tensor optimisation.
- Local model-free models were selected using *AICc* as well as with manual modifications for residues Gly^{175}, Leu^{199}, Glu^{201}, Arg^{234}, and Thr^{291}.
- Residues Gln^{293}, Ser^{294}, and Arg^{295} from the C-terminus, absent from the crystal structure, were fitted using a local τ_m parameter: 7.49 ($\pm$ 0.22) ns, 12.22 ($\pm$ 6.44) ns, and 3.58 ($\pm$ 0.19) ns, respectively.
- Important active site residues (Ser^{70}, Lys^{73}, Tyr^{105}, Ser^{130}, Glu^{166}, and Arg^{234}) are shown in bold red while residues from the Ω loop (residues 161–179) are coloured blue.
- n-ter: N-terminus amine (not observable).
- n.o.: non-observed N-H resonances (not assigned).
- o.l.: overlapped N-H resonances.

Appendix 4:
PSE-4 Amide Exchange Data

Table 10.4: PSE-4 amide exchange data

Residue		**EX2 ?**	*pH* **7.85**		*pH* **6.65**					
#	**aa**		k_{HX}	Δk_{HX}	k_{HX}	Δk_{HX}	k_{int}	*logSF*	K_{op}	ΔG_{HX}
			(s^{-1})	**(s^{-1})**	**(s^{-1})**	**(s^{-1})**	**(s^{-1})**			**(kcal mol^{-1})**
22	Ser	—	n-ter.	n-ter.	n-ter.	n-ter.	n-ter	—	—	—
23	Ser	—	n.o.	n.o.	n.o.	n.o.	4.4e+2	—	—	—
24	Ser	—	n.o.	n.o.	n.o.	n.o.	1.1e+1	—	—	—
25	Lys	—	o.l.	o.l.	>1e-3	>1e-3	8.4e-1	—	—	—
26	Phe	—	>1e-3	>1e-3	>1e-3	>1e-3	2.3e+0	—	—	—
27	Gln	—	>1e-3	>1e-3	>1e-3	>1e-3	5.6e+0	—	—	—
28	Gln	—	o.l.	o.l.	>1e-3	>1e-3	2.3e+0	—	—	—
29	Val	—	>1e-3	>1e-3	>1e-3	>1e-3	2.0e+0	—	—	—
30	Glu	EX2	1.8e-4	3.0e-5	1.7e-5	3.8e-7	1.3e+1	5.9	1.4e-6	8.2
31	Gln	—	o.l.	o.l.	o.l.	o.l.	6.6e+0	—	—	—
32	Asp	EX2	5.9e-4	9.3e-5	4.2e-5	6.6e-7	8.1e+0	5.3	5.2e-6	7.4
33	Val	EX2	1.1e-5	4.8e-7	1.3e-6	7.6e-8	5.6e+0	6.6	2.4e-7	9.2
34	Lys	EX2	2.3e-5	7.8e-7	2.8e-6	7.9e-8	6.7e-1	5.4	4.2e-6	7.5
35	Ala	EX2	5.1e-4	2.2e-4	4.8e-5	1.0e-6	1.3e+0	4.4	3.6e-5	6.2
36	Ile	EX2	3.5e-5	1.7e-6	2.8e-6	1.1e-7	4.2e-1	5.2	6.7e-6	7.2
37	Glu	—	o.l.	o.l.	o.l.	o.l.	4.8e+0	—	—	—
38	Val	—	o.l.	o.l.	3.6e-5	8.2e-7	5.6e+0	5.2	6.4e-6	7.2
39	Ser	—	>1e-3	>1e-3	>1e-3	>1e-3	8.5e+0	—	—	—
40	Leu	—	o.l.	o.l.	o.l.	o.l.	1.2e+0	—	—	—
41	Ser	—	>1e-3	>1e-3	>1e-3	>1e-3	3.3e+0	—	—	—
42	Ala	—	o.l.	o.l.	1.3e-4	2.5e-6	4.5e+0	4.6	2.8e-5	6.4
43	Arg	EX2	4.8e-4	1.3e-4	3.2e-5	9.0e-7	2.7e+0	4.9	1.2e-5	6.9
44	Ile	EX2	2.9e-4	3.8e-5	1.6e-5	5.3e-7	7.0e-1	4.6	2.3e-5	6.5
45	Gly	—	o.l.	o.l.	1.6e-6	7.5e-8	2.3e+0	6.2	7.1e-7	8.6
46	Val	EX2	7.7e-6	7.0e-7	1.2e-6	5.1e-8	4.8e+0	6.6	2.4e-7	9.2
47	Ser	EX2	7.1e-6	5.0e-7	1.9e-6	5.6e-8	8.5e+0	6.6	2.3e-7	9.3
48	Val	EX2	6.8e-6	5.7e-7	1.4e-6	5.7e-8	3.9e+0	6.5	3.5e-7	9.0
49	Leu	EX2	6.6e-6	6.8e-7	9.7e-7	3.5e-8	9.6e-1	6.0	1.0e-6	8.4
50	Asp	—	o.l.	o.l.	2.6e-5	8.1e-7	5.0e+0	5.3	5.3e-6	7.4
51	Thr	—	o.l.	o.l.	o.l.	o.l.	5.6e+0	—	—	—
52	Gln	—	>1e-3	>1e-3	>1e-3	>1e-3	3.6e+0	—	—	—
53	Asn	—	>1e-3	>1e-3	>1e-3	>1e-3	2.3e+0	—	—	—
54	Gly	—	>1e-3	>1e-3	>1e-3	>1e-3	4.0e+0	—	—	—
55	Glu	—	>1e-3	>1e-3	>1e-3	>1e-3	2.0e+1	—	—	—
56	Tyr	—	o.l.	o.l.	>1e-3	>1e-3	3.5e+0	—	—	—
57	Trp	EX2	6.1e-4	2.8e-4	3.9e-5	1.4e-6	9.9e-1	4.4	3.9e-5	6.1
59	Asp	EX2	>1e-3	>1e-3	1.7e-3	3.7e-4	6.3e+0	3.6	2.8e-4	5.0
60	Tyr	EX2	8.6e-6	7.6e-7	1.6e-6	6.4e-8	3.5e+0	6.3	4.7e-7	8.8
61	Asn	—	>1e-3	>1e-3	>1e-3	>1e-3	2.6e+0	—	—	—
62	Gly	—	>1e-3	>1e-3	2.5e-4	8.6e-5	4.0e+0	4.2	6.3e-5	5.9
63	Asn	—	>1e-3	>1e-3	>1e-3	>1e-3	5.6e+0	—	—	—
64	Gln	EX2	>1e-3	>1e-3	9.5e-5	2.8e-6	2.3e+0	4.4	4.2e-5	6.1
65	Arg	—	>1e-3	>1e-3	>1e-3	>1e-3	2.7e+0	—	—	—
66	Phe	EX2	3.3e-4	1.4e-4	2.4e-5	1.7e-6	6.6e+0	5.4	3.7e-6	7.6
67	Pro	—	—	—	—	—	—	—	—	—
68	Leu	EX2	>1e-3	>1e-3	3.3e-5	3.3e-6	6.0e-1	4.3	5.5e-5	5.9
69	Thr	—	>1e-3	>1e-3	>1e-3	>1e-3	1.2e+0	—	—	—

Table 10.4: PSE-4 amide exchange data (continued)

Residue		**EX2 ?**	*pH* **7.85**		*pH* **6.65**					
#	**aa**		k_{HX}	Δk_{HX}	k_{HX}	Δk_{HX}	k_{int}	*logSF*	K_{op}	ΔG_{HX}
			(s^{-1})	**(s^{-1})**	**(s^{-1})**	**(s^{-1})**	**(s^{-1})**			**(kcal mol^{-1})**
70	**Ser**	**—**	**n.o.**	**n.o.**	**n.o.**	**n.o.**	**8.5e+0**	**—**	**—**	**—**
71	Thr	—	>1e-3	>1e-3	>1e-3	>1e-3	3.9e+0	—	—	—
72	Phe	—	o.l.	o.l.	o.l.	o.l.	6.3e+0	—	—	—
73	**Lys**	**—**	**>1e-3**	**>1e-3**	**5.2e-4**	**7.3e-5**	**1.0e+0**	**3.3**	**5.0e-4**	**4.6**
74	Thr	EX2	>1e-3	>1e-3	1.0e-3	5.7e-4	1.2e+0	3.0	9.0e-4	4.2
75	Ile	EX2	2.9e-4	7.5e-5	2.1e-5	9.9e-7	6.7e-1	4.5	3.1e-5	6.3
76	Ala	EX2	1.2e-4	9.2e-6	9.1e-6	5.4e-7	1.3e+0	5.2	6.8e-6	7.2
77	Cys	EX2	1.3e-4	3.4e-5	1.3e-5	5.0e-7	8.1e+0	5.8	1.6e-6	8.1
78	Ala	EX2	1.3e-4	2.0e-5	1.0e-5	2.1e-7	6.6e+0	5.8	1.6e-6	8.1
79	Lys	EX2	9.1e-5	6.9e-6	9.8e-6	3.3e-7	4.2e-1	4.6	2.3e-5	6.5
80	Leu	—	o.l.	o.l.	o.l.	o.l.	3.6e-1	—	—	—
81	Leu	EX2	4.4e-5	4.3e-6	5.6e-6	3.4e-7	3.7e-1	4.8	1.5e-5	6.7
82	Tyr	EX2	6.3e-5	6.1e-6	7.0e-6	4.1e-7	7.5e-1	5.0	9.3e-6	7.0
83	Asp	EX2	1.2e-4	4.7e-5	1.3e-5	5.6e-7	9.1e+0	5.9	1.4e-6	8.2
84	Ala	EX2	1.8e-4	3.1e-5	1.3e-5	5.1e-7	6.6e+0	5.7	2.0e-6	8.0
85	Glu	EX2	>1e-3	>1e-3	6.7e-5	2.1e-6	8.1e+0	5.1	8.3e-6	7.1
86	Gln	—	o.l.	o.l.	>1e-3	>1e-3	6.6e+0	—	—	—
87	Gly	—	>1e-3	>1e-3	>1e-3	>1e-3	4.0e+0	—	—	—
88	Lys	—	>1e-3	>1e-3	>1e-3	>1e-3	1.0e+0	—	—	—
89	Val	EX2	>1e-3	>1e-3	5.9e-4	4.2e-5	1.2e+0	3.3	5.1e-4	4.6
90	Asn	—	o.l.	o.l.	o.l.	o.l.	3.6e+0	—	—	—
91	Pro	—	—	—	—	—	—	—	—	—
92	Asn	—	>1e-3	>1e-3	>1e-3	>1e-3	2.3e+0	—	—	—
93	Ser	—	>1e-3	>1e-3	>1e-3	>1e-3	5.3e+0	—	—	—
94	Thr	—	>1e-3	>1e-3	>1e-3	>1e-3	3.9e+0	—	—	—
95	Val	EX2	>1e-3	>1e-3	3.4e-4	3.5e-5	3.1e+0	4.0	1.1e-4	5.5
96	Glu	—	>1e-3	>1e-3	o.l.	o.l.	1.3e+1	—	—	—
97	Ile	—	>1e-3	>1e-3	>1e-3	>1e-3	1.2e+0	—	—	—
98	Lys	—	>1e-3	>1e-3	>1e-3	>1e-3	2.5e-1	—	—	—
99	Lys	—	o.l.	o.l.	o.l.	o.l.	2.5e-1	—	—	—
100	Ala	—	>1e-3	>1e-3	>1e-3	>1e-3	1.3e+0	—	—	—
101	Asp	—	>1e-3	>1e-3	>1e-3	>1e-3	8.1e+0	—	—	—
102	Leu	—	>1e-3	>1e-3	>1e-3	>1e-3	1.7e+0	—	—	—
103	Val	—	o.l.	o.l.	>1e-3	>1e-3	1.2e+0	—	—	—
104	Thr	—	o.l.	o.l.	o.l.	o.l.	3.1e+0	—	—	—
105	**Tyr**	**—**	**>1e-3**	**>1e-3**	**>1e-3**	**>1e-3**	**1.9e+0**	**—**	**—**	**—**
106	Ser	—	>1e-3	>1e-3	>1e-3	>1e-3	6.0e+0	—	—	—
107	Pro	—	—	—	—	—	—	—	—	—
108	Val	—	>1e-3	>1e-3	>1e-3	>1e-3	2.0e+0	—	—	—
109	Ile	—	>1e-3	>1e-3	>1e-3	>1e-3	6.7e-1	—	—	—
110	Glu	—	>1e-3	>1e-3	>1e-3	>1e-3	4.8e+0	—	—	—
111	Lys	—	>1e-3	>1e-3	>1e-3	>1e-3	1.2e+0	—	—	—
112	Gln	—	>1e-3	>1e-3	>1e-3	>1e-3	1.3e+0	—	—	—
113	Val	—	>1e-3	>1e-3	>1e-3	>1e-3	2.0e+0	—	—	—
114	Gly	—	>1e-3	>1e-3	>1e-3	>1e-3	6.3e+0	—	—	—
115	Gln	—	>1e-3	>1e-3	>1e-3	>1e-3	5.6e+0	—	—	—
116	Ala	—	>1e-3	>1e-3	>1e-3	>1e-3	2.3e+0	—	—	—

Table 10.4: PSE-4 amide exchange data (continued)

Residue		**EX2 ?**	*pH* **7.85**		*pH* **6.65**					
#	**aa**		k_{HX}	Δk_{HX}	k_{HX}	Δk_{HX}	k_{int}	*logSF*	K_{op}	ΔG_{HX}
			(s^{-1})	**(s^{-1})**	**(s^{-1})**	**(s^{-1})**	**(s^{-1})**			**(kcal mol^{-1})**
117	Ile	EX2	>1e-3	>1e-3	1.4e-4	1.2e-5	4.2e-1	3.5	3.3e-4	4.9
118	Thr	EX2	>1e-3	>1e-3	1.2e-4	1.4e-5	1.2e+0	4.0	1.1e-4	5.5
119	Leu	EX2	>1e-3	>1e-3	1.4e-4	1.1e-5	9.6e-1	3.8	1.5e-4	5.3
120	Asp	—	o.l.	o.l.	1.1e-5	9.2e-7	5.0e+0	5.7	2.2e-6	7.9
121	Asp	EX2	3.7e-4	1.4e-4	1.0e-4	5.3e-6	2.3e+1	5.4	4.4e-6	7.5
122	Ala	EX2	2.1e-4	3.4e-5	1.6e-5	6.3e-7	6.6e+0	5.6	2.4e-6	7.8
123	Cys	EX2	3.7e-4	7.9e-5	2.2e-5	7.9e-7	8.1e+0	5.6	2.7e-6	7.8
124	Phe	EX2	2.1e-4	5.4e-5	3.7e-5	6.5e-7	1.1e+1	5.5	3.2e-6	7.7
125	Ala	—	o.l.	o.l.	o.l.	o.l.	5.6e+0	—	—	—
126	Thr	EX2	>1e-3	>1e-3	1.8e-4	1.7e-5	2.0e+0	4.0	9.1e-5	5.6
127	Met	—	o.l.	o.l.	3.6e-4	6.3e-5	3.6e+0	4.0	9.9e-5	5.6
128	Thr	EX2	>1e-3	>1e-3	6.4e-4	1.6e-4	2.0e+0	3.5	3.3e-4	4.9
129	Thr	—	>1e-3	>1e-3	>1e-3	>1e-3	3.1e+0	—	—	—
130	**Ser**	**—**	**>1e-3**	**>1e-3**	**>1e-3**	**>1e-3**	**8.5e+0**	**—**	**—**	**—**
131	Asp	—	>1e-3	>1e-3	>1e-3	>1e-3	1.6e+1	—	—	—
132	Asn	—	>1e-3	>1e-3	>1e-3	>1e-3	6.6e+0	—	—	—
133	Thr	—	>1e-3	>1e-3	>1e-3	>1e-3	2.0e+0	—	—	—
134	Ala	—	>1e-3	>1e-3	>1e-3	>1e-3	3.6e+0	—	—	—
135	Ala	—	>1e-3	>1e-3	>1e-3	>1e-3	2.3e+0	—	—	—
136	Asn	—	o.l.	o.l.	>1e-3	>1e-3	2.3e+0	—	—	—
137	Ile	—	>1e-3	>1e-3	>1e-3	>1e-3	4.2e-1	—	—	—
138	Ile	EX2	2.0e-4	8.0e-5	1.8e-5	7.6e-7	2.5e-1	4.1	7.4e-5	5.8
139	Leu	EX2	1.9e-4	2.4e-5	1.7e-5	7.2e-7	3.6e-1	4.3	4.7e-5	6.0
140	Ser	EX2	>1e-3	>1e-3	1.2e-4	4.6e-6	3.3e+0	4.4	3.6e-5	6.2
141	Ala	EX2	>1e-3	>1e-3	6.6e-5	1.5e-6	4.5e+0	4.8	1.5e-5	6.7
142	Val	EX2	2.2e-4	3.1e-5	1.7e-5	5.4e-7	2.0e+0	5.1	8.7e-6	7.1
143	Gly	—	>1e-3	>1e-3	>1e-3	>1e-3	6.3e+0	—	—	—
144	Gly	EX2	3.6e-4	2.1e-4	4.7e-5	1.6e-6	9.7e+0	5.3	4.9e-6	7.4
145	Pro	—	—	—	—	—	—	—	—	—
146	Lys	—	o.l.	o.l.	o.l.	o.l.	4.2e-1	—	—	—
147	Gly	—	>1e-3	>1e-3	>1e-3	>1e-3	2.3e+0	—	—	—
148	Val	EX2	2.9e-4	6.1e-5	3.4e-5	8.6e-7	4.8e+0	5.1	7.1e-6	7.2
149	Thr	EX2	2.6e-4	5.3e-5	4.0e-5	1.6e-6	3.1e+0	4.9	1.3e-5	6.8
150	Asp	EX2	2.8e-4	1.2e-4	3.7e-5	1.2e-6	1.3e+1	5.5	2.9e-6	7.7
151	Phe	EX2	1.9e-4	5.2e-5	2.1e-5	9.8e-7	1.1e+1	5.7	1.9e-6	8.0
152	Leu	EX2	7.4e-5	3.0e-5	1.2e-5	8.5e-7	1.5e+0	5.1	7.8e-6	7.1
153	Arg	EX2	>1e-3	>1e-3	1.9e-5	6.7e-7	1.7e+0	5.0	1.1e-5	6.9
154	Gln	EX2	>1e-3	>1e-3	9.9e-5	5.7e-6	3.8e+0	4.6	2.6e-5	6.4
155	Ile	EX2	2.6e-4	7.9e-5	1.6e-5	6.0e-7	4.2e-1	4.4	3.8e-5	6.2
156	Gly	—	>1e-3	>1e-3	>1e-3	>1e-3	2.3e+0	—	—	—
157	Asp	EX2	>1e-3	>1e-3	2.3e-4	1.7e-5	2.0e+1	4.9	1.1e-5	6.9
158	Lys	—	>1e-3	>1e-3	>1e-3	>1e-3	1.2e+0	—	—	—
159	Glu	—	o.l.	o.l.	o.l.	o.l.	4.8e+0	—	—	—
160	Thr	EX2	8.4e-4	3.9e-4	9.1e-5	3.7e-6	5.6e+0	4.8	1.6e-5	6.7
161	Arg	EX2	>1e-3	>1e-3	8.4e-5	5.2e-6	4.3e+0	4.7	2.0e-5	6.6
162	Leu	EX2	>1e-3	>1e-3	6.5e-5	3.7e-6	1.0e+0	4.2	6.5e-5	5.8
163	Asp	EX2	>1e-3	>1e-3	2.2e-5	3.4e-6	5.0e+0	5.4	4.4e-6	7.5

Table 10.4: PSE-4 amide exchange data (continued)

Residue		**EX2 ?**	*pH* **7.85**		*pH* **6.65**					
#	**aa**		k_{HX}	Δk_{HX}	k_{HX}	Δk_{HX}	k_{int}	*logSF*	K_{op}	ΔG_{HX}
			(s^{-1})	**(s^{-1})**	**(s^{-1})**	**(s^{-1})**	**(s^{-1})**			**(kcal mol^{-1})**
164	Arg	EX2	>1e-3	>1e-3	4.4e-5	4.8e-6	7.8e+0	5.3	5.6e-6	7.3
165	Ile	—	>1e-3	>1e-3	5.3e-5	2.9e-6	7.0e-1	4.1	7.5e-5	5.7
166	**Glu**	**—**	**>1e-3**	**>1e-3**	**1.8e-5**	**1.7e-6**	**4.8e+0**	**5.4**	**3.7e-6**	**7.6**
167	Pro	—	—	—	—	—	—	—	—	—
168	Asp	—	o.l.	o.l.	o.l.	o.l.	8.1e+0	—	—	—
169	Leu	EX2	>1e-3	>1e-3	7.0e-5	4.3e-6	1.7e+0	4.4	4.0e-5	6.1
170	Asn	—	o.l.	o.l.	o.l.	o.l.	1.4e+0	—	—	—
171	Glu	—	>1e-3	>1e-3	>1e-3	>1e-3	8.1e+0	—	—	—
172	Gly	—	>1e-3	>1e-3	>1e-3	>1e-3	1.1e+1	—	—	—
173	Lys	—	o.l.	o.l.	o.l.	o.l.	1.0e+0	—	—	—
174	Leu	—	o.l.	o.l.	o.l.	o.l.	3.6e-1	—	—	—
175	Gly	—	o.l.	o.l.	>1e-3	>1e-3	2.4e+0	—	—	—
176	Asp	—	>1e-3	>1e-3	>1e-3	>1e-3	2.0e+1	—	—	—
177	Leu	—	n.o.	n.o.	>1e-3	>1e-3	1.7e+0	—	—	—
178	Arg	EX2	>1e-3	>1e-3	6.7e-4	3.9e-4	1.7e+0	3.4	4.0e-4	4.7
179	Asp	—	n.o.	n.o.	5.9e-5	6.3e-6	1.3e+1	5.4	4.4e-6	7.5
180	Thr	EX2	>1e-3	>1e-3	4.9e-5	1.2e-6	5.1e+0	5.1	8.7e-6	7.1
181	Thr	EX2	2.4e-4	1.2e-4	6.3e-5	3.9e-6	3.1e+0	4.7	2.0e-5	6.5
182	Thr	EX2	3.3e-4	7.8e-5	3.5e-5	1.3e-6	3.1e+0	4.9	1.1e-5	6.9
183	Pro	—	—	—	—	—	—	—	—	—
184	Lys	—	o.l.	o.l.	o.l.	o.l.	4.2e-1	—	—	—
185	Ala	—	o.l.	o.l.	o.l.	o.l.	1.3e+0	—	—	—
186	Ile	EX2	1.9e-4	2.1e-5	1.4e-5	6.6e-7	4.2e-1	4.5	3.4e-5	6.2
187	Ala	EX2	2.0e-4	3.1e-5	1.9e-5	6.6e-7	1.3e+0	4.8	1.4e-5	6.8
188	Ser	EX2	>1e-3	>1e-3	6.0e-5	2.8e-6	5.3e+0	4.9	1.1e-5	6.9
189	Thr	—	o.l.	o.l.	o.l.	o.l.	3.9e+0	—	—	—
190	Leu	EX2	1.4e-4	4.0e-5	1.4e-5	6.5e-7	9.6e-1	4.8	1.5e-5	6.7
191	Asn	EX2	1.6e-4	4.8e-5	2.0e-5	7.3e-7	1.4e+0	4.8	1.4e-5	6.7
192	Lys	—	2.8e-4	5.7e-5	o.l.	o.l.	4.2e-1	—	—	—
193	Phe	EX2	1.0e-4	1.2e-5	1.0e-5	4.4e-7	2.3e+0	5.4	4.5e-6	7.5
194	Leu	—	o.l.	o.l.	7.9e-6	4.2e-7	1.5e+0	5.3	5.3e-6	7.4
195	Phe	EX2	1.0e-4	4.2e-5	1.4e-5	5.1e-7	2.4e+0	5.3	5.6e-6	7.3
196	Gly	—	>1e-3	>1e-3	>1e-3	>1e-3	9.7e+0	—	—	—
197	Ser	—	o.l.	o.l.	>1e-3	>1e-3	1.3e+1	—	—	—
198	Ala	—	>1e-3	>1e-3	>1e-3	>1e-3	4.5e+0	—	—	—
199	Leu	EX2	>1e-3	>1e-3	2.6e-4	1.2e-5	6.0e-1	3.4	4.4e-4	4.7
200	Ser	—	>1e-3	>1e-3	>1e-3	>1e-3	3.3e+0	—	—	—
201	Glu	—	>1e-3	>1e-3	>1e-3	>1e-3	1.6e+1	—	—	—
202	Met	—	>1e-3	>1e-3	>1e-3	>1e-3	6.6e+0	—	—	—
203	Asn	—	>1e-3	>1e-3	>1e-3	>1e-3	2.3e+0	—	—	—
204	Gln	—	o.l.	o.l.	o.l.	o.l.	2.3e+0	—	—	—
205	Lys	—	o.l.	o.l.	o.l.	o.l.	4.2e-1	—	—	—
206	Lys	EX2	>1e-3	>1e-3	2.0e-4	1.6e-5	2.5e-1	3.1	8.1e-4	4.3
207	Leu	EX2	1.7e-4	4.2e-5	1.7e-5	5.9e-7	3.6e-1	4.3	4.7e-5	6.0
208	Glu	—	o.l.	o.l.	1.9e-5	6.5e-7	5.0e+0	5.4	3.9e-6	7.5
209	Ser	EX2	5.1e-4	7.5e-5	7.4e-5	2.3e-6	1.5e+1	5.3	4.8e-6	7.4
210	Trp	EX2	2.9e-4	4.2e-5	1.9e-5	7.3e-7	1.8e+0	5.0	1.1e-5	6.9

Table 10.4: PSE-4 amide exchange data (continued)

Residue		**EX2 ?**	*pH* **7.85**		*pH* **6.65**					
#	**aa**		k_{HX}	Δk_{HX}	k_{HX}	Δk_{HX}	k_{int}	*logSF*	K_{op}	ΔG_{HX}
			(s^{-1})	**(s^{-1})**	**(s^{-1})**	**(s^{-1})**	**(s^{-1})**			**(kcal mol^{-1})**
211	Met	—	o.l.	o.l.	1.3e-5	9.5e-7	1.8e+0	5.1	7.4e-6	7.2
212	Val	EX2	1.3e-4	5.0e-5	1.2e-5	7.4e-7	2.0e+0	5.2	6.4e-6	7.2
213	Asn	—	o.l.	o.l.	o.l.	o.l.	3.6e+0	—	—	—
214	Asn	—	>1e-3	>1e-3	>1e-3	>1e-3	2.3e+0	—	—	—
215	Gln	—	>1e-3	>1e-3	>1e-3	>1e-3	2.3e+0	—	—	—
216	Val	—	>1e-3	>1e-3	>1e-3	>1e-3	2.0e+0	—	—	—
217	Thr	—	>1e-3	>1e-3	>1e-3	>1e-3	3.1e+0	—	—	—
218	Gly	—	n.o.	n.o.	>1e-3	>1e-3	6.3e+0	—	—	—
219	Asn	—	n.o.	n.o.	>1e-3	>1e-3	5.6e+0	—	—	—
220	Leu	—	>1e-3	>1e-3	>1e-3	>1e-3	6.0e-1	—	—	—
221	Leu	—	>1e-3	>1e-3	>1e-3	>1e-3	3.7e-1	—	—	—
222	Arg	—	>1e-3	>1e-3	>1e-3	>1e-3	1.7e+0	—	—	—
223	Ser	—	>1e-3	>1e-3	>1e-3	>1e-3	8.9e+0	—	—	—
224	Val	EX2	>1e-3	>1e-3	4.6e-4	7.9e-5	3.9e+0	3.9	1.2e-4	5.5
225	Leu	EX2	>1e-3	>1e-3	1.9e-4	9.1e-6	9.6e-1	3.7	2.0e-4	5.2
226	Pro	—	—	—	—	—	—	—	—	—
227	Ala	—	>1e-3	>1e-3	>1e-3	>1e-3	2.3e+0	—	—	—
228	Gly	—	n.o.	n.o.	>1e-3	>1e-3	4.0e+0	—	—	—
229	Trp	EX2	>1e-3	>1e-3	4.3e-5	9.2e-6	2.2e+0	4.7	2.0e-5	6.6
230	Asn	EX2	9.8e-4	3.0e-4	6.5e-5	5.1e-6	1.8e+0	4.4	3.7e-5	6.2
231	Ile	—	o.l.	o.l.	1.7e-4	9.0e-6	4.2e-1	3.4	3.9e-4	4.8
232	Ala	EX2	5.6e-4	2.0e-4	3.8e-5	3.1e-6	1.3e+0	4.5	2.9e-5	6.3
233	Asp	EX2	>1e-3	>1e-3	1.7e-4	1.2e-5	8.1e+0	4.7	2.1e-5	6.5
234	**Arg**	**—**	**>1e-3**	**>1e-3**	**o.l.**	**o.l.**	**7.8e+0**	**—**	**—**	**—**
235	Ser	—	n.o.	n.o.	>1e-3	>1e-3	8.9e+0	—	—	—
236	Gly	—	>1e-3	>1e-3	>1e-3	>1e-3	7.9e+0	—	—	—
237	Ala	—	n.o.	n.o.	n.o.	n.o.	5.6e+0	—	—	—
238	Gly	—	>1e-3	>1e-3	>1e-3	>1e-3	4.0e+0	—	—	—
240	Gly	—	>1e-3	>1e-3	>1e-3	>1e-3	9.7e+0	—	—	—
241	Phe	—	>1e-3	>1e-3	>1e-3	>1e-3	9.7e+0	—	—	—
242	Gly	—	>1e-3	>1e-3	>1e-3	>1e-3	9.7e+0	—	—	—
243	Ala	—	>1e-3	>1e-3	>1e-3	>1e-3	5.6e+0	—	—	—
244	Arg	—	>1e-3	>1e-3	>1e-3	>1e-3	2.7e+0	—	—	—
245	Ser	—	o.l.	o.l.	o.l.	o.l.	8.9e+0	—	—	—
246	Ile	EX2	1.5e-5	1.5e-6	2.9e-6	1.1e-7	8.4e-1	5.5	3.4e-6	7.6
247	Thr	—	o.l.	o.l.	5.0e-5	3.1e-6	1.2e+0	4.4	4.3e-5	6.1
248	Ala	EX2	6.4e-6	4.5e-7	1.0e-6	4.2e-8	3.6e+0	6.6	2.8e-7	9.1
249	Val	EX2	3.9e-6	4.1e-7	4.8e-7	3.6e-8	2.0e+0	6.6	2.5e-7	9.2
250	Val	EX2	3.8e-6	5.1e-7	3.8e-7	4.5e-8	3.1e+0	6.9	1.2e-7	9.6
251	Trp	—	o.l.	o.l.	o.l.	o.l.	1.4e+0	—	—	—
252	Ser	EX2	>1e-3	>1e-3	4.8e-4	3.4e-4	4.1e+0	3.9	1.2e-4	5.5
254	Glu	—	o.l.	o.l.	>1e-3	>1e-3	1.6e+1	—	—	—
255	His	—	o.l.	o.l.	>1e-3	>1e-3	2.8e+1	—	—	—
256	Gln	—	>1e-3	>1e-3	>1e-3	>1e-3	1.1e+1	—	—	—
257	Ala	—	>1e-3	>1e-3	>1e-3	>1e-3	2.3e+0	—	—	—
258	Pro	—	—	—	—	—	—	—	—	—
259	Ile	EX2	9.4e-7	4.9e-7	2.6e-8	6.0e-9	4.2e-1	7.2	6.1e-8	10.1

Table 10.4: PSE-4 amide exchange data (continued)

Residue		**EX2 ?**	*pH* **7.85**		*pH* **6.65**					
#	**aa**		k_{HX}	Δk_{HX}	k_{HX}	Δk_{HX}	k_{int}	*logSF*	K_{op}	ΔG_{HX}
			(s^{-1})	**(s^{-1})**	**(s^{-1})**	**(s^{-1})**	**(s^{-1})**			**(kcal mol^{-1})**
260	Ile	EX2	5.6e-7	1.3e-7	2.6e-8	5.1e-9	2.5e-1	7.0	1.0e-7	9.7
261	Val	EX2	5.6e-7	1.4e-7	6.6e-8	2.1e-8	1.2e+0	7.2	5.7e-8	10.1
262	Ser	EX2	2.7e-6	6.4e-7	6.1e-8	9.4e-9	8.5e+0	8.1	7.3e-9	11.3
263	Ile	EX2	1.2e-6	2.7e-7	3.6e-8	2.5e-8	8.4e-1	7.4	4.2e-8	10.3
264	Tyr	EX2	1.6e-6	4.6e-7	9.1e-8	3.2e-8	7.2e-1	6.9	1.3e-7	9.6
265	Leu	—	o.l.	o.l.	4.7e-6	2.3e-7	6.8e-1	5.2	7.0e-6	7.2
266	Ala	EX2	1.4e-4	2.5e-5	1.3e-5	4.6e-7	1.4e+0	5.0	9.4e-6	7.0
267	Gln	—	>1e-3	>1e-3	>1e-3	>1e-3	2.3e+0	—	—	—
268	Thr	—	>1e-3	>1e-3	>1e-3	>1e-3	2.0e+0	—	—	—
269	Gln	—	o.l.	o.l.	>1e-3	>1e-3	3.6e+0	—	—	—
270	Ala	—	o.l.	o.l.	o.l.	o.l.	2.3e+0	—	—	—
271	Ser	—	o.l.	o.l.	>1e-3	>1e-3	5.3e+0	—	—	—
272	Met	—	n.o.	n.o.	>1e-3	>1e-3	4.5e+0	—	—	—
273	Glu	—	>1e-3	>1e-3	>1e-3	>1e-3	8.1e+0	—	—	—
274	Glu	—	>1e-3	>1e-3	>1e-3	>1e-3	2.3e+1	—	—	—
275	Arg	—	o.l.	o.l.	o.l.	o.l.	7.8e+0	—	—	—
276	Asn	—	>1e-3	>1e-3	>1e-3	>1e-3	3.8e+0	—	—	—
277	Asp	—	o.l.	o.l.	o.l.	o.l.	8.1e+0	—	—	—
278	Ala	EX2	>1e-3	>1e-3	1.3e-4	2.9e-6	6.6e+0	4.7	2.0e-5	6.6
279	Ile	EX2	2.5e-4	4.7e-5	1.2e-5	3.1e-7	4.2e-1	4.6	2.8e-5	6.3
280	Val	EX2	1.3e-5	6.0e-7	1.1e-6	6.6e-8	1.2e+0	6.0	9.7e-7	8.4
281	Lys	—	o.l.	o.l.	2.8e-6	7.3e-8	6.7e-1	5.4	4.2e-6	7.5
282	Ile	—	o.l.	o.l.	o.l.	o.l.	2.5e-1	—	—	—
283	Gly	EX2	1.1e-5	8.3e-7	3.0e-6	6.7e-8	2.3e+0	5.9	1.3e-6	8.2
284	His	—	o.l.	o.l.	4.5e-6	1.3e-7	2.4e+1	6.7	1.9e-7	9.4
285	Ser	EX2	7.3e-5	2.7e-5	1.2e-5	2.7e-7	2.6e+1	6.3	4.7e-7	8.8
286	Ile	EX2	8.4e-6	6.6e-7	3.8e-6	6.0e-7	8.4e-1	5.3	4.5e-6	7.5
287	Phe	—	o.l.	o.l.	o.l.	o.l.	2.3e+0	—	—	—
288	Asp	—	o.l.	o.l.	7.8e-6	2.0e-7	2.0e+1	6.4	3.9e-7	8.9
289	Val	EX2	>1e-3	>1e-3	2.0e-4	1.5e-5	5.6e+0	4.4	3.6e-5	6.2
290	Tyr	EX2	>1e-3	>1e-3	2.5e-4	2.0e-5	1.9e+0	3.9	1.3e-4	5.4
291	Thr	—	>1e-3	>1e-3	>1e-3	>1e-3	2.2e+0	—	—	—
292	Ser	—	>1e-3	>1e-3	>1e-3	>1e-3	8.5e+0	—	—	—
293	Gln	—	>1e-3	>1e-3	>1e-3	>1e-3	4.5e+0	—	—	—
294	Ser	—	>1e-3	>1e-3	>1e-3	>1e-3	5.3e+0	—	—	—
295	Arg	—	>1e-3	>1e-3	>1e-3	>1e-3	8.6e-2	—	—	—

- k_{int} values were obtained from an Excel spreadsheet from S. W. Englander (University of Pennsylvania, Philadelphia, PA, [11, 43]).
- Values presented here are rounded. Exact values can be obtained from BMRB (accession number 6838).
- Important active site residues (Ser^{70}, Lys^{73}, Tyr^{105}, Ser^{130}, Glu^{166} and Arg^{234}) are shown in bold red while the Ω loop (residues 161–179) is coloured blue.
- n-ter: N-terminus amine (not observable).
- n.o.: non-observed N-H resonances (not assigned).
- o.l.: overlapped N-H resonances.

Appendix 5:
cTEM-17m Backbone Chemical Shift Assignments

Table 10.5: cTEM-17m backbone chemical shifts

Residue		H_N	N	C_α	C_β	C’
#	aa	(ppm)	(ppm)	(ppm)	(ppm)	(ppm)
26	His	n-ter	n-ter	–	–	–
27	Pro	–	–	65.568	32.340	179.290
28	Glu	11.040	121.750	59.690	28.676	179.520
29	Thr	7.750	118.850	65.090	67.760	176.070
30	Leu	7.060	119.790	57.500	40.950	178.960
31	Val	7.500	119.720	66.890	31.330	178.330
32	Lys	7.250	119.230	57.170	30.380	178.450
33	Val	8.280	122.700	67.210	31.130	176.710
34	Lys	7.690	118.650	59.870	31.880	179.300
35	Asp	8.300	120.320	57.400	41.830	178.150
36	Ala	8.450	122.160	55.440	18.370	179.520
37	Glu	7.920	117.670	61.020	29.310	180.380
38	Asp	7.920	119.880	57.230	40.920	179.150
39	Gln	8.830	118.470	58.560	28.570	179.100
40	Leu	8.690	114.390	54.830	42.890	178.920
41	Gly	8.070	112.840	47.340	–	174.040
42	Ala	7.730	119.680	50.720	24.180	174.910
43	Arg	7.630	115.560	55.750	33.290	177.530
44	Val	10.560	128.190	61.290	34.248	172.740
45	Gly	8.800	111.280	44.090	–	172.360
46	Tyr	9.460	124.000	56.700	45.220	174.340
47	Ile	8.000	125.800	60.560	42.670	182.040
48	Glu	7.740	123.410	54.160	34.617	175.240
49	Leu	9.680	125.690	53.060	47.120	176.020
50	Asp	9.030	125.520	55.540	43.250	176.900
51	Leu	8.230	129.210	58.850	43.220	177.370
52	Asn	8.630	116.010	56.380	38.830	177.210
53	Ser	8.600	113.000	59.190	65.840	176.530
54	Gly	8.000	112.450	45.630	–	172.410
55	Lys	7.720	119.780	56.880	33.710	175.960
56	Ile	8.640	124.900	62.470	37.580	176.160
57	Leu	8.890	130.570	55.840	42.230	176.940
58	Glu	7.540	116.130	54.980	33.880	174.450
59	Ser	9.050	115.660	58.450	66.960	171.670
60	Phe	9.560	121.590	59.930	43.750	173.110
61	Arg	8.780	121.790	57.850	28.600	–
62	Pro	–	–	65.314	32.650	176.610
63	Glu	8.420	114.070	54.810	29.740	176.210
64	Glu	7.150	120.440	56.180	31.270	174.190
65	Arg	7.920	115.620	55.080	31.970	177.300
66	Phe	8.760	118.360	55.670	42.380	–
67	Pro	–	–	–	–	174.475
68	Met	7.862	119.515	58.424	–	179.789
69	Met	10.488	120.181	56.498	–	–
70	**Ser**	**–**	**–**	**57.812**	**–**	**176.090**
71	Thr	7.900	112.010	66.060	–	175.270
72	Phe	7.680	116.730	59.400	39.650	176.860
73	**Lys**	**7.430**	**122.390**	**60.170**	**31.900**	**177.480**
74	Val	6.660	114.670	66.200	32.650	176.040

Table 10.5: cTEM-17m backbone chemical shifts (continued)

Residue		H_N	N	C_α	C_β	C'
#	aa	(ppm)	(ppm)	(ppm)	(ppm)	(ppm)
75	Leu	6.740	117.750	57.260	40.640	178.060
76	Leu	7.990	116.970	57.540	42.440	177.240
77	Cys	7.460	113.680	63.810	44.870	175.620
78	Gly	8.380	110.860	47.960	–	173.170
79	Ala	7.870	124.380	54.990	17.120	180.700
80	Val	7.960	118.940	66.930	32.200	177.900
81	Leu	8.420	119.120	57.900	40.830	178.070
82	Ser	8.050	115.560	61.950	62.370	178.010
83	Arg	7.510	121.430	59.340	30.320	179.380
84	Val	8.350	124.230	65.090	31.090	180.810
85	Asp	9.010	123.500	57.290	40.800	177.780
86	Ala	7.520	118.750	52.320	19.480	177.920
87	Gly	8.190	107.600	45.760	–	174.930
88	Gln	8.370	117.340	55.630	30.100	173.560
89	Glu	7.360	118.050	52.930	33.670	172.700
90	Gln	10.130	125.120	54.850	31.460	176.030
91	Leu	9.020	122.960	57.650	41.570	177.350
92	Gly	8.360	102.011	44.520	–	173.820
93	Arg	7.320	122.530	58.020	31.920	174.700
94	Arg	8.500	127.260	56.550	31.660	174.470
95	Ile	9.080	130.220	60.240	38.940	174.510
96	His	8.440	124.650	55.400	31.040	174.150
97	Tyr	8.490	120.950	55.990	38.760	173.020
98	Ser	9.420	114.570	57.010	67.380	175.650
99	Gln	9.070	121.880	59.100	28.210	177.950
100	Asn	8.210	115.180	55.080	38.190	175.610
101	Asp	7.890	116.650	55.760	42.680	175.600
102	Leu	7.120	116.770	55.340	41.980	177.940
103	Val	7.730	117.160	58.830	34.470	176.560
104	Glu	8.510	123.220	57.930	30.230	174.930
105	**Tyr**	**8.670**	**121.230**	**60.520**	**36.130**	**172.120**
106	Ser	8.340	119.730	55.810	64.940	–
107	Pro	–	–	64.094	31.942	177.740
108	Val	8.660	118.380	64.570	33.140	179.060
109	Thr	9.630	113.620	63.970	69.270	181.920
110	Glu	8.170	119.980	58.840	28.590	176.430
111	Lys	7.420	116.200	55.890	32.560	177.260
112	His	7.120	116.190	55.240	28.730	174.490
113	Leu	7.840	120.230	58.220	42.020	179.130
114	Thr	8.290	109.270	64.400	68.870	175.610
115	Asp	8.770	117.120	53.950	40.460	177.650
116	Gly	7.900	110.780	45.110	–	171.630
117	Met	8.280	113.430	54.940	40.400	175.120
118	Thr	8.900	112.210	60.170	70.980	175.830
119	Val	8.090	121.970	68.170	31.760	177.930
120	Arg	9.030	118.350	60.200	31.350	177.590
121	Glu	7.620	118.310	58.440	30.080	180.510
122	Leu	9.070	122.820	58.040	41.130	179.070
123	Cys	8.110	118.910	62.300	42.460	175.960

Table 10.5: cTEM-17m backbone chemical shifts (continued)

Residue		H_N	N	C_α	C_β	C'
#	aa	(ppm)	(ppm)	(ppm)	(ppm)	(ppm)
124	Ser	7.710	113.340	61.400	62.610	178.980
125	Ala	8.480	124.560	55.640	17.520	180.210
126	Ala	8.630	120.810	55.120	17.540	178.440
127	Ile	8.210	113.640	65.020	38.180	176.610
128	Thr	8.960	109.770	65.340	–	175.930
129	Met	6.720	114.200	53.090	33.354	176.210
130	**Ser**	**7.130**	**114.910**	**59.410**	**–**	**–**
131	Asp	–	–	–	–	–
132	Asn	–	–	56.237	38.910	177.950
133	Thr	7.620	119.880	67.990	66.990	176.430
134	Ala	8.880	122.700	55.260	18.750	178.460
135	Ala	7.020	115.460	54.580	19.270	177.930
136	Asn	7.830	120.290	55.830	36.820	179.340
137	Leu	8.960	121.970	57.770	42.110	180.980
138	Leu	8.030	119.830	57.370	42.830	180.680
139	Leu	8.990	123.370	58.390	42.400	179.570
140	Thr	8.130	116.280	66.770	68.340	177.570
141	Thr	7.590	113.190	65.460	68.720	175.690
142	Ile	6.930	112.050	61.080	38.920	175.190
143	Gly	7.440	106.701	45.180	–	174.940
144	Gly	8.090	108.960	45.700	–	–
145	Pro	–	–	66.369	32.271	177.950
146	Lys	8.610	118.110	59.740	32.170	178.960
147	Glu	7.350	118.300	58.530	29.170	180.530
148	Leu	7.770	121.500	57.780	40.540	177.900
149	Thr	8.350	117.260	68.500	–	175.330
150	Asp	8.400	121.160	58.180	40.590	178.780
151	Phe	7.920	122.170	61.030	38.070	176.280
152	Leu	7.980	118.930	57.420	39.720	178.820
153	Arg	8.460	118.210	57.430	28.750	181.790
154	Gln	8.260	121.090	58.710	28.190	178.490
155	Ile	7.430	110.950	61.180	37.300	176.480
156	Gly	7.580	108.980	45.750	–	172.990
157	Asp	8.310	122.860	52.840	40.360	176.300
158	Lys	8.630	123.380	56.300	32.987	176.380
159	Glu	8.460	117.540	57.600	33.160	177.570
160	Thr	9.820	124.460	65.330	66.770	174.400
161	Arg	8.870	121.820	54.650	33.650	171.070
162	Leu	7.790	121.670	53.480	45.860	174.070
163	Asp	10.090	127.180	55.520	45.690	175.470
164	Arg	9.440	125.570	54.900	34.970	171.900
165	Ile	7.080	105.391	59.440	37.920	177.680
166	**Glu**	**9.273**	**116.456**	**55.050**	**–**	**–**
167	Pro	–	–	63.826	33.893	176.986
168	Asp	8.210	127.714	57.360	40.996	176.080
169	Leu	7.360	112.620	57.110	40.830	176.840
170	Asn	7.690	119.760	53.830	40.350	174.890
171	Glu	7.380	121.580	60.460	30.660	176.940
172	Gly	9.510	105.773	46.988	–	–

Table 10.5: cTEM-17m backbone chemical shifts (continued)

Residue		H_N	N	C_α	C_β	C’
#	aa	(ppm)	(ppm)	(ppm)	(ppm)	(ppm)
173	Lys	–	–	58.001	32.144	177.820
174	Leu	8.465	127.277	56.884	41.642	178.770
175	Gly	9.050	114.880	45.340	–	173.010
176	Asp	7.380	121.010	53.160	42.280	177.000
177	Leu	8.600	126.980	55.300	42.800	178.580
178	Arg	8.030	120.780	57.160	30.660	177.160
179	Asp	8.870	115.590	55.690	42.470	177.760
180	Thr	7.240	104.891	59.530	75.080	173.290
181	Thr	8.310	113.490	59.990	68.430	173.390
182	Thr	8.760	111.310	57.620	69.090	–
183	Pro	–	–	66.446	32.271	176.870
184	Lys	8.430	112.780	60.170	33.600	178.210
185	Ala	8.570	124.370	55.640	18.790	180.050
186	Ile	8.260	116.390	65.990	36.540	177.340
187	Ala	8.070	124.220	55.810	19.470	178.930
188	Ser	7.790	112.500	61.880	62.750	177.490
189	Thr	8.900	123.120	66.840	67.450	175.500
190	Leu	9.040	122.270	58.260	41.410	178.030
191	Arg	8.130	117.990	60.880	28.900	178.420
192	Lys	7.900	120.370	59.920	32.670	178.340
193	Leu	8.000	116.590	57.760	42.400	177.500
194	Leu	7.940	112.160	56.430	43.380	178.120
195	Thr	7.930	106.411	60.980	72.150	174.760
196	Gly	8.040	109.750	45.320	–	174.170
197	Glu	8.390	117.630	56.110	29.630	176.390
198	Leu	7.420	121.120	57.800	43.120	177.050
199	Leu	8.620	117.980	52.610	44.550	177.510
200	Thr	9.030	112.640	62.090	71.700	175.310
201	Leu	8.660	122.800	58.910	41.550	179.110
202	Ala	8.440	118.630	54.980	18.190	181.470
203	Ser	7.720	118.420	62.870	64.300	175.000
204	Arg	9.090	123.520	60.200	30.940	178.400
205	Gln	8.190	117.660	57.580	28.390	177.070
206	Gln	7.560	118.010	56.990	28.610	177.870
207	Leu	7.930	120.940	58.240	41.560	178.260
208	Ile	7.800	118.130	65.650	38.330	177.180
209	Asp	8.670	122.260	57.580	39.980	181.370
210	Trp	8.010	120.290	59.630	28.880	177.110
211	Met	7.750	115.840	59.590	35.690	180.150
212	Glu	9.650	124.690	59.710	31.790	178.150
213	Ala	7.310	119.520	51.760	19.145	–
214	Asp	–	–	–	–	–
215	Lys	9.522	127.500	56.982	–	–
216	Val	–	–	–	–	–
217	Ala	–	–	–	–	–
218	Gly	–	–	–	–	–
219	Pro	–	–	–	–	–
220	Leu	–	–	–	–	–
221	Leu	–	–	–	–	177.730

Table 10.5: cTEM-17m backbone chemical shifts (continued)

Residue		H_N	N	C_α	C_β	C’
#	aa	(ppm)	(ppm)	(ppm)	(ppm)	(ppm)
222	Arg	8.610	118.220	59.810	29.255	177.430
223	Ser	7.010	113.340	60.980	63.350	174.010
224	Ala	7.260	122.880	50.660	19.640	176.270
225	Leu	6.690	120.900	53.020	43.970	–
226	Pro	–	–	61.477	31.965	175.800
227	Ala	8.220	122.780	53.450	18.300	179.410
228	Gly	8.800	110.190	45.410	–	175.330
229	Trp	7.620	120.580	59.060	28.900	175.320
230	Phe	9.370	122.970	56.850	42.260	174.700
231	Ile	7.500	123.470	60.460	40.190	181.080
232	Ala	8.460	127.980	50.640	21.570	174.890
233	Asp	8.230	123.840	53.000	45.230	–
234	**Lys**	**–**	**–**	**–**	**–**	**–**
235	Ser	–	–	–	–	–
236	Gly	–	–	–	–	–
237	Ala	–	–	–	–	–
238	Gly	–	–	–	–	–
240	Glu	–	–	–	–	–
241	Arg	–	–	–	–	–
242	Gly	–	–	–	–	–
243	Ser	–	–	–	–	–
244	Arg	–	–	53.652	–	174.278
245	Gly	8.421	111.554	46.965	–	170.483
246	Ile	9.040	116.970	59.680	–	182.100
247	Ile	8.120	118.430	58.850	–	174.350
248	Ala	8.970	123.750	51.310	24.720	174.580
249	Ala	9.350	122.780	50.340	20.650	175.580
250	Leu	9.300	121.120	55.110	46.620	176.730
251	Gly	8.790	110.460	46.860	–	–
252	Pro	–	–	60.767	31.685	176.010
254	Asp	7.920	114.290	54.950	39.330	177.130
255	Gly	7.720	100.251	46.860	–	173.400
256	Lys	7.170	119.340	52.300	34.630	–
257	Pro	–	–	62.098	–	176.060
258	Ser	8.520	112.310	58.990	65.750	174.520
259	Arg	8.820	123.250	55.840	36.250	174.500
260	Ile	9.190	122.670	58.780	40.480	174.580
261	Val	9.190	126.310	59.630	36.280	173.340
262	Val	8.190	125.320	60.380	35.810	174.020
263	Ile	8.240	122.560	60.140	41.935	174.520
264	Tyr	8.790	122.620	56.920	44.971	174.420
265	Thr	8.930	110.750	59.540	70.821	–
266	Thr	–	–	–	–	–
267	Gly	–	–	45.638	–	174.480
268	Ser	8.360	114.500	58.940	65.645	175.820
269	Gln	8.830	123.360	55.740	29.055	175.910
270	Ala	8.650	123.320	52.280	20.590	178.690
271	Thr	8.650	112.880	61.680	70.950	–
272	Met	–	–	58.037	30.914	177.800

Table 10.5: cTEM-17m backbone chemical shifts (continued)

Residue		H_N	N	C_α	C_β	C'
#	aa	(ppm)	(ppm)	(ppm)	(ppm)	(ppm)
273	Asp	8.410	116.720	57.770	40.660	178.690
274	Glu	7.640	120.300	58.940	30.090	179.280
275	Arg	8.090	118.730	60.760	31.175	177.520
276	Asn	8.770	116.980	55.310	37.256	176.530
277	Arg	8.000	118.740	59.320	30.120	178.830
278	Gln	7.790	114.970	58.330	27.750	178.480
279	Ile	7.430	117.580	66.010	–	175.690
280	Ala	8.060	124.090	55.960	17.722	180.420
281	Glu	8.420	118.330	59.660	29.810	180.680
282	Ile	8.030	123.340	66.590	38.070	178.010
283	Gly	8.350	106.041	47.640	–	173.960
284	Ala	8.610	122.220	55.210	17.820	180.190
285	Ser	7.490	113.430	61.840	62.940	176.260
286	Leu	8.180	122.940	58.110	40.920	178.840
287	Ile	7.930	118.150	63.870	37.670	178.500
288	Lys	8.100	120.870	59.010	32.540	177.920
289	His	7.600	114.300	54.840	28.010	173.650
290	Trp	7.230	128.690	62.380	30.450	–

- Important active site residues (Ser^{70}, Lys^{73}, Tyr^{105}, Ser^{130}, Glu^{166}, and Arg^{234}) are shown in bold red while residues from the Ω loop (residues 161–179) are coloured blue.
- Chemical shifts have been deposited in the BMRB (under accession number 16598).
- n-ter: N-terminus amine (not observable).

Appendix 6:
Curriculum vitae

Sébastien Morin

Academic training

- **2006 – 2010**
  Ph.D. student in Biochemistry at Université Laval under the supervision of Dr Stéphane M. Gagné.
- **2004 – 2005**
  M.Sc. in Biochemistry at Université Laval under the supervision of Dr Stéphane M. Gagné.
- **2000 – 2003**
  B.Sc. in Biochemistry with Rouge et Or Distinction (Université Laval, with the last semester at Université Joseph Fourier, Grenoble, France).

Awards and Prizes

2010
- EMBO Long term fellowship.

2009
- Bourse PROTEO aux études supérieures.
- Bourse de congrès de PROTEO for 51st ENC, Daytona Beach (USA): April 18-23, 2010.
- Student Research Achievement Award (SRAA) Poster Competition, Molecular Biophysics Subgroup at 53rd Biophysical Society Annual Meeting, Boston (USA): February 28th to March 4th, 2009.
- Bourse du Fonds AELIÉS pour une présentation for 53rd Biophysical Society Annual Meeting, Boston (USA): February 28th to March 4th, 2009.

2008
- FRSQ Ph.D. research studentship: POSTPONED from 2006.
- Student Travel Award for MOOT XXI, Windsor (Canada): October 3-4, 2008.
- Bureau des bourses et de l'aide financière de l'Université Laval Travel Stipend for XXIIIrd ICMRBS, San Diego (USA): August 24-29, 2008.
- Best Poster Award at Symposium annuel du CREFSIP, Quebec City (Canada): May 28th, 2008.

2006
- Student Travel Grant for the 51st Biophysical Society Annual Meeting, Baltimore (USA): March 3-7, 2007.
- Bourse de congrès du CREFSIP for 51st Biophysical Society Annual Meeting, Baltimore (USA): March 3-7, 2007.
- NSERC Postgraduate Scholarship (BESC D).
- Fonds Hydro-Québec Ph.D. studentship (via Fondation de l'Université Laval): DECLINED.
- NSERC general fund for graduate studies studentship (via Fondation de l'Université Laval): DECLINED.

2005
- Fondation J.-Arthur Vincent studentship.

2003
- NSERC Postgraduate Scholarship (ES M).
- FRSQ M.Sc. research studentship: DECLINED.
- NSERC and Fondation de l'Université Laval excellence studentship.

2002
- NSERC Undergraduate Student Research Awards Program (USRA).

Publications

- Morin S., Clouthier C. M., Gobeil S., Pelletier J. N. & Gagné S. M. (In press) Backbone resonance assignments of a TEM-1/PSE-4 class A β-lactamase chimera. *Biomolecular NMR Assignments*.
- Fisette O., Morin S., Savard P.-Y., Lagüe P. & Gagné S. M. (2010) TEM-1 backbone dynamics – Insights from combined molecular dynamics and NMR. *Biophysical Journal*, **98:** 637–645.
- Morin S. & Gagné S. M. (2009) Simple tests for the validation of multiple field spin relaxation data. *Journal of Biomolecular NMR*, **45:** 361–372.
- Morin S. & Gagné S. M. (2009) NMR dynamics of PSE-4 β-lactamase: An interplay of ps-ns order and μs-ms motions in the active site. *Biophysical Journal*, **96:** 4681–4691.
- Morin S., Levesque R.C. & Gagné S. M. (2006) ^{1}H, ^{13}C and ^{15}N backbone resonance assignment for PSE-4, a 29.5 kDa class A β-lactamase from *Pseudomonas aeruginosa*. *Journal of Biomolecular NMR*, **36 Suppl 1:** 11.

Proceedings

- Morin S. & Gagné S. (2009) NMR dynamics of PSE-4 β-lactamase: An interplay of ps-ns order and μs-ms motions in the active site. *Biophysical Journal*: Biophysical Society 53rd Annual Meeting, Abstracts Issue, **96:** 74-A.
- Morin S. & Gagné S. (2007) Backbone dynamics and amide exchange for the 29.5 kDa class A β-lactamase PSE-4 by NMR. *Biophysical Journal*: Biophysical Society 51st Biophysical Society Annual Meeting, Abstracts Issue, **Suppl. S:** 641-A.

Oral Presentations

2010
- Interlabs-IBIS (Université Laval, Quebec City, Canada). RMN pour les nuls : des antibiotiques au VIH

2009
- 9th PROTEO Annual Symposium (Université Laval, Quebec City, Canada). Probing the dynamics of PSE-4: Motion or not ?
- Conference in Dr Rolf Boelens's laboratory (Bijvoet Center, Utrecht, The Netherlands). Dynamics of Class A β-lactamases: An interplay of ps-ns order and μs-ms motions
- Conference in Dr Volker Dötsch's laboratory (Johann Wolfgang Goethe Universität, Frankfurt, Germany). Dynamics of Class A β-lactamases: An interplay of ps-ns order and μs-ms motions
- Conference in Dr Stephan Grzesiek's laboratory (Biozentrum, Basel, Switzerland). Dynamics of Class A β-lactamases: An interplay of ps-ns order and μs-ms motions
- Conference in Dr Frédéric Allain's laboratory (ETH, Zürich, Switzerland). Dynamics of Class A β-lactamases: An interplay of ps-ns order and μs-ms motions
- Conference in Dr Frank D. Sönnichsen's laboratory (Christian-Albrechts-Universität, Kiel, Germany). Dynamics of Class A β-lactamases: An interplay of ps-ns order and μs-ms motions
- Conference in Dr Kalle Gehring's laboratory (McGill University, Montréal, Canada). NMR dynamics of PSE-4 β-lactamase: An interplay of ps-ns order and μs-ms motions in the active site

2008
- MOOT XXI (Windsor, Canada). NMR dynamics of PSE-4 β-lactamase: An interplay of ps-ns order and μs-ms motions in the active site

2007
- Conference in Dr. Matthew Crump's laboratory (Bristol University, Bristol, United Kingdom). Dynamics of class A β-lactamases by NMR and MM

Posters

2010

- 10th PROTEO Annual Symposium (Concordia University, Montreal, Canada). RNA binding characterization of the multifunctional protein p54^{nrb}. Mikaël BÉDARD, Sébastien MORIN, Sami Aziz AMEUR, Céline BRUELLE, Stéphane M. GAGNÉ & Michel VINCENT
- 51st ENC (Daytona Beach, FL, USA). Studying Dynamics of Class A β-lactamases with the use of a TEM-1/PSE-4 Chimera. Sébastien MORIN, Christopher M. CLOUTHIER, Sophie GOBEIL, Joëlle N. PELLETIER & Stéphane M. GAGNÉ
- 51st ENC (Daytona Beach, FL, USA). Initial characterization of RNA binding by the multifunctional protein p54^{nrb}. Mikaël BÉDARD, Sébastien MORIN, Sami Aziz AMEUR, Céline BRUELLE, Stéphane M. GAGNÉ & Michel VINCENT

2009

- MOOT XXII (Ottawa, Canada). A toolkit for dynamics relaxing the BMRB. Edward D'AUVERGNE, Chris MACRAILD, Sébastien MORIN, Gary THOMPSON, Eldon ULRICH
- MOOT XXII (Ottawa, Canada). Preliminary data for RNA binding by the multifunctional protein p54^{nrb}. Mikaël BÉDARD, Sébastien MORIN, Sami Aziz AMEUR, Céline BRUELLE, Stéphane M. GAGNÉ & Michel VINCENT
- 52nd Annual Meeting of the CSBMCB - Protein Folding Principles & Diseases (Niagara-on-the-Lake, Canada). Dynamics of class A β-lactamases from NMR and molecular dynamics: An interplay of ps-ns order and μs-ms motions. Stéphane M. GAGNÉ, Sébastien MORIN, Pierre-Yves SAVARD, Olivier FISETTE & Patrick LAGÜE
- 9th PROTEO Annual Symposium (Université Laval, Québec, Canada). A toolkit for dynamics and how to relax the BMRB. Edward D'AUVERGNE, Chris MACRAILD, Sébastien MORIN, Gary THOMPSON, Eldon ULRICH
- 5th Annual McGill Biophysical Chemistry Symposium (McGill University, Montreal, Canada). A toolkit for dynamics and how to relax the BMRB. Edward D'AUVERGNE, Chris MACRAILD, Sébastien MORIN, Gary THOMPSON, Eldon ULRICH
- 5th Annual McGill Biophysical Chemistry Symposium (McGill University, Montreal, Canada). Probing the dynamics of PSE-4: Motion or not ? Sébastien MORIN & Stéphane M. GAGNÉ
- 50th ENC (Asilomar, CA, USA). A toolkit for dynamics and how to relax the BMRB. Edward D'AUVERGNE, Chris MACRAILD, Sébastien MORIN, Gary THOMPSON, Eldon ULRICH
- Biophysical Society 53rd Annual Meeting (Boston, MA, USA). NMR dynamics of PSE-4 β-lactamase: An interplay of ps-ns order and μs-ms motions in the active site. Sébastien MORIN & Stéphane M. GAGNÉ

2008

- MOOT XXI (Windsor, Canada). Consistency tests of spin relaxation data at multiple fields: A prerequisite for the extraction of high quality dynamic information. Sébastien MORIN & Stéphane M. GAGNÉ
- XXIIIrd ICMRBS (San Diego, CA, USA). NMR dynamics of PSE-4 β-lactamase: An interplay of ps-ns order and μs-ms motions in the active site. Sébastien MORIN & Stéphane M. GAGNÉ
- 8th CREFSIP Annual Symposium (Quebec City, Canada). Kinetic and dynamic studies of chimeric β-lactamases. Christopher M. CLOUTHIER, Sébastien MORIN, Sophie GOBEIL, Stéphane M. GAGNÉ & Joëlle N. PELLETIER
- 8th CREFSIP Annual Symposium (Quebec City, Canada). NMR as a tool to study dynamics of class A β-lactamases. Sébastien MORIN & Stéphane M. GAGNÉ
- 91st Canadian Chemistry Conference and Exhibition (Edmonton, Canada). Kinetic and dynamic studies of chimeric β-lactamases. Christopher M. CLOUTHIER, Sébastien MORIN, Sophie GOBEIL, Stéphane M. GAGNÉ & Joëlle N. PELLETIER

- 4th Annual McGill Biophysical Chemistry Symposium (Montreal, Canada). NMR as a tool to study dynamics of class A β-lactamases. Sébastien MORIN & Stéphane M. GAGNÉ

2007

- MOOT XX (Ste-Adèle, Canada). NMR study of multiple timescale dynamics for PSE-4, a 30 kDa β-lactamase. Sébastien MORIN & Stéphane M. GAGNÉ
- 7th CREFSIP Annual Symposium (Quebec City, Canada). Dynamics of the 29.5 kDa Class A β-Lactamase PSE-4 by NMR. Sébastien MORIN & Stéphane M. GAGNÉ
- 3rd Annual McGill Biophysical Chemistry Symposium (Montreal, Canada). Dynamics of the 29.5 kDa class A β-lactamase PSE-4 by NMR. Sébastien MORIN & Stéphane M. GAGNÉ
- Biophysical Society 51st Annual Meeting (Baltimore, MD, USA). Backbone dynamics and amide exchange for the 29.5 kDa class A β-lactamase PSE-4 by NMR. Sébastien MORIN & Stéphane M. GAGNÉ

2006

- XXIInd ICMRBS (Göttingen, Germany). Backbone dynamics and amide exchange for the 29.5 kDa β-lactamase PSE-4 by liquid-state NMR. Sébastien MORIN & Stéphane M. GAGNÉ
- 6th CREFSIP Annual Symposium (Quebec City, Canada). Backbone resonance assignments, ^{15}N spin relaxation and amide exchange for the 29.5 kDa class A β-lactamase PSE-4 from *Pseudomonas aeruginosa* by liquid-state NMR. Sébastien MORIN, Roger C. LEVESQUE & Stéphane M. GAGNÉ

2005

- MOOT XVIII (Hamilton, Canada). Dynamics of the 29.5 kDa class A β-Lactamase PSE-4 by nuclear magnetic resonance: Preliminary results. Sébastien MORIN, Roger C. LEVESQUE & Stéphane M. GAGNÉ
- 5th CREFSIP Annual Symposium (Quebec City, Canada). Dynamics of the 29.5 kDa class A β-lactamase PSE-4 by nuclear magnetic resonance: Preliminary results. Sébastien MORIN, Roger C. LEVESQUE & Stéphane M. GAGNÉ
- 46th ENC (Providence, RI, USA). Dynamics of class A β-lactamase PSE-4 by liquid-state NMR: Preliminary results. Sébastien MORIN, Roger C. LEVESQUE & Stéphane M. GAGNÉ

2004

- Journée de la recherche de la faculté de médecine de l'Université Laval (Quebec City, Canada). Drosophila melanogaster's Hsp22 C-terminus seems flexible in solution within the oligomers. Sébastien MORIN, Stéphane M. GAGNÉ & Robert M. TANGUAY
- 4th CREFSIP Annual Symposium (Quebec City, Canada). Drosophila melanogaster's Hsp22 C-terminus seems flexible in solution within the oligomers. Sébastien MORIN, Stéphane M. GAGNÉ & Robert M. TANGUAY

Research Experience

- **2004 – 2010**
  Nuclear magnetic resonance laboratory: M.Sc. and Ph.D. student
  NMR study of the dynamics of the class A β-lactamase PSE-4.
  Université Laval, CREFSIP/PROTEO, IBIS. Supervisor: Dr Stéphane M. Gagné.
- **2003 – 2004**
  Cellular and developmental genetics laboratory: M.Sc. student
  Drosophila small heat shock protein Hsp22 structure characterisation by NMR.
  Université Laval, CREFSIP, RSVS. Supervisor and co-supervisor: Dr Robert M. Tanguay and Dr Stéphane M. Gagné.

- **2003**
  Protein mass spectrometry and signal transduction laboratories: B.Sc. student
  Development of a screening method for CK2 protein kinase ligands by MALDI-TOF mass spectrometry.
  Université Joseph Fourier, Institut de Biologie Structurale, Commissariat à l'Énergie Atomique (Grenoble, France). Supervisors: Dr Éric Forest and Dr Claude Cochet.
- **2002**
  Cellular and developmental genetics laboratory: B.Sc. student
  Preliminary work for Drosophila small heat shock protein Hsp22 structure characterisation by NMR
  Université Laval, CREFSIP, RSVS. Supervisor: Dr Robert M. Tanguay.
- **2001**
  Molecular endocrinology laboratory: B.Sc. student
  Participation in the different experiments for isolation, kinetics and crystallisation of a steroidian enzyme (17β-HSD type 5).
  Université Laval, Centre Hospitalier de l'Université Laval. Supervisor: Dr Sheng-Xiang Lin.

Other Experiences and Voluntary Work

- **2010**
  Teacher for part (2 weeks) of *Introduction à la bio-informatique* (BIF-1001, Université Laval).
- **2010**
  Teacher for part (2 weeks) of *Protéines* (BCM-2001, Université Laval).
- **2009**
  Teacher for part (6 weeks) of *Détermination de la structure des protéines* (BIF-3001/BCM-4100/BCM-7003, Université Laval).
- **2008 – 2010**
  minfx optimization library project, developer — voluntary work. Development of a collection of minimisation algorithms for use in other open-source programs.
- **2008 – 2009**
  Evaluation committee for the B.Sc. in biochemistry at Université Laval — voluntary work.
- **2008**
  Association des chercheurs étudiants en biochimie et microbiologie de l'Université Laval (ACEBMUL): External vice-president — voluntary work.
- **2008**
  Teaching assistant for *Laboratoire de protéines et d'enzymologie* (BCM-21141, Université Laval).
- **2007 – *Today***
  relax project, developer — voluntary work. Development of an open-source software for the study of protein dynamics by NMR.
- **2007 – 2008**
  Commission des études (Université Laval): Graduate student member (for AELIÉS). The role of this committee is to oversee the creation of new academic programs before they are submitted to the CREPUQ.
- **2007**
  Teaching assistant for *Laboratoire d'acides nucléiques* (BCM-18771, Université Laval).
- **2007**
  Association des chercheurs étudiants en biochimie et microbiologie de l'Université Laval (ACEBMUL): External vice-president — voluntary work.

- **2006 – 2010**
  Responsible for liquid nitrogen fills for the 600 MHz Varian INOVA NMR magnet in Dr Stéphane M. Gagné's laboratory.
- **2006 – 2009**
  BioConneXion 2007, 2008 and 2009 events (organised by CREFSIP students): Member of the organizing committee — voluntary work.
- **2006 – 2007**
  Biochemistry and Microbiology Department (Université Laval): Program committee member as students's representative — voluntary work.
- **2004 – 2007**
  Centre de recherche sur la fonction, la structure et l'ingénierie des protéines (CREFSIP): management committee as student member — voluntary work.
- **2004 – 2006**
  BioConneXion 2005 and 2006 events (organised by CREFSIP students): Manager of the event — voluntary work.

Bibliography

[1] Abragam, A. (1961) *The Principles of Nuclear Magnetism*. Oxford, Clarendon Press.

[2] Adachi, H., Ohta, T. & Matsuzawa, H. (1991) Site-directed mutants, at position 166, of RTEM-1 β-lactamase that form a stable acyl-enzyme intermediate with penicillin. *J. Biol. Chem.*, **266**: 3186–3191.

[3] Akaike, H. (1973) Information theory and an extension of the maximum likelihood principle. In *Proceedings of the 2nd International Symposium on Information Theory*, pages 267–281. Budapest, Akadémiai Kiadó.

[4] Akke, M. (2002) NMR methods for characterizing microsecond to millisecond dynamics in recognition and catalysis. *Curr. Opin. Struct. Biol.*, **12**: 642–647.

[5] Akke, M., Skelton, N. J., Kördel, J., Palmer, A. G. & Chazin, W. J. (1993) Effects of ion binding on the backbone dynamics of calbindin D9k determined by ^{15}N NMR relaxation. *Biochemistry*, **32**: 9832–9844.

[6] Allerhand, A., Doddrell, D., Glushko, V., Cochran, D. W., Wenkert, E., Lawson, P. J. & Gurd, F. R. (1971) Conformation and segmental motion of native and denatured ribonuclease A in solution. Application of natural-abundance carbon-13 partially relaxed Fourier transform nuclear magnetic resonance. *J. Am. Chem. Soc.*, **93**: 544–546.

[7] Ambler, R. P. (1980) The structure of β-lactamases. *Philos. Trans. R. Soc. Lond., B. Biol. Sci.*, **289**: 321–331.

[8] Ambler, R. P., Coulson, A. F., Frère, J. M., Ghuysen, J. M., Joris, B., Forsman, M., Levesque, R. C., Tiraby, G. & Waley, S. G. (1991) A standard numbering scheme for the class A β-lactamases. *Biochem. J.*, **276**: 269–270.

[9] Atanasov, B. P., Mustafi, D. & Makinen, M. W. (2000) Protonation of the β-lactam nitrogen is the trigger event in the catalytic action of class A β-lactamases. *Proc. Natl. Acad. Sci. U.S.A.*, **97**: 3160–3165.

[10] Atkins, P. & De Paula, J. (2006) *Physical Chemistry, 8th Edition*. Oxford University Press.

[11] Bai, Y., Milne, J. S., Mayne, L. & Englander, S. W. (1993) Primary structure effects on peptide group hydrogen exchange. *Proteins*, **17**: 75–86.

[12] Baryshnikova, O., Williams, T. & Sykes, B. (2008) Internal pH indicators for biomolecular NMR. *J. Biomol. NMR*, **41**: 5–7.

[13] Bax, A., Clore, G. M. & Gronenborn, A. M. (1990) ^{1}H—^{1}H correlation via isotropic mixing of ^{13}C magnetization, a new three-dimensional approach for assigning ^{1}H and ^{13}C spectra of ^{13}C-enriched proteins. *J. Magn. Reson.*, **88**: 425–431.

[14] Bebrone, C., Moali, C., Mahy, F., Rival, S., Docquier, J. D., Rossolini, G. M., Fastrez, J., Pratt, R. F., Frère, J. M. & Galleni, M. (2001) CENTA as a chromogenic substrate for studying β-lactamases. *Antimicrob. Agents Chemother.*, **45**: 1868–1871.

[15] Berman, H. M., Westbrook, J., Feng, Z., Gilliland, G., Bhat, T. N., Weissig, H., Shindyalov, I. N. & Bourne, P. E. (2000) The protein data bank. *Nucl. Acids Res.*, **28**: 235–242.

[16] Blackledge, M. (2005) Recent progress in the study of biomolecular structure and dynamics in solution

from residual dipolar couplings. *Prog. NMR. Spectr.*, **46**: 23–61.

[17] Blackledge, M., Cordier, F., Dosset, P. & Marion, D. (1998) Precision and uncertainty in the characterization of anisotropic rotational diffusion by ^{15}N relaxation. *J. Am. Chem. Soc.*, **120**: 4538–4539.

[18] Bloembergen, N., Purcell, E. M. & Pound, R. V. (1948) Relaxation effects in nuclear magnetic resonance absorption. *Phys. Rev.*, **73**: 679–712.

[19] Boissinot, M., Huot, A., Mercier, J. & Levesque, R. C. (1989) Development of gene probes and evolutionary relationships of the PSE-4 bla gene to plasmid-mediated β-lactamases of Gram-negative bacteria. *Mol. Cell. Probes*, **3**: 179–188.

[20] Boissinot, M. & Levesque, R. C. (1990) Nucleotide sequence of the PSE-4 carbenicillinase gene and correlations with the Staphylococcus aureus PC1 β-lactamase crystal structure. *J. Biol. Chem.*, **265**: 1225–1230.

[21] Bolduc, O. R., Clouthier, C. M., Pelletier, J. N. & Masson, J.-F. (2009) Peptide self-assembled monolayers for label-free and unamplified surface plasmon resonance biosensing in crude cell lysate. *Anal Chem*.

[22] Bradford, P. A. (2001) Extended-spectrum β-lactamases in the 21st century: Characterization, epidemiology, and detection of this important resistance threat. *Clin. Microbiol. Rev.*, **14**: 933–951.

[23] Branden, C. & Tooze, J. (1999) *Introduction to Protein Structure, 2nd edition*. Garland Publishing.

[24] Brown, N. G., Shanker, S., Prasad, B. V. V. & Palzkill, T. (2009) Structural and biochemical evidence that a TEM-1 β-lactamase N170G active site mutant acts via substrate-assisted catalysis. *J. Biol. Chem.*, **284**: 33703–33712.

[25] Burnham, K. P. & Andersen, D. R. (1998) *Model selection and inference: A practical information-theoretic approach.* Springer-Verlag.

[26] Bush, K. (2001) New β-lactamases in Gram-negative bacteria: Diversity and impact on the selection of antimicrobial therapy. *Clin. Infect. Dis.*, **32**: 1085–1089.

[27] Bush, K., Jacoby, G. A. & Medeiros, A. A. (1995) A functional classification scheme for β-lactamases and its correlation with molecular structure. *Antimicrob. Agents Chemother.*, **39**: 1211–1233.

[28] Bush, K., Macalintal, C., Rasmussen, B. A., Lee, V. J. & Yang, Y. (1993) Kinetic interactions of tazobactam with β-lactamases from all major structural classes. *Antimicrob. Agents Chemother.*, **37**: 851–858.

[29] Bös, F. & Pleiss, J. (2009) Multiple molecular dynamics simulations of TEM β-lactamase: Dynamics and water binding of the Ω-loop. *Biophys. J.*, **97**: 2550–2558.

[30] Carr, H. Y. & Purcell, E. M. (1954) Effects of diffusion on free precession in nuclear magnetic resonance experiments. *Phys. Rev.*, **94**: 630–638.

[31] Cartwright, S. J. & Coulson, A. F. (1980) Active site of staphylococcal β-lactamase. *Philos. Trans. R. Soc. Lond., B. Biol. Sci.*, **289**: 370–372.

[32] Cartwright, S. J., Tan, A. K. & Fink, A. L. (1989) Trapping the acyl-enzyme intermediate in β-lactamase I catalysis. *Biochem. J.*, **263**: 905–912.

[33] Case, D. A. (1999) Calculations of NMR dipolar coupling strengths in model peptides. *J. Biomol. NMR*, **15**: 95–102.

[34] Case, D. A. (2002) Molecular dynamics and NMR spin relaxation in proteins. *Acc. Chem. Res.*, **35**: 325–331.

[35] Cavanagh, J., Fairbrother, W. J., Palmer, A. G., Rance, M. & Skelton, N. J. (2007) *Protein NMR Spectroscopy: Principles and Practice, 2nd Edition*. Academic Press.

[36] Chain, E., Florey, H. W., Gardner, A. D., Heatley, N. G., Jennings, M. A., Orr-Ewing, J. & Sanders, A. G. (1940) Penicillin as a chemotherapeutic agents. *Lancet*, **236**: 226–228.

[37] Christensen, H., Martin, M. T. & Waley, S. G. (1990) β-lactamases as fully efficient enzymes. Determination of all the rate constants in the acyl-enzyme mechanism. *Biochem. J.*, **266**: 853–861.

[38] Clarke, J., Itzhaki, L. S. & Fersht, A. R. (1997) Hydrogen exchange at equilibrium: A short cut for analysing protein-folding pathways ? *Trends Biochem. Sci.*, **22**: 284–287.

[39] Clore, G. M., Driscoll, P. C., Wingfield, P. T. & Gronenborn, A. M. (1990) Analysis of the backbone dynamics of interleukin-1 β using two-dimensional inverse detected heteronuclear ^{15}N-^{1}H NMR spectroscopy. *Biochemistry*, **29**: 7387–7401.

[40] Clore, G. M., Szabo, A., Bax, A., Kay, L. E., Driscoll, P. C. & Gronenborn, A. M. (1990) Deviations from the simple 2-parameter model-free approach to the interpretation of nitrogen-15 nuclear magnetic-relaxation of proteins. *J. Am. Chem. Soc.*, **112**: 4989–4991.

[41] Cohen, S. A. & Pratt, R. F. (1980) Inactivation of bacillus cereus β-lactamase I by 6 β-bromopencillanic acid: Mechanism. *Biochemistry*, **19**: 3996–4003.

[42] Coles, M., Diercks, T., Muehlenweg, B., Bartsch, S., Zölzer, V., Tschesche, H. & Kessler, H. (1999) The solution structure and dynamics of human neutrophil gelatinase-associated lipocalin. *J. Mol. Biol.*, **289**: 139–157.

[43] Connelly, G. P., Bai, Y., Jeng, M. F. & Englander, S. W. (1993) Isotope effects in peptide group hydrogen exchange. *Proteins*, **17**: 87–92.

[44] Cooper, P. D. (1956) Site of action of radiopenicillin. *Bacteriol. Rev.*, **20**: 28–48.

[45] Cordier, F., Caffrey, M., Brutscher, B., Cusanovich, M. A., Marion, D. & Blackledge, M. (1998) Solution structure, rotational diffusion anisotropy and local backbone dynamics of Rhodobacter capsulatus cytochrome c2. *J. Mol. Biol.*, **281**: 341–361.

[46] Damblon, C., Raquet, X., Lian, L. Y., Lamotte-Brasseur, J., Fonzé, E., Charlier, P., Roberts, G. C. & Frère, J. M. (1996) The catalytic mechanism of β-lactamases: NMR titration of an active-site lysine residue of the TEM-1 enzyme. *Proc. Natl. Acad. Sci. U.S.A.*, **93**: 1747–1752.

[47] d'Auvergne, E. J. (2006) *Protein dynamics: A study of the model-free analysis of NMR relaxation data.* Ph.D. thesis, Biochemistry and Molecular Biology, University of Melbourne (Australia). http://eprints.infodiv.unimelb.edu.au/archive/00002799/.

[48] d'Auvergne, E. J. & Gooley, P. R. (2003) The use of model selection in the model-free analysis of protein dynamics. *J. Biomol. NMR.*, **25**: 25–39.

[49] d'Auvergne, E. J. & Gooley, P. R. (2006) Model-free model elimination: A new step in the model-free dynamic analysis of NMR relaxation data. *J. Biomol. NMR*, **35**: 117–135.

[50] d'Auvergne, E. J. & Gooley, P. R. (2007) Set theory formulation of the model-free problem and the diffusion seeded model-free paradigm. *Mol. Biosyst.*, **3**: 483–494.

[51] d'Auvergne, E. J. & Gooley, P. R. (2008) Optimisation of NMR dynamic models I. Minimisation algorithms and their performance within the model-free and brownian rotational diffusion spaces. *J. Biomol. NMR*, **40**: 107–119.

[52] d'Auvergne, E. J. & Gooley, P. R. (2008) Optimisation of NMR dynamic models II. A new methodology for the dual optimisation of the model-free parameters and the Brownian rotational diffusion tensor. *J. Biomol. NMR*, **40**: 121–133.

[53] Davies, J. (1994) Inactivation of antibiotics and the dissemination of resistance genes. *Science*, **264**: 375–382.

[54] De Wals, P.-Y., Doucet, N. & Pelletier, J. N. (2009) High tolerance to simultaneous active-site mutations in TEM-1 β-lactamase: Distinct mutational paths provide more generalized β-lactam recognition. *Protein*

Sci., **18**: 147–160.

[55] Delaglio, F., Grzesiek, S., Vuister, G. W., Zhu, G., Pfeifer, J. & Bax, A. (1995) NMRPipe: A multidimensional spectral processing system based on UNIX pipes. *J. Biomol. NMR*, **6**: 277–293.

[56] Dellwo, M. J. & Wand, A. J. (1989) Model-independent and model-dependent analysis of the global and internal dynamics of cyclosporin A. *J. Am. Chem. Soc.*, **111**: 4571–4578.

[57] Devore, J. (1982) *Probability and Statistics for Engineering and the Sciences*. Brooks/Cole Publishing Company.

[58] Ding, Z., Lee, G., Liang, X., Gallazzi, F., Arunima, A. & Doren, S. R. V. (2005) PhosphoThr peptide binding globally rigidifies much of the FHA domain from Arabidopsis receptor kinase-associated protein phosphatase. *Biochemistry*, **44**: 10119–10134.

[59] Dive, G. & Dehareng, D. (1999) Serine peptidase catalytic machinery: Cooperative one-step mechanism. *Int. J. Quant. Chem.*, **73**: 161–174.

[60] Dosset, P., Hus, J. C., Blackledge, M. & Marion, D. (2000) Efficient analysis of macromolecular rotational diffusion from heteronuclear relaxation data. *J. Biomol. NMR*, **16**: 23–28.

[61] Doucet, N. & Pelletier, J. N. (2007) Simulated annealing exploration of an active-site tyrosine in TEM-1 β-lactamase suggests the existence of alternate conformations. *Proteins*, **69**: 340–348.

[62] Doucet, N., Savard, P.-Y., Pelletier, J. N. & Gagné, S. M. (2007) NMR investigation of Tyr105 mutants in TEM-1 β-lactamase: Dynamics are correlated with function. *J. Biol. Chem.*, **282**: 21448–21459.

[63] Doucet, N., Wals, P.-Y. D. & Pelletier, J. N. (2004) Site-saturation mutagenesis of Tyr-105 reveals its importance in substrate stabilization and discrimination in TEM-1 β-lactamase. *J. Biol. Chem.*, **279**: 46295–46303.

[64] Drummond, D. A., Silberg, J. J., Meyer, M. M., Wilke, C. O. & Arnold, F. H. (2005) On the conservative nature of intragenic recombination. *Proc. Natl. Acad. Sci. U.S.A.*, **102**: 5380–5385.

[65] Díaz, N., Sordo, T. L., Merz Jr., K. M. & Suárez, D. (2003) Insights into the acylation mechanism of class A β-lactamases from molecular dynamics simulations of the TEM-1 enzyme complexed with benzylpenicillin. *J. Am. Chem. Soc.*, **125**: 672–684.

[66] Díaz, N., Suárez, D., Merz, K. M. & Sordo, T. L. (2005) Molecular dynamics simulations of the TEM-1 β-lactamase complexed with cephalothin. *J. Med. Chem.*, **48**: 780–791.

[67] Díaz, N., Suárez, D., Sordo, T. & Merz, K. (2001) Acylation of class A β-lactamases by penicillins: A theoretical examination of the role of Serine 130 and the β-lactam carboxylate group. *J. Phys. Chem., Ser. B*, **105**: 11302–11313.

[68] Einstein, A. (1905) Über die von der molekularkinetischen Theorie der Wärme geforderte Bewegung von in ruhenden Flüssigkeiten suspendierten Teilchen. *Ann. Phys.*, **17**: 891–921.

[69] Englander, S. W. & Kallenbach, N. R. (1983) Hydrogen exchange and structural dynamics of proteins and nucleic acids. *Q. Rev. Biophys.*, **16**: 521–655.

[70] Englander, S. W. & Mayne, L. (1992) Protein folding studied using hydrogen-exchange labeling and two-dimensional NMR. *Annu. Rev. Biophys. Biomol. Struct.*, **21**: 243–265.

[71] Englander, S. W., Mayne, L., Bai, Y. & Sosnick, T. R. (1997) Hydrogen exchange: The modern legacy of Linderstrøm-Lang. *Protein Sci.*, **6**: 1101–1109.

[72] Errington, J., Daniel, R. A. & Scheffers, D.-J. (2003) Cytokinesis in bacteria. *Microbiol. Mol. Biol. Rev.*, **67**: 52–65.

[73] Escobar, W. A., Tan, A. K. & Fink, A. L. (1991) Site-directed mutagenesis of β-lactamase leading to accumulation of a catalytic intermediate. *Biochemistry*, **30**: 10783–10787.

[74] Eyles, S. J. & Kaltashov, I. A. (2004) Methods to study protein dynamics and folding by mass

spectrometry. *Methods*, **34**: 88–99.

[75] Farrow, N., Zhang, O., Szabo, A., Torchia, D. & Kay, L. E. (1995) Spectral density function mapping using ^{15}N relaxation data exclusively. *J. Biomol. NMR*, **6**: 153–162.

[76] Farrow, N. A., Muhandiram, R., Singer, A. U., Pascal, S. M., Kay, C. M., Gish, G., Shoelson, S. E., Pawson, T., Forman-Kay, J. D. & Kay, L. E. (1994) Backbone dynamics of a free and phosphopeptide-complexed Src homology 2 domain studied by ^{15}N NMR relaxation. *Biochemistry*, **33**: 5984–6003.

[77] Fetrow, J. S. (1995) Omega loops: Nonregular secondary structures significant in protein function and stability. *FASEB J.*, **9**: 708–717.

[78] Fischer, M. W. F., Majumdar, A. & Zuiderweg, E. R. P. (1998) Protein NMR relaxation: Theory, application and outlook. *Prog. Nucl. Magn. Reson. Spec.*, **33**: 207–272.

[79] Fisette, O., Morin, S., Savard, P.-Y., Lagüe, P. & Gagné, S. (2010) TEM-1 backbone dynamics – Insights from combined molecular dynamics and nuclear magnetic resonance. *Biophys. J.*, **98**: 637–645.

[80] Fisher, J., Charnas, R. L., Bradley, S. M. & Knowles, J. R. (1981) Inactivation of the RTEM β-lactamase from Escherichia coli. Interaction of penam sulfones with enzyme. *Biochemistry*, **20**: 2726–2731.

[81] Fisher, J. F., Meroueh, S. O. & Mobashery, S. (2005) Bacterial resistance to β-lactam antibiotics: Compelling opportunism, compelling opportunity. *Chem. Rev.*, **105**: 395–424.

[82] Fleming, A. (1929) On the antibacterial action of cultures of a penicillium, with special reference to their use in the isolation of B. influenzae. *Br. J. Exp. Path.*, **10**: 226–236.

[83] Fonzé, E., Charlier, P., To'th, Y., Vermeire, M., Raquet, X., Dubus, A. & Frère, J. M. (1995) TEM1 β-lactamase structure solved by molecular replacement and refined structure of the S235A mutant. *Acta Crystallogr. D. Biol. Crystallogr.*, **51**: 682–694.

[84] Franzoni, L., Lücke, C., Pérez, C., Cavazzini, D., Rademacher, M., Ludwig, C., Spisni, A., Rossi, G. L. & Rüterjans, H. (2002) Structure and backbone dynamics of apo- and holo-cellular retinol-binding protein in solution. *J. Biol. Chem.*, **277**: 21983–21997.

[85] Frère, J. M. (1995) β-lactamases and bacterial resistance to antibiotics. *Mol. Microbiol.*, **16**: 385–395.

[86] Furth, A. J. (1975) Purification and properties of a constitutive β-lactamase from Pseudomonas aeruginosa strain Dalgleish. *Biochim. Biophys. Acta.*, **377**: 431–443.

[87] Fushman, D., Cahill, S. & Cowburn, D. (1997) The main-chain dynamics of the dynamin pleckstrin homology (PH) domain in solution: Analysis of ^{15}N relaxation with monomer/dimer equilibration. *J. Mol. Biol.*, **266**: 173–194.

[88] Fushman, D., Tjandra, N. & Cowburn, D. (1998) Direct measurement of ^{15}N chemical shift anisotropy in solution. *J. Am. Chem. Soc.*, **120**: 10947–10952.

[89] Fushman, D., Tjandra, N. & Cowburn, D. (1999) An approach to direct determination of protein dynamics from ^{15}N NMR relaxation at multiple fields, independent of variable ^{15}N chemical shift anisotropy and chemical exchange contributions. *J. Am. Chem. Soc.*, **121**: 8577–8582.

[90] Gabel, F., Bicout, D., Lehnert, U., Tehei, M., Weik, M. & Zaccai, G. (2002) Protein dynamics studied by neutron scattering. *Q. Rev. Biophys.*, **35**: 327–367.

[91] Gagné, S. M., Tsuda, S., Spyracopoulos, L., Kay, L. E. & Sykes, B. D. (1998) Backbone and methyl dynamics of the regulatory domain of troponin C: Anisotropic rotational diffusion and contribution of conformational entropy to calcium affinity. *J. Mol. Biol.*, **278**: 667–686.

[92] García de la Torre, J., Huertas, M. L. & Carrasco, B. (2000) HYDRONMR: Prediction of NMR relaxation of globular proteins from atomic-level structures and hydrodynamic calculations. *J. Magn. Reson.*, **147**: 138–146.

[93] Ghrayeb, J., Kimura, H., Takahara, M., Hsiung, H., Masui, Y. & Inouye, M. (1984) Secretion cloning vectors in Escherichia coli. *EMBO J.*, **3**: 2437–2442.

[94] Ghuysen, J. M. (1991) Serine β-lactamases and penicillin-binding proteins. *Annu. Rev. Microbiol.*, **45**: 37–67.

[95] Gibson, R. M., Christensen, H. & Waley, S. G. (1990) Site-directed mutagenesis of β-lactamase I. Single and double mutants of Glu-166 and Lys-73. *Biochem. J.*, **272**: 613–619.

[96] Go, A., Kim, S., Baum, J. & Hecht, M. H. (2008) Structure and dynamics of de novo proteins from a designed superfamily of 4-helix bundles. *Protein Sci.*, **17**: 821–832.

[97] Golemi-Kotra, D., Meroueh, S. O., Kim, C., Vakulenko, S. B., Bulychev, A., Stemmler, A. J., Stemmler, T. L. & Mobashery, S. (2004) The importance of a critical protonation state and the fate of the catalytic steps in class A β-lactamases and penicillin-binding proteins. *J. Biol. Chem.*, **279**: 34665–34673.

[98] Gretes, M., Lim, D. C., de Castro, L., Jensen, S. E., Kang, S. G., Lee, K. J. & Strynadka, N. C. (2009) Insights into positive and negative requirements for protein-protein interactions by crystallographic analysis of the β-lactamase inhibitory proteins BLIP, BLIP-I, and BLP. *J. Mol. Biol.*, **389**: 289–305.

[99] Gronwald, W., Boyko, R., Sönnichsen, F., Wishart, D. & Sykes, B. D. (1997) Orb, a homology-based program for the prediction of protein NMR chemical shifts. *J. Biomol. NMR*, **10**: 165–181.

[100] Grzesiek, S., Anglister, J. & Bax, A. (1993) Correlation of backbone amide and aliphatic side-chain resonances in $^{13}C/^{15}N$-enriched proteins by isotropic mixing of ^{13}C magnetization. *J. Magn. Reson., Ser. B*, **101**: 114–119.

[101] Grzesiek, S. & Bax, A. (1992) Correlating backbone amide and side chain resonances in larger proteins by multiple relayed triple resonance NMR. *J. Am. Chem. Soc.*, **114**: 6291–6293.

[102] Grzesiek, S. & Bax, A. (1992) Improved 3D triple-resonance NMR techniques applied to a 31 kDa proteins. *J. Magn. Reson.*, **96**: 432–440.

[103] Grzesiek, S. & Bax, A. (1997) A three-dimensional NMR experiment with improved sensitivity for carbonyl-carbonyl J correlation in proteins. *J. Biomol. NMR*, **9**: 207–211.

[104] Guillaume, G., Vanhove, M., Lamotte-Brasseur, J., Ledent, P., Jamin, M., Joris, B. & Frère, J. M. (1997) Site-directed mutagenesis of glutamate 166 in two β-lactamases. Kinetic and molecular modeling studies. *J. Biol. Chem.*, **272**: 5438–5444.

[105] Hahn, E. L. (1950) Spin echoes. *Phys. Rev.*, **80**: 580–594.

[106] Hall, B. G. & Barlow, M. (2004) Evolution of the serine β-lactamases: Past, present and future. *Drug. Resist. Updat.*, **7**: 111–123.

[107] Hall, J. B. & Fushman, D. (2003) Characterization of the overall and local dynamics of a protein with intermediate rotational anisotropy: Differentiating between conformational exchange and anisotropic diffusion in the B3 domain of protein G. *J. Biomol. NMR*, **27**: 261–275.

[108] Hansen, D. F., Vallurupalli, P. & Kay, L. E. (2008) An improved ^{15}N relaxation dispersion experiment for the measurement of millisecond time-scale dynamics in proteins. *J. Phys. Chem. B*, **112**: 5898–5904.

[109] Hansen, D. F., Yang, D., Feng, H., Zhou, Z., Wiesner, S., Bai, Y. & Kay, L. E. (2007) An exchange-free measure of ^{15}N transverse relaxation: An NMR spectroscopy application to the study of a folding intermediate with pervasive chemical exchange. *J. Am. Chem. Soc.*, **129**: 11468–11479.

[110] Hayes, F., Hallet, B. & Cao, Y. (1997) Insertion mutagenesis as a tool in the modification of protein function. Extended substrate specificity conferred by pentapeptide insertions in the Ω-loop of TEM-1 β-lactamase. *J. Biol. Chem.*, **272**: 28833–28836.

[111] Hedstrom, L. (2002) Serine protease mechanism and specificity. *Chem. Rev.*, **102**: 4501–4524.

[112] Hermann, J. C., Hensen, C., Ridder, L., Mulholland, A. J. & Höltje, H.-D. (2005) Mechanisms

of antibiotic resistance: QM/MM modeling of the acylation reaction of a class A β-lactamase with benzylpenicillin. *J. Am. Chem. Soc.*, **127**: 4454–4465.

[113] Hermann, J. C., Pradon, J., Harvey, J. N. & Mulholland, A. J. (2009) High level QM/MM modeling of the formation of the tetrahedral intermediate in the acylation of wild type and K73A mutant TEM-1 class A β-lactamase. *J. Phys. Chem. A*, **113**: 11984–11994.

[114] Hermann, J. C., Ridder, L., Höltje, H.-D. & Mulholland, A. J. (2006) Molecular mechanisms of antibiotic resistance: QM/MM modelling of deacylation in a class A β-lactamase. *Org. Biomol. Chem.*, **4**: 206–210.

[115] Hermann, J. C., Ridder, L., Mulholland, A. J. & Höltje, H.-D. (2003) Identification of Glu166 as the general base in the acylation reaction of class A β-lactamases through QM/MM modeling. *J. Am. Chem. Soc.*, **125**: 9590–9591.

[116] Herzberg, O. & Moult, J. (1987) Bacterial resistance to β-lactam antibiotics: Crystal structure of β-lactamase from Staphylococcus aureus PC1 at 2.5 Å resolution. *Science*, **236**: 694–701.

[117] Horn, J. R. & Shoichet, B. K. (2004) Allosteric inhibition through core disruption. *J. Mol. Biol.*, **336**: 1283–1291.

[118] Huang, W., Petrosino, J., Hirsch, M., Shenkin, P. S. & Palzkill, T. (1996) Amino acid sequence determinants of β-lactamase structure and activity. *J. Mol. Biol.*, **258**: 688–703.

[119] Hung, L.-H. & Samudrala, R. (2003) Accurate and automated classification of protein secondary structure with PsiCSI. *Protein Sci.*, **12**: 288–295.

[120] Hurvich, C. & Tsai, C.-L. (1989) Regression and time series model selection in small samples. *Biometrika*, **76**: 297–307.

[121] Igumenova, T. I., Frederick, K. K. & Wand, A. J. (2006) Characterization of the fast dynamics of protein amino acid side chains using NMR relaxation in solution. *Chem. Rev.*, **106**: 1672–1699.

[122] Ikura, M., Kay, L. E. & Bax, A. (1990) A novel approach for sequential assignment of ^{1}H, ^{13}C, and ^{15}N spectra of proteins: Heteronuclear triple-resonance three-dimensional NMR spectroscopy. Application to calmodulin. *Biochemistry*, **29**: 4659–4667.

[123] Imtiaz, U., Billings, E., Knox, J. R., Manavathu, E. K., Lerner, S. A. & Mobashery, S. (1993) Inactivation of class A β-lactamases by clavulanic acid: The role of arginine-244 in a proposed nonconcerted sequence of events. *J. Am. Chem. Soc.*, **115**: 4435–4442.

[124] Imtiaz, U., Billings, E. M., Knox, J. R. & Mobashery, S. (1994) A structure-based analysis of the inhibition of class A β-lactamases by sulbactam. *Biochemistry*, **33**: 5728–5738.

[125] Ishima, R. & Torchia, D. A. (1999) Estimating the time scale of chemical exchange of proteins from measurements of transverse relaxation rates in solution. *J. Biomol. NMR*, **14**: 369–372.

[126] Ishima, R. & Torchia, D. A. (2000) Protein dynamics from NMR. *Nat. Struct. Biol.*, **7**: 740–743.

[127] Jarymowycz, V. A. & Stone, M. J. (2006) Fast time scale dynamics of protein backbones: NMR relaxation methods, applications, and functional consequences. *Chem. Rev.*, **106**: 1624–1671.

[128] Jaurin, B. & Grundström, T. (1981) AmpC cephalosporinase of Escherichia coli K-12 has a different evolutionary origin from that of β-lactamases of the penicillinase type. *Proc. Natl. Acad. Sci. U.S.A.*, **78**: 4897–4901.

[129] Jelsch, C., Mourey, L., Masson, J. M. & Samama, J. P. (1993) Crystal structure of Escherichia coli TEM1 β-lactamase at 1.8 Å resolution. *Proteins*, **16**: 364–383.

[130] John, B. K., Plant, D. & Hurd, R. E. (1993) Improved proton-detected heteronuclear correlation using gradient-enhanced z and zz filters. *J. Magn. Reson., Ser. A*, **101**: 113–117.

[131] Johnson, B. & Blevins, R. (1994) NMR view: A computer program for the visualization and analysis of NMR data. *J. Biomol. NMR.*, **4**: 603–614.

[132] Jones, R. N., Wilson, H. W., Novick, W. J., Barry, A. L. & Thornsberry, C. (1982) In vitro evaluation of CENTA, a new β-lactamase-susceptible chromogenic cephalosporin reagent. *J. Clin. Microbiol.*, **15**: 954–958.

[133] Kabsch, W. & Sander, C. (1983) Dictionary of protein secondary structure: Pattern recognition of hydrogen-bonded and geometrical features. *Biopolymers*, **22**: 2577–2637.

[134] Karplus, M. (2003) Molecular dynamics of biological macromolecules: A brief history and perspective. *Biopolymers*, **68**: 350–358.

[135] Kather, I., Jakob, R. P., Dobbek, H. & Schmid, F. X. (2008) Increased folding stability of TEM-1 β-lactamase by in vitro selection. *J. Mol. Biol.*, **383**: 238–251.

[136] Kay, L. E. (1998) Protein dynamics from NMR. *Biochem. Cell. Biol.*, **76**: 145–152.

[137] Kay, L. E. (2005) NMR studies of protein structure and dynamics. *J. Magn. Reson.*, **173**: 193–207.

[138] Kay, L. E., Keifer, P. & Saarinen, T. (1992) Pure absorption gradient enhanced heteronuclear single quantum correlation spectroscopy with improved sensitivity. *J. Am. Chem. Soc.*, **114**: 10663–10665.

[139] Kay, L. E., Torchia, D. A. & Bax, A. (1989) Backbone dynamics of proteins as studied by ^{15}N inverse detected heteronuclear NMR spectroscopy: Application to staphylococcal nuclease. *Biochemistry*, **28**: 8972–8979.

[140] Kay, L. E., Xu, G.-Y., Singer, A., Muhandiram, D. & Forman-Kay, J. (1993) A gradient-enhanced HCCH-TOCSY experiment for recording side-chain ^{1}H and ^{13}C correlations in H_2O samples of proteins. *J. Magn. Reson., Ser. B*, **101**: 333–337.

[141] Kay, L. E., Xu, G. Y. & Yamazaki, T. (1994) Enhanced-sensitivity triple-resonance spectroscopy with minimal H_2O saturation. *J. Magn. Reson., Ser. A*, **109**: 129–133.

[142] Kempf, J. G., Jung, J.-Y., Ragain, C., Sampson, N. S. & Loria, J. P. (2007) Dynamic requirements for a functional protein hinge. *J. Mol. Biol.*, **368**: 131–149.

[143] Kempf, J. G. & Loria, J. P. (2003) Protein dynamics from solution NMR: Theory and applications. *Cell. Biochem. Biophys.*, **37**: 187–211.

[144] Knox, J. R. (1995) Extended-spectrum and inhibitor-resistant TEM-type β-lactamases: Mutations, specificity, and three-dimensional structure. *Antimicrob. Agents Chemother.*, **39**: 2593–2601.

[145] Koch, A. L. (2003) Bacterial wall as target for attack: Past, present, and future research. *Clin. Microbiol. Rev.*, **16**: 673–687.

[146] Koradi, R., Billeter, M. & Wüthrich, K. (1996) Molmol: a program for display and analysis of macromolecular structures. *J. Mol. Graph.*, **14**: 51–55.

[147] Korzhnev., D. M., Billeter, M., Arseniev, A. S. & Orekhov, V. Y. (2001) NMR studies of Brownian tumbling and internal motions in proteins. *Prog. Nucl. Magn. Reson. Spectros.*, **38**: 197–266.

[148] Korzhnev, D. M., Neudecker, P., Mittermaier, A., Orekhov, V. Y. & Kay, L. E. (2005) Multiple-site exchange in proteins studied with a suite of six NMR relaxation dispersion experiments: An application to the folding of a Fyn SH3 domain mutant. *J. Am. Chem. Soc.*, **127**: 15602–15611.

[149] Korzhnev, D. M., Salvatella, X., Vendruscolo, M., Nardo, A. A. D., Davidson, A. R., Dobson, C. M. & Kay, L. E. (2004) Low-populated folding intermediates of Fyn SH3 characterized by relaxation dispersion NMR. *Nature*, **430**: 586–590.

[150] Kovrigin, E. L., Kempf, J. G., Grey, M. J. & Loria, J. P. (2006) Faithful estimation of dynamics parameters from CPMG relaxation dispersion measurements. *J. Magn. Reson.*, **180**: 93–104.

[151] Krishna, M. M. G., Hoang, L., Lin, Y. & Englander, S. W. (2004) Hydrogen exchange methods to study protein folding. *Methods*, **34**: 51–64.

[152] Kroenke, C. D., Rance, M. & Palmer, A. G. (1999) Variability of the ^{15}N chemical shift anisotropy in

Escherichia coli ribonuclease H in solution. *J. Am. Chem. Soc.*, **121**: 10119–10125.

[153] Kuriyan, J., Petsko, G. A., Levy, R. M. & Karplus, M. (1986) Effect of anisotropy and anharmonicity on protein crystallographic refinement. An evaluation by molecular dynamics. *J. Mol. Biol.*, **190**: 227–254.

[154] Křížová, H., Žídek, L., Stone, M. J., Novotny, M. V. & Sklenář, V. (2004) Temperature-dependent spectral density analysis applied to monitoring backbone dynamics of major urinary protein-I complexed with the pheromone 2-sec-butyl-4,5-dihydrothiazole. *J Biomol. NMR*, **28**: 369–384.

[155] Lamotte-Brasseur, J., Dive, G., Dideberg, O., Charlier, P., Frère, J. M. & Ghuysen, J. M. (1991) Mechanism of acyl transfer by the class A serine β-lactamase of Streptomyces albus G. *Biochem. J.*, **279**: 213–221.

[156] Lamotte-Brasseur, J., Jacob-Dubuisson, F., Dive, G., Frère, J. M. & Ghuysen, J. M. (1992) Streptomyces albus G serine β-lactamase. Probing of the catalytic mechanism via molecular modelling of mutant enzymes. *Biochem. J.*, **282**: 189–195.

[157] Lamotte-Brasseur, J., Lounnas, V., Raquet, X. & Wade, R. C. (1999) pKa calculations for class A β-lactamases: Influence of substrate binding. *Protein Sci.*, **8**: 404–409.

[158] Lee, A. L., Kinnear, S. A. & Wand, A. J. (2000) Redistribution and loss of side chain entropy upon formation of a calmodulin-peptide complex. *Nat. Struct. Biol.*, **7**: 72–77.

[159] Lee, A. L. & Wand, A. J. (1999) Assessing potential bias in the determination of rotational correlation times of proteins by NMR relaxation. *J. Biomol. NMR*, **13**: 101–112.

[160] Lefèvre, J. F., Dayie, K. T., Peng, J. W. & Wagner, G. (1996) Internal mobility in the partially folded DNA binding and dimerization domains of GAL4: NMR analysis of the N-H spectral density functions. *Biochemistry*, **35**: 2674–2686.

[161] Levitt, M. (2001) *Spin Dynamics*. John Wiley & Sons.

[162] Li, Z., Raychaudhuri, S. & Wand, A. J. (1996) Insights into the local residual entropy of proteins provided by NMR relaxation. *Protein Sci.*, **5**: 2647–2650.

[163] Lietz, E. J., Truher, H., Kahn, D., Hokenson, M. J. & Fink, A. L. (2000) Lysine-73 is involved in the acylation and deacylation of β-lactamase. *Biochemistry*, **39**: 4971–4981.

[164] Lim, D., Park, H. U., Castro, L. D., Kang, S. G., Lee, H. S., Jensen, S., Lee, K. J. & Strynadka, N. C. (2001) Crystal structure and kinetic analysis of β-lactamase inhibitor protein-II in complex with TEM-1 β-lactamase. *Nat. Struct. Biol.*, **8**: 848–852.

[165] Lim, D., Sanschagrin, F., Passmore, L., Castro, L. D., Levesque, R. C. & Strynadka, N. C. (2001) Insights into the molecular basis for the carbenicillinase activity of PSE-4 β-lactamase from crystallographic and kinetic studies. *Biochemistry*, **40**: 395–402.

[166] Linderstrøm-Lang, K. (1955) Deuterium exchange between peptides and water. *Chem. Soc. Spec. Publ.*, **2**: 1–20.

[167] Lipari, G. & Szabo, A. (1982) Model-free approach to the interpretation of nuclear magnetic resonance relaxation in macromolecules. 1. Theory and range of validity. *J. Am. Chem. Soc.*, **104**: 4546–4559.

[168] Lipari, G. & Szabo, A. (1982) Model-free approach to the interpretation of nuclear magnetic resonance relaxation in macromolecules. 2. Analysis of experimental results. *J. Am. Chem. Soc.*, **104**: 4559–4570.

[169] Lowbury, E. J., Lilly, H. A., Kidson, A., Ayliffe, G. A. & Jones, R. J. (1969) Sensitivity of Pseudomonas aeruginosa to antibiotics: Emergence of strains highly resistant to carbenicillin. *Lancet*, **2**: 448–452.

[170] Lyons, B. A. & Montelione, G. T. (1993) An HCCNH triple-resonance experiment using carbon-13 isotropic mixing for correlating backbone amide and side-chain aliphatic resonances in isotopically enriched proteins. *J. Magn. Reson., Ser. B*, **101**: 206–209.

[171] Ma, L., Hass, M. A. S., Vierick, N., Kristensen, S. M., Ulstrup, J. & Led, J. J. (2003) Backbone dynamics

of reduced plastocyanin from the cyanobacterium Anabaena variabilis: Regions involved in electron transfer have enhanced mobility. *Biochemistry*, **42**: 320–330.

[172] Mack, J. W., Usha, M. G., Long, J., Griffin, R. G. & Wittebort, R. J. (2000) Backbone motions in a crystalline protein from field-dependent ^{2}H-NMR relaxation and line-shape analysis. *Biopolymers*, **53**: 9–18.

[173] Madgwick, P. J. & Waley, S. G. (1987) β-lactamase I from Bacillus cereus. Structure and site-directed mutagenesis. *Biochem. J.*, **248**: 657–662.

[174] Mandel, A. M., Akke, M. & Palmer, A. G. (1995) Backbone dynamics of Escherichia coli ribonuclease HI: Correlations with structure and function in an active enzyme. *J. Mol. Biol.*, **246**: 144–163.

[175] Marciano, D. C., Pennington, J. M., Wang, X., Wang, J., Chen, Y., Thomas, V. L., Shoichet, B. K. & Palzkill, T. (2008) Genetic and structural characterization of an L201P global suppressor substitution in TEM-1 β-lactamase. *J. Mol. Biol.*, **384**: 151–164.

[176] Massova, I. & Mobashery, S. (1998) Kinship and diversification of bacterial penicillin-binding proteins and β-lactamases. *Antimicrob. Agents Chemother.*, **42**: 1–17.

[177] Matagne, A., Dubus, A., Galleni, M. & Frère, J. M. (1999) The β-lactamase cycle: A tale of selective pressure and bacterial ingenuity. *Nat. Prod. Rep.*, **16**: 1–19.

[178] Matagne, A., Lamotte-Brasseur, J. & Frère, J. M. (1998) Catalytic properties of class A β-lactamases: Efficiency and diversity. *Biochem. J.*, **330**: 581–598.

[179] Maveyraud, L., Massova, I., Birck, C., Miyashita, K., Samama, J.-P. & Mobashery, S. (1996) Crystal structure of 6α-(hydroxymethyl)penicillanate complexed to the TEM-1 β-lactamase from Escherichia coli: Evidence on the mechanism of action of a novel inhibitor designed by a computer-aided process. *J. Am. Chem. Soc.*, **118**: 7435–7440.

[180] Maveyraud, L., Mourey, L., Kotra, L., Pedelacq, J., Guillet, V., Mobashery, S. & Samama, J. (1998) Structural basis for clinical longevity of carbapenem antibiotics in the face of challenge by the common class A β-lactamase from antibiotic-resistant bacteria. *J. Am. Chem. Soc.*, **120**: 9748–9752.

[181] Maveyraud, L., Pratt, R. F. & Samama, J. P. (1998) Crystal structure of an acylation transition-state analog of the TEM-1 β-lactamase. Mechanistic implications for class A β-lactamases. *Biochemistry*, **37**: 2622–2628.

[182] McIntosh, L. P. & Dahlquist, F. W. (1990) Biosynthetic incorporation of ^{15}N and ^{13}C for assignment and interpretation of nuclear magnetic resonance spectra of proteins. *Q. Rev. Biophys.*, **23**: 1–38.

[183] Meiboom, S. & Gill, D. (1958) Modified spin-echo method for measuring nuclear relaxation times. *Rev. Sci. Instrum.*, **29**: 688–691.

[184] Meroueh, S. O., Fisher, J. F., Schlegel, H. B. & Mobashery, S. (2005) Ab initio QM/MM study of class a β-lactamase acylation: Dual participation of Glu166 and Lys73 in a concerted base promotion of Ser70. *J. Am. Chem. Soc.*, **127**: 15397–15407.

[185] Meroueh, S. O., Roblin, P., Golemi, D., Maveyraud, L., Vakulenko, S. B., Zhang, Y., Samama, J.-P. & Mobashery, S. (2002) Molecular dynamics at the root of expansion of function in the M69L inhibitor-resistant TEM β-lactamase from Escherichia coli. *J. Am. Chem. Soc.*, **124**: 9422–9430.

[186] Metropolis, N. & Ulam, S. (1949) The Monte Carlo method. *J. Am. Stat. Assoc.*, **44**: 335–341.

[187] Meyer, M. M., Silberg, J. J., Voigt, C. A., Endelman, J. B., Mayo, S. L., Wang, Z.-G. & Arnold, F. H. (2003) Library analysis of SCHEMA-guided protein recombination. *Protein Sci.*, **12**: 1686–1693.

[188] Michaelis, L. & Menten, M. L. (1913) Kinetik der Invertinwirkung. *Biochem. Z.*, **49**: 333–369.

[189] Millet, O., Loria, J., Kroenke, C., Pons, M. & Palmer, A. (2000) The static magnetic field dependence of chemical exchange linebroadening defines the NMR chemical shift time scale. *J. Am. Chem. Soc.*, **122**: 2867–2877.

[190] Minasov, G., Wang, X. & Shoichet, B. K. (2002) An ultrahigh resolution structure of TEM-1 β-lactamase suggests a role for Glu166 as the general base in acylation. *J. Am. Chem. Soc.*, **124**: 5333–5340.

[191] Moews, P. C., Knox, J. R., Dideberg, O., Charlier, P. & Frère, J. M. (1990) β-lactamase of Bacillus licheniformis 749/C at 2 Å resolution. *Proteins*, **7**: 156–171.

[192] Moffat, K. (2001) Time-resolved biochemical crystallography: A mechanistic perspective. *Chem. Rev.*, **101**: 1569–1582.

[193] Morin, S., Clouthier, C. M., Gobeil, S., Pelletier, J. N. & Gagné, S. M. (In press) Backbone resonance assignments of a TEM-1/PSE-4 class A β-lactamase chimera. *Biomol. NMR Assign.*

[194] Morin, S. & Gagné, S. M. (2009) NMR dynamics of PSE-4 β-lactamase: An interplay of ps-ns order and μs-ms motions in the active site. *Biophys. J.*, **96**: 4681–4691.

[195] Morin, S. & Gagné, S. M. (2009) Simple tests for the validation of multiple field spin relaxation data. *J. Biomol. NMR*, **45**: 361–372.

[196] Morin, S., Levesque, R. C. & Gagné, S. M. (2006) ^{1}H, ^{13}C, and ^{15}N backbone resonance assignments for PSE-4, a 29.5 kDa class A β-lactamase from Pseudomonas aeruginosa. *J. Biomol. NMR*, **36 Suppl 1**: 11.

[197] Muhandiram, D. R. & Kay, L. E. (1994) Gradient-enhanced triple-resonance three-dimensional NMR experiments with improved sensitivity. *J. Magn. Reson., Ser. B*, **103**: 203–216.

[198] Mulder, F. A., Skrynnikov, N. R., Hon, B., Dahlquist, F. W. & Kay, L. E. (2001) Measurement of slow (μs-ms) time scale dynamics in protein side chains by ^{15}N relaxation dispersion NMR spectroscopy: Application to Asn and Gln residues in a cavity mutant of T4 lysozyme. *J. Am. Chem. Soc.*, **123**: 967–975.

[199] Ness, S., Martin, R., Kindler, A. M., Paetzel, M., Gold, M., Jensen, S. E., Jones, J. B. & Strynadka, N. C. (2000) Structure-based design guides the improved efficacy of deacylation transition state analogue inhibitors of TEM-1 β-lactamase. *Biochemistry*, **39**: 5312–5321.

[200] Newsom, S. W. (1969) Carbenicillin-resistant Pseudomonas. *Lancet*, **2**: 1141.

[201] Newsom, S. W., Sykes, R. B. & Richmond, M. H. (1970) Detection of a β-lactamase markedly active against carbenicillin in a strain of Pseudomonas aeruginosa. *J. Bacteriol.*, **101**: 1079–1080.

[202] O'Callaghan, C. H., Morris, A., Kirby, S. M. & Shingler, A. H. (1972) Novel method for detection of β-lactamases by using a chromogenic cephalosporin substrate. *Antimicrob. Agents Chemother.*, **1**: 283–288.

[203] Oefner, C., D'Arcy, A., Daly, J. J., Gubernator, K., Charnas, R. L., Heinze, I., Hubschwerlen, C. & Winkler, F. K. (1990) Refined crystal structure of β-lactamase from Citrobacter freundii indicates a mechanism for β-lactam hydrolysis. *Nature*, **343**: 284–288.

[204] Oliva, M., Dideberg, O. & Field, M. J. (2003) Understanding the acylation mechanisms of active-site serine penicillin-recognizing proteins: A molecular dynamics simulation study. *Proteins*, **53**: 88–100.

[205] Orekhov, V., Noldeand, D., Golovanov, A., Korzhnev, D. & Arseniev, A. (1995) Processing of heteronuclear NMR relaxation data with the new software DASHA. *Appl. Magn. Reson.*, **9**: 581–588.

[206] Orekhov, V. Y., Korzhnev, D. M., Diercks, T., Kessler, H. & Arseniev, A. S. (1999) ^{1}H-^{15}N NMR dynamic study of an isolated alpha-helical peptide (1–36)-bacteriorhodopsin reveals the equilibrium helix-coil transitions. *J. Biomol. NMR*, **14**: 345–356.

[207] Orencia, M. C., Yoon, J. S., Ness, J. E., Stemmer, W. P. & Stevens, R. C. (2001) Predicting the emergence of antibiotic resistance by directed evolution and structural analysis. *Nat. Struct. Biol.*, **8**: 238–242.

[208] Ottiger, M. & Bax, A. (1998) Determination of relative N-HN, N-C', CR-C', and CR-HR effective bond lengths in a protein by NMR in a dilute liquid crystalline phase. *J. Am. Chem. Soc.*, **120**: 12334–12341.

[209] Ouellette, M., Bissonnette, L. & Roy, P. H. (1987) Precise insertion of antibiotic resistance determinants into Tn21-like transposons: Nucleotide sequence of the OXA-1 β-lactamase gene. *Proc. Natl. Acad. Sci. U.S.A.*, **84**: 7378–7382.

[210] Palmer, A. G. (2001) NMR probes of molecular dynamics: Overview and comparison with other techniques. *Annu. Rev. Biophys. Biomol. Struct.*, **30**: 129–155.

[211] Palmer, A. G. (2004) NMR characterization of the dynamics of biomacromolecules. *Chem. Rev.*, **104**: 3623–3640.

[212] Palmer, A. G., Cavanagh, J., Wright, P. E. & Rance, M. (1991) Sensitivity improvement in proton detected heteronuclear correlation experiments. *J. Magn. Reson.*, **93**: 151–170.

[213] Palmer, A. G., Kroenke, C. D. & Loria, J. P. (2001) Nuclear magnetic resonance methods for quantifying microsecond-to-millisecond motions in biological macromolecules. *Methods Enzymol.*, **339**: 204–238.

[214] Palmer, A. G., Rance, M. & Wright, P. E. (1991) Intramolecular motions of a zinc finger DNA-binding domain from Xfin characterized by proton-detected natural abundance ^{13}C heteronuclear NMR spectroscopy. *J. Am. Chem. Soc.*, **113**: 4371–4380.

[215] Palzkill, T. & Botstein, D. (1992) Identification of amino acid substitutions that alter the substrate specificity of TEM-1 β-lactamase. *J. Bacteriol.*, **174**: 5237–5243.

[216] Palzkill, T., Le, Q. Q., Venkatachalam, K. V., LaRocco, M. & Ocera, H. (1994) Evolution of antibiotic resistance: Several different amino acid substitutions in an active site loop alter the substrate profile of β-lactamase. *Mol. Microbiol.*, **12**: 217–229.

[217] Pawley, N. H., Wang, C., Koide, S. & Nicholson, L. K. (2001) An improved method for distinguishing between anisotropic tumbling and chemical exchange in analysis of ^{15}N relaxation parameters. *J. Biomol. NMR*, **20**: 149–165.

[218] Peng, J. & Wagner, G. (1992) Mapping of spectral density functions using heteronuclear NMR relaxation measurements. *J. Magn. Reson., Ser. B*, **98**: 308–332.

[219] Peng, J. W. & Wagner, G. (1995) Frequency spectrum of NH bonds in eglin c from spectral density mapping at multiple fields. *Biochemistry*, **34**: 16733–16752.

[220] Pervushin, K., Riek, R., Wider, G. & Wüthrich, K. (1997) Attenuated T_2 relaxation by mutual cancellation of dipole-dipole coupling and chemical shift anisotropy indicates an avenue to NMR structures of very large biological macromolecules in solution. *Proc. Natl. Acad. Sci. U.S.A.*, **94**: 12366–12371.

[221] Petrosino, J., Cantu, C. & Palzkill, T. (1998) β-lactamases: Protein evolution in real time. *Trends Microbiol.*, **6**: 323–327.

[222] Petrosino, J. F. & Palzkill, T. (1996) Systematic mutagenesis of the active site Ω loop of TEM-1 β-lactamase. *J. Bacteriol.*, **178**: 1821–1828.

[223] Phan, I. Q. H., Boyd, J. & Campbell, I. D. (1996) Dynamic studies of a fibronectin type I module pair at three frequencies: Anisotropic modelling and direct determination of conformational exchange. *J. Biomol. NMR*, **8**: 369–378.

[224] Prescott, L. M., Harley, J. P. & Klein, D. A. (1993) *Microbiology, 2nd edition*. W.C. Brown Publishers.

[225] Quenouille, M. (1949) Approximate tests of correlation in time series. *J. Roy. Stat. Soc., Ser. B*, **11**: 18–84.

[226] Raquet, X., Lamotte-Brasseur, J., Fonzé, E., Goussard, S., Courvalin, P. & Frère, J. M. (1994) TEM β-lactamase mutants hydrolysing third-generation cephalosporins. A kinetic and molecular modelling analysis. *J. Mol. Biol.*, **244**: 625–639.

[227] Raquet, X., Lounnas, V., Lamotte-Brasseur, J., Frère, J. M. & Wade, R. C. (1997) pKa calculations for class A β-lactamases: Methodological and mechanistic implications. *Biophys. J.*, **73**: 2416–2426.

[228] Reddy, T. & Rainey, J. K. (2010) Interpretsation of biomolecular NMR spin relaxation parameters. *Biochem. Cell Biol.*, **88**: 131–142.

[229] Reichmann, D., Cohen, M., Abramovich, R., Dym, O., Lim, D., Strynadka, N. C. J. & Schreiber, G. (2007) Binding hot spots in the TEM1-BLIP interface in light of its modular architecture. *J. Mol. Biol.*, **365**: 663–679.

[230] Reichmann, D., Rahat, O., Albeck, S., Meged, R., Dym, O. & Schreiber, G. (2005) The modular architecture of protein-protein binding interfaces. *Proc. Natl. Acad. Sci. U.S.A.*, **102**: 57–62.

[231] Reid, A. J., Simpson, I. N., Harper, P. B. & Amyes, S. G. (1988) The differential expression of genes for the PSE-4 β-lactamase in Pseudomonas aeruginosa and the enterobacteriaceae. *J. Antimicrob. Chemother.*, **21**: 525–533.

[232] Reincke, B., Pérez, C., Pristovsek, P., Lücke, C., Ludwig, C., Löhr, F., Rogov, V. V., Ludwig, B. & Rüterjans, H. (2001) Solution structure and dynamics of the functional domain of Paracoccus denitrificans cytochrome c_{552} in both redox states. *Biochemistry*, **40**: 12312–12320.

[233] Richardson, J. S. & Richardson, D. C. (1989) *Prediction of protein structure and the principles of protein conformation*. Plenum Press.

[234] Roccatano, D., Sbardella, G., Aschi, M., Amicosante, G., Bossa, C., Nola, A. & Mazza, F. (2005) Dynamical aspects of TEM-1 β-lactamase probed by molecular dynamics. *J. Comput. Aided Mol. Des.*, **19**: 329–340.

[235] Sabbagh, Y., Thériault, E., Sanschagrin, F., Voyer, N., Palzkill, T. & Levesque, R. C. (1998) Characterization of a PSE-4 mutant with different properties in relation to penicillanic acid sulfones: Importance of residues 216 to 218 in class A β-lactamases. *Antimicrob. Agents Chemother.*, **42**: 2319–2325.

[236] Salkind, A. R., Cuddy, P. G. & Foxworth, J. W. (2001) Is this patient allergic to penicillin?: An evidence-based analysis of the likelihood of penicillin allergy. *JAMA*, **285**: 2498–2505.

[237] Sambrook, J. & Russel, D. W. (2001) *Molecular cloning*. Cold Spring Harbor.

[238] Sanschagrin, F., Thériault, E., Sabbagh, Y., Voyer, N. & Levesque, R. C. (2000) Combinatorial biochemistry and shuffling of TEM, SHV and Streptomyces albus Ω loops in PSE-4 class A β-lactamase. *J. Antimicrob. Chemother.*, **45**: 517–520.

[239] Savard, P.-Y. (2008) *Caractérisation structurale et dynamique de la β-lactamase TEM-1 de la bactérie Escherichia coli par RMN liquide.* Ph.D. thesis, Biochimie et microbiologie, Université Laval (Canada). http://archimede.bibl.ulaval.ca/archimede/uid/5655dbc3-abbd-430d-931b-3caa28e8cd0a.

[240] Savard, P.-Y. & Gagné, S. M. (2006) Backbone dynamics of TEM-1 determined by NMR: Evidence for a highly ordered protein. *Biochemistry*, **45**: 11414–11424.

[241] Savard, P.-Y., Sosa-Peinado, A., Levesque, R. C., Makinen, M. W. & Gagné, S. M. (2004) ^{1}H, ^{13}C and ^{15}N backbone resonance assignments for TEM-1, a 28.9 kDa β-lactamase from E. coli. *J. Biomol. NMR*, **29**: 433–434.

[242] Savoie, A., Sanschagrin, F., Palzkill, T., Voyer, N. & Levesque, R. C. (2000) Structure-function analysis of α-helix H4 using PSE-4 as a model enzyme representative of class A β-lactamases. *Protein Eng.*, **13**: 267–274.

[243] Saxena, A., Udgaonkar, J. B. & Krishnamoorthy, G. (2005) *Fluorescence Spectroscopy in Biology*, chapter Protein Dynamics and Protein Folding Dynamics Revealed by Time-Resolved Fluorescence, pages 163–179. Springer Berlin Heidelberg.

[244] Schurr, J. M., Babcock, H. P. & Fujimoto, B. S. (1994) A test of the model-free formulas. Effects of anisotropic rotational diffusion and dimerization. *J. Magn. Reson., Ser. B*, **105**: 211–224.

[245] Schwarz, G. (1978) Estimating dimension of a model. *Ann. Stat.*, **6**: 461–464.

[246] Shapiro, Y. E., Kahana, E., Tugarinov, V., Liang, Z., Freed, J. H. & Meirovitch, E. (2002) Domain flexibility in ligand-free and inhibitor-bound Escherichia coli adenylate kinase based on a mode-coupling analysis of ^{15}N spin relaxation. *Biochemistry*, **41**: 6271–6281.

[247] Sharma, D. & Rajarathnam, K. (2000) ^{13}C NMR chemical shifts can predict disulfide bond formation. *J. Biomol. NMR*, **18**: 165–171.

[248] Slupsky, C. M., Boyko, R. F., Booth, V. K. & Sykes, B. D. (2003) Smartnotebook: A semi-automated approach to protein sequential NMR resonance assignments. *J. Biomol. NMR*, **27**: 313–321.

[249] Smoluchowski, M. (1906) Zur kinetischen Theorie der Brownschen Molekularbewegung und der Suspensionen. *Ann. Phys.*, **21**: 756–780.

[250] Soss, S. E. & Flynn, P. F. (2007) Functional implications for a prototypical k-turn binding protein from structural and dynamical studies of 15.5K. *Biochemistry*, **46**: 14979–14986.

[251] Spyracopoulos, L. (2006) A suite of Mathematica notebooks for the analysis of protein main chain ^{15}N NMR relaxation data. *J. Biomol. NMR*, **36**: 215–224.

[252] Stec, B., Holtz, K. M., Wojciechowski, C. L. & Kantrowitz, E. R. (2005) Structure of the wild-type TEM-1 β-lactamase at 1.55 Å and the mutant enzyme Ser70Ala at 2.1 Å suggest the mode of noncovalent catalysis for the mutant enzyme. *Acta Crystallogr. D. Biol. Crystallogr.*, **61**: 1072–1079.

[253] Strateva, T. & Yordanov, D. (2009) Pseudomonas aeruginosa - A phenomenon of bacterial resistance. *J. Med. Microbiol.*, **58**: 1133–1148.

[254] Strominger, J. L. & Tipper, D. J. (1965) Bacterial cell wall synthesis and structure in relation to the mechanism of action of penicillins and other antibacterial agents. *Am. J. Med.*, **39**: 708–721.

[255] Strynadka, N. C., Adachi, H., Jensen, S. E., Johns, K., Sielecki, A., Betzel, C., Sutoh, K. & James, M. N. (1992) Molecular structure of the acyl-enzyme intermediate in β-lactam hydrolysis at 1.7 Å resolution. *Nature*, **359**: 700–705.

[256] Swarén, P., Golemi, D., Cabantous, S., Bulychev, A., Maveyraud, L., Mobashery, S. & Samama, J. P. (1999) X-ray structure of the Asn276Asp variant of the Escherichia coli TEM-1 β-lactamase: Direct observation of electrostatic modulation in resistance to inactivation by clavulanic acid. *Biochemistry*, **38**: 9570–9576.

[257] Swarén, P., Maveyraud, L., Guillet, V., Masson, J. M., Mourey, L. & Samama, J. P. (1995) Electrostatic analysis of TEM1 β-lactamase: Effect of substrate binding, steep potential gradients and consequences of site-directed mutations. *Structure*, **3**: 603–613.

[258] Thai, Q. K., Bös, F. & Pleiss, J. (2009) The lactamase engineering database: A critical survey of TEM sequences in public databases. *BMC Genomics*, **10**: 390.

[259] Therrien, C., Kotra, L. P., Sanschagrin, F., Mobashery, S. & Levesque, R. C. (2000) Evaluation of inhibition of the carbenicillin-hydrolyzing β-lactamase PSE-4 by the clinically used mechanism-based inhibitors. *FEBS Lett.*, **470**: 285–292.

[260] Therrien, C. & Levesque, R. C. (2000) Molecular basis of antibiotic resistance and β-lactamase inhibition by mechanism-based inactivators: Perspectives and future directions. *FEMS Microbiol. Rev.*, **24**: 251–262.

[261] Therrien, C., Sanschagrin, F., Palzkill, T. & Levesque, R. C. (1998) Roles of amino acids 161 to 179 in the PSE-4 Ω loop in substrate specificity and in resistance to ceftazidime. *Antimicrob. Agents Chemother.*, **42**: 2576–2583.

[262] Thomas, V. L., Golemi-Kotra, D., Kim, C., Vakulenko, S. B., Mobashery, S. & Shoichet, B. K. (2005) Structural consequences of the inhibitor-resistant Ser130Gly substitution in TEM β-lactamase. *Biochemistry*, **44**: 9330–9338.

[263] Tipper, D. J. & Strominger, J. L. (1965) Mechanism of action of penicillins: A proposal based on their

structural similarity to acyl-D-alanyl-D-alanine. *Proc. Natl. Acad. Sci. U.S.A.*, **54**: 1133–1141.

[264] Tjandra, N., Szabo, A. & Bax, A. (1996) Protein backbone dynamics and ^{15}N chemical shift anisotropy from quantitative measurement of relaxation interference effects. *J. Am. Chem. Soc.*, **118**: 6986–6991.

[265] Tjandra, N., Wingfield, P., Stahl, S. & Bax, A. (1996) Anisotropic rotational diffusion of perdeuterated HIV protease from ^{15}N NMR relaxation measurements at two magnetic fields. *J. Biomol. NMR*, **8**: 273–284.

[266] Tollinger, M., Skrynnikov, N. R., Mulder, F. A., Forman-Kay, J. D. & Kay, L. E. (2001) Slow dynamics in folded and unfolded states of an SH3 domain. *J. Am. Chem. Soc.*, **123**: 11341–11352.

[267] Tolman, J. R. (2001) Dipolar couplings as a probe of molecular dynamics and structure in solution. *Curr. Opin. Struct. Biol.*, **11**: 532–539.

[268] Tsan, P., Hus, J.-C., Caffrey, M., Marion, D. & Blackledge, M. (2000) Rotational diffusion anisotropy and local backbone dynamics of carbon monoxide bound Rhodobacter capsulatus cytochrome c'. *J. Am. Chem. Soc.*, **122**: 5603–5612.

[269] Ulrich, E. L., Akutsu, H., Doreleijers, J. F., Harano, Y., Ioannidis, Y. E., Lin, J., Livny, M., Mading, S., Maziuk, D., Miller, Z., Nakatani, E., Schulte, C. F., Tolmie, D. E., Wenger, R. K., Yao, H. & Markley, J. L. (2008) Biomagresbank. *Nucl. Acids Res.*, **36**: D402–D408.

[270] Vanhove, M., Guillaume, G., Ledent, P., Richards, J. H., Pain, R. H. & Frère, J. M. (1997) Kinetic and thermodynamic consequences of the removal of the Cys-77-Cys-123 disulphide bond for the folding of TEM-1 β-lactamase. *Biochem. J.*, **321**: 413–417.

[271] Vijayakumar, S., Ravishanker, G., Pratt, R. F. & Beveridge, D. L. (1995) Molecular dynamics simulation of a class A β-lactamase: Structural and mechanistic implications. *J. Am. Chem. Soc.*, **117**: 1722–1730.

[272] Voigt, C. A., Martinez, C., Wang, Z.-G., Mayo, S. L. & Arnold, F. H. (2002) Protein building blocks preserved by recombination. *Nat. Struct. Biol.*, **9**: 553–558.

[273] Wand, A. J. (2001) Dynamic activation of protein function: A view emerging from NMR spectroscopy. *Nat. Struct. Biol.*, **8**: 926–931.

[274] Wang, A. C. & Bax, A. (1993) Minimizing the effects of radio-frequency heating in multidimensional NMR experiments. *J. Biomol. NMR*, **3**: 715–720.

[275] Wang, C. & Palmer, A. G. (2003) Solution NMR methods for quantitative identification of chemical exchange in ^{15}N-labeled proteins. *Magn. Reson. Chem.*, **41**: 866–876.

[276] Wang, J., Palzkill, T. & Chow, D.-C. (2009) Structural insight into the kinetics and ΔCp of interactions between TEM-1 β-lactamase and β-lactamase inhibitory protein (BLIP). *J. Biol. Chem.*, **284**: 595–609.

[277] Wang, X., Minasov, G., Blázquez, J., Caselli, E., Prati, F. & Shoichet, B. K. (2003) Recognition and resistance in TEM β-lactamase. *Biochemistry*, **42**: 8434–8444.

[278] Wang, X., Minasov, G. & Shoichet, B. K. (2002) Evolution of an antibiotic resistance enzyme constrained by stability and activity trade-offs. *J. Mol. Biol.*, **320**: 85–95.

[279] Wang, X., Minasov, G. & Shoichet, B. K. (2002) Noncovalent interaction energies in covalent complexes: TEM-1 β-lactamase and β-lactams. *Proteins*, **47**: 86–96.

[280] Wang, X., Minasov, G. & Shoichet, B. K. (2002) The structural bases of antibiotic resistance in the clinically derived mutant β-lactamases TEM-30, TEM-32, and TEM-34. *J. Biol. Chem.*, **277**: 32149–32156.

[281] Waxman, D. J., Yocum, R. R. & Strominger, J. L. (1980) Penicillins and cephalosporins are active site-directed acylating agents: Evidence in support of the substrate analogue hypothesis. *Philos. Trans. R. Soc. Lond., B. Biol. Sci.*, **289**: 257–271.

[282] Willard, L., Ranjan, A., Zhang, H., Monzavi, H., Boyko, R. F., Sykes, B. D. & Wishart, D. S. (2003)

VADAR: A web server for quantitative evaluation of protein structure quality. *Nucl. Acids Res.*, **31**: 3316–3319.

[283] Wishart, D. S. & Sykes, B. D. (1994) The ^{13}C chemical-shift index: A simple method for the identification of protein secondary structure using ^{13}C chemical-shift data. *J. Biomol. NMR*, **4**: 171–180.

[284] Witte, W. (1998) Medical consequences of antibiotic use in agriculture. *Science*, **279**: 996–997.

[285] Wittekind, M. & Mueller, L. (1993) HNCACB, a high-sensitivity 3D NMR experiment to correlate amide-proton and nitrogen resonances with the α- and β-carbon resonances in proteins. *J. Magn. Reson., Ser. B*, **101**: 201–205.

[286] Wolfe, S., Kim, C.-K. & Yang, K. (1994) Ab initio molecular orbital calculations on neutral hydrolysis and methanolysis of azetidinones, including catalysis by water. Relationship to the mechanism of action of β-lactam antibiotics. *Can. J. Chem.*, **72**: 1033–1043.

[287] Xu, X. P. & Case, D. A. (2001) Automated prediction of ^{15}N, $^{13}C_\alpha$, $^{13}C_\beta$ and ^{13}C' chemical shifts in proteins using a density functional database. *J. Biomol. NMR*, **21**: 321–333.

[288] Yamazaki, T., Lee, W., Arrowsmith, C. H., Muhandiram, D. R. & Kay, L. E. (1994) A suite of triple resonance NMR experiments for the backbone assignment of ^{15}N, ^{13}C, ^{2}H labeled proteins with high sensitivity. *J. Am. Chem. Soc.*, **116**: 11655–11666.

[289] Yang, D. & Kay, L. E. (1996) Contributions to conformational entropy arising from bond vector fluctuations measured from NMR-derived order parameters: Application to protein folding. *J. Mol. Biol.*, **263**: 369–382.

[290] Yang, D., Mok, Y.-K., Forman-Kay, J. D., Farrow, N. A. & Kay, L. E. (1997) Contributions to protein entropy and heat capacity from bond vector motions measured by NMR spin relaxation. *J. Mol. Biol.*, **272**: 790–804.

[291] Yip, G. N. B. & Zuiderweg, E. R. P. (2004) A phase cycle scheme that significantly suppresses offset-dependent artifacts in the R_2-CPMG ^{15}N relaxation experiment. *J. Magn. Reson.*, **171**: 25–36.

[292] Yip, G. N. B. & Zuiderweg, E. R. P. (2005) Improvement of duty-cycle heating compensation in NMR spin relaxation experiments. *J. Magn. Reson.*, **176**: 171–178.

[293] Yon, J. M., Perahia, D. & Ghélis, C. (1998) Conformational dynamics and enzyme activity. *Biochimie*, **80**: 33–42.

[294] Zhang, H., Neal, S. & Wishart, D. S. (2003) RefDB: A database of uniformly referenced protein chemical shifts. *J. Biomol. NMR*, **25**: 173–195.

[295] Zhuravleva, A. V., Korzhnev, D. M., Kupče, E., Arseniev, A. S., Billeter, M. & Orekhov, V. Y. (2004) Gated electron transfers and electron pathways in azurin: A NMR dynamic study at multiple fields and temperatures. *J. Mol. Biol.*, **342**: 1599–1611.

Thesis prepared with LaTeX.